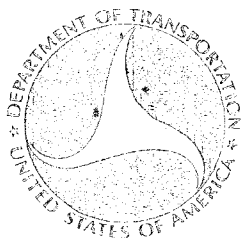


AERODYNAMIC FORCES ON FREIGHT TRAINS
VOLUME II
TEST RESULTS REPORT
FULL-SCALE AERODYNAMIC VALIDATION TESTS
OF TRAILER-ON-A-FLAT CAR (SERIES II)

ENGINEERING TEST AND ANALYSIS DIVISION
ENSCO, INC.
ALEXANDRIA, VIRGINIA 22303



MARCH 1978

Document is available to the public through the
National Technical Information Service,
Springfield, Virginia 22161.

Prepared for
U.S. DEPARTMENT OF TRANSPORTATION
FEDERAL RAILROAD ADMINISTRATION

Office of Freight Systems
Washington, D.C. 20590

NOTICE

This document is disseminated under the sponsorship of the Department of Transportation in the interest of information exchange. The United States Government assumes no liability for the contents or use thereof.

NOTICE

The United States Government does not endorse products or manufacturers. Trade or manufacturer's names appear herein solely because they are considered essential to the object of this report.

1. Report No. FRA/ORD-76-295.II		2. Government Accession No.		3. Recipient's Catalog No. 70481823	
4. Title and Subtitle AERODYNAMIC FORCES ON FREIGHT TRAINS VOLUME II - Full-Scale Aerodynamic Validation Tests of Trailer-on-a-Flat Car (Series II)				5. Report Date March 1978	
				6. Performing Organization Code	
7. Author(s) Prakash B. Joshi				8. Performing Organization Report No. DOT-FR-78-19	
9. Performing Organization Name and Address ENSCO, INC. 2560 Huntington Ave. Alexandria, VA 22303				10. Work Unit No. (TRAIS)	
				11. Contract or Grant No. DOT-FR-64113	
12. Sponsoring Agency Name and Address U.S. Department of Transportation Federal Railroad Administration, OFS 2100 Second Street, S.W. Washington, DC 20590				13. Type of Report and Period Covered Test Results Report June 1976-December 1977	
				14. Sponsoring Agency Code	
15. Supplementary Notes Vol. I -Wind Tunnel Test of Containers and Trailers on Flat Cars - December 1976 - A.G. Hammitt. Vol.III - Correlation of Wind Tunnel and Full Scale Test Data - To be published. Vol. IV - Wind Tunnel Tests of Conventional Rail Freight Rolling Stock - To be published.					
16. Abstract Aerodynamic forces were measured on full-scale Trailer-on-a-Flat Car (TOFC) configurations and a reliable data base was established for validation of wind tunnel test programs. The drag, side and lift forces were determined on two trailers mounted on an instrumented flat car, each by means of a specially designed force-balance system. Two TOFC configurations (Configuration 1 with a loaded buffer car leading the instrumented flat car and Configuration 2 with an empty buffer car) were tested under different wind conditions. In addition to the aerodynamic resistance of the trailers, total tractive resistance of the TOFC was measured via instrumented couplers. The results indicate good agreement between the full-scale aerodynamic drag data and the wind tunnel data from the tests at the Calspan Corporation. The wind tunnel tests conducted at the California Institute of Technology exhibited significantly higher drag values than the full-scale measurements, especially at high wind angles. The foregoing conclusions apply to both Configurations 1 and 2. It was found that Configuration 2 experienced consistently larger drag than Configuration 1. Measurement of the total tractive resistance enabled a rough estimation of the rolling resistance of the instrumented flat car. The present tests show that at 50 mph the aerodynamic drag accounts for 50 to 60 percent of total train resistance and the rolling resistance takes the remaining share. At 90 mph, the drag force amounts to approximately 55 to 70 percent of the total resistance.					
17. Key Words Train Resistance Aerodynamic Drag on Freight Trains Rolling Resistance TOFC Aerodynamics			18. Distribution Statement Document available to the Public through the National Technical Information Service, Springfield, VA 22161		
19. Security Classif. (of this report) Unclassified		20. Security Classif. (of this page) Unclassified		22. Price PC A17 MFA01	

ACKNOWLEDGMENTS

The success of the AERO/TOFC (Series II) Program has been a result of the hard work and the contribution of ideas on the part of several individuals. Thanks are due to Mr. Arne Bang, FRA, Chief Freight Service Division and Mr. John Koper, the FRA Program Manager; Dr. A.G. Hammitt, the Principal Investigator; Mssrs. Given Brewer, LaVerne Wallace and Hemant Limaye of Brewer Engineering Laboratories; Mr. Lorin Staten, Mr. Bruce Morrell, and Mr. Lane Maxwell of the Transportation Test Center. Special thanks go to the following ENSCO personnel: Mr. Carl T. Jones, the Project Manager, Mr. Robert Scofield, the Project Engineer, and Mr. Robert Hendrickson for engineering and managerial support; Mr. Bryan Stewart, Mr. John Berglund, Mr. John Hight, Mr. Herschel Cannon, and Mr. Don Chaffel who provided instrumentation design, installation and data processing support. Finally, thanks are also due to the members of the TTC machine shops, the locomotive crew and the administrative personnel with the participating organizations.

METRIC CONVERSION FACTORS

Approximate Conversions to Metric Measures

Symbol	When You Know	Multiply by	To Find	Symbol
LENGTH				
in	inches	*2.5	centimeters	cm
ft	feet	30	centimeters	cm
yd	yards	0.9	meters	m
mi	miles	1.6	kilometers	km
AREA				
in ²	square inches	6.5	square centimeters	cm ²
ft ²	square feet	0.09	square meters	m ²
yd ²	square yards	0.8	square meters	m ²
mi ²	square miles	2.6	square kilometers	km ²
	acres	0.4	hectares	ha
MASS (weight)				
oz	ounces	28	grams	g
lb	pounds	0.45	kilograms	kg
	short tons (2000 lb)	0.9	tonnes	t
VOLUME				
tsp	teaspoons	5	milliliters	ml
Tbsp	tablespoons	15	milliliters	ml
fl oz	fluid ounces	30	milliliters	ml
c	cups	0.24	liters	l
pt	pints	0.47	liters	l
qt	quarts	0.95	liters	l
gal	gallons	3.8	liters	l
ft ³	cubic feet	0.03	cubic meters	m ³
yd ³	cubic yards	0.76	cubic meters	m ³
TEMPERATURE (exact)				
°F	Fahrenheit temperature	5/9 (after subtracting 32)	Celsius temperature	°C

*1 in = 2.54 (exact). For other exact conversions and more detailed tables, see NBS Misc. Publ. 286, Units of Weights and Measures, Price \$2.25, SD Catalog No. C13.10/286.

Approximate Conversions from Metric Measures

Symbol	When You Know	Multiply by	To Find	Symbol
LENGTH				
mm	millimeters	0.04	inches	in
cm	centimeters	0.4	inches	in
m	meters	3.3	feet	ft
m	meters	1.1	yards	yd
km	kilometers	0.6	miles	mi
AREA				
cm ²	square centimeters	0.16	square inches	in ²
m ²	square meters	1.2	square yards	yd ²
km ²	square kilometers	0.4	square miles	mi ²
ha	hectares (10,000 m ²)	2.5	acres	
MASS (weight)				
g	grams	0.035	ounces	oz
kg	kilograms	2.2	pounds	lb
t	tonnes (1000 kg)	1.1	short tons	
VOLUME				
ml	milliliters	0.03	fluid ounces	fl oz
l	liters	2.1	pints	pt
l	liters	1.06	quarts	qt
l	liters	0.26	gallons	gal
m ³	cubic meters	35	cubic feet	ft ³
m ³	cubic meters	1.3	cubic yards	yd ³
TEMPERATURE (exact)				
°C	Celsius temperature	9/5 (then add 32)	Fahrenheit temperature	°F

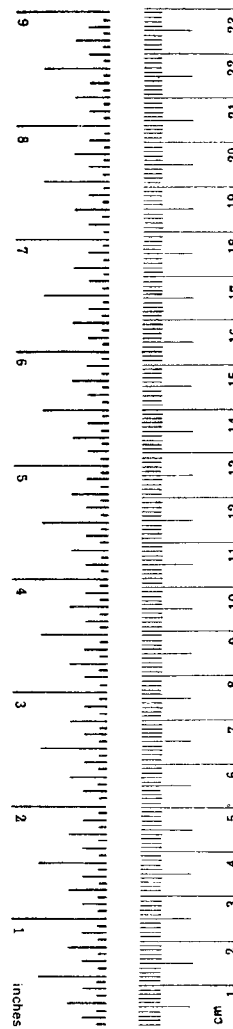
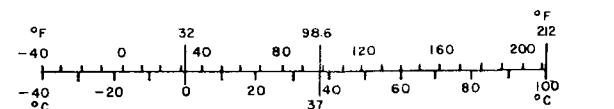


TABLE OF CONTENTS

<u>SECTION</u>	<u>TITLE</u>	<u>PAGE</u>
	ACKNOWLEDGEMENTS	i
	METRIC CONVERSION FACTORS	ii
	TABLE OF CONTENTS	iii
	LIST OF ILLUSTRATIONS	vi
	LIST OF TABLES	xi
	SUMMARY	xii
1.0	INTRODUCTION	1
1.1	BACKGROUND	1
1.2	OBJECTIVE	3
1.3	SUMMARY OF RESULTS	3
1.4	REPORT ORGANIZATION	4
2.0	TEST DESCRIPTION	6
2.1	GENERAL	6
2.2	TEST ZONE	8
2.3	TEST CONSIST	11
2.4	INSTRUMENTATION	19
2.4.1	General	19
2.4.2	Primary Instrumentation	19
2.4.2.1	Force Balance System	21
2.4.2.2	Instrumented Couplers	26
2.4.2.3	Onboard Wind Speed and Direction Indicator	30
2.4.2.4	Wayside Weather Station	33
2.4.2.5	Train Speed Measurement	34
2.4.2.6	Automatic Location Detectors (ALD)	35
2.4.3	Secondary Instrumentation	35
2.4.3.1	Accelerometers	35
2.4.3.2	Displacement Transducers	36
2.4.3.3	Vertical Gyroscope	36
2.4.3.4	Relative Speed Transducer	36
2.4.4	Signal Conditioning, Filtering and Recording	36
2.4.5	List of Data Channels	37
2.5	TEST PROCEDURES	40
3.0	DEVELOPMENT OF DATA ANALYSIS PROCEDURES AND ERROR ESTIMATION	44
3.1	GENERAL	44
3.2	MAGNITUDES OF FORCES OF INTEREST	45
3.2.1	Aerodynamic Forces	45
3.2.2	Gravitational Forces	45
3.2.3	Inertial Forces	47
3.2.3.1	Linear Accelerations	47
3.2.3.2	Centripetal Acceleration	48

TABLE OF CONTENTS (CONT)

3.3	MODELS FOR LONGITUDINAL AND LATERAL MOTIONS	49
3.3.1	Model for Longitudinal Motion	50
3.4	DERIVATION OF EQUATIONS OF MOTION	51
3.4.1	Equation for Longitudinal Motion	54
3.4.2	Equation of Lateral Motion	57
3.5	METHODS OF AERODYNAMIC FORCE DETERMINATION	59
3.5.2	Momentum Approach	61
3.5.3	Energy Approach	64
3.6	COMPUTATIONAL PROCEDURE FOR ON-BOARD PROCESSING	66
3.6.1	Drag Force	67
3.6.2	Side Force	69
3.7	ESTIMATION OF ERRORS	71
3.7.1	Errors in Drag Force Determination	71
3.7.2	Errors in Side Force Determination	83
4.0	REDUCTION OF TEST DATA	95
4.1	GENERAL	95
4.2	ONBOARD DATA REDUCTION	95
4.3	POST-TEST DATA REDUCTION	98
4.3.1	Comparison of Relative Velocity Data Between Onboard and Wayside Measurements	98
4.3.2	Comparison of Force Area Data Based on Onboard Wind Data and Vectored Wind Data	101
4.3.3	Derivation of Rolling Resistance Information	102
4.3.4	Changes in Attitude of Flat Car Deck Plate	104
5.0	ANALYSIS OF TEST DATA	141
5.1	GENERAL	141
5.2	FORCE AREA PLOTS BASED ON ONBOARD WIND DATA WITH OFFSET	142
5.3	FORCE AREA PLOTS BASED ON CALCULATED RELATIVE WIND DATA	143
5.4	FORCE AREA DATA BASED ON ONBOARD WIND DATA CORRECTED FOR OFFSET	153
5.5	ANALYSIS OF ROLLING RESISTANCE INFORMATION	162

TABLE OF CONTENTS (CONT)

6.0	COMPARISON OF FULL-SCALE AND WIND TUNNEL DATA	171
6.1	GENERAL	171
6.2	BRIEF DESCRIPTION OF WIND TUNNEL TESTS	171
6.3	COMPARISON OF CONFIGURATION 1 DATA	176
6.3.1	Drag Area	176
6.3.2	Side Force Area	176
6.4	COMPARISON OF CONFIGURATION 2 DATA	179
6.4.1	Drag Area	179
6.4.2	Side Force Area	179
6.5	DISCUSSION OF RESULTS	179
7.0	CONCLUSIONS	184
8.0	REFERENCES	186
APPENDIX A	- FULL-SCALE AERODYNAMIC LOAD MEASURING SYSTEM FOR AERO/TOFC (SERIES II)	A-1
APPENDIX B	- TEST EVENTS REPORT	B-1
APPENDIX C	- MATHEMATICAL DERIVATIONS	C-1
APPENDIX D	- PROCEDURE FOR ONBOARD COMPUTATION OF DRAG AND SIDE FORCES	D-1

LIST OF ILLUSTRATIONS

<u>Figure No.</u>	<u>Title</u>	<u>Page</u>
2-1(a)	Transportation Test Center Facilities	9
2-1(b)	Topographical Map of AERO/TOFC(Series II) Test Zone	10
2-2(a)	Test Consist - Configuration 1	12
2-1(b)	Test Consist - Configuration 2	12
2-3	DOT-001 Locomotive in Configuration 1	13
2-4(a)	Buffer Flat Car	14
2-4(b)	Instrumented Flat Car	14
2-5	Instrumented Coupler (Trailing)	15
2-6	Trailer Mounted on Buffer Flat Car	16
2-7	Trailer Mounted on Instrumented Flat Car	17
2-8	Wood/Sheel Metal Wheel Assembly Underneath Trailer	17
2-9(a)	Cross-Bracing Inside Trailer-View A	18
2-9(b)	Cross-Bracing Inside Trailer-View B	18
2-10	Flexure Arrangement - Schematic Diagram	20
2-11	Schematic of Perspective View of Force - Balance System	22
2-12(a)	Flexure Assembly at Kingpin - View A	23
2-12(b)	Flexure Assembly at Kingpin - View B	23
2-12(c)	Flexure Assembly at Kingpin - View C	24
2-13(a)	Rear Flexure Assembly - Vertical	24
2-13(b)	Rear Flexure Assembly - Lateral	24(a)
2-14(a)	Jacking Calibration of Right-Rear, Vertical Flexure	27
2-14(b)	Jacking Calibration of Right-Rear, Vertical Flexure - Closeup View	27

LIST OF ILLUSTRATIONS (CONT)

<u>Figure No.</u>	<u>Title</u>	<u>Page</u>
2-15(a)	Longitudinal Wind Calibration	28
2-15(b)	Lateral Wind Calibration	28
2-16	Engineering Drawing of Instrumented Coupler	29
2-17	Exploded View of Instrumented Coupler	30(a)
2-18	Spring Assembly Inside Barrel Housing of Instrumented Coupler	31
2-19	On-board Wind Speed and Direction Sensor Mounted in Wind Tunnel	32
2-20(a)	Wayside Weather Station With Test Consist In Background	33
2-20(b)	Wayside Weather Station	34
2-21	Displacement Transducer Between Flat Car and Truck Frame	37
3-1(a)	Typical Drag Force Variation With Speed	46
3-1(b)	Typical Side Force Variation With Speed	46
3.2	Contribution of Trailer Weight to Longitudinal and Lateral Load Cells	47
3-3	Component of Trailer Weight Versus Tilt Angle	48
3-4	Model for Longitudinal Motion	50
3-5	Model for Lateral Motion	52
3-6	Coordinate System	53
3-7(a)	Longitudinal Motion of Trailer	55
3-7(b)	Free Body Diagram for Longitudinal Motion	55
3-7(c)	Free Body Diagram for Lateral Motion	56
3-8	Sign Convention for Restoring Forces	57

LIST OF ILLUSTRATIONS (CONT)

<u>Figure No.</u>	<u>Title</u>	<u>Page</u>
3-9	Approximation for Gravitational Force	68
3-10	Load Cell and Signal Processing Errors	81
3-11	Motion of Trailer Center of Gravity in x-y Plane	91
4-1(a)	Coordinate System for Wayside Wind Direction	99
4-1(b)	Coordinate System for Onboard Wind Direction	99
4-2	Calculation of Relative Wind Vector From Wayside Wind Data	100
5-1(a)	Total Drag Area Versus Onboard Relative Wind Direction with Offset-Configuration 1	144
5-1(b)	Total Drag Area Versus Onboard Relative Wind Direction with Offset-Configuration 2	145
5-2(a)	Total Side Force Area Versus Onboard Relative Wind Direction with Offset-Configuration 1	146
5-2(b)	Total Side Force Area Versus Onboard Relative Wind Direction with Offset-Configuration 2	147
5-3(a)	Total Calculated Drag Area Versus Calculated Relative Wind Direction-Configuration 1	149
5-3(b)	Total Calculated Drag Area Versus Calculated Wind Direction-Configuration 2	150
5-4(a)	Total Calculated Side Force Area Versus Calculated Relative Wind Direction-Configuration 1	151
5-4(b)	Total Calculated Side Force Area Versus Calculated Relative Wind Direction-Configuration 2	152
5-5	Comparison of Calculated Relative Wind Direction and Onboard Relative Wind Direction with Offset	154

LIST OF ILLUSTRATIONS (CONT)

<u>Figure No.</u>	<u>Title</u>	<u>Page</u>
5-6(a)	Total Drag Area Versus Onboard Relative Wind Direction - Configuration 1	156
5-6(b)	Total Drag Area Versus Onboard Relative Wind Direction - Configuration 2	157
5-7(a)	Total Side Force Area Versus Onboard Relative Wind Direction- Configuration 1	158
5-7(b)	Total Side Force Area Versus Onboard Relative Wind Direction - Configuration 2	159
5-8(a)	Total Lift Force Area Versus Onboard Relative Wind Direction - Configuration 1	160
5-8(b)	Total Lift Area Versus Onboard Relative Wind Direction - Configuration 2	161
5-9(a)	Total Tracitve Resistance for Configuration 1	163
5-9(b)	Total Tracitve Resistance for Configuration 2	164
5-10(a)	Rolling Resistance Information Versus Onboard Relative Wind Speed-Configuration 1	166
5-10(b)	Rolling Resistance Information Versue Onboard Relative Wind Speed-Configuration 2	167
5-11(a)	Rolling Resistance Information Versus Average Train Speed - Configuration 1	168
5-11(b)	Rolling Resistance Information Versus Average Train Speed - Configuration 2	169
6-1(a)	Mean Drag Area as a Function of Wind Angle- Configuration 1	172
6-1(b)	Mean Drag Area as a Function of Wind Angle- Configuration 2	173
6-2(a)	Mean Side Force Area as a Function of Wind Angle - Configuration 1	174
6-2(b)	Mean Side Force Area as a Function of Wind Angle - Configuration 2	175

LIST OF ILLUSTRATIONS (CONT)

<u>Figure No.</u>	<u>Title</u>	<u>Page</u>
6-3	Comparison of Full-Scale Drag Area With Wind Tunnel Results - Configuration 1	177
6-4	Comparison of Full-Scale Side Force Area With Wind Tunnel Results - Configuration 1	178
6-5	Comparison of Full-Scale Drag Area with Wind Tunnel Results - Configuration 2	180
6-6	Comparison of Full-Scale Side Force Area With Wind Tunnel Results- Configuration 2	181

LIST OF TABLES

<u>Table No.</u>	<u>Title</u>	<u>Page</u>
2-1	General Test Conditions	8
2-2	AERO/TOFC (Series II) Instrumentation	38
2-3	Test Matrix	40
3-1	Amplitudes and Frequencies of Carbody Oscillatory Modes	75
3-2	Errors in Drag Force Determination	84
4-1(A)	Wind Speed and Direction Data - Configuration 1	106
4-1(B)	Wind Speed and Direction Data - Configuration 2	109
4-2(A)	Force Data for Configuration 1	111
4-2(B)	Force Data for Configuration 2	114
4-3(A)	Force Area Data Based on Onboard Relative Wind - Configuration 1	116
4-3(B)	Force Area Data Based on Onboard Relative Wind - Configuration 2	119
4-4(A)	Force Area Data Based on Calculated Relative Wind - Configuration 1	121
4-4(B)	Force Area Data Based on Calculated Relative Wind- Configuration 2	124
4-5(A)	Rolling Resistance Data for Configuration 1	126
4-5(B)	Rolling Resistance Data for Configuration 2	129
4-6(A)	Zero Changes of Measurement Transducers - Configuration 1	131
4-6(B)	Zero Changes of Measurement Transducers - Configuration 2	136
4-7	Changes in Carbody Attitude - Pitch and Roll	140
5-1	Zero Offset of Onboard Wind Instrument	155
5-2	Approximate Range of TTX Rolling Resistance	170
6-1	Approximate Percent Agreement Between Full- Scale and Wind Tunnel Results	183

SUMMARY

Full-scale aerodynamic validation tests (AERO/TOFC (Series II)) were successfully conducted on two Trailer-on-a-Flat-Car Configurations at the Transportation Test Center (TTC). ENSCO, Inc. developed and executed the planning of these tests. Brewer Engineering Laboratories (BEL) were the subcontractors for design and installation of the mechanical force-balance system which was used for measuring the aerodynamic forces. The TTC instrumentation group designed and fabricated the leading and trailing couplers which measured total tractive resistance of the TOFC configuration. The test data was collected onboard data acquisition car T-5 owned by the Federal Railroad Administration (FRA). ENSCO, Inc. handled the data acquisition and processing, pre-test and post-test analysis and preparation of the final test results report. ENSCO also coordinated the activities of the test participants, namely BEL, TTC, FRA and Dr. Andrew G. Hammitt, principal investigator under contract to FRA. The AERO/TOFC (Series II) test program was managed by the FRA Office of Freight Systems.

The AERO/TOFC (Series II) test data was found to be reasonable and repeatable, and established a reliable basis for validation of the wind tunnel test programs. The test results indicate that the aerodynamic drag data is in good agreement (within 20 percent) with the wind tunnel tests conducted at Calspan Corporation. The California Institute of Technology (CIT) wind tunnel results showed significantly larger drag values (at high wind angles) than the full-scale measurements. The foregoing results apply to both TOFC configurations tested. It was found that the configuration with empty buffer car (Configuration 1) consistently experienced larger drag (10 percent for wind angles near zero and up to 20 percent at six degrees) than the configuration with the loaded buffer car (Configuration 2). Measurement of total tractive resistance enabled a rough estimation of flat-car rolling

resistance. The present results show that at 50 mph for Configuration 2 (which has more drag), the aerodynamic resistance accounts for 50 to 60 percent of the total train resistance and the rolling resistance takes the remaining share. At 90 mph, the drag force accounts for approximately 50 to 70 percent of the total tractive resistance.

1.0 INTRODUCTION

1.1 BACKGROUND

The tractive resistance of railroad trains, both passenger and freight, has long been a subject of interest to the industry. There is, however, a lack of good engineering data for making reliable predictions of tractive resistance. Tractive resistance consists of aerodynamic resistance and rolling resistance, and in practice, rolling resistance is difficult to measure under controlled conditions. In the past, the wind tunnel has been used extensively to determine the aerodynamic resistance of scale models of trains. However, the applicability of data obtained in model tests and extrapolated to full-scale configurations is inconclusive for a variety of reasons. These reasons include the lack of proper ground plane simulation, the necessity of Reynolds number extrapolation and the size of the model relative to boundary layer thickness on the ground plane. Earlier work in the measurement of aerodynamic resistance was oriented towards high-speed passenger transport and the wind tunnel was used rather extensively. Comparatively, only a small body of work exists in the area of aerodynamic resistance of freight trains.

With the introduction of new designs, i.e., cars of the rack and piggyback types, there has been a resurgence of interest in the aerodynamics of freight trains. Railroads have experienced the need for additional power when pulling a train of rack or piggyback cars as opposed to pulling a train of standard railcars. The economic impact of increased train resistance is of great importance to the operating railroads because increased resistance translates into greater power requirements, fuel consumption and locomotive maintenance.

Wind tunnel tests of two freight-train configurations, Trailer-on-a-Flatcar (TOFC) and Container-on-Flatcar (COFC), were conducted by Andrew G. Hammitt Associates (Reference 1) using the

facilities at California Institute of Technology (CIT). In these tests aerodynamic resistance exerted on some basic blocks and on 1/43-scale models of TOFC and COFC configurations were measured. The ground plane was simulated by stationary ground board, the Reynolds number of the model based on trailer length was 1.2×10^6 (1/20 of full-scale value) and the ratio of boundary layer thickness to model height was approximately 1:4. Experiments with the same models at higher Reynolds numbers (up to 5.6×10^6) were run subsequently in the variable density wind tunnel at Calspan Corporation by the same investigator (Reference 2). The boundary layer thickness was approximately 1/5 of the model height in the latter tests.

The first series of tests (AERO/TOFC (Series I), Reference 3) aimed at determining the aerodynamic forces and moments on full-scale TOFC configurations was carried out at the Transportation Test Center (TTC) in 1976. The tests involved suspending two van-trailers by means of two mechanical force-balance systems on a flat car and operating the consist containing the flat car at different speeds under various wind conditions. The following difficulties were immediately obvious:

- The inability of the balance systems to return to zero readings at the end of a test run, i.e., non-repeatability.
- The presence of large dynamic forces especially those due to lateral accelerations.
- The non-linearities in the calibration of the force-balance system.

Although these problems made it difficult to obtain definitive information regarding aerodynamic forces, valuable information was obtained on the behavior of the system which was useful in planning future testing. For instance, coupling existed between the dynamics of the carbody and the trailers on their mechanical supports; this resulted in large resonant amplitudes. Also, the trailer tilted when loads were applied during calibration. This

caused spurious components of trailer weight in the lateral-force readings.

Finally, the observed non-repeatability of the system was due to a combination of the coupling and the trailer tilt. Thus, AERO/TOFC (Series I) tests showed the complications involved in the measurement of aerodynamic forces in the presence of relatively large inertial and gravitational forces. The AERO/TOFC (Series II) tests were designed taking these problems into account. This second test series is the primary subject of this report.

1.2 OBJECTIVE

The primary objective of the AERO/TOFC (Series II) tests was to perform measurements of aerodynamic resistance (mainly drag and side forces) on full-scale trailer-on-a-flat car configurations and to obtain reliable engineering data which would serve to validate the wind tunnel results described in References 1 and 2.

A secondary goal of the AERO/TOFC (Series II) tests was to measure the entire tractive resistance of the TOFC configuration simultaneously with the aerodynamic resistance in order to derive rolling resistance information.

1.3 SUMMARY OF RESULTS

The AERO/TOFC (Series I) test results demonstrated the necessity for:

- Using a force-balance system of improved design which could be accurately aligned and precisely calibrated.
- Reducing the magnitude of dynamic (inertial) forces relative to the anticipated aerodynamic forces.
- Stiffening the trailer and flat car structures to maintain alignment and calibration during testing.

These modifications were incorporated in the AERO/TOFC (Series II) tests and the performance of the trailer-flat car force-balance

system was predictable and repeatable. The aerodynamic-force data displayed minimal scatter and clear trends. The tractive resistance data and the rolling resistance information derived therefrom appeared reasonable.

A comparison of AERO/TOFC (Series II) results with the wind tunnel data described in Reference 1 and 2 reveal the following:

- The full-scale drag area data is in good agreement with the Calspan tests. The CIT experiments indicate significantly larger values of drag than the AERO/TOFC (Series II) measurements.
- In contrast to the drag area data the side force data is in closer agreement with the CIT tests. The Calspan data gives relatively lower values of side forces than the full-scale measurements.

A rough estimate indicates that, at 50mph, aerodynamic drag accounts for 50 to 60 percent of total train resistance and the remainder is rolling resistance. At 90 mph, aerodynamic drag accounts for approximately 50 to 70 percent of total train resistance.

1.4 REPORT ORGANIZATION

This report describes the AERO/TOFC (Series II) test procedures, the data reduction and analysis, and the results of comparing the full-scale aerodynamic data with the wind tunnel data collected previously. This introductory chapter is followed by a description of the test which includes descriptions of the test consist, the test zone, the instrumentation including the force-balance system, and the test procedures. An in-depth review of methods used to scientifically analyze the experimental data is presented in Section 3.0, along with the computational scheme for on-board data processing and the error sources present in force determination. Section 4.0 includes sample

calculations used in the reduction of the test data and tabulations of same. In Section 5.0, the data is presented graphically and analytical curve-fits are developed. A detailed comparison between the full-scale tests and the wind tunnel results is the subject of Section 6.0. Finally, in Section 7.0 conclusions derived from this test series are presented.

2.0 TEXT DESCRIPTION

2.1 GENERAL

The AERO/TOFC (Series II) test was performed by operating a special freight consist over a specified test zone at several constant speeds under different wind conditions. The consist was made up of a locomotive, a buffer flat car, an instrumented flat car and a data collection vehicle. Three different train speeds of 50, 70 and 90 mph were used. Tests were conducted under calm weather conditions as well as under wind speeds ranging up to 20 mph at various azimuth angles.

Aerodynamic forces were measured on two van-trailers carried in the consist. Each trailer was supported by a force-balance system rigidly attached to the instrumented flat car. The combined tractive resistance of the trailer and the flat car was obtained by means of instrumented couplers at the leading and trailing ends of the flat car. Load cells were used as force measuring devices in all cases.

The levels of inertial forces experienced by the trailers and the flat car were determined by monitoring their accelerations. Displacement between the deck of the flat car and the truck side frames (both leading and trailing) was measured at four points to estimate the extent of roll and pitch of the carbody relative to the track. A vertical gyroscope was also provided to measure the roll of one trailer relative to the local gravity vector. It will be shown in Section 3.0 that angular displacement of the trailers due to changes in carbody orientation causes components of trailer weight to contaminate the aerodynamic force data.

An instrument was mounted to the locomotive to measure

the speed and direction of airflow relative to the train. A wayside weather station was located near the center of the test zone and recorded wind speed and direction at two heights above the ground. Relative humidity and barometric pressure readings were also taken during each test run.

Train speed was measured using an optical tachometer on the data collection vehicle (T-5). The relative speed between T-5 and the instrumented flat car was also measured so that the absolute speed of the latter could be obtained. An Automatic Location Detector mounted underneath the instrumented flat car was used to determine location of the consist in the test zone when passing over the targets placed along the track. This detector was also used to automatically turn on the data acquisition system when the consist entered the test zone and turn it off at the end of the zone.

The analog outputs of measurement transducers were passed through conditioning amplifiers, converted to digital form and recorded on magnetic tape. On a typical test day, the instrument zeros were read when the flat car was parked at a specified location inside an enclosed building at the test facility. Data was collected during each run and subsequently processed using the Raytheon 704 Computer onboard T-5. At the end of a test day, the instrumented flat car was brought back to its original position and transducer zeros were recorded again. This exercise provided zero-shift data for each day which is a useful indicator of system performance and integrity.

Pre-test checkout runs were conducted on 21 November and 2 December 1977. Actual tests were run on 5, 6, 7, 9, 12, 14, 15 and 16 December 1977. A final calibration of the system was performed on 17 December 1977. Table 2 - 1 summarizes the general test conditions on each day.

TABLE 2-1

GENERAL TEST CONDITIONS

TEST DATE	BUFFER CAR CONFIGURATION	WIND SPEED RANGE (MPH)	WIND DIRECTION* RANGE (DEGREES)	TEST RUN NUMBERS
12/5/77	UNLOADED	8-13	420-450	23-31
12/6/77	UNLOADED	0-5	60-360	32-40
12/8/77	UNLOADED	7-12	370-410	41-50
12/9/77	TWO TRAILERS	0-6	380-460	51-61
12/12/77	TWO TRAILERS	4-16	100-430	62-73
12/14/77	TWO TRAILERS	2-11	240-470	74-82
12/15/77	TWO TRAILERS	0-13	90-300	83-93
12/16/77	TWO TRAILERS	10-19	230-310	94-102
12/16/77	UNLOADED	7-9	250-270	103-108

*Defined relative to the coordinate system described in Section 4.3.

2.2 TEST ZONE

The test zone for the AERO/TOFC (Series II) tests was a part of the east tangent of the Railroad Test Track (RTT) at the Transportation Test Center (TTC) in Pueblo, Colorado. The latitude of Pueblo is 30° 17' N and the climatological data published by the National Oceanographic and Atmospheric Association (NOAA) indicates the prevalence of high winds in this area around November and December (Reference 4). Figure 2-1(a) shows the layout at TTC and the location of the test track. The consist ran downhill over a distance of 4000 feet from station 140 to station 180. Altitudes of these locations above mean sea level are 4873 feet and 4862 feet respectively (Reference 5). Therefore, the average downgrade was 0.275 percent. The railroad track was made of 136-pound continuously welded rail with wooden ties on 19.5-inch centers. This section of RTT was

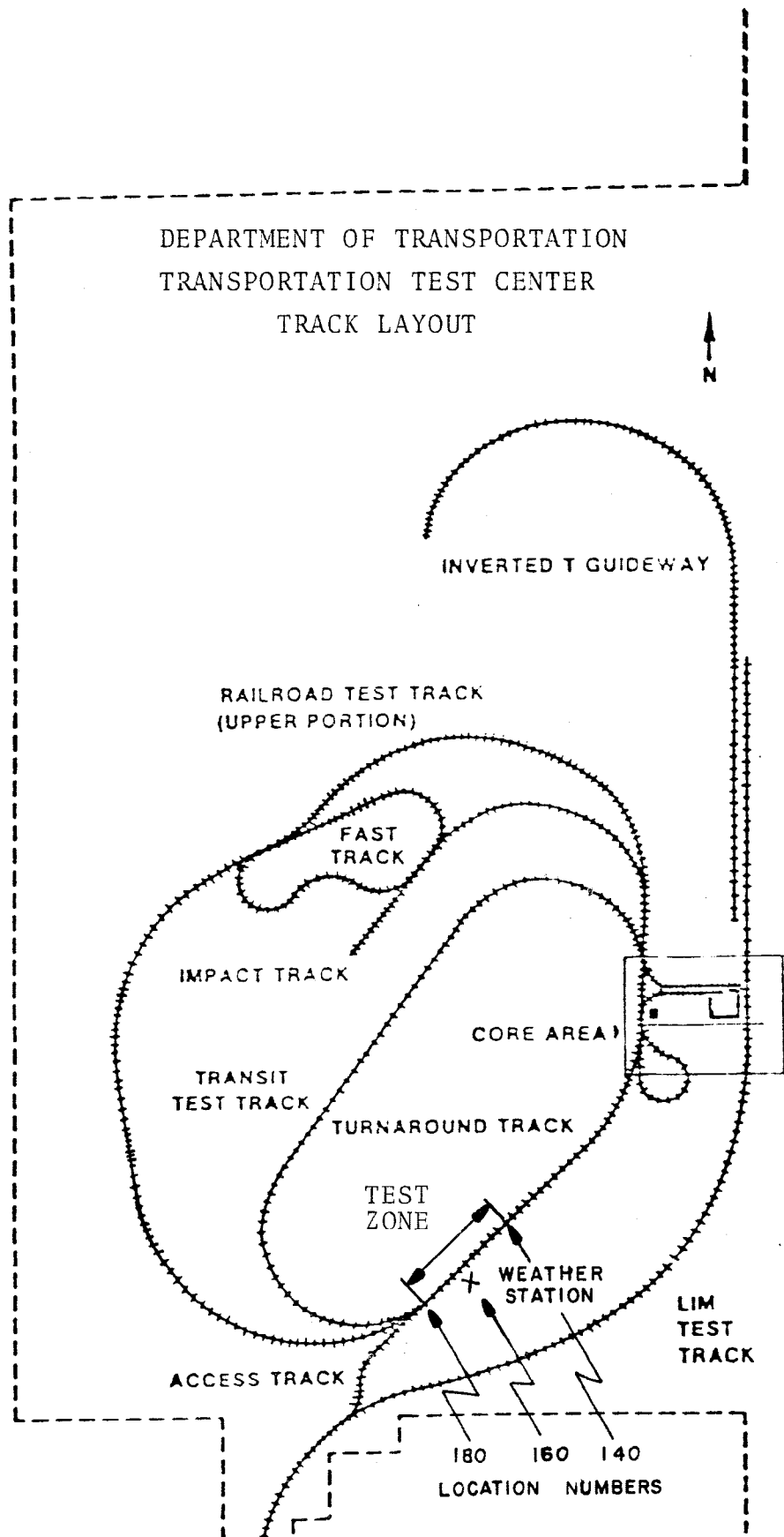


Figure 2-1(a). Transportation Test Center Facilities

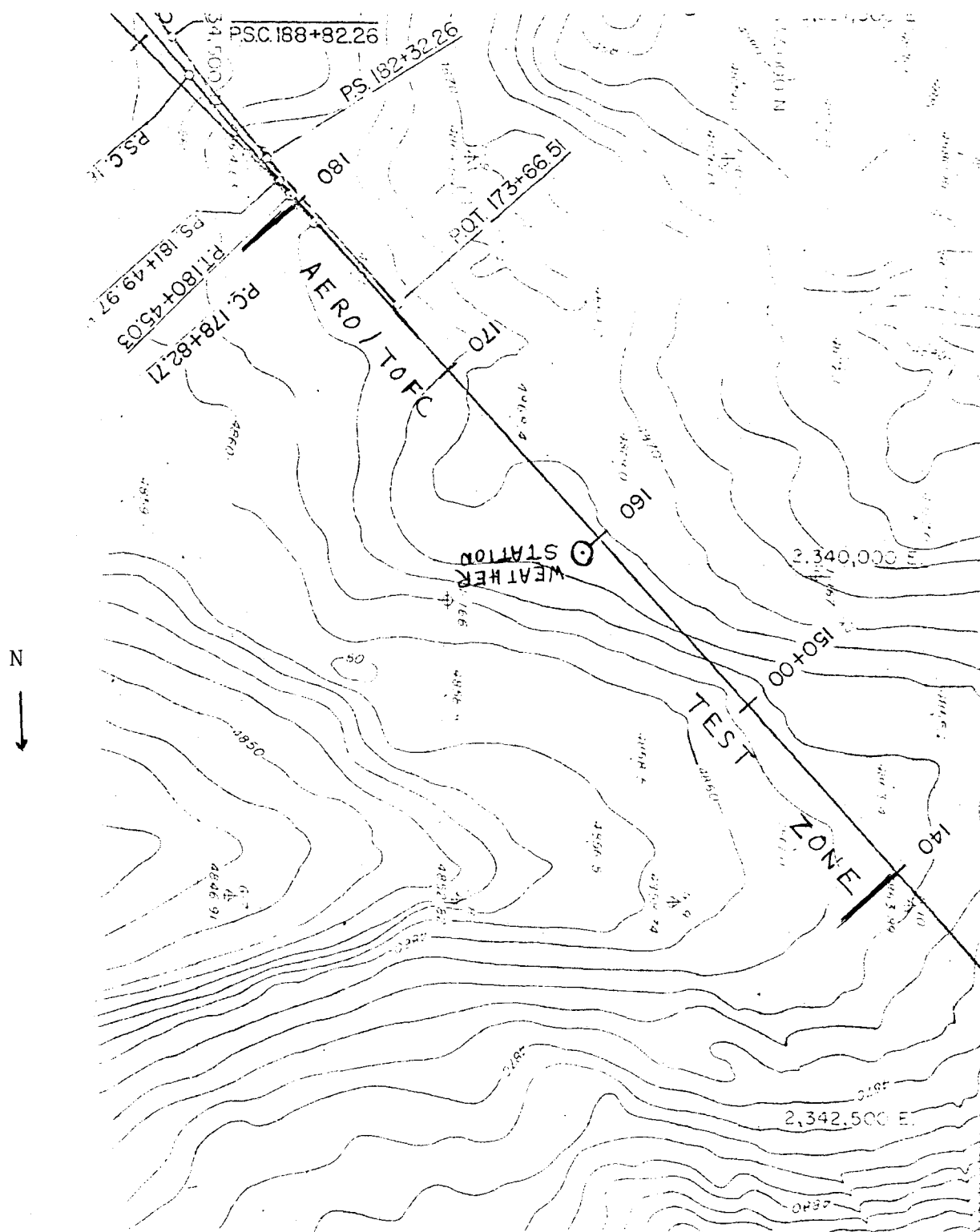


Figure 2-1(b). Topographical Map of AERO/TOFC Series II) Test Zone

completed in 1976 and has been maintained to meet FRA track classification 6. Two track surveys were conducted prior to the test using the Track Survey Device (TSD) on 19 September and 11 November 1977 to ensure that the track geometry was within the required standards. A post-test track survey was performed using the Plasser track geometry car on 21 December 1977.

The test zone was divided into five sections, each 800 feet long, by means of location detector targets. Data was processed separately over each subzone and also collectively over the entire zone. This enables one to compare results over parts of the test zone and also provides some redundancy in the case of a system malfunction during a portion of a test run. A wayside weather station was located at the middle of the test zone (Station 160) approximately 100 feet off the track as shown in Figure 2-1 (a). Figure 2-1(b) is a topographical map of the test area.

2.3 TEST CONSIST

The test article consisted of a locomotive, a buffer flat car, an instrumented flat car and a data collection car (T-5). Two consist configurations, designated 1 and 2, were tested. In configuration 1 the buffer car was loaded with two trailers and in configuration 2 it was empty (Figures 2-2 (a) and 2-2(b)). The consist entered the test zone with the locomotive leading in all tests.

The locomotive used for all tests was DOT-001 which is a General Electric U -30C built in June 1971. Figure 2-3 shows the locomotive in Configuration 1 with a wind speed and direction sensor fixed to its leading end. The buffer and instrumented flat cars were TTX 256054 and TTX 256034 respectively (Figures 2-4(a) and 2-4(b)). These rail cars are standard piggyback type built by Pullman Standard in April 1975. The

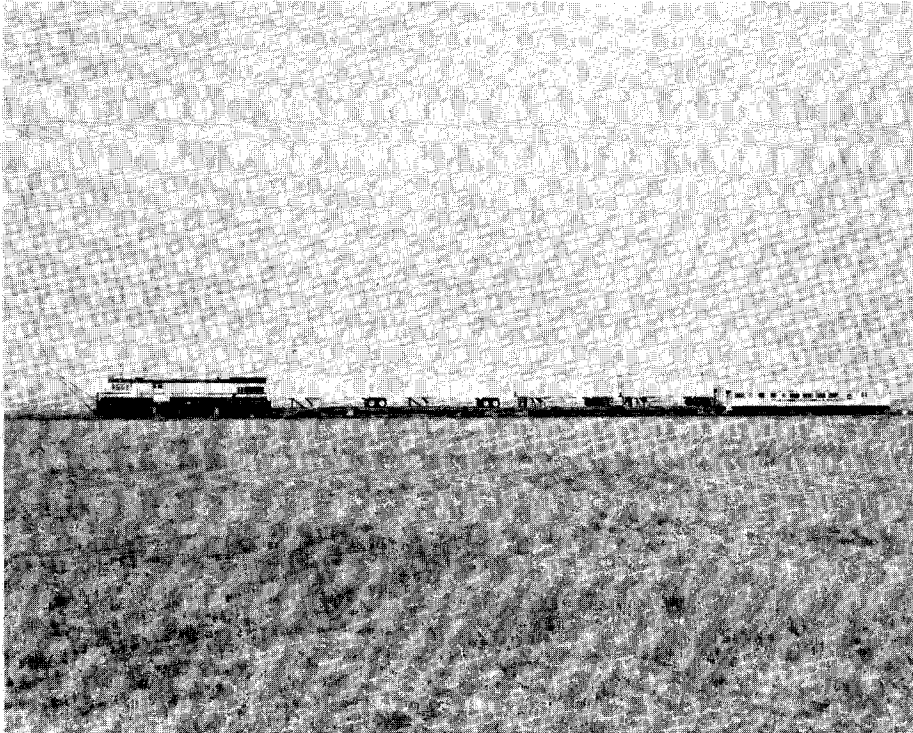


Figure 2-2(a). Test Consist - Configuration 1

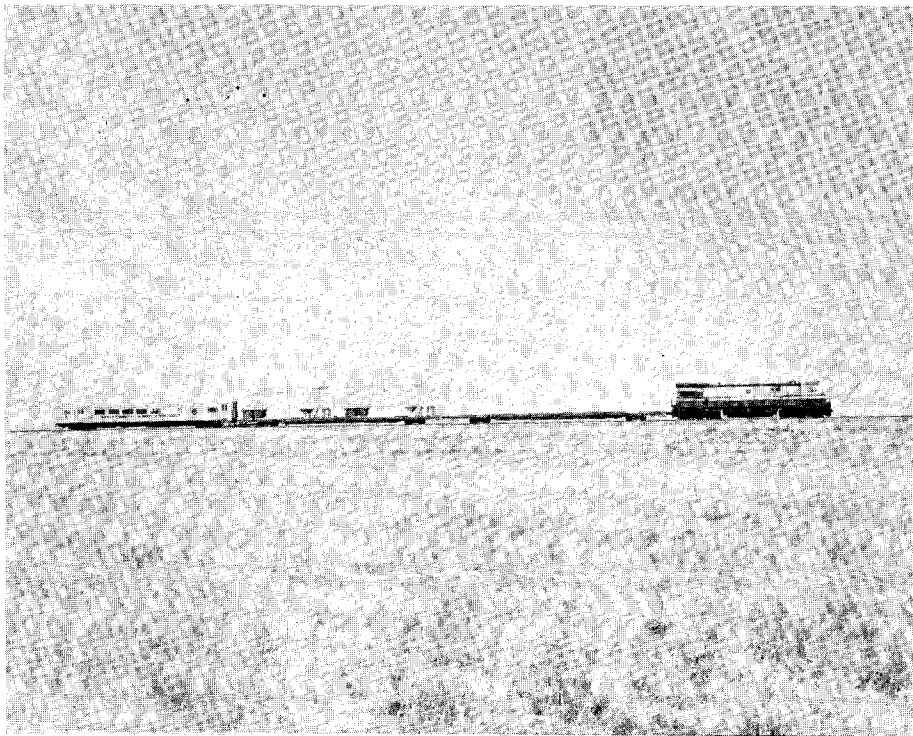


Figure 2-2(b). Test Consist - Configuration 2

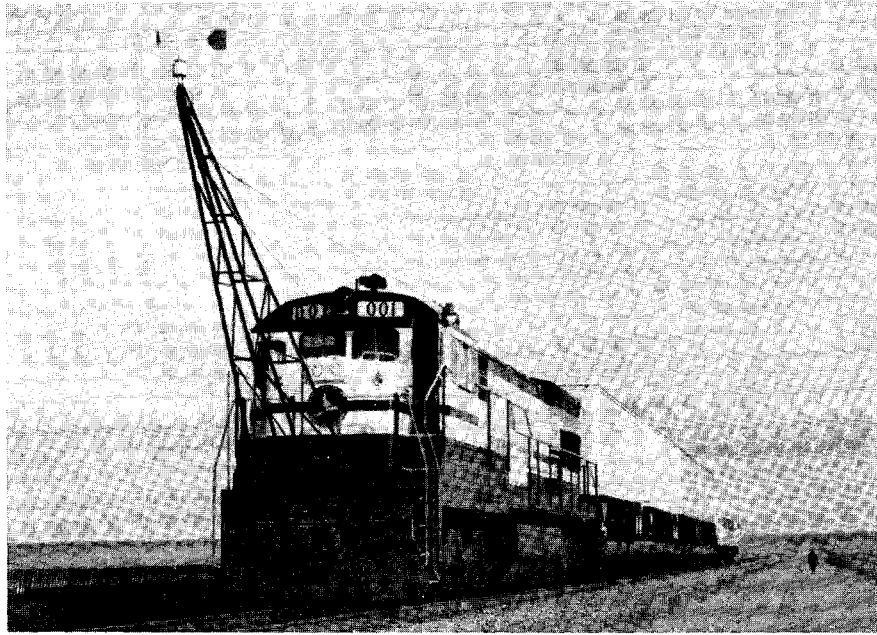


Figure 2-3 . DOT-001 Locomotive in Configuration 1

instrumented flat car was modified by introducing appropriate structural stiffeners to facilitate installation of the force-balance system described in Section 2.4.2.1. Details of these modifications are described in Appendix A. The TTX cars were oriented with their B-end leading during all test runs. The empty weight of each car is 67500 pounds.

The trucks on both cars were ASF Ride Control with 33-inch wheels and 6 x 11-inch roller bearings. These were specially modified for the AERO/TOFC (Series II) tests in order to minimize the forces due to lateral and vertical car-dynamics. For example, wheels on both cars were turned cylindrical, constant contact side bearings were installed and softer spring groups were used in the primary suspension. A TTC Test Specification (Reference 6) contains the details of the truck modifications.

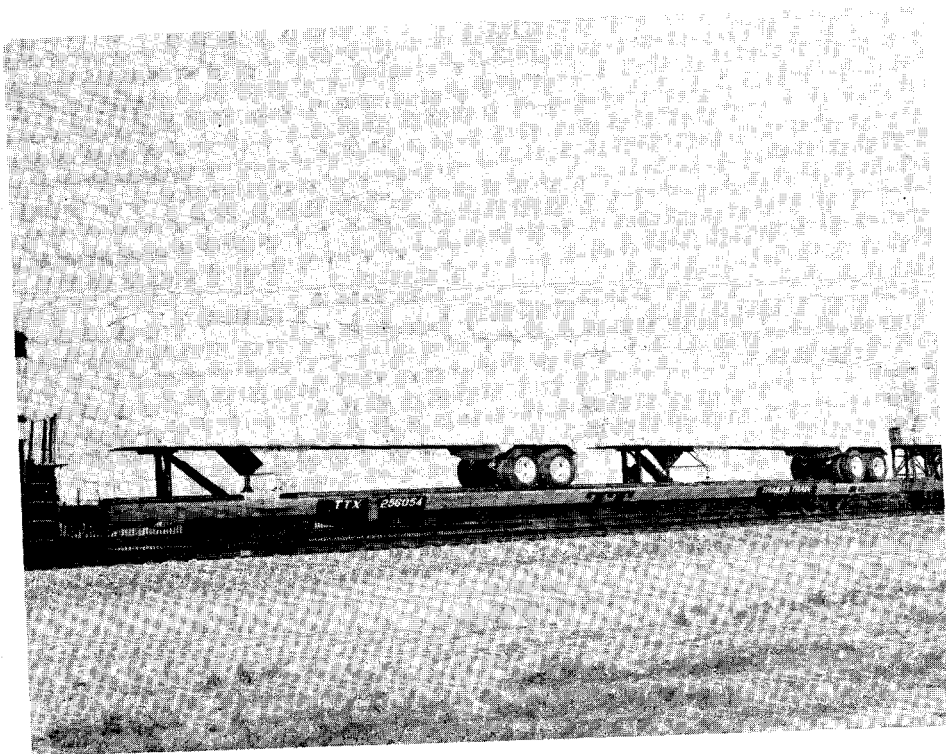


Figure 2-4(a). Buffer Flat Car

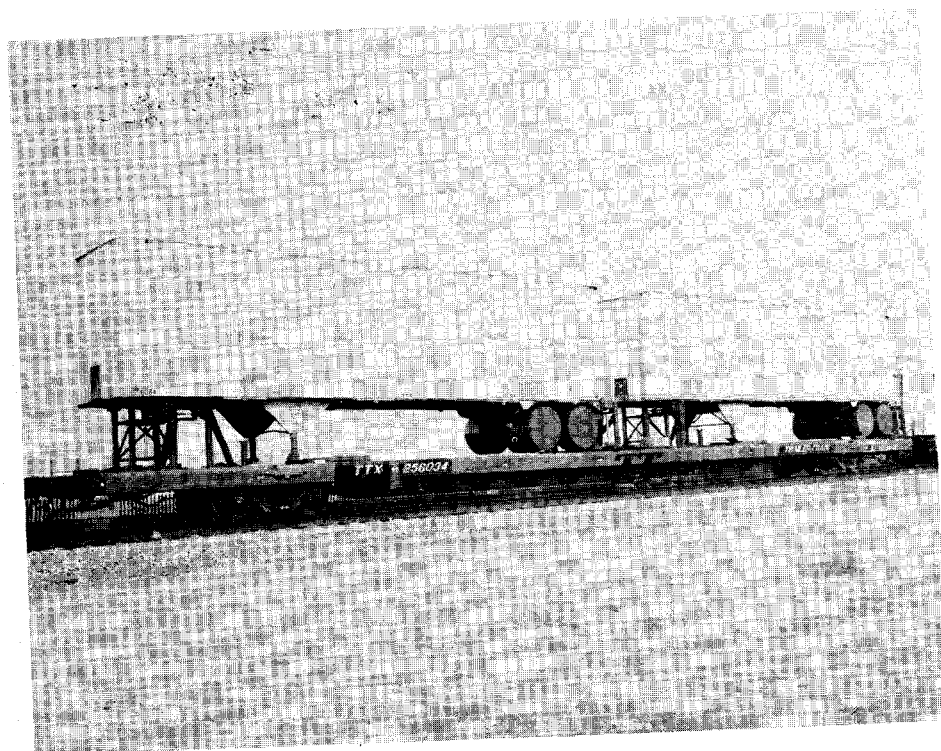


Figure 2-4(b). Instrumented Flat Car

The couplers at both ends of the instrumented car were 60-inch, swivel shank, E-type with standard draft gears. Strain-gage type load cells were employed to measure the compressive and tensile forces experienced by the couplers. Figure 2-5 shows the instrumented coupler between T-5 and the adjacent flat car.

The trailers carried on the buffer car were 40-foot long, vertical, exterior post-type manufactured by Trailmobile and were mounted in the conventional manner. Figure 2-6 is a close-up view of one trailer. The height of the trailer ceiling above the ground was 13 1/2 feet. Serial number 5974 was placed on the B-end and serial number 5987 on the A-end of the buffer rail car. Both trailers were empty for all tests (empty weight was 12400 pounds per each).

The trailers mounted on the instrumented flat car were also made by Trailmobile but were interior-post type with horizontally corrugated sides and four rounded vertical corners as shown in

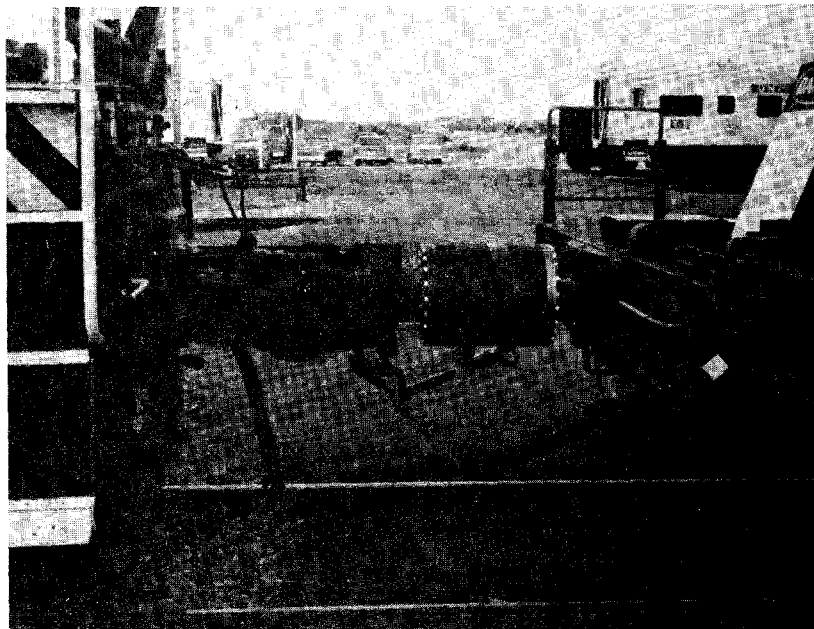


Figure 2-5. Instrumented Coupler (Trailing)

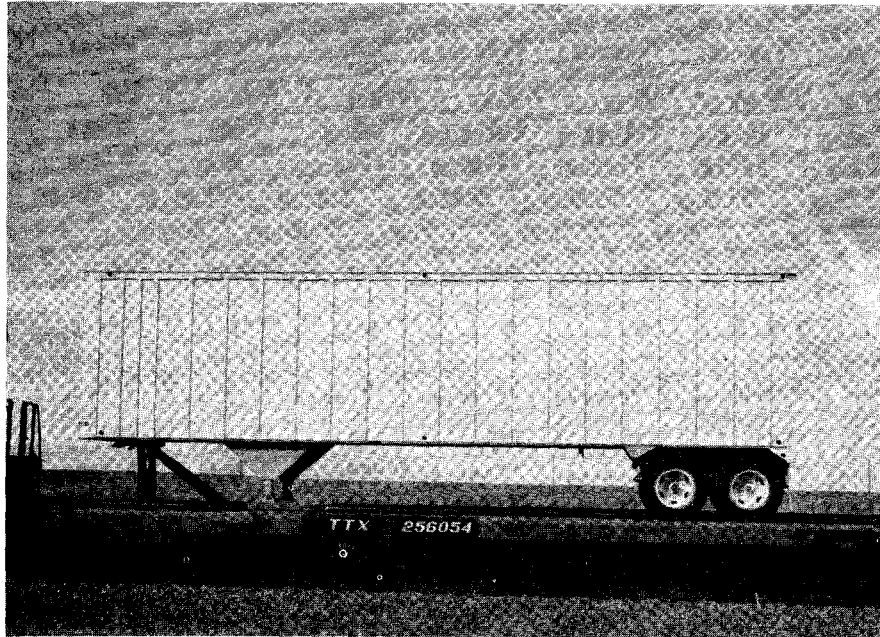


Figure 2-6. Trailer Mounted on Buffer Flat Car

Figure 2-7. These trailers were attached to a force-balance system (described in Section 2.4.2.1) which was mounted on the flat car. Serial number 6084 was located at the B-end and serial number 6078 at the A-end. Extensive modifications were introduced in order to reduce the deadweight of the trailers and to increase stiffness in torsion and bending. For instance, the original wheel bogies were removed and replaced by light sheet metal/wood structures with similar aerodynamic profile as shown in Figure 2-8. This reduced trailer weight from 12400 to 9850 pounds each. Tension cables were fastened diagonally across the trailer cross-section at four stations as shown by the photographs in Figure 2-9(a) and (b). The trailer doors were shut and joined together by a rigid bracing to permit transfer of shear force. These stiffening procedures raised the natural frequencies of the trailer, thereby promoting its decoupling from carbody dynamics. The trailers on the instrumented flat car were 78 inches apart. The spacing between the trailers on the A-end of the buffer car and B-end of the instrumented car was 115 inches.

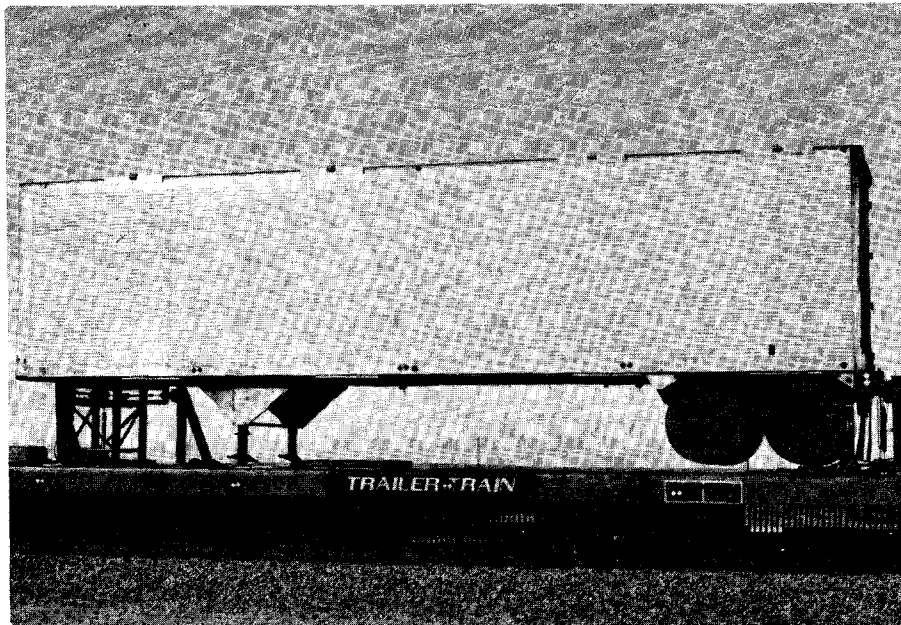


Figure 2-7. Trailer Mounted on Instrumented Flat Car

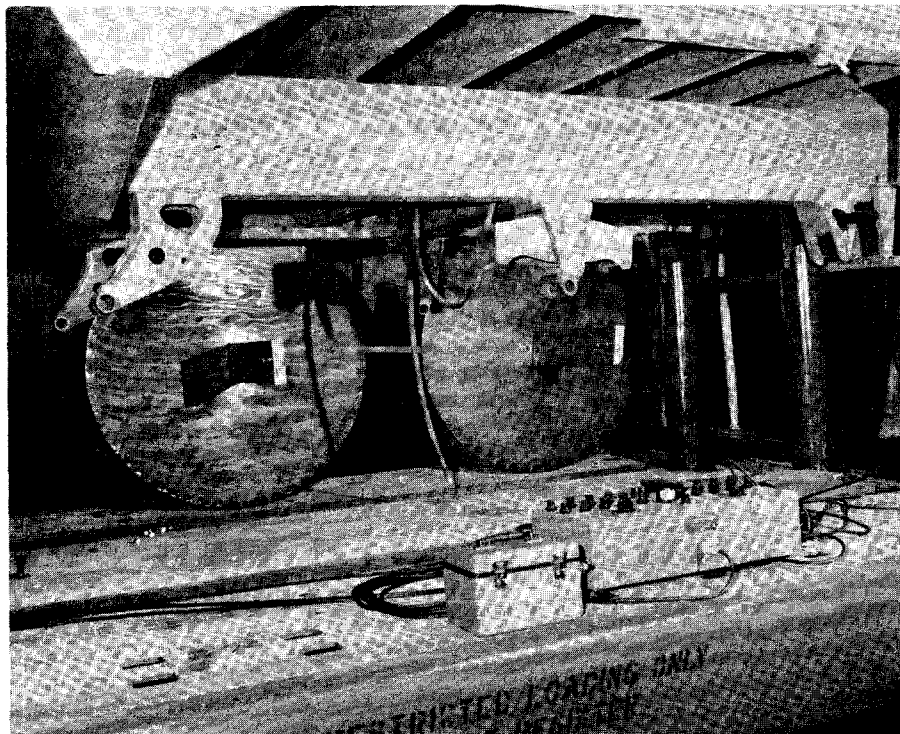


Figure 2-8. Wood/Sheet Metal Wheel Assembly Underneath Trailer

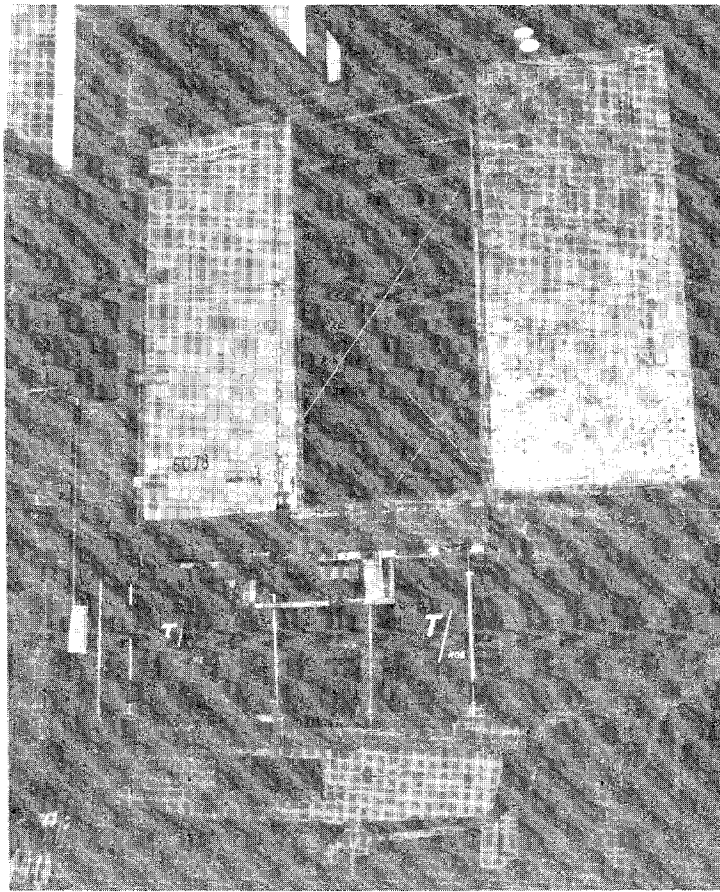


Figure 2-9(a). Cross-Bracing Inside Trailer - View A

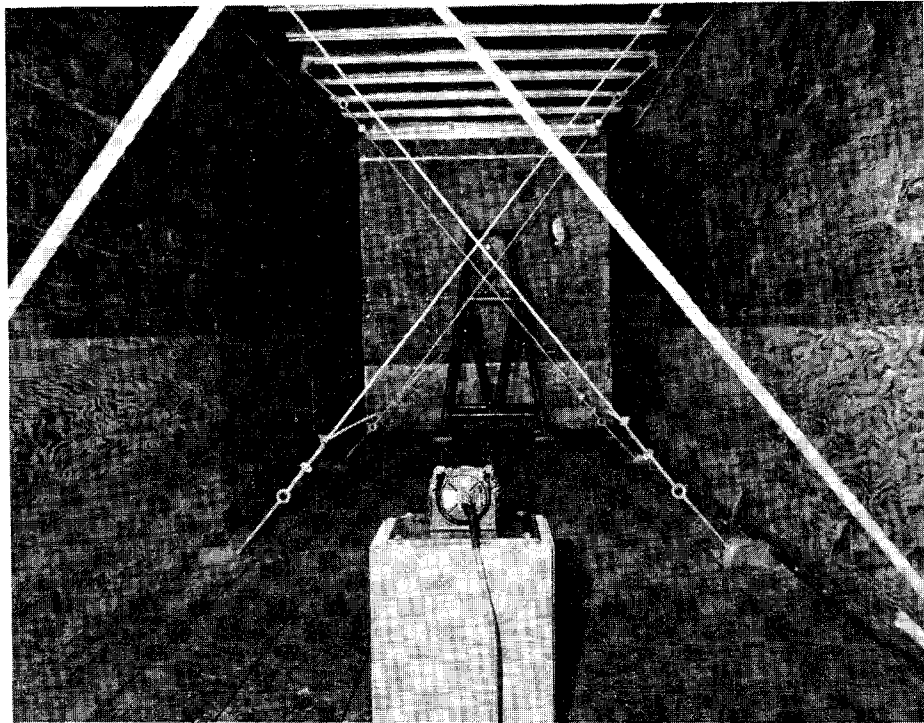


Figure 2-9(b). Cross-Bracing Inside Trailer - View B

The A-end trailer on the instrumented car was separated by 82 inches from data collection vehicle T-5.

The last member of the test consist (data collection vehicle T-5) is a standard ambulance car built by St. Louis Car Company in 1958. The car has been modified internally to house the data acquisition system which includes signal conditioning amplifiers, filters, an analog to digital converter, a Raytheon 704 mini-computer, a digital to analog converter, two tape drives, a strip chart recorder and a high speed line printer.

2.4 INSTRUMENTATION

2.4.1 General

The analysis procedures developed in Section 3.0 define the physical quantities that must be measured during the test in order to determine the aerodynamic forces and the rolling resistance. Accordingly, the instrumentation was designed principally to measure these quantities. In addition, it was desirable to have a certain degree of redundancy in some measurements which would enable data recovery in the event of an instrumentation malfunction. Thus, the instrumentation may be divided into two categories (primary and secondary) and these are described in the following paragraphs.

2.4.2 Primary Instrumentation

The physical parameters of major interest were the three components of aerodynamic force, i.e., longitudinal (drag), lateral (side force) and vertical (lift); tractive forces experienced by the leading and trailing couplers on the instrumented car; speed and direction of airflow as seen by the train; train speed and location in the test zone; and wayside wind conditions near the test track. The instrumentation employed to obtain these measurements is discussed in the following paragraphs.

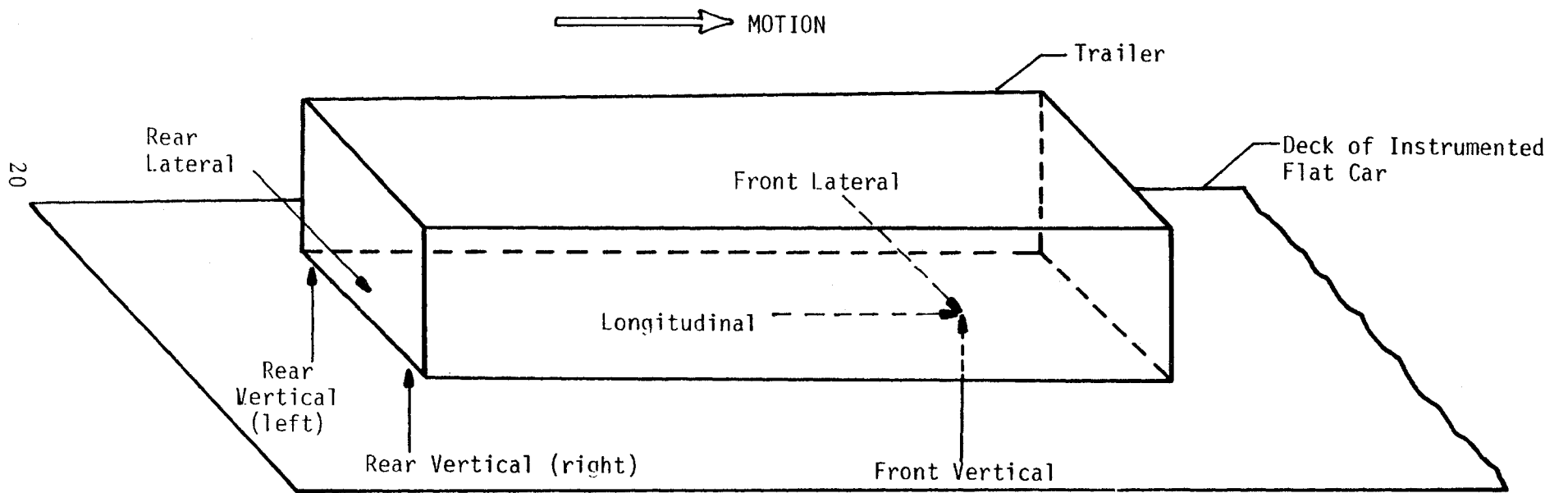


Figure 2-10. Flexure Arrangement - Schematic Diagram

2.4.2.1 Force Balance System

A mechanical force-balance system was used to determine the aerodynamic forces exerted on the trailers mounted on the instrumented flat car. The balance system supported each trailer at the kingpin and at two points at the rear of the trailer by means of flexures. The flexures are long slender columns designed to be strong in tension or compression but weak in bending for reasons which will be explained shortly. There were three mutually orthogonal flexures at the kingpin each with a load cell in series, to measure longitudinal, lateral and vertical forces. At the rear there were two vertical flexures and a flexure for lateral force measurement, all with a load cell in series. Figure 2-10 is a schematic of the flexure arrangement. The drag force on each trailer was measured by a single longitudinal load cell, the side force was obtained from the front and rear lateral load cells, the lift force was obtained from the three vertical load cells.

The force-balance system for the AERO/TOFC (Series II) tests was designed by Andrew G. Hammitt Associates (Reference 8) and fabricated, installed, aligned and calibrated by Brewer Engineering Laboratories (BEL) and is discussed in their report included herein as Appendix A.

The longitudinal and lateral flexures were attached to the deck of the flat car by massive support frames which were anchored to rigid members of the flat car structure. The vertical flexures were directly connected to the rigid structural components of the flat car. A schematic of a perspective view of the balance system is shown in Figure 2-11.

Figure 2-12(a) shows the flexure assembly at the kingpin with the front, lateral support frame at the left. Another view (Figure 2-12(b)) shows the support structure for the longitudinal flexure. The channel members around the longitudinal and lateral flexures form an overload protection system and carry the load in

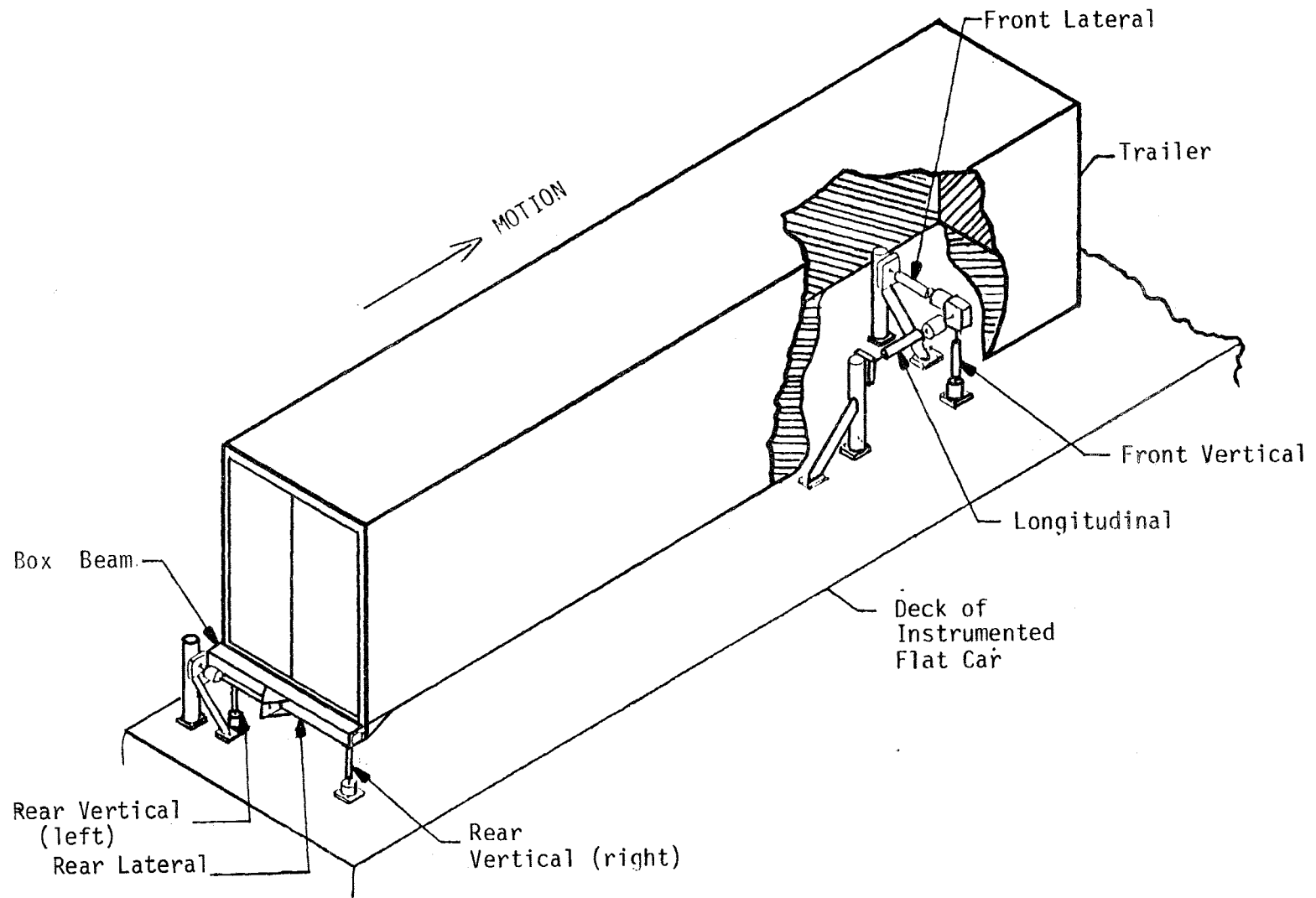


Figure 2-11. Schematic of Perspective View of Force-Balance System

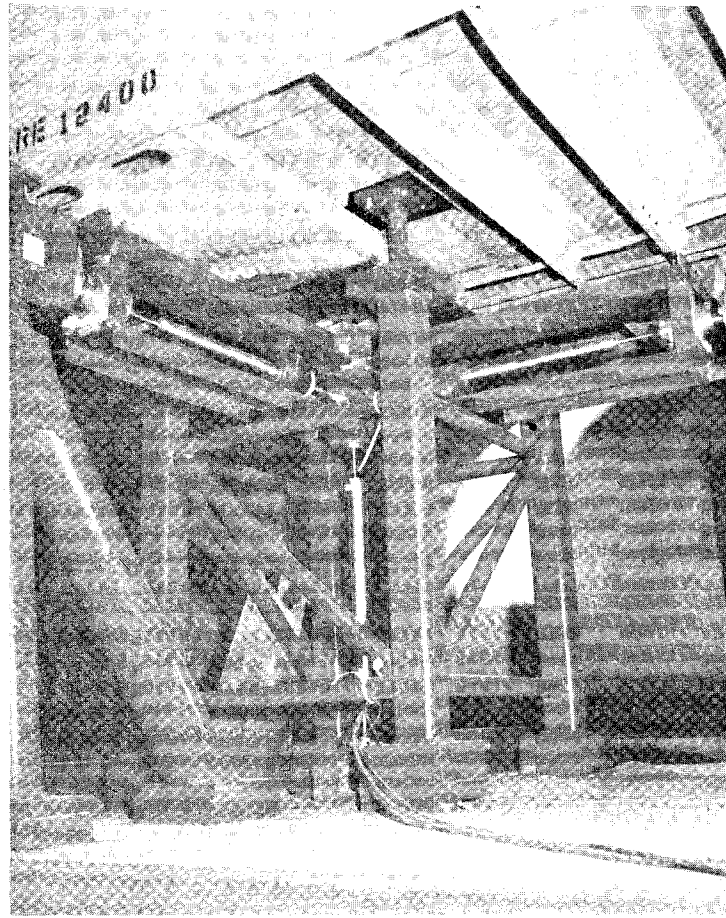


Figure 2-12(a). Flexure Assembly at Kingpin - View A

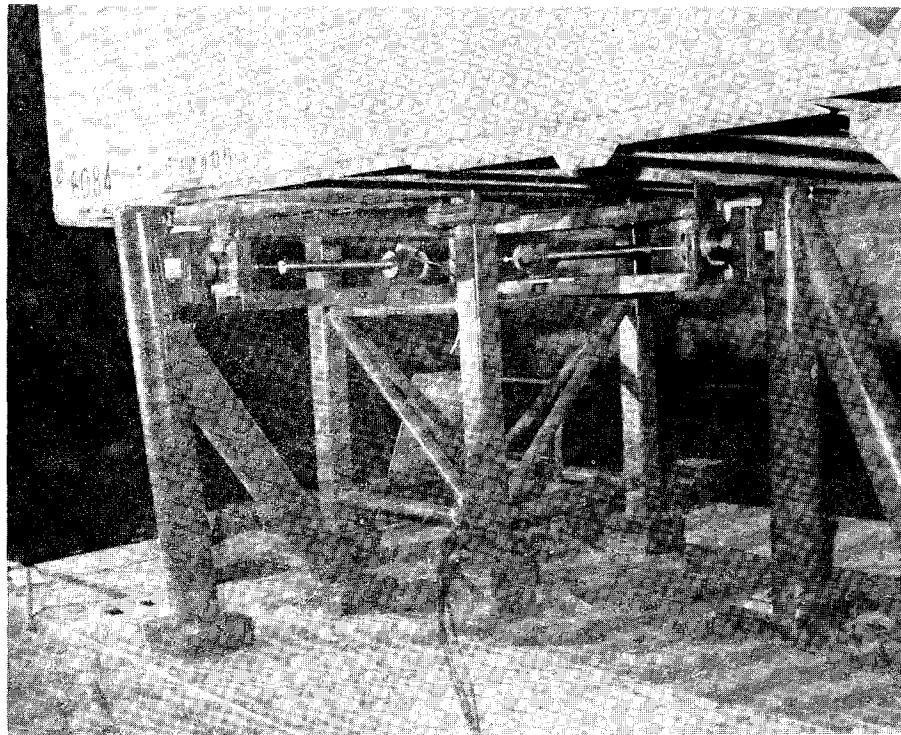


Figure 2-12(b). Flexure Assembly at Kingpin - View B

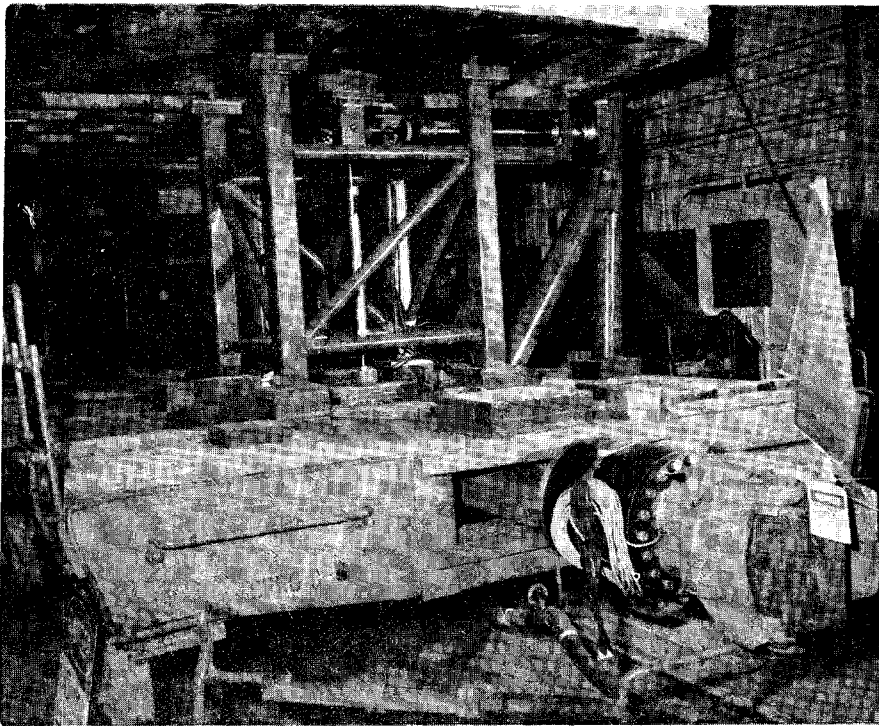


Figure 2-12(c). Flexure Assembly at Kingpin - View C

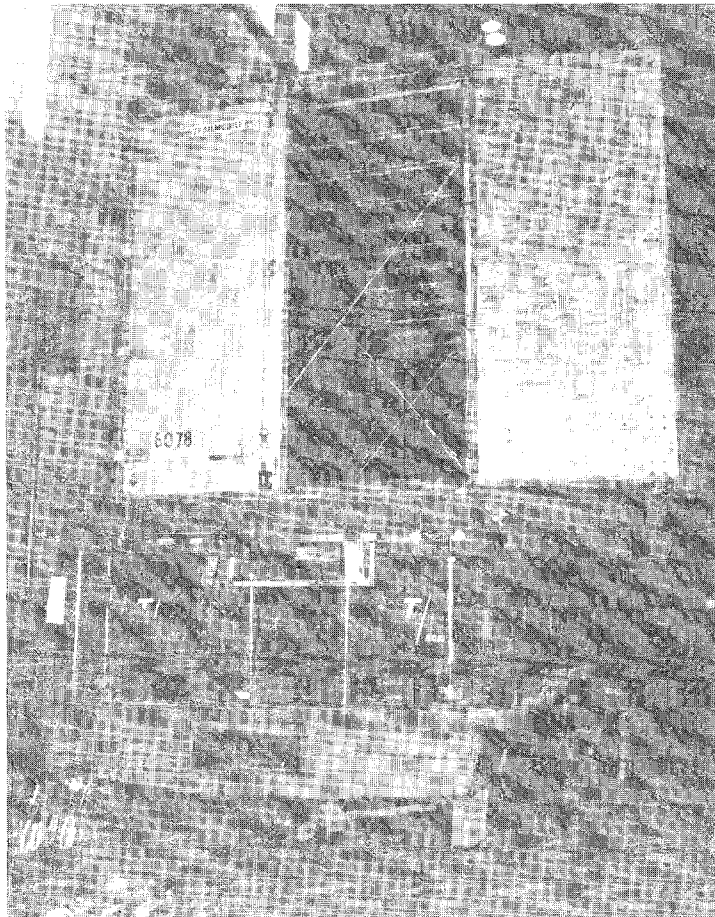


Figure 2-13(a). Rear Flexure Assembly - Vertical

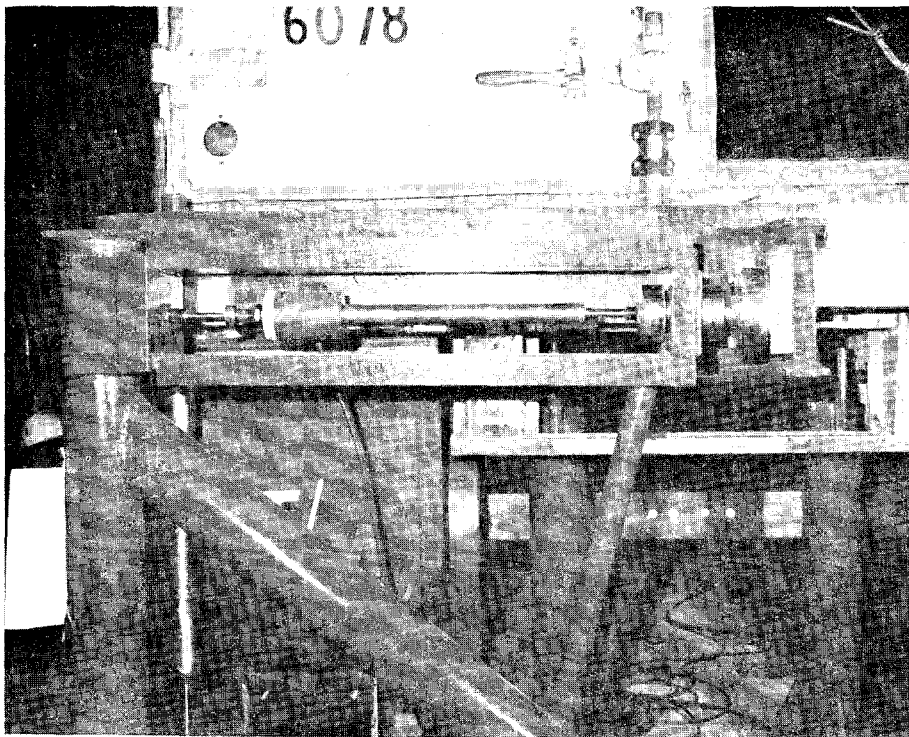


Figure 2-13(b). Rear Flexure Assembly - Lateral

the event of flexure failure. The four box-beams surrounding the vertical flexure are parts of a tower (which extends inside the trailer) used for applying jacking-loads to align the balance system. Figure 2-12(c) provides a clear view of this assembly and the portion inside the trailer is shown in (Figure 2-9) The load cells in series with the flexures are also shown in Figures 2-12(a,b and c). Figures 2-13 (a and b) show the rear flexure and load cell assemblies. The vertical flexures supporting the trailer at two points on a box beam (welded to the trailer) are shown in Figure 2-13(a) and a close-up of the rear lateral flexure with its overload protection system is shown in Figure 2-13(b).

The flexures employed in the force-balance system were specially constructed by BEL using a flexural pivot design which provided maximum axial stiffness and at the same time minimized lateral stiffness. Thus, the greatest portion of the applied load is registered by a load cell with its axis in the same direction as the external load. For example, drag force on the trailer is transferred almost entirely to the longitudinal flexure with a negligibly small portion being taken up by bending of the vertical flexures. This was important in the AERO/TOFC (Series II) tests because the aerodynamic forces to be measured were small relative to the inertial forces in the same environment. This flexural-pivot design also allowed the use of a simple and effective overload protection system. The details of flexure and overload stop designs are described in Appendix A.

The accuracy of a force-balance system depends on its alignment in the orthogonal planes. Any misalignment can result in an interaction between flexures in two different planes. For instance, if the vertical and lateral flexures are not perfectly perpendicular, a portion of trailer weight will be erroneously read as lateral force. Given the massive trailers (9850 pounds each), this can lead to significant values of spurious forces. In order

to minimize such interactions, each flexure was loaded independently along its axis and readings in the five other load cells were taken. Fine adjustments were then made to the flexure alignment to reduce the interaction-forces to an acceptable minimum (within two percent of applied load). Typically, this exercise can lead to a protracted trial and error process. However, the care exercised in flexure alignment at the time of installation made it a relatively simple matter to achieve the desired accuracy. The procedure described herein, called "jacking calibration" by BEL, is described in Appendix A.

Removable frames, shown in Figure 2-14(a) were used in jacking the right-rear vertical flexure to apply external loads. A closeup view (Figure 2-14(b) shows tubing for hydraulic fluid, a precision load cell to measure applied loads and a long column which serves as the load path.

The entire balance system was calibrated by applying known loads to the front and sides of both trailers at several locations. The load cell outputs were recorded and forces were summed in all three directions. A comparison was then made with the applied force. The results of this procedure, termed "wind load simulation jacking", are tabulated in Appendix A. The overall calibration accuracy achieved by the BEL-designed balance system was one percent and two percent of applied load for longitudinal and lateral load applications, respectively. Representative test set-ups for longitudinal and lateral force applications are illustrated in Figure 2-15 (a and b) respectively.

2.4.2.2 Instrumented Couplers

As mentioned earlier, couplers at the leading and trailing ends of the instrumented TTX car were used to measure tractive resistance of the rail car/trailer combination. The instrumented couplers for the AERO/TOFC (Series II) tests were designed, developed and fabricated by the TTC Instrumentation and Facility Service Groups. The basic measurement element in the couplers

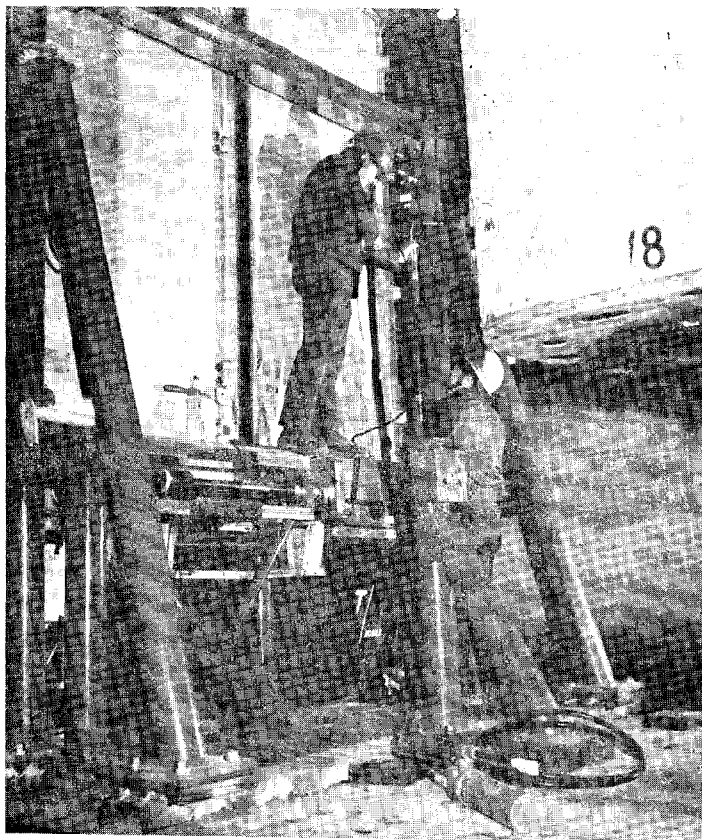


Figure 2-14(a). Jacking Calibration of Right-Rear, Vertical Flexure

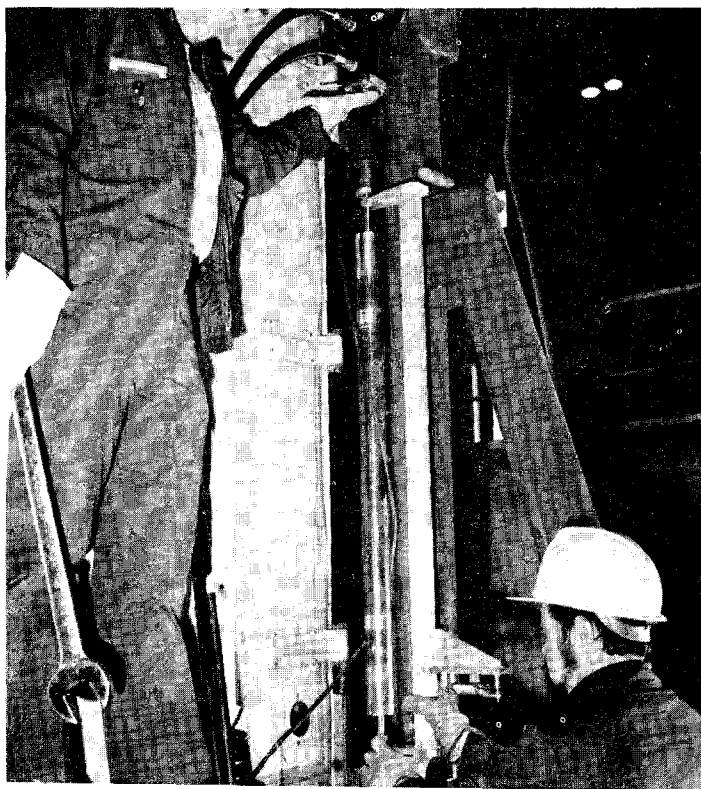


Figure 2-14(b). Jacking Calibration of Right-Rear, Vertical Flexure - Closeup View

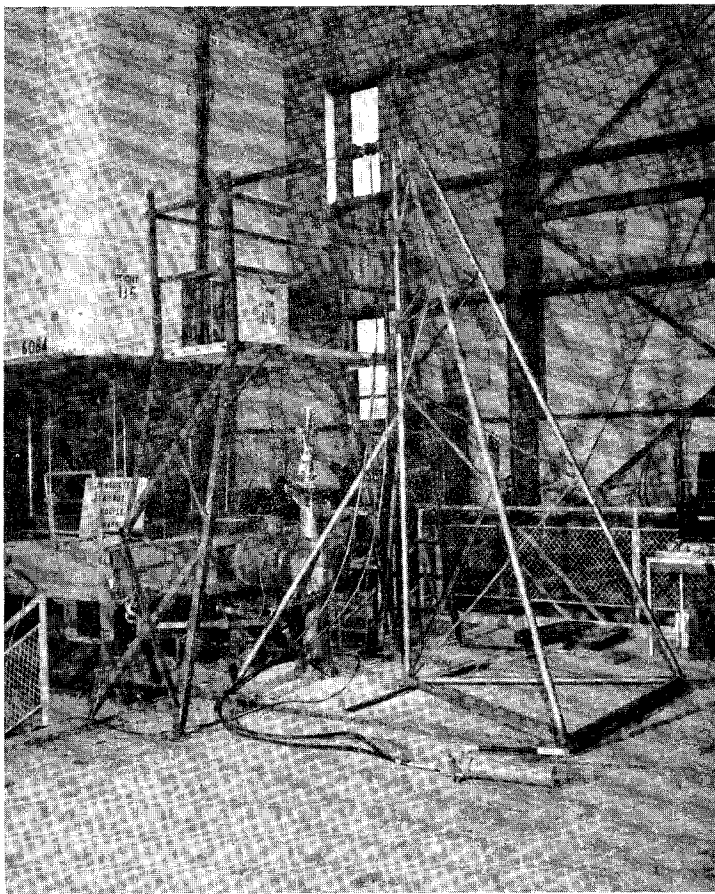


Figure 2-15(a). Longitudinal Wind Calibration

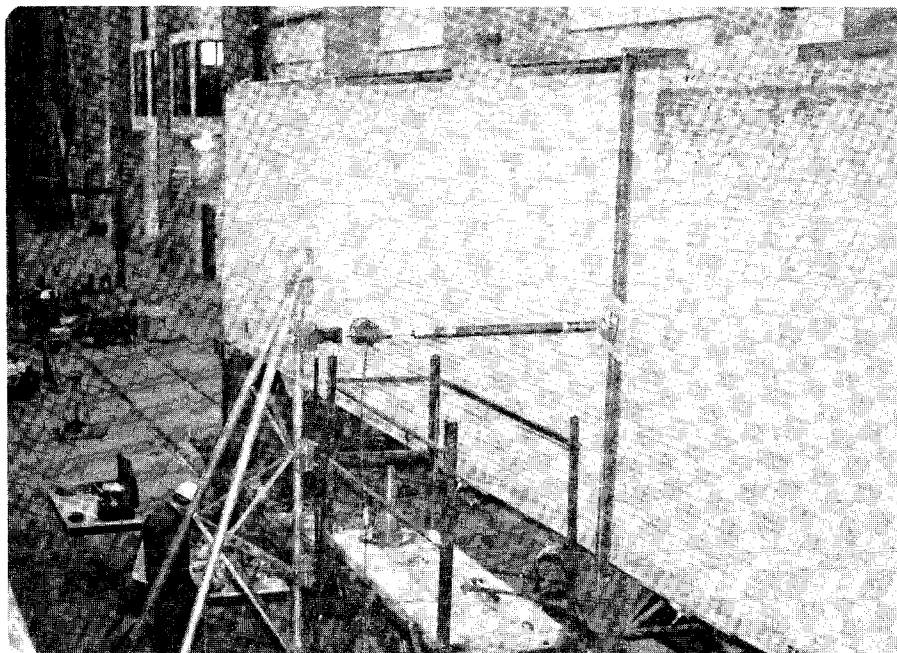


Figure 2-15(b). Lateral Wind Calibration

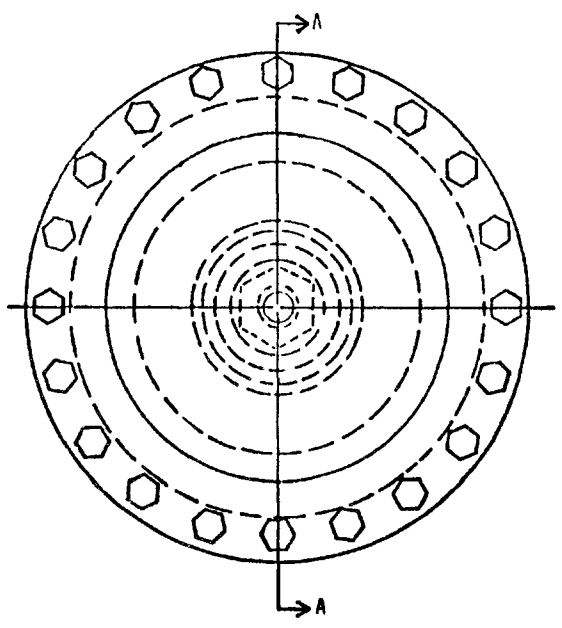
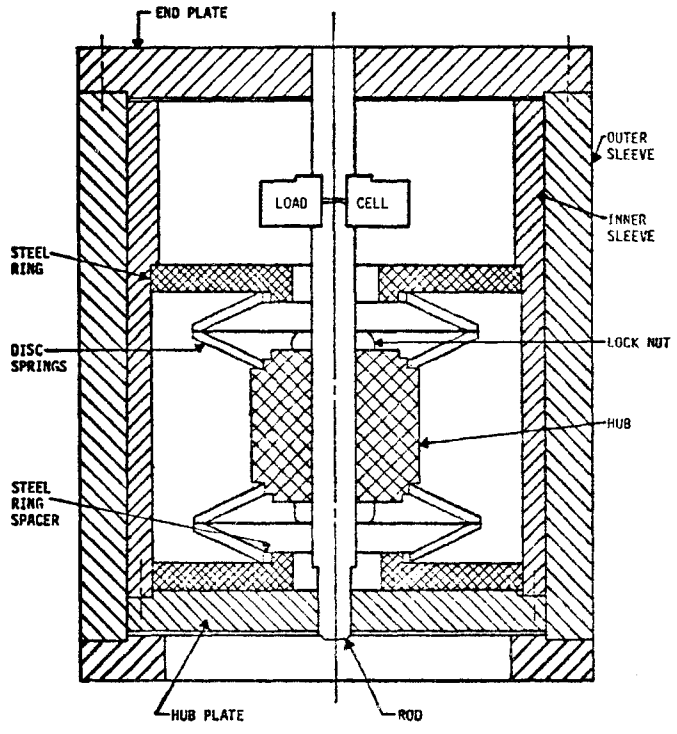
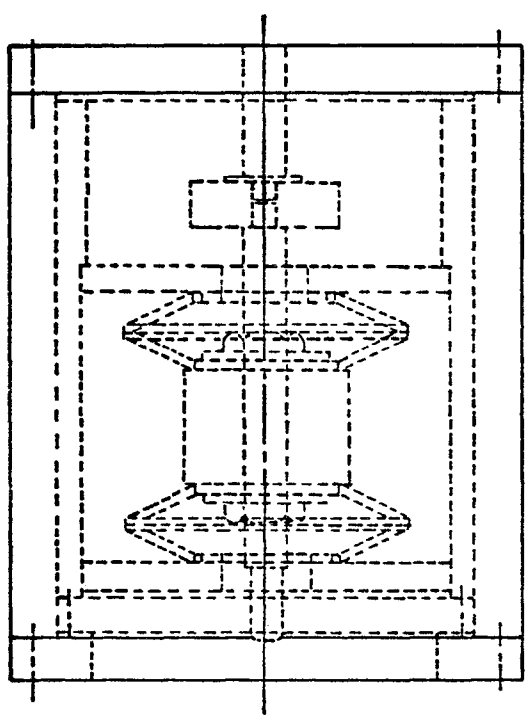


Figure 3-16. Engineering Drawing of Instrumented Coupler

is an Interface, shear-web load cell. The coupler design is shown in the engineering drawing in Figure 2-16 and an exploded view is shown in the photograph of Figure 2-17. The load cell is installed in series with the coupler shank and is protected by the outer cylindrical housing, which serves as a load-stop mechanism. The mechanical clearance is set so that maximum allowable deflection corresponds to one-half the maximum allowable overload capability of the load cell as specified by the manufacturer (Interface, Inc.). If the load exceeds the design limit, and therefore exceeds the allowable deflection, the load will be carried by the load-stop mechanism. In the coupler design, the load cell deflection is made less sensitive by adding Belleville spring washers (Figure 2-18). The springs allow the load path to deflect to a greater degree so that the load-stop adjustment is less sensitive. The purpose of the two concentric cylinders in the coupler design is to protect the load cell from large bending and torsional movements. The outer cylinder has grease fittings and the space between the cylinders is filled with grease to reduce friction between the cylinders.

The instrumented coupler underwent extensive calibration and the procedures and results are described in Appendix B. Although the coupler exhibited some hysteresis, an overall accuracy of five percent of applied load was achieved.

2.4.2.3 Onboard Wind Speed and Direction Indicator

The speed and direction of the wind relative to the train was measured by a probe mounted on a tower attached to the locomotive (Figure 2-3). The tower projected the instrument forward of and over the top of the locomotive by a distance equal to locomotive height. This was done to insure that the probe extended into

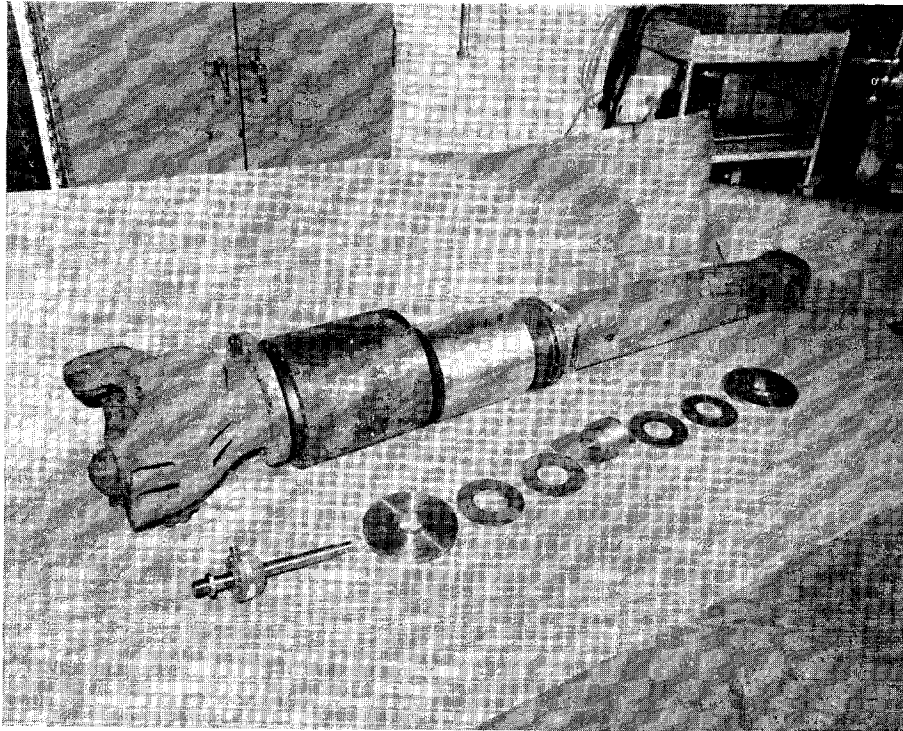


Figure 2-17. Exploded View of Instrumented Coupler

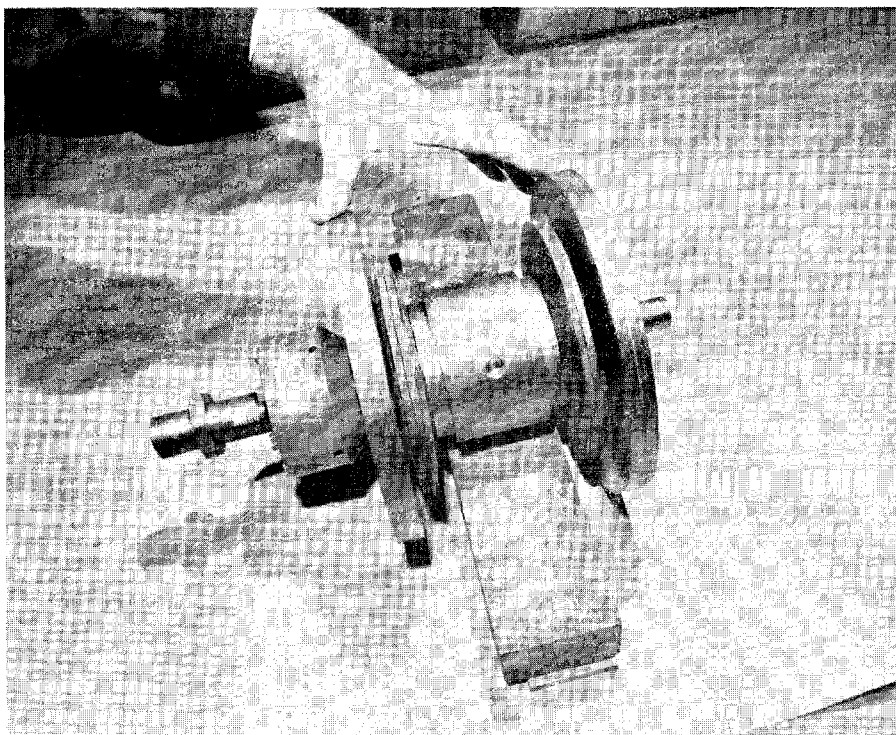


Figure 2-18. Spring Assembly Inside Barrel Housing of Instrumented Coupler

the free stream and was not affected by viscous effects near the locomotive body. The height of the speed and direction sensor above the rail was approximately 19.5 feet. This instrument was a Propvane model 8002, manufactured by R.M. Young, Inc. The speed measurement was obtained by a d-c generator driven by the propeller of the instrument and the instrument was capable of measuring wind speeds up to 200 mph. The direction sensor was a slide-wire potentiometer with a range of ± 171 degrees. The direction of the relative wind was defined such that head wind corresponded to zero degrees and tail wind to 180 degrees. The instrument was calibrated in a wind tunnel at the conclusion of the tests and was found to have a one-degree offset with respect to true wind direction for wind speeds in the range of 30 to 50 and 60 to 100 mph. The offset was zero for wind speed between 50 and 60 mph. The speed measurement accuracy of the speed and direction indicator was about one percent and the direction indicator was accurate to within one degree.

Figure 2-19 is a closeup view of the sensor mounted in the wind tunnel.

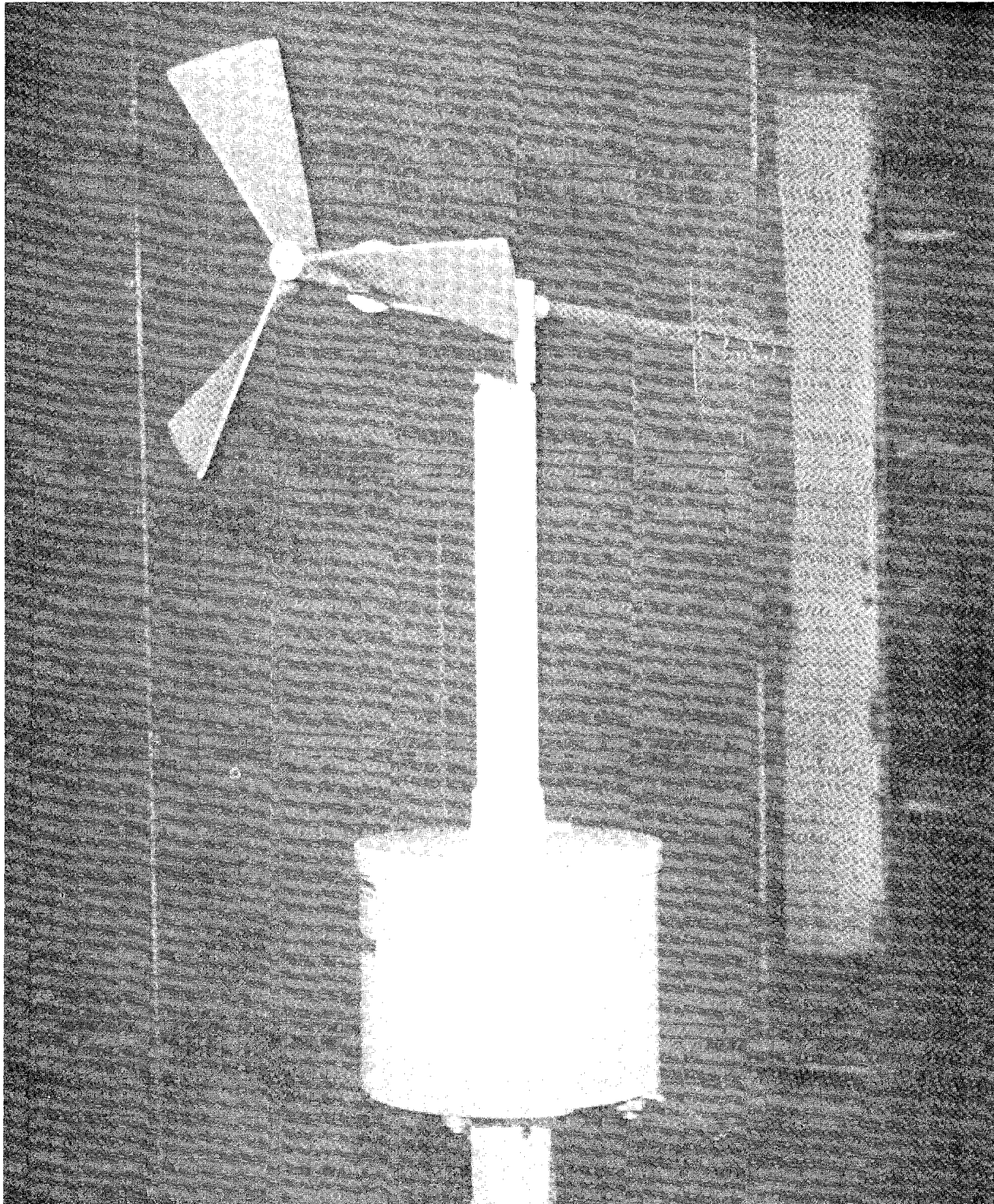


Figure 2-19 . On-Board Wind Speed and Direction Sensor Mounted In Wind Tunnel

2.4.2.4 Wayside Weather Station

The weather station was located at the center of the test zone (station 160 in Figure 2-1(a)) to determine the wind conditions near the test track. Figure 2-20(a) shows the weather station with the test consist in the background. Wind speed and direction were measured at two elevations, 20 feet and 8 feet above the top of the rail (as shown in Figure 2-20(b)) in order to detect wind shear. The direction sensor was aligned so that wind along the track in the direction of train motion corresponded to zero degrees and the wind in the opposite direction corresponded to 180 degrees. The sensors used at both locations were Climatronics Mark 3 units. The signals from these transducers were transmitted via FM telemetry to the data collection car for conditioning and recording on a digital tape. The range of the sensors was 0 to 50 mph and 0 to 540 degrees. Due to the drift problems associated with the FM transmission system, the overall

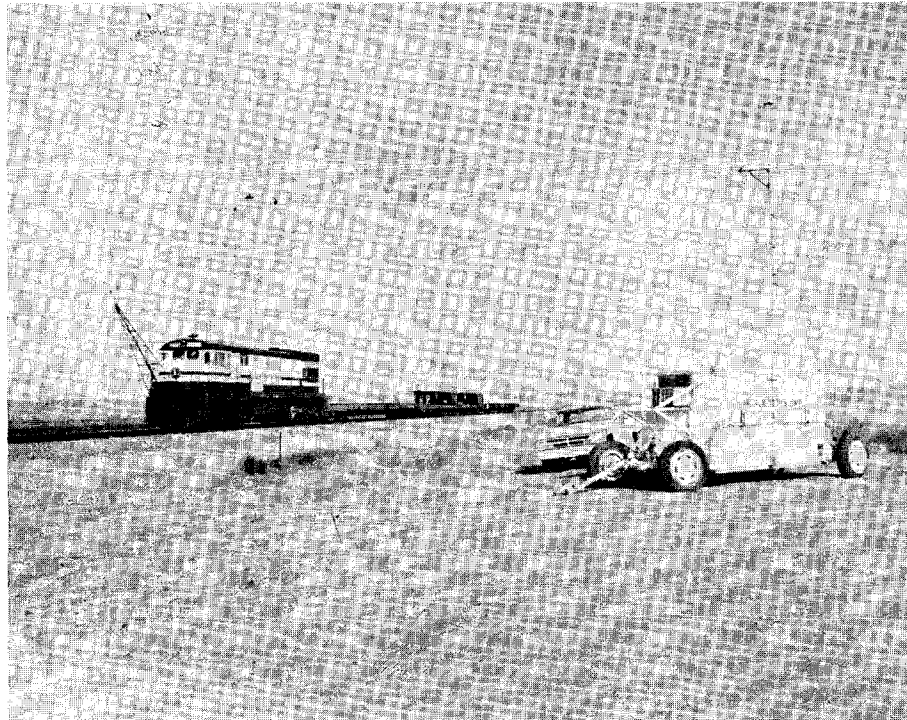


Figure 2-20(a). Wayside Weather Station with Test Consist In Background

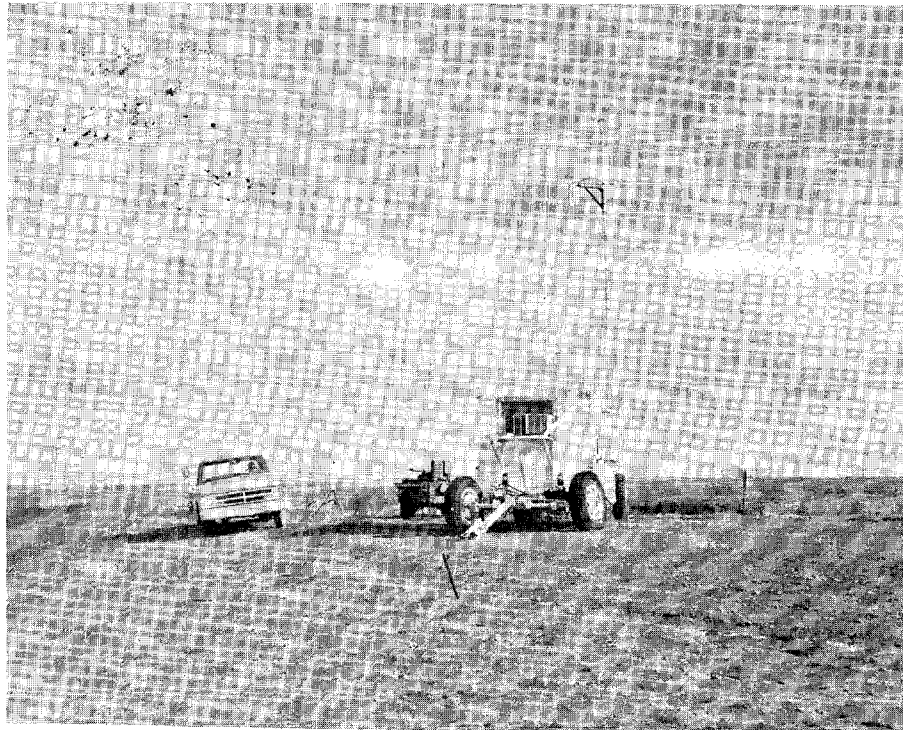


Figure 2-20 (b). Wayside Weather Station

long-term accuracy was two percent for both speed and direction. The wayside barometric pressure was measured by a Wallace and Tiernan, 8-inch dial barometer with a range of 30 inches of Hg. The temperature and relative humidity values were obtained from the equipment in the Office of Central Control (OCC) at TTC and radioed to T-5. Details of the weather station equipment and its calibration are contained in the TTC report included as Appendix B.

2.4.2.5 Train Speed Measurement

Train speed was measured by an optical tachometer attached to the No. 1 axle of T-5. The output of this transducer was conditioned by an ENSCO-built speed and distance processor mounted in the T-5 computer racks. The optical encoder built by Triumph-Ross had a range of 100 mph. The present method of aerodynamic force determination (described in Section 3.4) requires the measurement of instantaneous train speed at the beginning and

end of the test zone. In order to ensure the necessary accuracy of this measurement, some modifications were introduced in the speed and distance processor as described in Appendix C.

2.4.2.6 Automatic Location Detectors (ALD)

The location of the consist along the test track was determined by an eddy-current transducer detecting metal targets placed on the track. The sensor, built by Kaman Sciences, was attached to the center sill of the test vehicle at the longitudinal midpoint. The signal pulse was transmitted by multiconductor cables into T-5 for conditioning and transmission to the weather station.

2.4.3 Secondary Instrumentation

Physical quantities such as trailer and flat car accelerations, flat car roll and pitch displacements, and relative speed between T-5 and the instrumented flat car are also of interest as described in the next section. Therefore, in addition to the instrumentation described previously, the transducers described in the following paragraphs were used to obtain supplementary information.

2.4.3.1 Accelerometers

Two accelerometers were located at the center of gravity of each trailer to measure longitudinal and lateral accelerations. Accelerations were also measured at the center of the flat car in the longitudinal, lateral, and vertical directions. These measurements were made to estimate the magnitude of the inertial forces acting on the trailer-flat car system. The frequency response of the accelerometers was limited to 15 Hz in order to sense only the low-frequency, rigid body motions which are of interest. The lateral accelerometers were Stratham \pm 0.5g strain gage units and the vertical accelerometers were \pm 0.5g. The flat car accelerations were measured using a ride quality sensing unit which contained a Schaevitz fluid-damped accelerometer. The Stratham accelerometers were calibrated by the TTC Instrumentation Group and had an accuracy of 2.5 percent.

2.4.3.2 Displacement Transducer

Displacement transducers were located at the four corners of the instrumented flat car to measure displacements between the carbody and the truck side frame. The transducers used were ± 5 -inch, cableometric transducers made by ENSCO and were calibrated by inducing known displacements. The body of each string potentiometer was mounted to the side sill of the TTX car and the measurement string was attached to the truck side frame below the spring as shown in Figure 2-21. This resulted in use of long strings and hence the errors caused by lateral motion of the strings are small. The displacement data can be used to obtain roll and pitch of the flat car deck plate. As shown in Section 3.0, this motion can introduce components of trailer weight into longitudinal and lateral force-balance transducers and can contaminate drag and side-force data.

2.4.3.3 Vertical Gyroscope

The pitch and roll motions of the A-end trailer (serial number 6078) were measured by a gravity-oriented vertical reference gyro. This unit was manufactured by Bendix (Model 14168-2C) and had a range of ± 10 degrees with a frequency response of 10Hz. Figure 2-9 (b) shows the gyro mounted at the center of gravity of the trailer.

2.4.3.4 Relative Speed Transducer

Since the speed measurement unit was located on T-5 and all other measurements were made on the instrumented TTX car, it was necessary to obtain the absolute speed of the latter. A relative speed transducer built by ENSCO was installed between T-5 and the TTX car for this purpose. It was a d-c generator unit which produced a voltage output proportional to speed and was calibrated using a linear rate table.

2.4.4 Signal Conditioning, Filtering and Recording

The outputs of all measurement transducers were transmitted to T-5 via cables for conditioning. Signal conditioning amplifiers

having high thermal stability made by Dynamics, Inc., were used. The data channels were then fed in parallel into filters so that each channel was filtered at 1.0 Hz and 80.0 Hz by a programmable, four-pole, Bessel filter. The next step was to digitize each channel at 256 samples per second and record this information on a 1/2-inch, 800 bpi magnetic tape at a speed of 45 inches per second. The Gould strip-chart recorder on T-5 allowed the display of any six data channels in real time.

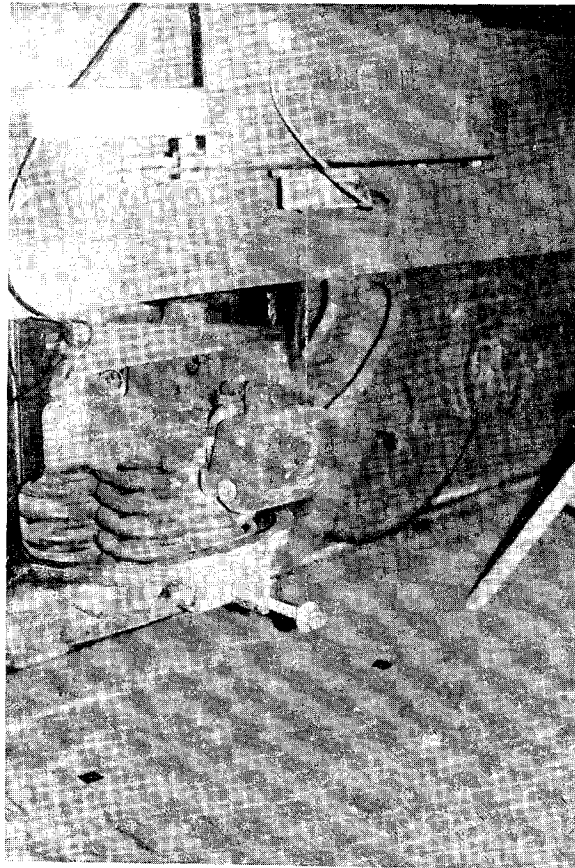


Figure 2-21. Displacement Transducer Between Flat Car and Truck Frame

2.4.5 List of Data Channels

Table 2-2 summarizes the data channel assignments for AERO/TOFC (Series II) instrumentation.

TABLE 2-2

AERO/TOFC (SERIES II) INSTRUMENTATION

PRIMARY INSTRUMENTATION

TRANSDUCER	LOCATION	CHANNEL No ***	SCALE FACTOR
F1 Load Cell	A Trailer Vertical Front	11 (71)	1 mv/lb
F2 Load Cell	A Trailer Lateral Front	12 (72)	2 mv/lb
F3 Load Cell	A Trailer Longitudinal Front	13 (73)	2 mv/lb
F4 Load Cell	A Trailer Vertical Rear Left	14 (74)	1 mv/lb
F5 Load Cell	A Trailer Vertical Rear Right	15 (75)	1 mv/lb
F6 Load Cell	A Trailer Lateral Rear	16 (76)	2 mv/lb
F7 Load Cell	B Trailer Vertical Front	17 (77)	1 mv/lb
F8 Load Cell	B Trailer Lateral Front	18 (78)	2 mv/lb
F9 Load Cell	B Trailer Longitudinal Front	19 (79)	2 mv/lb
F10 Load Cell	B Trailer Vertical Rear Left	20 (80)	1 mv/lb
F11 Load Cell	B Trailer Vertical Rear Right	21 (81)	1 mv/lb
F12 Load Cell	B Trailer Lateral Rear	22 (82)	2 mv/lb
F13 Load Cell	Leading Coupler Longitudinal	23 (83)	2 mv/lb
F14 Load Cell	Trailing Coupler Longitudinal	24 (84)	2 mv/lb
V Wind Speed	Locomotive Boom	29 (89)	0.05v/mpH
α Wind Direction	Locomotive Boom	30 (46)	2.0v/90°
W Wind Speed	Wayside 0*	31 (47)	40 mph/volt
β Wind Direction	Wayside 0*	32 (48)	216°/volt
W_1 Wind Speed	Wayside 1**	33 (49)	40 mph/volt
β_1 Wind Direction	Wayside 1**	34 (50)	216°/volt
Automatic Location Detector	Truck of TTX	1 (61)	None
Train Speed	Trailing Axle of T-5	2 (62)	10 mph/volt

*Measured 8 feet above top of rail

**Measured 19 1/2 feet above top of rail

***First number is arbitrary channel number. Number in parenthesis is T-5 channel number.

TABLE 2-2 (CONT)

AERO/TOFC (SERIES II) INSTRUMENTATION

SECONDARY INSTRUMENTATION

TRANSDUCER	LOCATION	CHANNEL NO ***	SCALE FACTOR
A1 Accelerometer	A Trailer Longitudinal	25 (85)	---
A2 Accelerometer	A Trailer Lateral	26 (86)	20 volt/g
A3 Accelerometer	B Trailer Longitudinal	27 (87)	---
A4 Accelerometer	B Trailer Lateral	28 (88)	20 volt/g
A5 Longitudinal Ride Quality	Center Deck TTX	9 (69)	10 volt/g
A6 Lateral Ride Quality	Center Deck TTX	10 (70)	10 volt/g
A7 Vertical Ride Quality	Center Deck TTX	8 (68)	10 volt/g
D1 Displacement Transducer	A End Truck TTX Right Side	4 (64)	1 volt/inch
D2 Displacement Transducer	A End Truck TTX Left Side	5 (65)	1 volt/inch
D3 Displacement Transducer	B End Truck TTX Right Side	6 (66)	1 volt/inch
D4 Displacement Transducer	B End Truck TTX Left Side	7 (67)	1 volt/inch
G1 Gyro Pitch	A Trailer	37 (53)	0.47°/volt
G2 Gyro Roll	A Trailer	38 (54)	0.497°/volt
U Rel. TTX Speed	Between TTX & T-5	3 (63)	2.43 volt/ mph
t Time Code	Wayside	35 (51)	None

2.5 TEST PROCEDURES

Tests were performed by operating the test consist over the test zone at constant speeds, and under different wind conditions for each system configuration. Table 2-3 contains the test matrix.

TABLE 2-3

TEST MATRIX

TEST SERIES	CONFIGURATION	TRAIN SPEEDS MPH	WIND CONDITIONS (MPH)*
1	1	50, 70, 90	0 - 6
2	1	50, 70, 90	4 - 16
3	1	50, 70, 90	2 - 11
4	1	50, 70, 90	0 - 13
5	1	50, 70, 90	10 - 19
6	2	50, 70, 90	8 - 13
7	2	50, 70, 90	0 - 5
8	2	50, 70, 90	7 - 12
9	2	50, 70, 90	7 - 9

*Wind conditions prevailing during the test period were obtained from Table 2-1

The actual test runs were preceded by several pre-test runs to checkout the system. Proper operation of all transducers and associated instrumentation, under both static and dynamic conditions, was verified first. A long-term, thermal-stability check was performed on the electronic system before beginning the tests. The alignment and calibration of the force-balance system was performed before, after and once during the test period. The instrumentation was also electrically calibrated and scale factors were checked. All calibrations were conducted inside the Central Services Building (CSB) when the trailers were not exposed to external wind conditions.

The schedule of activities on a typical test day was as follows: All transducer zeroes were recorded prior to each test series. The location of the instrumented TTX car on the track inside the CSB was marked at this time. The test consist was then moved to the north end of the test zone. A surveillance and conditioning run was made over the test track before the start of actual test runs. This was a low-speed (20-30 mph) run over the entire test track to determine the general condition of the track and to resolve any potential hazards. These and other safety precautions were handled in accordance with the TTC Operational Test Procedures (Reference 7).

At the completion of the surveillance run, the consist was backed to about 1000 feet north of the test zone entry point. During this move a stop was made at the weather station for calibration of wind instruments. The test run was then started. The train first came out of a curve and accelerated downhill before entering the test zone. The DOT-001 locomotive undergoes a speed transition around 45 mph subjecting the test consist to a rather sharp jerk. The locomotive engineer was instructed to overcome this transition quickly so as to avoid damage to the force-balance system. The train speed was maintained as steady as possible by an appropriate coordination of throttle setting and brakes by the engineer. Data was recorded from the force-

balance transducers, the couplers, the accelerometers, and the supplementary instrumentation as the consist traversed the test zone. Weather station data was received by the data acquisition system via telemetry during this period.

After leaving the test zone, the consist was gradually decelerated to a stop using the air brakes. Throughout the test program, the consist speed was regulated so that there was no severe lurching at any time, including start-up and braking. Immediately following a run, the weather conditions measured at the Office of Central Control (OCC) were radioed to T-5 by a weather station operator for a post-test comparison with the telemetered data. This completed the operational procedures for a test run. The consist was then backed to its starting point to initiate another run.

When three passes through the test zone (at the same speed) were completed, the test data was processed by the computer onboard T-5. The resulting aerodynamic forces, fore area (defined in Section 4-2) and wind directions were checked for repeatability from test run to test run. A spot comparison was also made with the wind tunnel test results (Reference 1 and 2) to determine whether the values of forces and force areas were reasonable. Some of the other indicators used to evaluate the quality of the recorded data were: (1) distance traveled by the consist based on the number of data samples collected, (2) relative magnitudes of average, initial, and final train speeds, (3) comparison of onboard relative wind speed and direction measurement with calculations based on vector subtraction of average train speed from wayside wind vector, and (4) other factors indicative of validity of data, e.g., signs of forces on the A and B trailers, etc. Upon establishing that the test runs at one speed yielded meaningful data, a decision was made to conduct tests at another speed.

The test consist was brought back to the CSB at the end of a test series and the instrumented TTX car was located exactly at the same location as that prior to the test series. Transducer readings were recorded and compared with the earlier readings taken before the test series in order to insure that significant zero shifts did not occur. This concluded the test day. The power supplies for the instrumentation and the electronics were left on for the entire period in which the AERO/TOFC (Series II) tests were conducted.

3.0 DEVELOPMENT OF DATA ANALYSIS PROCEDURES AND ERROR ESTIMATION

3.1 GENERAL

This section includes a critical examination of the methods for determining aerodynamic forces (mainly drag and side forces) using a mechanical balance system. The possible sources of error in the system are identified and their magnitudes are estimated.

The force-balance system has been described in Section 2.4.2.1. As shown in Figure 2-10, each trailer is supported vertically by three flexures (one in the front and two at the rear), restrained longitudinally by one flexure (in the front) and arrested laterally by two flexures (one forward and one aft).

A load cell is connected to each flexure and the outputs of these cells are related to the external forces and moments acting on the trailer. These external forces include aerodynamic forces and components of trailer weight due to its orientation in the earth's gravitational field. Thus, it should be possible, in principle, to determine the aerodynamic forces from load cell responses and trailer orientation. In practice, however, two additional forces appear due to (1) longitudinal and lateral accelerations of the carbody on which the trailer is mounted and (2) centripetal accelerations due to track curvature. These accelerations are small in magnitude and should average out to zero over the test zone. Any net non-zero accelerations, however, can lead to significant inertial forces due to the large mass of the trailer. These considerations show that the AERO/TOFC (Series II) test required determination of aerodynamic forces in the presence of contaminating gravitational and inertial forces. An estimation of orders of magnitudes of various forces of interest is presented in the next section.

3.2 MAGNITUDES OF FORCES OF INTEREST

3.2.1 Aerodynamic Forces

The flow of air about an object causes a certain pressure distribution to be established on its surface. When the pressure is integrated over the entire body surface, it can be translated into a single force vector (called aerodynamic force), and a moment vector acting through the center of gravity of the body. In the present context, the component of aerodynamic force in the direction of train motion is defined as drag force and a perpendicular component in the local horizontal plane is termed side force. Lift is the remaining component, orthogonal to the drag and side forces, and to the plane of the ground. The moment vector has three components which represent rotational motions about the three orthogonal directions mentioned earlier.

The drag force offers resistance to motion which increases with train speed and is of major interest in the AERO/TOFC (Series II) work. Typical variations of the drag and side forces with the speed of the air stream relative to the train are shown in Figures 3-1(a) and 3-1(b). The force values at 90 mph were obtained from the wind tunnel/model tests described in Reference 8 and the values at other speeds are based on an ideal square law variation, i.e.,

$$\text{Aerodynamic Force} = KV_{\text{rel}}^2 \quad (3.1)$$

where K is a constant of proportionality and V_{rel} is the relative wind speed.

3.2.2 Gravitational Forces

The roll and pitch motions of the trailer (defined precisely in Section 3.3) add components of trailer weight to the longitudinal and lateral load cells as shown in Figure 3-2. Such

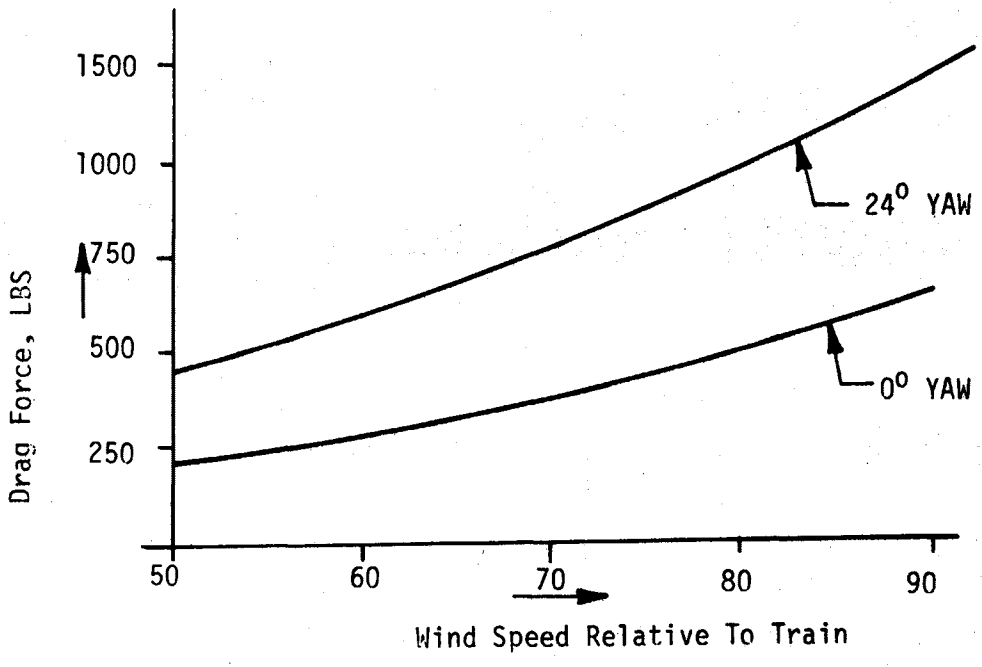


Figure 3-1a. Typical Drag Force Variation with Speed.

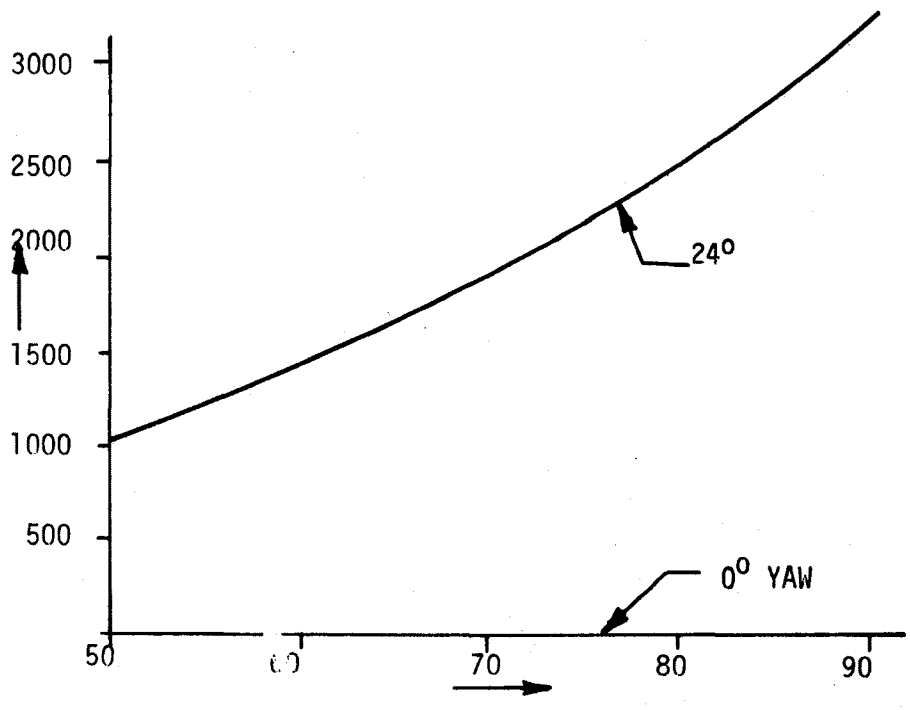


Figure 3-1b. Typical Side Force Variation with Speed

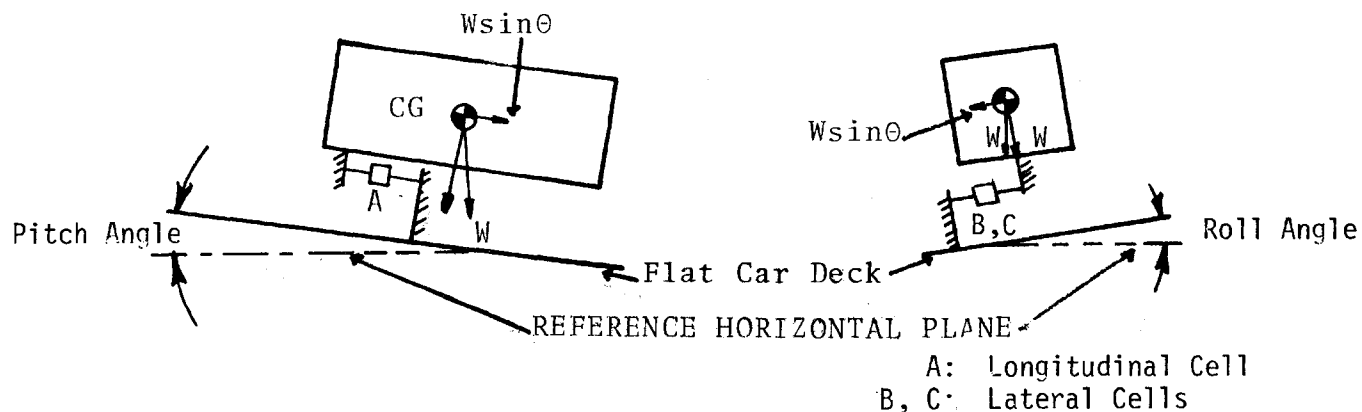


Figure 3-2. Contribution of Trailer Weight to Longitudinal and Lateral Load Cells

motions may occur as a result of topographical changes under the track or from changes in orientation of the flatcar on its suspension.

The component of trailer weight (9850 pounds) is plotted against the angle of tilt in Figure 3-3. This relationship is linear for the small angles likely to be encountered in practice.

3.2.3 Inertial Forces

These forces are due to linear and centripetal accelerations which are described below.

3.2.3.1 Linear Accelerations

Representative values for lateral and longitudinal acceleration as recommended by Reference 8 for the AERO/TOFC (Series II) experimental design were:

Lateral acceleration	0.35 g
Longitudinal acceleration	0.33 g

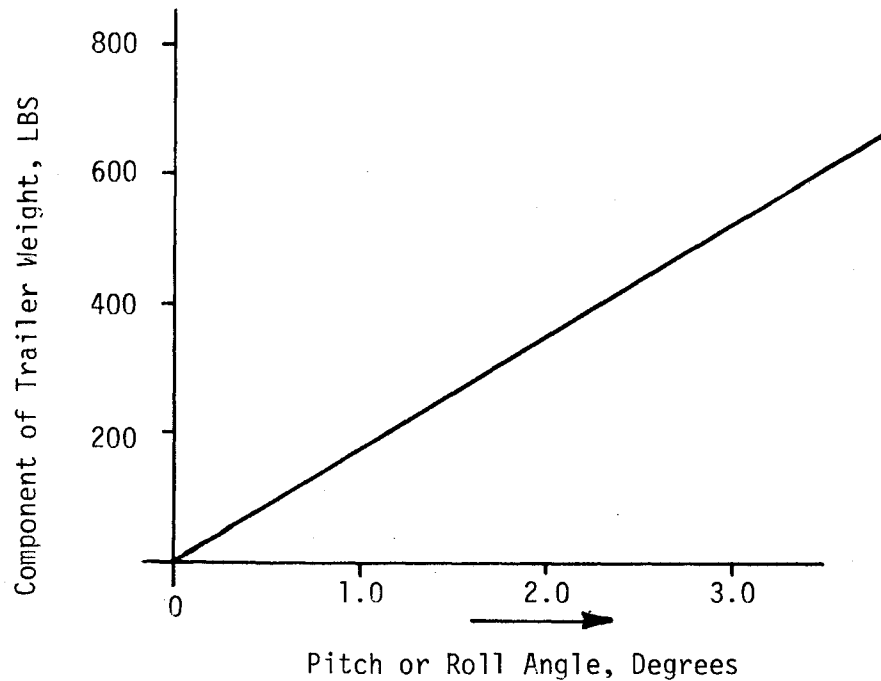


Figure 3-3. Component of Trailer Weight Versus Tilt Angle

These were, however, worst case estimates and the maximum accelerations (or decelerations) were expected to be limited to 0.1 g. For a 9850 pound trailer, this meant inertial forces in the order of 1000 pounds.

3.2.3.2 Centripetal Acceleration

The AERO/TOFC (Series II) test requirements (Reference 9) stipulated that the track alignment be maintained within 1/4-inch for a 62-foot mid-chord. This corresponds to a radius of curvature (see Appendix C)

$$R = \frac{(31)^2 + \sigma^2}{2\sigma} \text{ feet} \quad (3.2)$$

which, for $\sigma = 1/48$ foot has the value 4.4 miles. The corresponding centripetal acceleration has a maximum value

$$\begin{aligned}
 a_c &= \frac{V^2}{R} \\
 &= \frac{(90 \times 22/15)^2}{(4.4)(5280)(32.2)} \\
 &= 0.023 \text{ g at 90 mph train speed} \qquad (3.3)
 \end{aligned}$$

This acceleration leads to a maximum centrifugal force of 227 pounds at 90 mph.

The above discussion shows that, in the longitudinal direction, the drag and gravitational forces are of the same order of magnitude, especially at low train speeds and small angles of yaw. In the lateral direction, the side force, the gravitational force and the centrifugal force can be of the same order of magnitude at small angles of yaw and high train speeds, especially when the alignment deviations in the track do not average out to zero over the test zone. In both directions, the inertial forces can be very large compared to aerodynamic forces. It is clear, therefore, that the determination of aerodynamic forces in the presence of contaminating inertial, gravitational and centrifugal forces presented a difficult problem. The side force, in particular, is less amenable to an accurate evaluation due to centrifugal force contributions in addition to the gravitational and inertia forces.

The next task was to define appropriate mechanical systems and to derive the dynamic equations. This is the subject of the following two sections.

3.3 MODELS FOR LONGITUDINAL AND LATERAL MOTIONS

In the following analysis, the longitudinal and lateral motions of the trailer mass were assumed to be decoupled from the vertical motion and from each other. This is a very good assumption since the support flexures of the balance system

are very weak in the transverse direction as compared to the axial direction (Section 2.4.2.2). Table I in Appendix A summarizes the stiffness characteristics of the flexures and provides a justification for the foregoing assumption. Models for longitudinal and lateral motion will now be defined.

3.3.1 Model for Longitudinal Motion

Figure 3-4 illustrates the longitudinal model for one trailer with mass m . K_L and C_L represent spring stiffness and damping coefficients of the longitudinal flexure. F_L denotes symbolically a readout device for the longitudinal load cell. Let r_s be the motion (at point A) of the support which connects the flexure to the carbody deck plate. θ_g is the (pitch) angle between the local vertical and the normal to the plane of the track segment on which the carbody is resting. θ_c is the angle between the normal to the carbody deck plate (referred to as carbody deck plane in Figure 3-4) and the normal

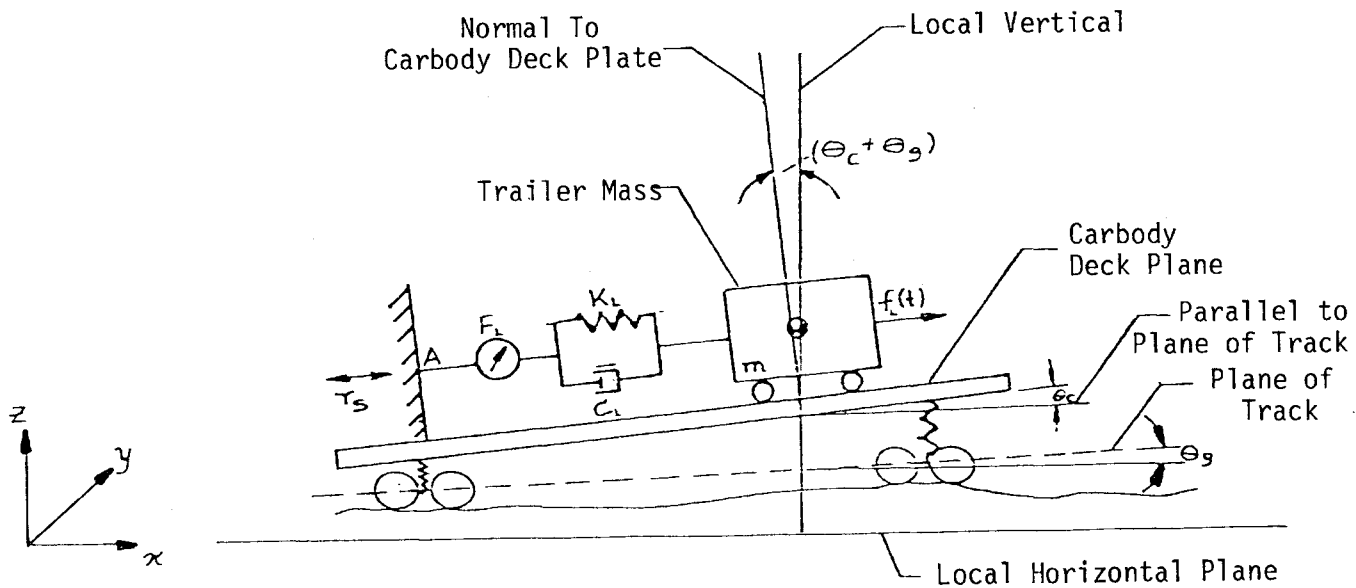


Figure 3-4. Model for Longitudinal Motion

to the plane of the track. The force $f_L(t)$ on mass m stands for the external forces acting on the system. In the case of longitudinal motion, these forces are the gravitational force due to the tilt $(\theta_c + \theta_g)$ and the aerodynamic drag force.

The system for lateral motion is shown in Figure 3-5 for one trailer. F_{s1} and F_{s2} correspond to the two lateral load cell readouts. K_{s1} and C_{s1} are stiffness and damping coefficients for the rear lateral flexure, respectively. Similarly, K_{s2} and C_{s2} represent stiffness and damping coefficients for the front lateral flexure. As shown in the side view, ψ_c is the roll angle between the normal to the deck plane and the normal to the plane of the track. ψ_g is the roll angle between the normal to the plane of the track and the local vertical. The external force f_s consists of aerodynamic side force, the gravitational force due to tilt $(\psi_c + \psi_g)$ and the centrifugal force due to local track curvature.

3.4 DERIVATION OF THE EQUATIONS OF MOTION

Figure 3-6 shows the coordinate system adopted for the derivation of the governing equations.

The coordinates x, y and z form an inertial reference frame with the x axis along the track and $\tilde{x}, \tilde{y}, \tilde{z}$ is a moving reference frame fixed to the carbody center of gravity. The latter frame of reference has an angular velocity $\vec{\omega}$ with respect to the inertial reference. Let $(\tilde{x}, \tilde{y}, \tilde{z})$ be the instantaneous coordinates of the center of gravity of the trailer relative to the moving reference and let (x, y, z) be the instantaneous position of the origin of the moving reference with respect to the inertial frame. Let \vec{R} and $\vec{\rho}$ denote the position vectors of O' relative to O and C relative to O' , respectively (Figure 3-6). Let α and ϕ be the angles made by \vec{R} and $\vec{\rho}$ with respect to Ox and $O'\tilde{x}$, respectively. The sum of the vectors \vec{R} and $\vec{\rho}$ is given by the resultant vector \vec{r} .

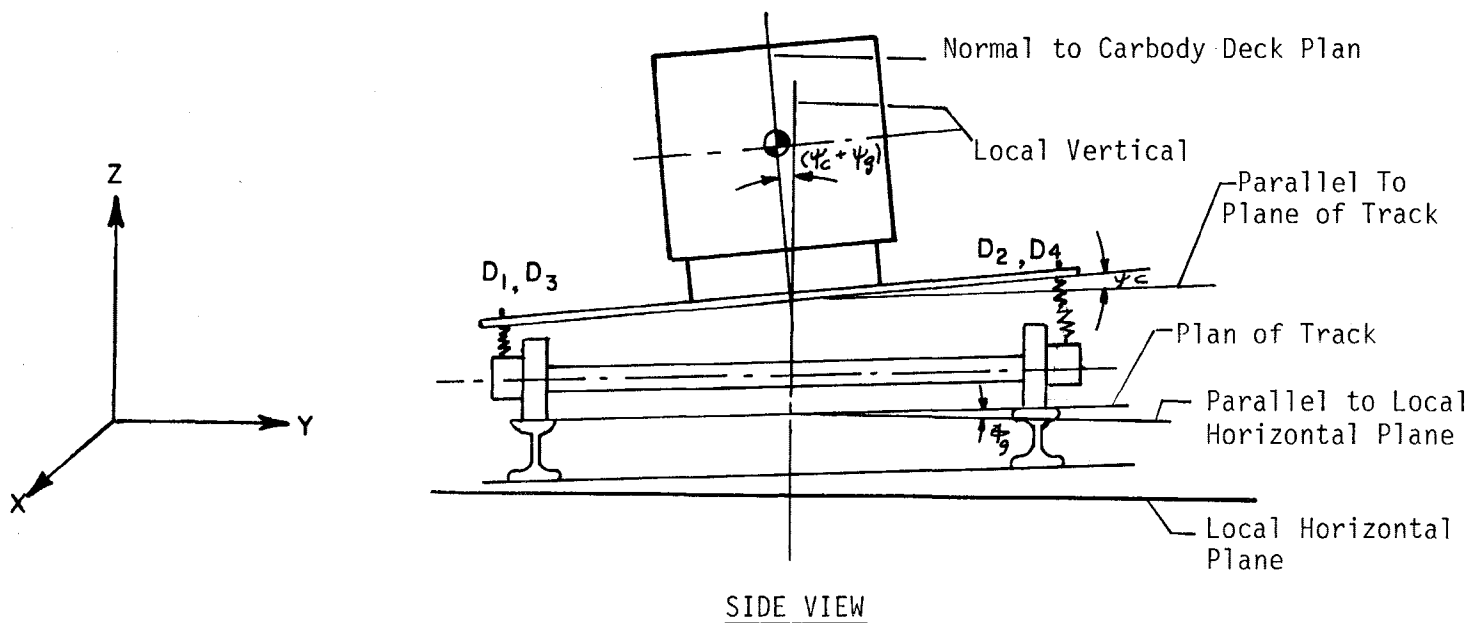
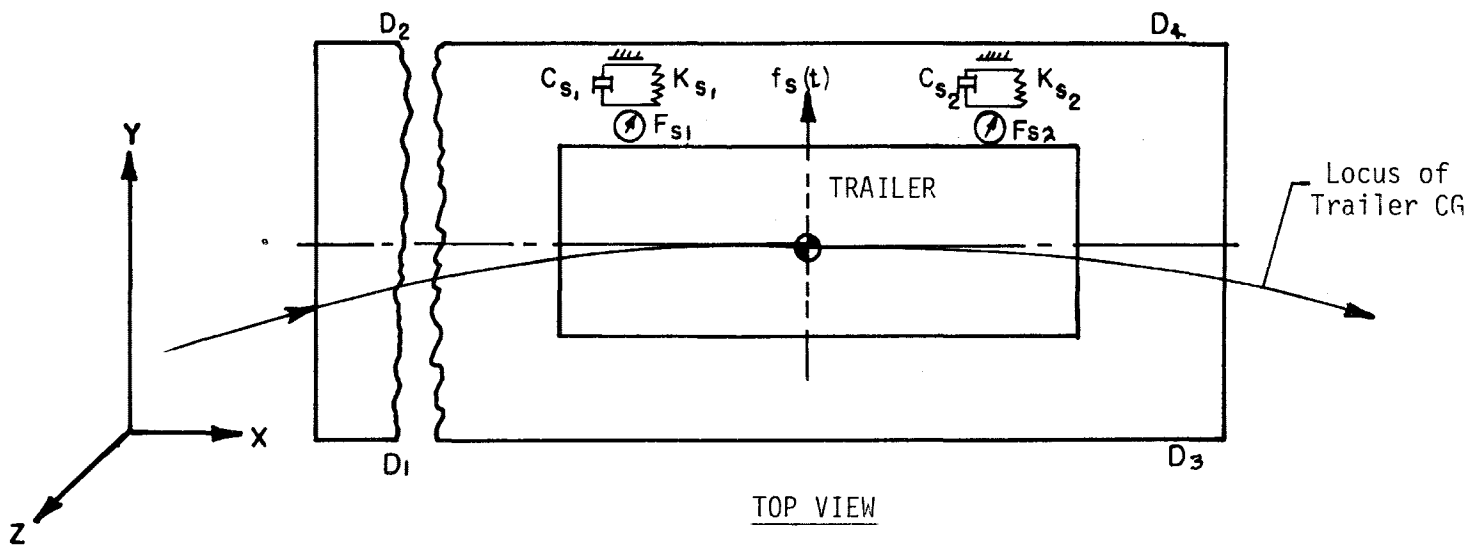


Figure 3-5. Model for Lateral Motion

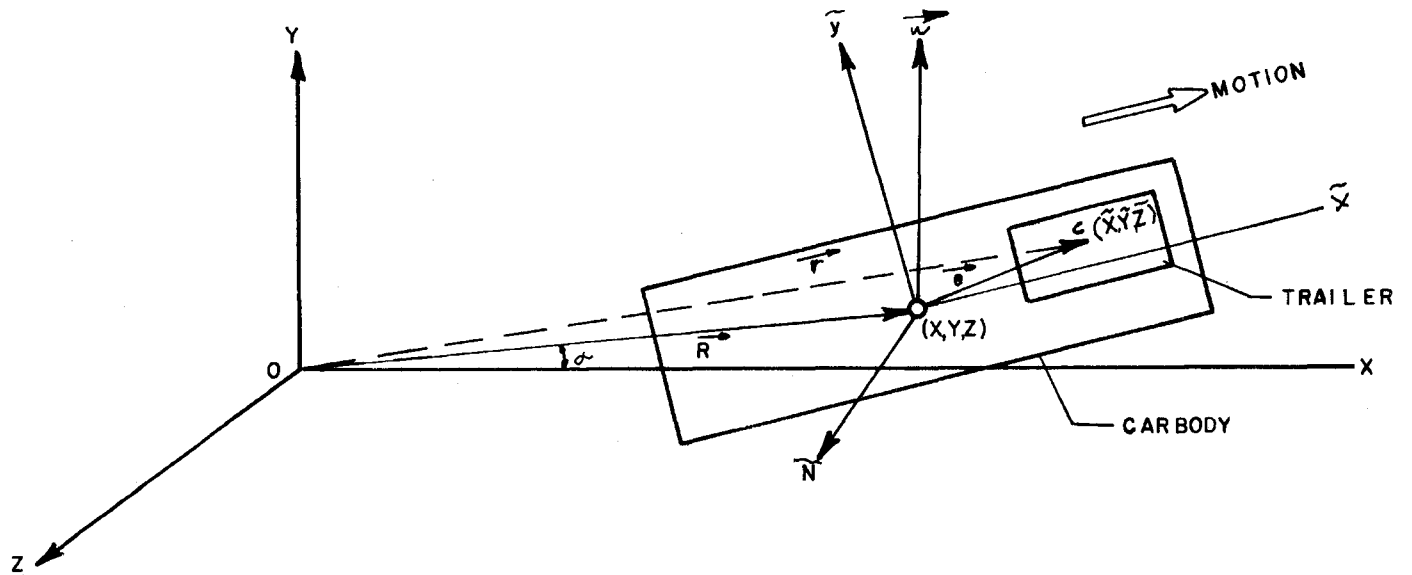


Figure 3-6. Coordinate System for Derivation of Governing Equations

If the trailer were rigidly fastened to the carbody deck plate, its center of gravity would move along \vec{r} . In reality, however, the trailer executes vibratory motions longitudinally (i.e., parallel to the carbody longitudinal axis) and laterally (i.e., parallel to the carbody transverse axis). The vertical motions of the trailer are not of interest in the present work.

The following assumptions are introduced to simplify the analysis. The first assumption was set forth earlier in Section 3.3 and is repeated here for the sake of completeness.

- Longitudinal and lateral motions of the trailer mass are assumed to be decoupled from the vertical motion and from each other.

- The trailers and the carbody are assumed to be perfectly rigid. Thus these bodies do not undergo flexural and torsional vibrations which may be coupled with their rigid body motions.
- The track is assumed to be almost tangent and the flexures to be fairly stiff so that the following conditions hold at all times:
 - Small carbody lateral motion
 $y(t) \ll x(t)$
 - Small trailer lateral motion
 $\tilde{y}(t) \ll \tilde{x}(t)$
 - Small angular displacement of the carbody
 $\alpha(t) \approx 0$
 - Small angular displacement of the trailer
 $\phi(t) \approx 0$

Under these assumptions the equations of motion were derived as described in the following paragraphs.

3.4.1 Equation for Longitudinal Motion

The longitudinal motion of a trailer occurs along a direction \vec{r}_L parallel to the longitudinal axis of symmetry of the carbody as shown in Figure 3-7(a). The free body diagram of mass m is shown in Figure 3-7(b).

Note that θ is positive in the counterclockwise direction in the vertical (x-z) plane. In other words, θ is positive when the leading end of the carbody tilts upward. The restoring force $\{K_L(r_L - r_S) + c_L(\dot{r}_L - \dot{r}_S)\}$ is given by the

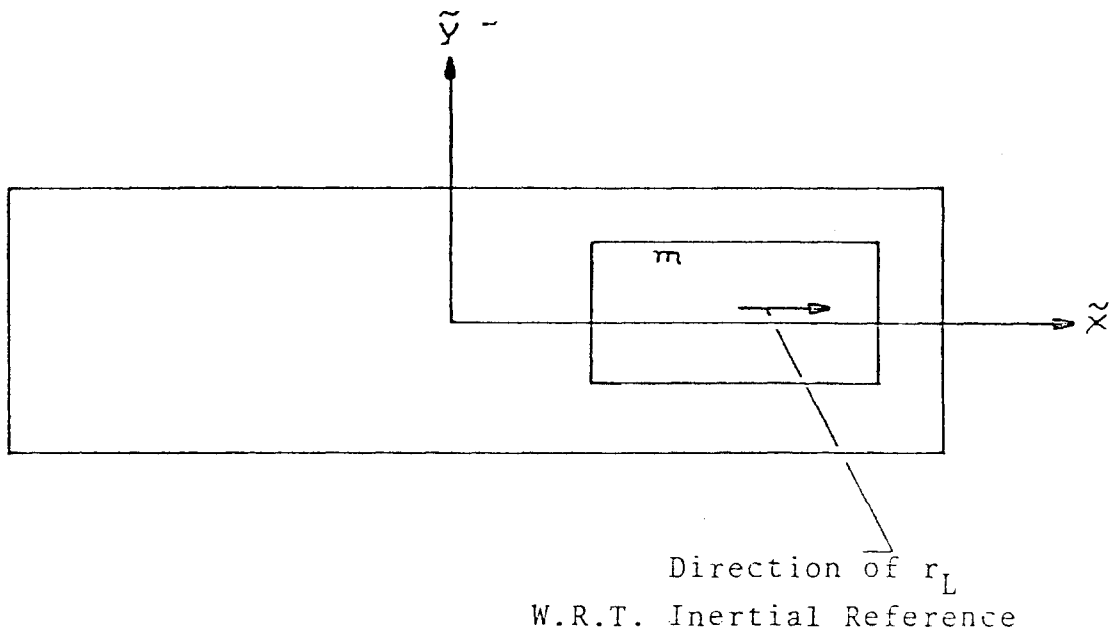


Figure 3-7(a). Longitudinal Motion of Trailer

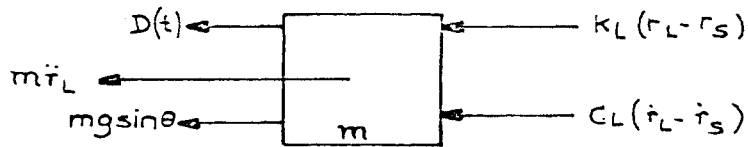


Figure 3-7(b). Free Body Diagram for Longitudinal Motion

meter readout F_L and it may be positive or negative. A sign convention was, therefore, necessary and was established as follows. The actual arrangement for the longitudinal force transducer (of which Figure 3-4 is a model) has been described in detail in Section 2.4.2.1 and is shown in Figure 3-7(c).

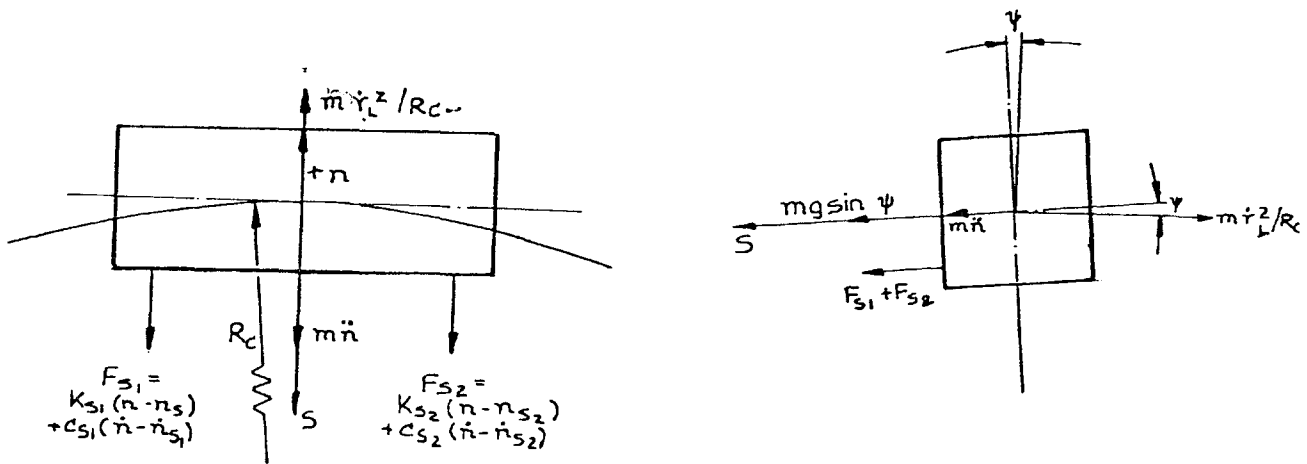


Figure 3-7c. Free Body Diagram for Lateral Motion

It is evident that a positive displacement in the \vec{r}_L direction causes the load cell to be in tension and this should, according to the sign convention for the load cell (Reference 10), correspond to a positive reading. Summing the forces in Figure 3-7(b), the equation of longitudinal motion is:

$$m\ddot{r}_L + mg\sin\theta(t) + D(t) + K_L(r_L - r_S) + C_L(\dot{r}_L - \dot{r}_S) = 0 \quad (3.4)$$

where $D(t)$ is the instantaneous drag force.

Since

$$K_L(r_L - r_S) + C_L(\dot{r}_L - \dot{r}_S) = +F_L(t) \quad (3.5)$$

$$m\ddot{r}_L + mg\sin\theta(t) + D(t) + F_L(t) = 0 \quad (3.6)$$

For small angles, $\sin\theta(t) \approx \theta(t)$ and thus

$$m\ddot{r}_L = -F_L(t) - D(t) - mg\theta(t) \quad (3.7)$$

This is the equation of longitudinal motion.

3.4.2 Equation of Lateral Motion

Figure 3-8 shows the free body diagram for lateral motion. This motion occurs along a direction \vec{n} parallel to the transverse axis of symmetry of the carbody.

The equation of motion is obtained by summing the forces in the \vec{n} direction. Hence,

$$m\ddot{n} + mg\sin\psi(t) + S(t) - F_{s1}(t) - F_{s2}(t) = \frac{m\dot{r}_L^2}{R_C(t)} \cos\psi(t) \quad (3.8)$$

where $S(t)$ is the instantaneous aerodynamic side force and $R_C(t)$ is the radius of curvature of the locus of the trailer center of gravity at time t . Note that the load cells are in compression for a positive displacement n and therefore negative signs appear in front of F_{s1} and F_{s2} in the above equation. The term on the right hand side in Equation 3.8 is due to the centrifugal force.

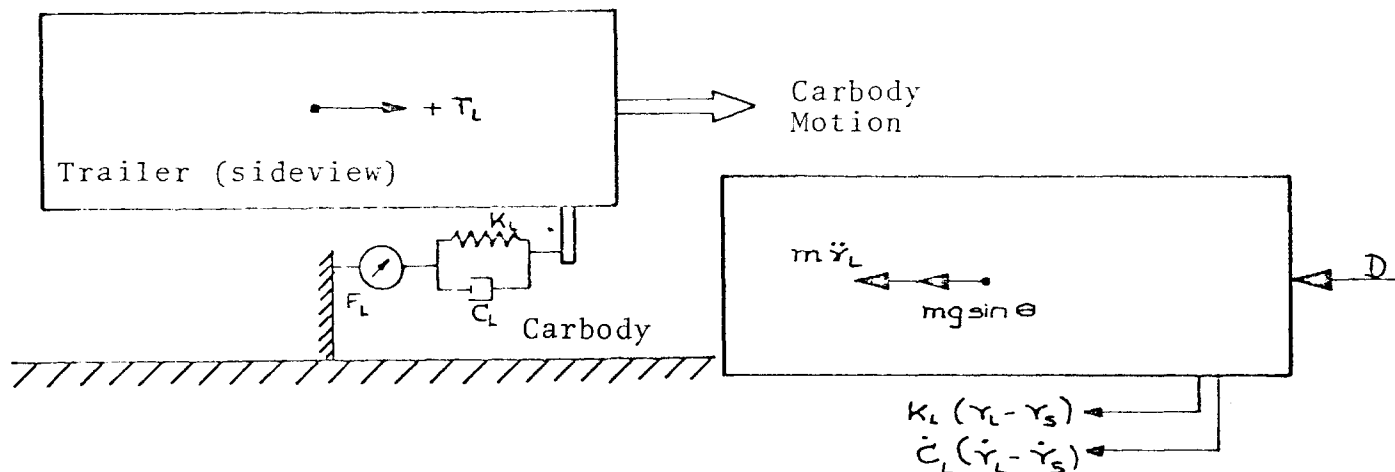


Figure 3-8. Sign Convention for Restoring Forces

For small angles, $\sin\psi(t) \approx \psi(t)$ and $\cos\psi(t) \approx 1$ and

$$m\ddot{n} = F_{s1}(t) + F_{s2}(t) - S(t) - mg\psi(t) + \frac{mr_L^2}{R_c(t)} \quad (3.9)$$

Equation 3.9 is the equation for lateral motion.

In Equations 3.7 and 3.9, the angles $\theta(t)$ and $\psi(t)$ are positive in the counterclockwise direction and are the orientations of the normal to the carbody with respect to the local vertical in the x-z and y-z planes, respectively. These angles consist of the following components:

- Inclination of the plane of the track with respect to the local vertical θ_g (Figure 3-4) or ψ_g (Figure 3-5).
- Inclination of the carbody deck plate relative to the plane of the track θ_c (Figure 3-4) and ψ_c (Figure 3-5).
- Flexural and torsional vibrations of the carbody during motion.
- Local buckling of the carbody deck plate and the bottom plate of the trailer.
- Permanent deformations of the carbody and other structural elements.

The angles θ and ψ can be very accurately measured using a vertical gyro. This measurement, however, is difficult due to performance limitations in severe dynamic environments.

It may, therefore, be necessary to obtain θ and ψ values by alternate means. Angles θ_g and ψ_g can be determined through careful surveying, and angles θ_c and ψ_c can be determined via displacement transducers as described in Section 3.6. The stiffening of the carbody and the trailers as described in Appendix A should eliminate the possibility of buckling and permanent deformation. Angular deflections were expected to be periodic and to lead to zero net contribution when averaged over a long period of time.

3.5 METHODS OF AERODYNAMIC FORCE DETERMINATION

Solving Equation 3.7 and 3.9 for instantaneous drag and side force, respectively

$$D(t) = -F_L(t) - m\ddot{r}_L - mg\theta(t) \quad (3.10)$$

and

$$S(t) = F_{s1}(t) + F_{s2}(t) - m\ddot{n} - mg\psi(t) + \frac{m\dot{r}_L^2}{R_c(t)} \quad (3.11)$$

The purpose of AERO/TOFC (Series II) tests was to determine the aerodynamic forces averaged over the duration of the test. This can be accomplished by the following three methods.

3.5.1 Straight-Forward Averaging Approach

Averaging Equations (3.10) and (3.11) over the duration of the test run and assuming this averaging time to be sufficiently long

$$\bar{D} = -\bar{F}_L - m\bar{\ddot{r}}_L - mg\bar{\theta} \quad (3.12)$$

$$\bar{S} = \bar{F}_{s1} + \bar{F}_{s2} - m\bar{n}\ddot{n} - mg\bar{\psi} + m \left[\frac{\dot{r}_L^2}{R_c} \right] \quad (3.13)$$

This approach involves averaging the longitudinal acceleration \ddot{r}_L and the transverse acceleration \ddot{n} . In view of the massiveness of the trailers (306 slugs each), it is necessary that these averages be computed very accurately. For example, in order to keep the error in inertial force below 10 pounds, $\bar{\ddot{r}}_L$ must be determined within 0.0019. Apart from the errors associated with the averaging process, errors of the above magnitude can be caused by an 0.05-degree misalignment of the accelerometer itself. The preceding considerations apply to the average transverse acceleration \bar{n} as well.

Aerodynamic force determination using Equation 3.12 and 3.13 also requires accurate measurement of average longitudinal (pitch) and transverse (roll) orientations $\bar{\theta}$ and $\bar{\psi}$, respectively. The sensitivity of the gravitational forces to these angles has already been discussed in Section 3.2.2. The difficulty with direct gyroscopic measurement of θ and ψ (which has been mentioned in Section 3.4.2) coupled with averaging errors, would not allow evaluation of gravitational forces to the required accuracy. For instance, a ± 10 -pound error in the gravitational force terms requires that the average angular orientations be determined within 0.05 degree. A moderately expensive gyroscope (such as the Bendix Type 14168-2C) provides a typical accuracy of 0.1 degree. Therefore, a 0.05-degree accuracy would be extremely difficult to achieve with a sufficient margin of reliability and the necessary instrumentation would be prohibitively expensive.

In addition to the average acceleration and average angular orientation measurements, determination of side force from Equation 3.13 requires computation of average centrifugal force. This task presents difficulties because, strictly speaking, an instantaneous measurement of the radius of

curvature (R_c) is necessary. Such a measurement is very difficult to obtain with sufficient accuracy and is very expensive.

The straight-forward averaging approach was employed in the initial data reduction stages of the AERO/TOFC (Series I) tests (Reference 3), and the resulting force values appeared to be erratic and inconsistent. These force computations had the following disadvantages:

- Longitudinal and lateral accelerations suffered from bias and averaging errors.
- Gravitational force correction was applied to drag forces alone and only the contribution due to track elevation was accounted for.
- Centrifugal force corrections to side force data were not computed because of unavailability of curvature data.

This experience suggested the need for an alternate approach to force evaluation which would eliminate the need for average acceleration and employ simple corrections to account for gravitational and centrifugal forces. Two possible techniques are discussed in the following paragraphs.

3.5.2 Momentum Approach

The case for drag force is described first. Integrating Equation 3.10 over the duration of the test run (from $t=0$ to $t=T$), dividing by T and rearranging terms

$$\begin{aligned} \frac{m}{T} \left[\dot{r}_L(T) - \dot{r}_L(0) \right] &= \frac{-1}{T} \int_0^T F_L(t) dt - \frac{1}{T} \int_0^T D(t) dt \\ &\quad - \frac{1}{T} \int_0^T mg\theta(t) dt \end{aligned} \quad (3.14)$$

This equation shows that the rate of change of momentum equals the net external force. The external forces are stiffness and damping force (F_L), aerodynamic drag (D) and gravitational force ($mg\theta$). Another interpretation of Equation 3.14, obtained by multiplying through by T , is that the change in momentum equals the net external impulse. The latter consists of stiffness and damping, aerodynamic drag and gravitational impulses. Equation 3.14 suggests a method for measuring the average drag force.

$$\begin{aligned}\bar{D} &= \frac{1}{T} \int_0^T D(t) dt \\ &= \frac{-1}{T} \int_0^T F_L(t) dt - \frac{mg}{T} \int_0^T \theta(t) dt - \frac{m}{T} [\dot{r}_L(T) - \dot{r}_L(0)]\end{aligned}$$

or

$$\bar{D} = -\bar{F}_L - mg\bar{\theta} - \frac{m}{T} [\dot{r}_L(T) - \dot{r}_L(0)] \quad (3.15)$$

Equation 3.15 assumes that the averages are independent of the starting instant of time and that the averaging time is sufficiently long. In other words, the random processes (D , F_L and θ) are assumed to be statistically stationary and ergodic.

It is shown in Appendix C that to a good approximation

$$\dot{r}_L(t) = \dot{R}_x(t)$$

where R_x is the speed of the carbody along the track which is aligned with the x axis. It should be borne in mind that the track may have a very small net curvature, in which case the inertial coordinate system of Figure 3-6 is actually a curvilinear system. Equation 3.15 now takes the form

$$\bar{D} = -\bar{F}_L - mg\bar{\theta} - \frac{m}{T} [\dot{R}_X(T) - \dot{R}_X(0)] \quad (3.16)$$

The advantage of Equation 3.16 is that the acceleration terms are replaced by velocity terms. The measurement of instantaneous longitudinal velocities at the beginning and at the end of the test zone is a relatively simple task.

Equation 3.16 has the limitation that a measurement of absolute longitudinal orientation θ is required and this presents the same difficulties as in the case of the straight-forward averaging approach. It is possible, however, to provide an approximation to the gravitational force term in Equations 3.15 and 3.16. This correction will be derived in Section 3.6.

Returning to the side force Equation 3.11 and performing similar manipulations, one obtains

$$\begin{aligned} \bar{S}(t) &= \frac{1}{T} \int_0^T S(t) dt \\ &= \bar{F}_{S_1} + \bar{F}_{S_2} - mg\bar{\psi} - \frac{m}{T} [\dot{n}(T) - \dot{n}(0)] \\ &\quad + \frac{m}{T} \int_0^T \frac{\dot{r}_L^2(t)}{R_C(t)} dt \end{aligned} \quad (3.17)$$

Again, as shown in Appendix C, the transverse velocity \dot{n} can be approximated as

$$\dot{n}(t) = \dot{R}_y(t)$$

where \dot{R}_y is the lateral speed of the carbody (i.e., normal to the track in the local horizontal plane). Equation 3.17 then becomes

$$\bar{S}(t) = \bar{F}_{s_1} + \bar{F}_{s_2} - mg\bar{\psi} - \frac{m}{T} [\dot{R}_y(T) - \dot{R}_y(0)] + m \left[\frac{\dot{R}_x^2(t)}{R_c(t)} \right] \quad (3.18)$$

Notice that this equation contains the track curvature (i.e., curvature of the x-axis) in the centrifugal force term. In contrast to the drag force, the replacement of acceleration by velocity in the lateral direction is not useful. This is because absolute lateral velocities of the trailer are very difficult to measure and the AERO/TOFC (Series II) tests did not incorporate such a measurement. The gravitational term in Equation 3.18 implies the same difficulties as before and the centrifugal force term presents additional problems. An estimation for the last three terms in Equation 3.18 is presented in Section 3.7.

3.5.3 Energy Approach

Consider the drag force equation first. Multiplying Equation 3.10 by the longitudinal velocity \dot{r}_L and integrating over the duration of the test run,

$$\begin{aligned} \int_0^T m \dot{r}_L \ddot{r}_L dt &= \frac{m}{2} \int_0^T d(\dot{r}_L^2) \\ &= - \int_0^T \dot{r}_L(t) F_L(t) dt - \int_0^T \dot{r}_L(t) D(t) dt \\ &\quad - mg \int_0^T \dot{r}_L(t) \theta(t) dt \end{aligned}$$

or

$$\begin{aligned} \frac{1}{2}m \left[\dot{r}_L^2(T) - \dot{r}_L^2(0) \right] = & - \int_0^T \dot{r}_L(t) F_L(t) dt - \int_0^T \dot{r}_L(t) D(t) dt \\ & - mg \int_0^T \dot{r}_L(t) \theta(t) dt \end{aligned} \quad (3.19)$$

This equation shows that the change in kinetic energy of the trailer between the beginning and the end of the test zone equals the work done by external forces acting on the trailer. These forces are stiffness and damping force, aerodynamic drag and gravitational force. Using the approximation $\dot{r}_L(t) \approx \dot{R}_X(t)$ in Equation 3.19 and dividing by the test duration T ,

$$\begin{aligned} \frac{1}{T} \int_0^T \dot{R}_X(t) D(t) dt = & -\frac{1}{T} \int_0^T \dot{R}_X(t) F_L(t) dt - \frac{mg}{T} \int_0^T \dot{R}_X(t) \theta(t) dt \\ & - \frac{1}{2}m \left[\dot{R}_X^2(T) - \dot{R}_X^2(0) \right] \end{aligned} \quad (3.20)$$

or

$$\begin{aligned} \overline{\dot{R}_X(t) D(t)} = & \overline{\dot{R}_X(t) F_L(t)} - mg \overline{\dot{R}_X(t) \theta(t)} \\ & - \frac{1}{2} m \left[\dot{R}_X^2(T) - \dot{R}_X^2(0) \right] \end{aligned} \quad (3.21)$$

Thus the energy approach requires computation of averages of products under the barred quantities in Equation 3.21, and together with the change in kinetic energy, the result is average drag power. The final desired quantity is the average drag force \bar{D} , which can be recovered through an iterative scheme described in Appendix C.

A similar series of operations on the side force equation (3.11) yields the following relation after employing the approximation $\dot{n}(t) \approx \dot{R}_y(t)$

$$\overline{\dot{R}_y(t)S(t)} = \overline{-\dot{R}_y(t)F_{S_1}(t)} - \overline{\dot{R}_y(t)F_{S_2}(t)} - mg \overline{\dot{R}_y(t)\psi(t)} \\ - \frac{1}{2} m \left[\dot{R}_y^2(T) - \dot{R}_y^2(0) \right] + m \left[\frac{\dot{R}_x^2(t)\dot{R}_y(t)}{R_c(t)} \right] \quad (3.22)$$

As in the case of the momentum approach, Equation 3.22 is not useful for determining the average side force \bar{S} and it has been listed here only for the sake of completeness.

3.6 COMPUTATIONAL PROCEDURE FOR ON-BOARD PROCESSING

Three possible methods of computation were discussed in the previous section and their relative merits and demerits were pointed out. The choice of a particular method for on-board processing is dictated by the following criteria.

- The method should be free of any inherent inaccuracies.
- It should be relatively simple in nature and easy to apply.
- It should lend itself to simple corrections, if necessary.
- It should be compatible with the rather limited software capabilities of the T-5 test car, especially with regard to the amount of available storage.

As is evident from the discussions in Section 3.5, the straightforward averaging approach contains some inherent inaccuracies, but the energy approach is somewhat involved and relatively difficult to apply. Thus the momentum approach seems to be the

appropriate choice. This method readily satisfies the first three criteria. However, some elaboration is necessary with respect to the corrections. This is the subject of the following paragraphs.

3.6.1 Drag Force

The average drag force as given by Equation 3.16 is:

$$\bar{D} = -\bar{F}_L - \frac{m}{T} [\dot{R}_x(T) - \dot{R}_x(0)] - mg\bar{\theta} \quad (3.16)$$

As mentioned in Sections 3.5.2, it is easy to determine the velocities \dot{R}_x of the carbody (corrected for the relative motion between T-5 and the carbody) at the beginning and at the end of the test zone. The software on-board T-5 should provide an accurate average transducer reading \bar{F}_L which is corrected for cross-axis response and zero errors. Appendix D contains computational procedures for \dot{R}_x and \bar{F}_L . The measurement of θ using a vertical gyro may not be sufficiently accurate and reliable. Therefore, in spite of the fact that gyroscopic measurements were incorporated into AERO/TOFC (Series II) it was decided to approximate the gravitational term for purposes of on-board computation. Referring to Section 3.4.2, the term $mg\bar{\theta}$ can be written as

$$mg\bar{\theta} = mg(\bar{\theta}_g + \bar{\theta}_c + \bar{\theta}_d)$$

or

$$mg\bar{\theta} = mg\bar{\theta}_g + mg\bar{\theta}_c + mg\bar{\theta}_d \quad (3.23)$$

where $\bar{\theta}_d$ is an additional component due to flexural deflections of the carbody and may represent permanent deformation of the carbody or its static deflection. $\bar{\theta}_c$ is the carbody tilt relative to plane of the track, and $\bar{\theta}_g$ is the angle between

the plane of the track and the local horizontal plane. Under the present plan of simplified on-board processing, the approximation introduced is:

$$mg\bar{\theta} \approx mg\bar{\theta}_g \quad (3.24)$$

With this approximation, the trailer center of gravity follows the track profile in the x,z plane and θ_g becomes the slope of the track (Figure 3-9).

It is shown in Section 3.7 and in Appendix C that

$$mg\bar{\theta} \approx \frac{mg}{\dot{T}R_{x_{av}}} \Delta H \quad (3.25)$$

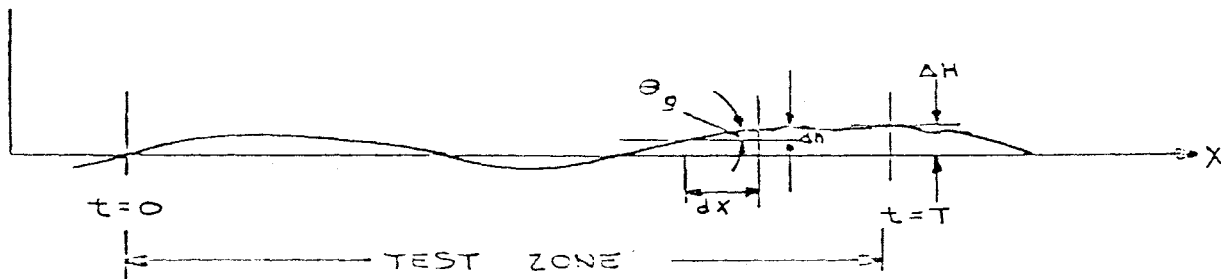


Figure 3-9. Approximation for Gravitational Force

where ΔH is the change in elevation between the beginning and the end of the test zone. The accuracy of the approximation in Equation 3.25 is examined in detail in Appendix C. From Equations 3.24 and 3.25

$$mg\bar{\theta} \approx \frac{mg \Delta H}{T\dot{R}_{x_{av}}} \quad (3.26)$$

Finally, the approximate drag force equation is

$$\bar{D} \approx -\bar{F}_L - \frac{m}{T} [\dot{R}_x(T) - \dot{R}_x(0)] - \frac{mg}{T\dot{R}_{x_{av}}} \Delta H \quad (3.27)$$

This equation was incorporated into the software on-board T-5 for near-real time data processing (Appendix D). The validity of approximating Equation 3.23 by Equation 3.24 can only be justified a posteriori by analyzing the displacement transducer data and the gyroscopic data. Referring to Figures 3-4 and 3-5, it is seen that the pitch angle $\bar{\theta}_c$ in Equation 3.23 is given by

$$\bar{\theta}_c = \frac{\frac{1}{2}(\bar{D}_3 + \bar{D}_4) - \frac{1}{2}(\bar{D}_1 + \bar{D}_2)}{L} \quad (3.28)$$

where the displacements $D_{1,2,3,4}$ are defined positive in the +z direction (Figure 3-4) and L is the distance between the transducers D_1 (or D_2) and D_3 (or D_4).

3.6.2 Side Force

Equation 3.18 yields the average side force as

$$\bar{S} = \bar{F}_{s_1} + \bar{F}_{s_2} - mg\bar{\psi} - \frac{m}{T} [\dot{R}_y(T) - \dot{R}_y(0)] + m \left[\frac{\dot{R}_x^2(t)}{R_c(t)} \right] \quad (3.29)$$

The unavailability of lateral velocity (\dot{R}_y) data and curvature data makes it imperative that the following approximation be used without any a priori knowledge of the last two terms in Equation 3.29.

$$\bar{S} \approx \bar{F}_{s_1} + F_{s_2} - mg\bar{\psi} \quad (3.30)$$

Further, since the absolute roll angle $\bar{\psi}$ derived from gyroscopic measurements may suffer from problems mentioned earlier, it becomes necessary to simply ignore the last term in Equation 3.30 for purposes on on-board processing (Appendix D). Thus

$$\bar{S} = \bar{F}_{s_1} + \bar{F}_{s_2} \quad (3.31)$$

It should be emphasized that Equation 3.31 represents only a very rough approximation to the side force.

It is convenient to divide the gravitational term in Equation 3.30 in a fashion similar to Equation 3.23. Hence

$$mg\bar{\psi} = mg\bar{\psi}_g + mg\bar{\psi}_c + mg\bar{\psi}_d \quad (3.32)$$

Unlike the case of drag force, it is not possible to obtain a good estimate for the component $mg\bar{\psi}_g$ in terms of change in elevation. Rather, an accurate survey is necessary to determine the orientation (ψ_g) of the normal to the plane of the track relative to the local vertical in the y-z plane (Figure 3-5). This was done (Refernece 12) and a correction for the term $mg\bar{\psi}_g$ was applied during post-test analysis of AERO/TOFC (Series II) data. The roll angle ψ_c can be determined by the equation

$$\bar{\psi}_c = \frac{\frac{1}{2}(D_2 + D_4) - \frac{1}{2}(D_1 + D_3)}{\ell} \quad (3.33)$$

where ℓ is the distance between the transducers D_1 (or D_3) and D_2 (or D_4). The side force discussion in this section has been limited to the momentum approach because this method was employed for on-board processing.

3.7 ESTIMATION OF ERRORS

The purpose of this section is to identify the sources of error in drag and side force determination and to evaluate these errors wherever possible. In general, errors can be broadly classified into two categories:

- Systematic errors which arise due to certain approximations introduced into the force determination methods. These errors are so termed because they bear exact relationship to certain governing physical parameters.
- Random errors which are due to statistical fluctuations of measured parameter about a certain mean value. These errors are random in the sense that the exact nature of the governing physical processes is not known. Some examples are, nonlinearity, hysteresis, non-repeatability, etc.

3.7.1 Errors in Drag Force Determination

Equation 3.16 is an exact formula for the drag force. In going from Equation 3.16 to Equation 3.27, which was used for on-board computation, two approximations have been made. These are:

$$mg\bar{\theta} = mg\bar{\theta}_g + mg\bar{\theta}_c + mg\bar{\theta}_d \approx mg\bar{\theta}_g$$

$$mg\bar{\theta}_g \approx \frac{mg}{TR_{x_{av}}} \Delta H$$

The error (ϵ_g) in the latter approximation is considered first. As developed in Appendix C.4

$$mg\bar{\theta}_g = \frac{mg\Delta H}{TR_{x_{av}}} + \epsilon_g \quad (3.34)$$

where

$$\epsilon_g \equiv 0 \quad (3.35a)$$

if disturbance in the track profile (wavelength λ) and variations in the average train speed (frequency f) do not possess any common frequencies, i.e., $f\lambda \neq 1$. Notice that both profile and speed are assumed to be sinusoidal. In the event that a common frequency does exist, the error is given by the relation

$$\epsilon_g = -mg\pi \frac{A}{\lambda} \frac{B}{\dot{R}_{x_{av}}} \cos \frac{\pi\ell}{\lambda} \sin \left(\phi - \frac{\pi\ell}{\lambda} \right) \quad (3.35b)$$

In Equation 3.35b, A and λ are the amplitude and wavelength, respectively, of the track disturbances and B is the maximum value of variations in train speed about the average value $\dot{R}_{x_{av}}$. " ℓ " denotes the carbody bolster spacing and ϕ stands for the phase angle between the two sinusoids. The reader is referred to the discussion under Equation C.70 in Appendix C for a more complete explanation of the terms in Equation 3.35b. The maximum value of ϵ_g occurs when both sine and cosine terms in the preceding equation are unity.

Thus,

$$|\epsilon_g|_{\max} = mg\pi \frac{A}{\lambda} \frac{B}{\dot{R}_{x_{av}}} \quad (3.36)$$

The variations B are most likely to be derived from the exchange of potential and kinetic energies as the carbody traverses the sinusoidal track. In this case the amplitude B is extremely small as shown in Appendix C. However, for purposes of worst case error estimation, it may be assumed that B is ± 3 percent of the average speed. Also, for a typical track profile variation of 1/4-inch ($=2A$) with 39 feet length ($=\lambda/2$), the error is

$$|\epsilon_g|_{\max} = 9850\pi \frac{1/8}{12 \times 78} \quad (0.03)$$

$$= 0.12 \text{ pound}$$

For track disturbances and speed variations that are not necessarily sinusoid, but which can be expressed in terms of Fourier series, the error is given by (Appendix C)

$$|\epsilon_g| = mg \frac{\pi}{2} \sum_{p=0}^{\infty} \sum_{q=0}^{\infty} \frac{A_p}{\lambda_p} \frac{B_q}{\dot{R}_x} \sin \frac{2\pi \ell}{\lambda_p} \quad (3.37)$$

av

Although this equation contains infinite summations, the amplitudes A_p and B_q fall off rapidly due to the convergence property of the Fourier series, and the error remains finite. In view of these additional contributions, the error ϵ_g may be rounded off to 0.5 pounds.

Consider now the remaining gravitational force terms. One can write Equation 3.23 as

$$\begin{aligned} mg\bar{\theta}(t) &= mg\bar{\theta}_g(t) + mg\bar{\theta}_c(t) + mg\bar{\theta}_d(t) \\ &= mg\bar{\theta}_g(t) + mg[\bar{\theta}_{c_o}(t) + \bar{\Delta\theta}_c(t)] \\ &\quad + mg[\bar{\theta}_{d_o}(t) + \bar{\Delta\theta}_d(t)] \end{aligned} \quad (3.38)$$

where $\theta_{c_0}(t)$ is a slowly varying part of θ_c which is not necessarily periodic and $\Delta\theta_c(t)$ is a fast varying periodic part. Similar distinctions apply to $\theta_{d_0}(t)$ and $\Delta\theta_d(t)$. The terms $\Delta\theta_c$ and $\Delta\theta_d$ should be interpreted as pitching and bending (i.e., flexural) oscillations of the carbody supporting two empty trailers. Physically, $\theta_{c_0}(t)$ and $\theta_{d_0}(t)$ account for the fact that the carbody and the trailer may not return to the original spatial orientation at the end of a test. In other words, the quantity $[\theta_{c_0}(T) - \theta_{c_0}(0)]$ represents permanent change in the orientation of the carbody plane relative to the plane of the track. Similarly, $[\theta_{d_0}(T) - \theta_{d_0}(0)]$ accounts for the permanent change in the static flexural deflection of the carbody. Such non-cyclic changes are a result of hysteresis phenomena which can be caused by structural damping in the system.

It is appropriate to first determine errors in averaging the terms $\Delta\theta_c(t)$ and $\Delta\theta_d(t)$. Ideally, these terms should produce zero averages. Deviations from zero, however, will occur due to finite averaging time and their magnitudes will depend upon the amplitude and frequency of $\Delta\theta_c$ oscillations. As shown in Appendix C, the maximum averaging error for a sinusoidal signal is given by:

$$\text{Averaging Error} = \pm \frac{A}{\pi f T} \quad (3.39)$$

where

A = signal amplitude

f = signal frequency

T = averaging time

Therefore, in order to estimate errors according to Equation 3.39, it is necessary to know the frequency and amplitude of the pitching and bending modes. Although this information is not available for a TTX carbody supporting two empty trailers, the frequency and amplitude can be suggested from similar configurations tested in the Lightweight Flatcar Program conducted by ENSCO, Inc., for the Federal Railroad Administration. In the present report, approximate parameters have been provided by Reference 13 and are listed below:

Table 3-1. Amplitudes and Frequencies of Carbody Oscillatory Modes

Mode	Frequency (Hz)	Acceleration Amplitude (g)
First Bending	3.5	0.2
Pitch	3.0	0.2
Roll	3.0	0.1
Lateral Rigid Body Motion	2.5	0.2
Yaw	2.5	0.2

Thus, error in $mg\overline{\Delta\theta}_c$ is

$$\epsilon_c = mg \frac{\text{Displacement Amplitude}/L}{\pi f T} \quad (3.40)$$

where L is the distance defined in Equation 3.28 and the displacement amplitude is related to the acceleration amplitude through the relation

$$\text{Displacement Amplitude} = \frac{a_c}{4\pi^2 f^2} \quad (3.41)$$

with a_c denoting the acceleration amplitude in ft/sec^2

$$\epsilon_c = \pm \frac{a_c mg}{4\pi^3 f_c^3 TL} \quad (3.42)$$

For pitching mode, $a_c = (0.2)(32.2) \text{ ft}/\text{sec}^2$, $f_c = 3.0 \text{ Hz}$,
 $L = 60 \text{ ft.}$, $T = (4000 \text{ ft})/(132 \text{ ft}/\text{sec}) = 30.3 \text{ sec}$ at 90 mph
and the trailer weight $mg = 9850 \text{ pounds}$

$$\begin{aligned} \epsilon_c &= \pm \frac{(0.2)(32.2)(9850)}{4\pi^3 (3.0)^3 (30.3)(60)} \\ &= \pm 0.10 \text{ pound at 90 mph} \end{aligned}$$

and

$$= \pm 0.06 \text{ pound at 50 mph}$$

Similarly, the averaging error in $mg\overline{\Delta\theta}_d$ is

$$\epsilon_d = \pm \frac{a_d mg}{4\pi^3 f_d^3 TL} \quad (3.43)$$

For the bending mode, $a_d = (0.2)(32.2) \text{ ft}/\text{sec}^2$ and $f_d = 3.5 \text{ Hz}$.
The remaining quantities in Equation 3.43 have the same values
as in Equation 3.42 and the resulting error has the value

$$\begin{aligned} \epsilon_d &= \pm \frac{(0.2)(32.2)(9850)}{4\pi^3 (3.5)^3 (30.3)(60)} \\ &= \pm 0.07 \text{ pound at 90 mph} \end{aligned}$$

and

$$= \pm 0.04 \text{ pound at 50 mph}$$

Returning to Equation 3.38 and incorporating Equation 3.34,

$$mg\bar{\theta}(t) = \frac{mg}{\dot{R}_{x_{av}}^T} \Delta H + mg\bar{\theta}_{c_o}(t) + mg\bar{\theta}_{d_o}(t) + \epsilon_g + \epsilon_c + \epsilon_d \quad (3.44)$$

Errors in determining the slowly varying terms $mg\bar{\theta}_{c_o}(t)$ and $mg\bar{\theta}_{d_o}(t)$ do not lend themselves to rigorous estimation. These terms have very large periods (by definition) which are difficult to estimate for lack of any reasonable basis. Therefore, it is assumed that $\theta_{c_o}(t)$ varies linearly from a value $\theta_{c_o}(o)$ to a value $\theta_{c_o}(T)$ and has the average value

$$\bar{\theta}_{c_o} = \frac{\theta_{c_o}(o) + \theta_{c_o}(T)}{2}$$

In the onboard computation, the term $mg\bar{\theta}_{c_o}$ is being ignored altogether, and therefore, the associated error term is:

$$\begin{aligned} \epsilon_{c_o} &= mg\bar{\theta}_{c_o} \\ &= mg \left[\frac{\theta_{c_o}(o) + \theta_{c_o}(T)}{2} \right] \end{aligned} \quad (3.45)$$

Based on a 2-inch peak-to-peak relative displacement between the A end and B end of the carbody (60-foot wheelbase),

$$\begin{aligned} \frac{1}{2} \left[\theta_{c_o}(o) + \theta_{c_o}(T) \right]_{\max} &= \frac{1}{2} \frac{2 \text{ in}}{60 \times 12 \text{ in}} \\ &= 1.39 \times 10^{-3} \text{ radian} \end{aligned}$$

Hence,

$$\begin{aligned}\epsilon_{c_o} &= (9850)(1.39 \times 10^{-3}) \\ &= 13.7 \text{ pounds}\end{aligned}$$

A posteriori verification of the magnitude of θ_{c_o} was made using the displacement transducer data before and after a test series. This procedure is discussed in Section 4.0 and the results are listed in Tables 4-6A, 4-6B and 4-7. It was found that the average displacements were very small and the corresponding value of $mg\theta_c$ had a maximum value of 1.03 pounds.

A similar argument can be advanced for the term $mg\theta_{d_o}$. Assuming a 1-inch peak-to-peak displacement of the static position of the center of the carbody,

$$\begin{aligned}\epsilon_{d_o} &= mg \frac{\theta_{d_o}(0) + \theta_{d_o}(T)}{2} \tag{3.46} \\ &= (9850) \frac{1}{2} \frac{1 \text{ in}}{30 \times 12 \text{ in}} \\ &= 13.7 \text{ pounds}\end{aligned}$$

Again, this computation is a worst case estimate and the error magnitude in practice was probably much lower.

Finally, Equation 3.38 takes the form:

$$mg\bar{\theta}(t) = \frac{mg}{\dot{R}_x T_{av}} \Delta H + \epsilon_g + \epsilon_{c_o} + \epsilon_{d_o} + \epsilon_c + \epsilon_d \tag{3.47}$$

The only remaining errors due to drag force determination from Equation 3.27 are due to inaccuracies in the instantaneous speed difference $[\dot{R}_x(T) - \dot{R}_x(0)]$ and the load cell reading F_L . The error in instantaneous speed measurement is derived in Appendix C.6 and has the value 0.18 percent at 90 mph and 0.32 percent at 50 mph. Therefore, the errors in force measurement are

$$\begin{aligned}\epsilon_s &= \frac{m}{T} \times (\text{maximum error in speed}) \\ &= \frac{9850}{32.2} \cdot \frac{1}{30.3} \cdot 2 (0.0018 \times 132) \\ &= 4.80 \text{ pounds at 90 mph}\end{aligned}$$

and

$$\begin{aligned}\epsilon_s &= \frac{9850}{32.2} \cdot \frac{1}{54.5} \cdot 2(0.0032 \times 73.3) \\ &= 2.63 \text{ pounds at 50 mph}\end{aligned}$$

where the test duration $T = 30.3$ seconds at 90 mph and 54.5 seconds at 50 mph.

In addition to ϵ_s , errors are also incurred due to the assumed decoupling between carbody rotation and translation. These errors (ϵ_{dc}) are derived in Appendix C.2 where it is shown that

$$\begin{aligned}\epsilon_{dc} &= 4.77 \text{ pounds at 90 mph} \\ &= 2.62 \text{ pounds at 50 mph}\end{aligned}$$

Also, as pointed out in Appendix C.2, there are small errors in speed computation due to trailer translation relative to the carbody.

Thus

$$\begin{aligned}\epsilon_t &= 0.20 \text{ pounds at 90 mph} \\ &= 0.11 \text{ pounds at 50 mph}\end{aligned}$$

Finally, the errors in load cell reading \bar{F}_L in Equation 3.16 need to be considered. These are affected by (1) misalignments and nonlinearities in the force-balance system, (2) errors in the load cell itself and its associated electronics, and (3) errors due to averaging the \bar{F}_L signal. This error estimation is described below.

The calibration tests conducted by Brewer Engineering Laboratories (Appendix A) indicate that there was a maximum of one pound of nonlinearity in 1000 pounds longitudinal load. Also, the maximum error in the longitudinal load cell due to misalignment was found to be 18 pounds when a lateral load of 1390 pounds was applied. The point of application of this load was about one-fourth the trailer length off center and forward. With the lateral load applied at the center of the trailer, the maximum error was eight pounds in 1418 pounds.

Therefore, the worst case total RMS error is $\sqrt{(18)^2 + (1)^2}$
= 18.03 pounds and it is designated ϵ_{bal} .

Figure 3-10 is a schematic diagram of load cell and signal processing errors. The load cell accuracy applied to a BLH type U3G1 (capacity 5000 pounds) used in the longitudinal and lateral flexures. The overall figure of 0.03 millivolt accounts for nonlinearity, hysteresis and repeatability when a 10-volt excitation is employed. Using the scale factor of

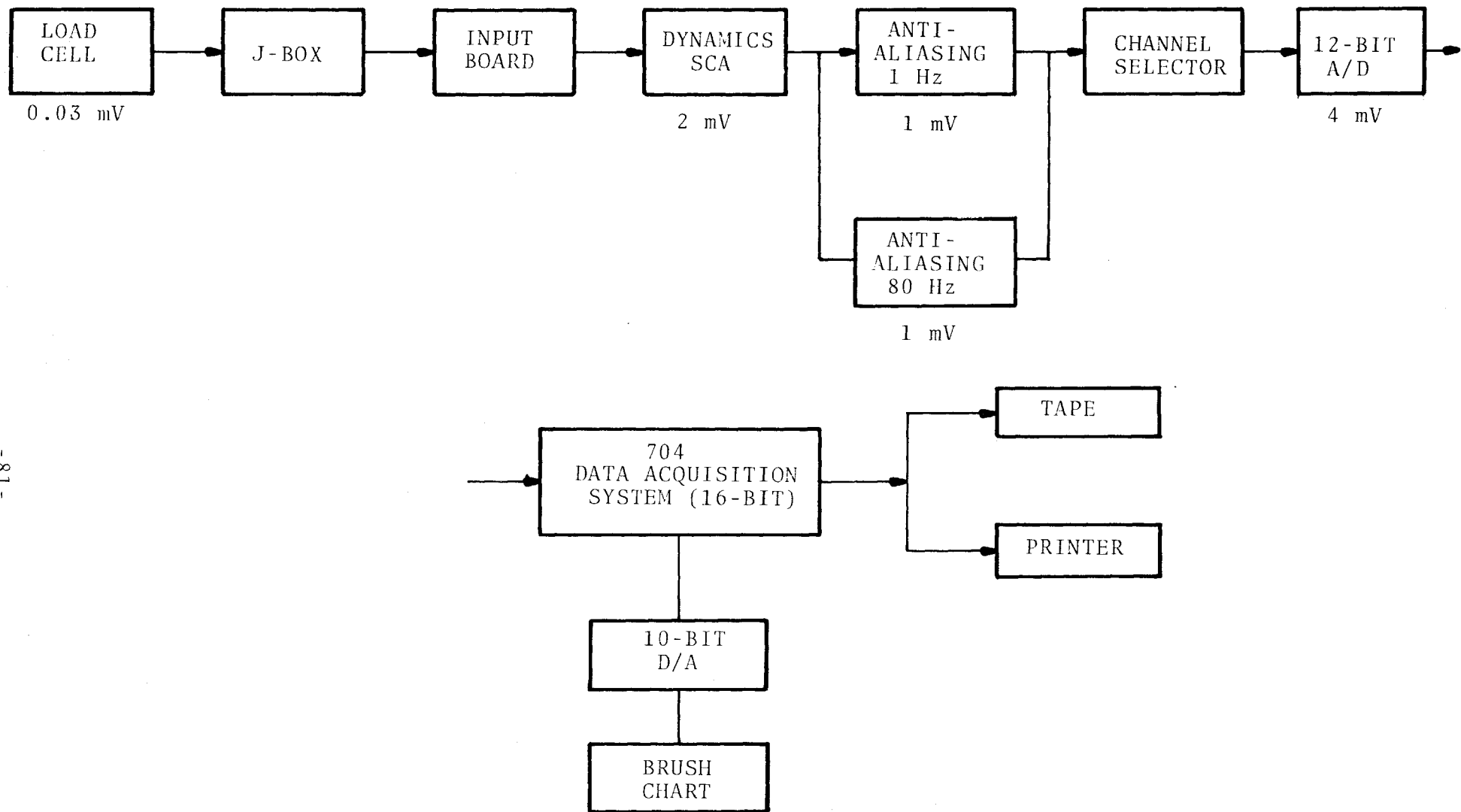


Figure 3-10. Load Cell and Signal Processing Errors

2 mV/lb for longitudinal and lateral load cells (Table 2-2) and the rated output of U3G1 (0.3 mV per volt excitation). the gain setting of the signal conditioning amplifier had the value

$$\frac{2 \text{ mV/lb} \times 5000 \text{ lb}}{3 \text{ mV/V} \times 10 \text{ V}} = 333.3$$

This is the factor by which the load cell nonlinearity errors are magnified and the resulting value is $0.03 \times 333.3 = 10 \text{ mV}$. Combining all the errors of Figure 3-10 in RMS manner, the load cell and signal processing errors are

$$\begin{aligned} \epsilon_L &= \sqrt{(10)^2 + (2)^2 + (1)^2 + (4)^2} \\ &= 11 \text{ millivolts} \end{aligned}$$

and the corresponding error in load cell reading is, for the scale factor 2 mV/lb,

$$\epsilon_L = \frac{11}{2} = 5.5 \text{ pounds}$$

The error due to averaging the longitudinal load cell reading F_L is given by Equation 3.39. The AERO/TOFC (Series II) raw data indicates that this signal displays a predominant frequency of 6 Hz with an amplitude of ± 750 pounds (at 70 mph). Hence, the averaging error is

$$\begin{aligned} \epsilon_{L_{av}} &= \frac{750}{\pi(6)(30.3)} = 1.3 \text{ pounds at 90 mph} \\ &= \frac{750}{\pi(6)(54.5)} = 0.73 \text{ pounds at 50 mph} \end{aligned}$$

In the preceding computations, it has been assumed that the signal frequency and amplitude do not vary appreciably with speed.

The drag force equation 3.16 now has the final form

$$\begin{aligned} \bar{D} = & -\bar{F}_L - \frac{m}{T} \left[\dot{R}_X(T) - \dot{R}_X(O) \right] - \frac{mg\Delta H}{\dot{R}_{X_{av}} T} - \epsilon_L - \epsilon_{L_{av}} - \epsilon_{bal} \\ & - \epsilon_s - \epsilon_{dc} - \epsilon_t - \epsilon_g - \epsilon_{c_o} - \epsilon_c - \epsilon_d \end{aligned} \quad (3.48)$$

Since the Equation 3.27

$$\bar{D} \approx -\bar{F}_L - \frac{m}{T} \left[\dot{R}_X(T) - \dot{R}_X(O) \right] - \frac{mg\Delta H}{\dot{R}_{X_{av}} T}$$

has been employed in onboard data processing, the RMS error in \bar{D} is, assuming independence of individual errors

$$\begin{aligned} \epsilon = & \left[\epsilon_L^2 + \epsilon_{L_{av}}^2 + \epsilon_{bal}^2 + \epsilon_s^2 + \epsilon_{dc}^2 + \epsilon_t^2 + \epsilon_g^2 \right. \\ & \left. + \epsilon_{c_o}^2 + \epsilon_{d_o}^2 + \epsilon_c^2 + \epsilon_d^2 \right]^{1/2} \end{aligned} \quad (3.49)$$

Table 3-2 is a list of error sources.

3.7.3 Errors in Side Force Determination

This error estimation follows closely the procedures for the drag force. Equation 3.31 was used for on-board computation of the side force and it is an approximation of the exact Equation 3.18. The errors are derived as follows:

Table 3-2. Errors in Drag Force Determination

Source of Error	Symbol	Magnitude (Pounds)	
		50 mph	90 mph
Load Cell and Signal Processing	ϵ_L	5.50	5.50
Averaging Longitudinal Load Cell Signal	$\epsilon_{L_{av}}$	0.73	1.30
Balance Misalignments and Nonlinearities	ϵ_{bal}	18.03*	18.03
Instantaneous Speed Measurement	ϵ_{bal}	2.63	4.80
Decoupling Between Rotational and Translational Motions	ϵ_{dc}	2.62	4.77
Trailer Translation Relative to Carbody	ϵ_t	0.11	0.20
Gravitational Force Approximation	ϵ_g	0.50	0.50
Permanent Change in Pitch Attitude of Carbody	ϵ_{c_o}	1.03†	1.03†
Permanent Change in Flexural Shape of Carbody	ϵ_{d_o}	13.70*	13.70*
Averaging Pitching Oscillations	ϵ_c	0.06	0.10
Averaging Flexural Oscillations	ϵ_d	0.04	0.06
Total RMS Error (Incl. Perm. Def.)	ϵ	23.60	24.30
Total RMS Error (Excl. Perm. Def.)	$\hat{\epsilon}$	19.20	20.10

* Absolute worst case estimates, actual values are probably as much as 50 percent lower. This reduces ϵ to 20.7 pounds and to 17.0 pounds at 50 mph and the corresponding values at 90 mph are 21.5 and 18.0 pounds, respectively.

† Based on post-test analysis of data.

3.7.2.1 Error Due to Ignoring the Gravitational Term $mg\bar{\psi}$ in Equation 3.18

The contribution $mg\bar{\psi}$ as given by Equation 3.32 can be further divided as follows

$$\begin{aligned} mg\bar{\psi} &= mg\bar{\psi}_g + mg\bar{\psi}_c + mg\bar{\psi}_d \\ &= mg\bar{\psi} + mg(\bar{\psi}_{c_o} + \Delta\bar{\psi}_c) + mg\bar{\psi}_d \end{aligned}$$

or

$$mg\bar{\psi} = mg\bar{\psi}_g + mg\bar{\psi}_{c_o} + mg\Delta\bar{\psi}_c + mg\bar{\psi}_d \quad (3.50)$$

The contribution of each term in Equation 3.50 will now be estimated. $\bar{\psi}_g$ is the average angle between the normal to the plane of the track and the local vertical direction measured in the y-z plane (Figure 3-5). Results of a recent survey (Reference 12) of the AERO/TOFC (Series II) test track indicate existence of a uniform 0.1-inch crosslevel ($\bar{\psi}_g$ positive in Figure 3-5). The corresponding systematic error in side force is

$$\begin{aligned} \bar{\psi}_g &= mg\bar{\psi}_g \\ &= +9850 \text{ lbf} \times \frac{0.1 \text{ inch}}{56 \text{ inch}} \\ &= +17.6 \text{ pound feet} \end{aligned} \quad (3.51)$$

$\bar{\psi}_{c_o}$ represents a slowly varying term analogous to $\bar{\theta}_{c_o}$ and may be replaced by the linear approximation

$$\bar{\psi}_{c_o} = \left[\frac{\psi_{c_o}(o) + \psi_{c_o}(T)}{2} \right]$$

Since $mg\bar{\psi}_{c_o}$ is neglected altogether, the resulting error is

$$\begin{aligned}\delta_{c_o} &= mg\psi_{c_o} \\ &= mg \left[\frac{\psi_{c_o}(o) + \psi_{c_o}(T)}{2} \right] \quad (3.52)\end{aligned}$$

Introducing an estimate of a one-inch peak-to-peak relative displacement between the right side and the left side of the carbody,

$$\begin{aligned}\frac{1}{2} \left[\psi_{c_o}(o) + \psi_{c_o}(T) \right]_{\max} &= \frac{1}{2} \frac{1 \text{ in}}{60 \text{ in}} \\ &= 8.33 \times 10^{-3} \text{ radian} \\ &\quad (0.48 \text{ degree})\end{aligned}$$

$$\text{Hence, } \delta_{c_o} = (9850)(8.33 \times 10^{-3})$$

$$= 82.1 \text{ pounds}$$

A post-test verification of the magnitude of ψ_{c_o} was carried out using the displacement transducer data before and after a test series (Section 4.0). The results are listed in Tables 4-6A, 4-6B and 4-7. It was found that the displacements were very small and the maximum value of $mg\psi_{c_o}$ was 8.5 pounds. The error due to averaging $mg\Delta\psi_c$ will be small as indicated by the computations of $mg\bar{\psi}_c$ and need not be calculated. Also, flexural deformations in the lateral direction are negligible compared with other deformations. Therefore, the associated force errors can be ignored in comparison with other error contributions.

3.7.2.2 Error Due to Ignoring the Momentum Term
in Equation 3.18

This error is

$$\delta_s = \frac{m}{T} \left[\dot{R}_y(T) - \dot{R}_y(o) \right] \quad (3.53)$$

An estimate for the lateral speed can be obtained using the data of Table 3-1. For the sway mode with a frequency of 2.5 Hz and an acceleration amplitude 0.2 g

$$\begin{aligned} \dot{R}_y &\approx \frac{(0.2)(32.2) \text{ ft/sec}^2}{2\pi(2.5)/\text{sec}} \\ &= 0.41 \text{ feet per second} \end{aligned}$$

Thus

$$\left[\dot{R}_y(T) - \dot{R}_y(o) \right]_{\max} = 2(0.41) = 0.82 \text{ feet per second}$$

Hence

$$\begin{aligned} \delta_s &= \frac{9850}{32.2} \left(\frac{1}{30.3} \right) (0.82) \\ &= 8.3 \text{ pounds at 90 mph} \end{aligned}$$

and

$$\begin{aligned} \delta_s &= \frac{9850}{32.2} \left(\frac{1}{54.5} \right) (0.82) \\ &= 4.6 \text{ pounds at 50 mph} \end{aligned}$$

As in the case of drag force, the side force determination is subject to errors due to decoupling of translational and rotational trailer motions relative to the carbody. As shown in Appendix C.7 these errors are

$$\begin{aligned}\delta_{dc} &= 16.1 \text{ pounds at 90 mph} \\ &= 8.9 \text{ pounds at 50 mph}\end{aligned}$$

In addition, small errors are present due to translation of the trailer relative to the carbody and from Appendix C.7

$$\begin{aligned}\delta_t &= 0.20 \text{ pound at 90 mph} \\ &= 0.11 \text{ pound at 50 mph}\end{aligned}$$

3.7.2.3 Error in Rear Lateral Load Cell Reading F_{s_1}

For a BLH U3G1 (5000-pound) load cell in conjunction with an amplifier of gain 333.3, the RMS error in Figure 3-10 has the value

$$\sqrt{(0.03 \times 333.3)^2 + (2)^2 + (1)^2 + (4)^2} = 11 \text{ millivolts}$$

The load-cell scale factor is 2 mV/lb (Table 2-2), therefore, the error in F_{s_1} is

$$\delta_{s_1} = \frac{11}{2} = 5.5 \text{ pounds}$$

3.7.2.4 Error in Front Lateral Load Cell Reading F_{s_2}

For the same load cell (Paragraph 3.7.2.3) with an amplifier gain of 333.3 and a scale factor equal to 2 mV/lb, the error is

$$\delta_{s_2} = 5.5 \text{ pounds}$$

The error due to averaging the load cell signals F_{s_1} and F_{s_2} is given by Equation 3.39. As indicated by the AERO/TOFC (Series II) raw data, both the front and rear lateral-load-cell outputs are characterized by a predominant low frequency of 1.8 Hz with an amplitude of ± 1000 pounds. Then the error due to averaging is

$$\delta_{s_{1_{av}}} = \delta_{s_{2_{av}}} = \frac{1000}{\pi(1.8)(30.3)} = 5.84 \text{ pounds at 90 mph}$$

$$\delta_{s_{1_{av}}} = \delta_{s_{2_{av}}} = \frac{1000}{\pi(1.8)(54.5)} = 3.24 \text{ pounds at 50 mph}$$

The preceding computations assume that the signal amplitude and frequency do not vary appreciably with speed.

Finally, errors in F_{s_1} and F_{s_2} also occur due to misalignments and nonlinearities in the force balance system. The calibration data in Appendix A reveals that there is a maximum combined nonlinearity of 26 pounds in the front and rear lateral load cells. Also, maximum error due to misalignment was found to be 13 pounds in the two lateral load cells. Therefore, the total RMS error is

$$\delta_{bal} = \sqrt{(26)^2 + (13)^2} = 29.1 \text{ pounds}$$

3.7.2.5 Error Due to Omission of the Centrifugal Force Term in Equation 3.18

The average centrifugal force, CF is given by

$$CF = m \left[\frac{\dot{R}_x^2(t)}{\dot{R}_c(t)} \right] = \frac{m}{T} \int_0^T \frac{\dot{R}_x^2(t)}{\dot{R}_c(t)} dt$$

Using the distance-time transformation

$$t = t(x)$$

$$CF = \frac{m}{T} \int_0^{\Lambda} \frac{\dot{R}_x^2[t(x)]}{\dot{R}_c[t(x)]} \frac{d[t(x)]}{dx} dx \quad (3.54)$$

Expressing the integral explicitly as a function of x

$$CF = \frac{m}{T} \int_0^{\Lambda} \frac{\dot{R}_x^2(x)}{\dot{R}_c(x)} \frac{dt}{dx} dx$$

It may be recalled that $R_c(x)$ is the radius of curvature of the locus of the trailer center of gravity in the x-y plane (Figure 3-5). Let the equation of this locus be

$$y = q(x) \quad (3.55)$$

Then the curvature is given by

$$\frac{1}{R_c(x)} = \frac{q''}{(1 + q'^2)^{3/2}} \quad (3.56)$$

The locus of the center of gravity of the trailer deviates from the centerline of the track for two reasons: (1) lateral movement of the carbody within the rails and (2) lateral motion of the trailer relative to the longitudinal axis of symmetry of the carbody. These motions, however, will be confined within a small distance $\pm\mu$ from the centerline of the track. This situation is illustrated in Figure 3-11.

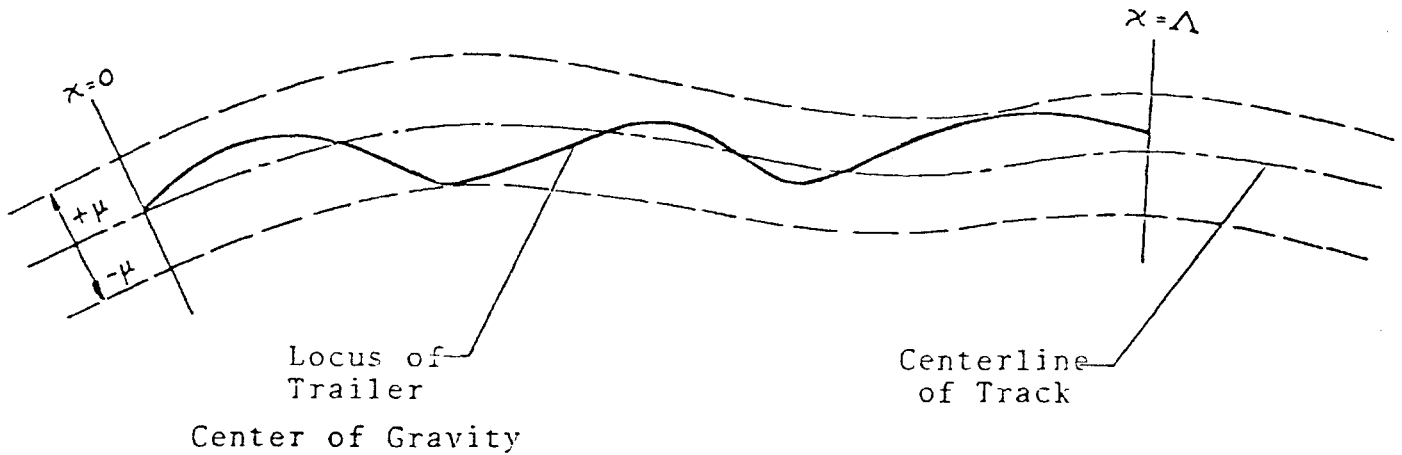


Figure 3-11. Motion of Trailer Center of Gravity in x-y Plane

Due to the inertia of the massive trailer in the direction of motion, the excursions of its center of gravity must occur gradually and, therefore, the slope $q'(x)$ is expected to be small, i.e.,

$$q'^2(x) \ll 1, \quad 0 \leq x \leq \Lambda \quad (3.57)$$

Then Equation 3.56 becomes

$$\frac{1}{R_c(x)} \approx q'' \quad (3.58)$$

and Equation 3.54 reads

$$CF = \frac{m}{T} \int_0^{\Lambda} q''(x) \dot{R}_x^2(x) \frac{dt}{dx} dx$$

Further, for purposes of error estimation, it may be assumed that

$$\dot{R}_x(x) = \frac{dx}{dt} = \dot{R}_{x_{av}} = \text{constant}$$

Hence,

$$CF = \frac{m\dot{R}_{xav}}{T} \int_0^{\Lambda} q'' dx$$

or

$$CF = \frac{m\dot{R}_{xav}}{T} [q'(\Lambda) - q'(0)] \quad (3.59)$$

It is, therefore, necessary to estimate the slope of the locus in Equation 3.59. The slope q' is affected by the slope of the track itself, the position of the wheels of the carbody on the rails and the yawing of the carbody with respect to the trucks in addition to the trailer motions relative to the carbody. A very rough estimate is obtained as follows. The track survey of Reference 12 indicates a maximum slope (alignment deviation) of 0.004 radian. If the relative lateral motion between the front axle of the front truck and the rear axle of the front truck and the rear axle of the rear truck is 2 inches over the carbody wheelbase of 60 feet, the corresponding angle is 0.003 radian. Accounting for carbody yaw and trailer motions, a reasonable value of the slope is ± 0.01 radian (5.7 degrees). Substituting approximate numbers in Equation 3.59,

$$CF = \frac{9850}{32.2} \left(\frac{132}{30.2} \right) (\pm 0.01 \pm 0.01)$$

$$= \pm \frac{9850 \times 132 \times 0.02}{32.2 \times 30.3}$$

$$= \pm 26.8 \text{ pounds at 90 mph}$$

and

$$CF = \pm \frac{12400 \times 73.3 \times 0.02}{32.2 \times 54.5}$$

$$= \pm 8.3 \text{ pounds at 50 mph}$$

Thus, the error due to ignoring the centrifugal force is

$$\begin{aligned}\delta_{cf} &= 26.8 \text{ pounds at 90 mph} \\ &= 8.3 \text{ pounds at 50 mph}\end{aligned}$$

Finally, Equation 3.18 can be written very closely as

$$\begin{aligned}\bar{S} &= \bar{F}_{s1} + \bar{F}_{s2} + \delta_{s1_{av}} + \delta_{s2} + \delta_{s2_{av}} + \delta_{bal} + \delta_g \\ &+ \delta_{co} + \delta_s + \delta_{dc} + \delta_t + \delta_{cf}\end{aligned}\quad (3.60)$$

A compilation of errors in side force is presented in Table 3-3. Excluding the systematic error δ_g , the other errors can be combined to yield a RMS type composite error as follows

$$\begin{aligned}\delta &= \sqrt{\left[\delta_{s1}^2 + \delta_{s1_{av}}^2 + \delta_{s2}^2 + \delta_{s2_{av}}^2 + \delta_{bal}^2 + \delta_{co}^2 \right. \\ &\quad \left. + \delta_s^2 + \delta_{dc}^2 + \delta_t^2 + \delta_{cf}^2 \right]}\end{aligned}\quad (3.61)$$

Table 3-3
 ERRORS IN SIDE FORCE DETERMINATION

Source of Error	Symbol	Magnitude (Pounds)	
		50 mph	90 mph
Front Lateral Load Cell and Signal Processing	δ_{s_2}	5.50	5.50
Averaging Front Lateral Cell Signal	$\delta_{s_2_{av}}$	3.24	5.84
Rear Lateral Load Cell and Signal Processing	δ_{s_1}	5.50	5.50
Averaging Rear Lateral Load Cell Signal	$\delta_{s_1_{av}}$	3.24	5.84
Blance Misalignments and Nonlinearities	δ_{bal}	29.10*	29.10*
Gravitational Force Due to Crosslevel	δ_g	17.60†	17.60†
Permanent Change in Roll Attitude of Carbody	δ_{c_o}	8.50	8.50
Lateral Momentum of Carbody	δ_s	4.60	8.30
Decoupling Between Translational and Rotational Motions	δ_{dc}	8.90	16.10
Trailer Translation Relative to Carbody	δ_t	0.11	0.20
Centrifugal Force	δ_{cf}	8.30	26.80
Total RMS Error (Incl. Perm. Def.)	δ	34.20	45.80
Total RMS Error (Excl. Perm. Def.)	$\hat{\delta}$	33.10	45.00

* A worst case estimate, actual values are probably much lower.

† Based on post-test analysis of data.

4.0 REDUCTION OF TEST DATA

4.1 GENERAL

The process of data reduction involves performing certain operations on the voluminous raw data to put it into a manageable and useful intermediate form. Data analysis consists of manipulating and interpreting the reduced data to produce certain results. The test data collected in AERO/TOFC (Series II) was reduced and analyzed in two phases. In the first phase, data was processed in near-real time onboard T-5, using computational procedures developed in the previous section. A preliminary analysis was conducted simultaneously to examine the quality of the data and to establish its repeatability and meaningfulness. The second phase included additional calculations and an in-depth analysis to ascertain the fine structure and the behavior of the data.

This section deals with the details of onboard and post-test data reduction methods and includes tables of AERO/TOFC (Series II) data. The analysis procedures including the graphic display of the data are covered in Section 5.0.

4.2 ONBOARD DATA REDUCTION

As mentioned in Section 2.4.4, the AERO/TOFC (Series II) data was filtered at two frequencies, one Hz and 80 Hz. Data reduction was performed on the one-Hz filtered data using procedures described in Appendix D. The first step was to average all data channels over the duration of the test run. This process was straight forward with the exception of the onboard and wayside wind vectors \vec{V} and \vec{W} , respectively. The individual components of these quantities were averaged as follows,

$$\bar{V}_x = \overline{|\vec{V}| \cos\alpha} \quad (4.1a)$$

$$\bar{V}_y = \overline{|\vec{V}| \sin\alpha} \quad (4.1b)$$

$$\bar{W}_x = \overline{|\vec{W}| \cos\beta} \quad (4.2a)$$

$$\bar{W}_y = \overline{|\vec{W}| \sin\beta} \quad (4.2b)$$

where $|\vec{V}|$ and $|\vec{W}|$ denote the onboard and wayside wind speed, respectively. α and β are the wind directions relative to the direction of train motion. $|\vec{V}|$, $|\vec{W}|$, α and β were measured continuously during test runs (Section 2.4).

The drag and side forces were calculated by applying Equations 3.27 and 3.31 to each trailer. The load cell term \bar{F}_9 was replaced by \bar{F}_3 for Trailer A and by \bar{F}_q for Trailer B. Similarly, \bar{F}_{S_1} and \bar{F}_{S_2} are substituted by \bar{F}_2 and \bar{F}_6 for Trailer A and by \bar{F}_8 and \bar{F}_{12} for Trailer B. The reader is referred to Table 2-2 for the load cell identifications. No cross-axis response correction was necessary to the averaged load cell readings due to careful flexure alignment prior to the test (Appendix A). The momentum and gravitational contributions in Equation 3.27 were computed using the relative velocity (between the instrumented TTX and T-5) data as detailed in Appendix D. In addition to drag and side forces, the complimentary lift force on each trailer was computed by the formulas

$$L\bar{F}_A = \bar{F}_1 + \bar{F}_4 + \bar{F}_5 \quad (4.3a)$$

and
$$L\bar{F}_B = \bar{F}_7 + \bar{F}_{10} + \bar{F}_{11} \quad (4.3b)$$

As pointed out in References 1 and 2, the aerodynamic force scale with respect to the dynamic pressure which is defined as

$$q = \frac{1}{2} \rho V_{rel}^2 \quad (4.4)$$

where ρ is the density of the air and V_{rel} is the speed of the air relative to the train. During the AERO/TOFC (Series II) tests, the air density was computed at the beginning of each test series using the procedure described in Appendix D. The square of onboard relative wind speed was obtained from the equation

$$V_{rel}^2 = \left| \bar{V}_{rel} \right|^2 = (\bar{V}_x)^2 + (\bar{V}_y)^2 \quad (4.5)$$

where \bar{V}_x and \bar{V}_y are given by Equations 4.1a and 4.1b. The force area for each trailer was computed by dividing the drag, side and lift forces by the dynamic pressure. Thus

$$\text{Drag Area} = \frac{\text{Drag Force}}{\text{Dynamic Pressure}} \quad (4.6a)$$

$$\text{Side Force Area} = \frac{\text{Side Force}}{\text{Dynamic Pressure}} \quad (4.6b)$$

and
$$\text{Lift Area} = \frac{\text{Lift Force}}{\text{Dynamic Pressure}} \quad (4.6c)$$

The total force areas for the two trailers were obtained by summing corresponding force areas of each trailer. Again, the details of this procedure are listed in Appendix D.

The results of onboard data processing are shown in a sample computer output in Appendix D. Some minor corrections were applied to the onboard reduced data. For example, during the first two days of testing (5 and 6 December 1977), the measured onboard relative wind direction was reduced by a factor of 0.78 due to an electrical gain factor error. Also, the electrical zero was found to have an offset of 0.8 degrees and an appropriate correction was made. Another problem of an intermittent nature was the saturation of the electrical output of the onboard speed indicator. When this occurred, relative wind

speed and direction was calculated using average train speed and wayside wind vector (Section 4.3) and used in subsequent computations. As mentioned in Section 3.7.2, there is a systematic error of +17.6 pounds per trailer in the side force and it was subtracted before calculating side force areas for final tabulation. The final results of the AERO/TOFC (Series II) onboard data reduction are presented in Tables 4-1A, 4-2A and 4-3A for Configuration 1 and Tables 4-1B, 4-2B and 4-3B for Configuration 2. These tables are included at the end of this section.

4.3 POST-TEST DATA REDUCTION

The exercise in this phase consisted of (1) a comparison between onboard wind measurements and those resulting from combining the average train speed with the wayside wind vector, (2) calculation of force areas based on calculated relative wind data, (3) derivation of rolling resistance information, and (4) determining changes in roll and pitch attitudes of the deck plate of the instrumented TTX car during the test series. These are described in the following sections.

4.3.1 Comparison of Relative Velocity Data Between Onboard and Wayside Measurements

Figures 4-1a and 4-1b show the coordinate systems used for wayside and onboard wind directions. The average train speed and the wayside wind vector are combined as shown in Figure 4-2.

Therefore

$$|\vec{V}|^2 = |\vec{T}|^2 + |\vec{W}|^2 - 2|\vec{T}| |\vec{W}| \cos\beta \quad (4.7a)$$

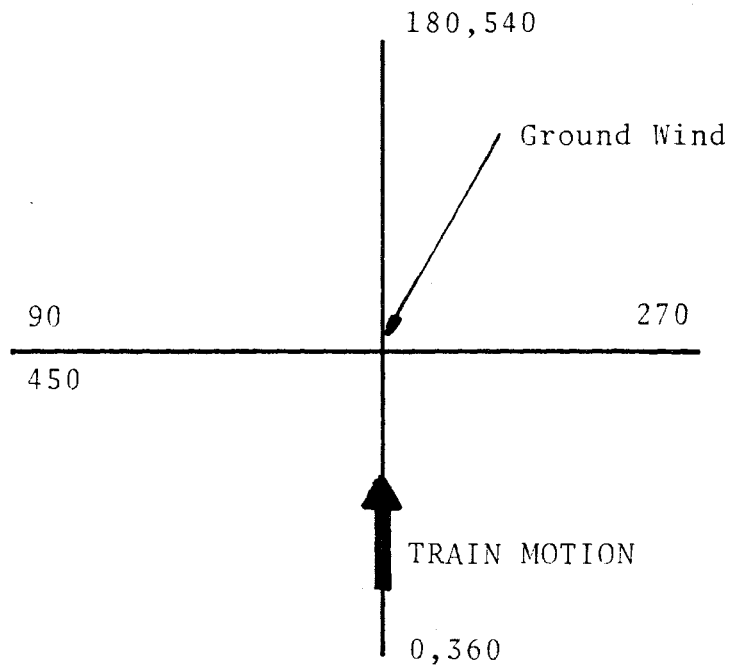


Figure 4-1a. Coordinate System for Wayside Wind Direction.

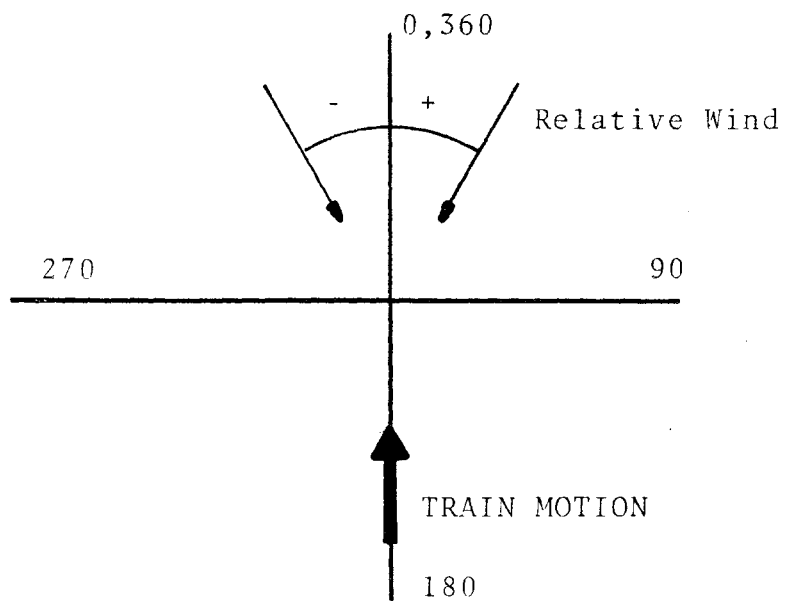


Figure 4-1b. Coordinate System for Onboard Wind Direction.

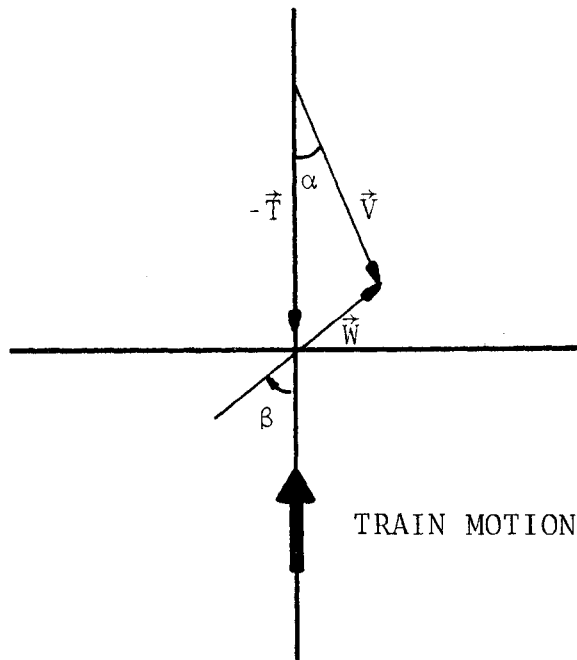


Figure 4-2. Calculation of Relative Wind Vector from Wayside Wind Data

and

$$\alpha = \tan^{-1} \left[\frac{-W \sin \beta}{T - W \cos \beta} \right] \quad (4.7b)$$

where β is measured in the coordinate system of Figure 4-1a. The resulting value of α from Equation 4.7b corresponds to the coordinate system of Figure 4-1b.

Sample Calculation: Consider Run Number 98 in Table 4-1A where,

$$|\vec{T}| = 127.55 \text{ feet/second}$$

$$|\vec{W}| = 24.53 \text{ feet/second}$$

$$\beta = 252.53 \text{ degrees}$$

Then, from Equation (4.6a),

$$|\vec{T}|^2 = (127.55)^2 + (24.53)^2 - 2(127.55)(24.53) \cos(252.53) = 18749.3$$

or

$$|\vec{V}| = 136.93 \text{ feet/second}$$

and

$$\alpha = \tan^{-1} \left[\frac{(24.53) \sin(252.53)}{127.55 - 24.53 \cos(252.53)} \right] \\ = 9.84 \text{ degrees}$$

Adding 180 degrees, the calculated wind direction appears as 189.84 degrees in Table 4-1A.

4.3.2 Comparison of Force Area Data Based on Onboard Wind Data and Vectored Wind Data

As described in Section 4.2, onboard data reduction resulted in force areas based on onboard relative wind speed. A similar computation was performed to obtain force areas based on calculated relative wind speed (Section 4.3.1). First, dynamic pressure based on calculated wind speed was obtained using the relation,

$$\frac{q_{\text{cal}}}{q_{\text{onboard}}} = \frac{|\vec{V}|_{\text{cal}}^2}{|\vec{V}|_{\text{onboard}}^2} \quad (4.8)$$

Next, the force areas were computed from the ratio

$$\frac{\text{Calculated Force Area}}{\text{Onboard Force Area}} = \frac{q_{\text{onboard}}}{q_{\text{cal}}}$$

Sample calculation: Again consider Run Number 98 in Table 4-1A, where

$$|\vec{V}|_{\text{cal}} = 136.93 \text{ feet/second}$$

$$|\vec{V}|_{\text{onboard}} = 151.29 \text{ feet/second}$$

From Table 4-3A

$$q_{\text{onboard}} = 22.90 \text{ pounds/square foot}$$

$$\text{Total Drag Area} = 73 \text{ square feet}$$

Then, using Equation 4.7

$$\begin{aligned} q_{\text{cal}} &= 22.90 \frac{(136.93)^2}{(151.29)^2} \\ &= 18.76 \text{ pounds/square foot} \end{aligned}$$

and Equation 4.8 yields

$$\begin{aligned} (\text{Drag Area})_{\text{cal}} &= \frac{22.90}{18.76} (73) \\ &= 89.11 \text{ square feet} \end{aligned}$$

Results of these computations are compiled in Tables 4-4A and 4-4B.

4.3.3 Derivation of Rolling Resistance Information

As shown in Appendix C.9, the average rolling resistance \bar{R} of the instrumented TTX car (combined with its average aerodynamic drag \bar{D}_C) is given by

$$\begin{aligned}
(\bar{R} + \bar{D}_C) &= (\bar{F}_{\text{lead}} - \bar{F}_{\text{trail}}) + (m_C + 2m)g\sin\theta \\
&- (\bar{D}_A + \bar{D}_B) - \frac{1}{T} (m_C + 2m) [\dot{x}(T) - \dot{x}(0)]
\end{aligned}
\tag{4.10}$$

where \bar{F}_{lead} and \bar{F}_{trail} are the average leading and trailing coupler forces and \bar{D}_A and \bar{D}_B are average drag forces on Trailers A and B, respectively. The quantities m and m_C denote the mass of one trailer and the mass of the instrumented TTX car including the force-balance structure, respectively. $\dot{x}(0)$ and $\dot{x}(T)$ are initial and final train speed of the TTX car. A typical calculation of rolling resistance was performed as follows:

Sample calculation: Consider Run Number 98 in Table 4-2A

$$\bar{D}_A + \bar{D}_B = 1691 \text{ pounds}$$

The weight of the balance structures and the support frames on the TTX car was calculated from drawings and has the value 9850 pounds. Adding this to the weight of the flat car (67,000 pounds), the total weight is 76,850 pounds which is believed to be accurate within one percent. Since the trailer weighs 9,850 pounds

$$(m_C + 2m)g = 97050 \text{ pounds}$$

so that $(m_C + 2m) = \frac{97050}{32.14} = 3019.60$ slugs. For the AERO/TOFC (Series II) test zone the average downhill grade is 0.275 percent, i.e.,

$$\sin\theta \approx \theta = 0.00275 \text{ radian}$$

From Table 4-5A for Run Number 98

$$\bar{F}_{\text{lead}} = 1881 \text{ pounds}$$

$$\bar{F}_{\text{trail}} = -82 \text{ pounds}$$

$$\dot{x}(0) = 131.45 \text{ feet/second}$$

$$\dot{x}(T) = 124.22 \text{ feet/second}$$

$$T = 31.50 \text{ seconds (calculated from the total number of samples divided by the sampling rate of 256 Hz)}$$

Finally,

$$\begin{aligned}(\bar{R} + \bar{D}_C) &= 1881 - (-82) + 97050 \times 0.00275 \\ &\quad - (1691) - \frac{3019.60}{31.50} [124.22 - 131.45] \\ &= 1963 + 267 - 1691 + 693 \\ &= 1232 \text{ pounds}\end{aligned}$$

It should be noted that the term $(\bar{F}_{\text{lead}} - \bar{F}_{\text{trail}})$ in Equation 4.10 represents the total tractive resistance (rolling plus aerodynamic) of the flat car with two trailers. It has a value of 1963 pounds in the above example. The rolling resistance data for Configurations 1 and 2 are listed in Tables 4-5A and 4-5B, respectively.

4.3.4 Changes in Attitude of Flat Car Deck Plate

As pointed out in Sections 3.7.1 and 3.7.2, large errors can occur in drag and side force measurements due to permanent changes in the pitch and roll attitudes of the carbody deck plate. Therefore, a post-test verification of these changes was conducted, along with a compilation of zero-shifts of the force-balance and coupler transducers. The results are given in Table 4-6A for Configuration 1 and Table 4-6B for Configuration 2. The zero changes have been computed between the

beginning and the end of a test series, when the instrumented flat car was parked at the same location inside the CSB. Displacement transducer data in Tables 4-6A and 4-6B was used to determine the roll and pitch angle from Equations 3.28 and 3.33. The corresponding trailer-weight components were also calculated and are listed in Table 4-7. It is evident that the carbody underwent negligible changes in pitch and very small changes in roll attitude. The maximum trailer weight components were 1.03 pounds due to pitch and 8.52 pounds due to roll.

The aforementioned attitude information was obtained from displacement transducer data rather than the gyroscopic data because the latter appeared to be erroneous. The average carbody roll and pitch during the test runs were computed onboard using displacement data as shown on the sample computer output (Appendix D). The pitch angles were insignificant (maximum value 0.001 degrees) and roll angles were very small (largest value 0.003 degrees). The corresponding errors in longitudinal force (0.17 pound) and lateral force (0.52) pound were negligibly small.

Table 4-1A
Wind Speed and Direction Data - Configuration 1

Run No.	Nom. Train Speed	Avg. Train Speed	Wayside Wind		Onboard Relative Wind		Calculated Relative Wind	
			Speed	Dir.†	Speed	Dir.††	Speed	Dir.††
	mph	Ft/Sec	Ft/Sec	Degrees	Ft/Sec	Degrees	Ft/Sec	Degrees
51*	50	69.68*	7.82	471.87	69.91	173.15	72.95*	174.29*
52	50	75.38	6.91	434.76	71.98	175.95	73.86	174.82
53	50	68.96	6.83	457.52	70.16	175.53	70.18	174.46
54	70	97.94	7.63	424.11	91.62	177.78	94.85	175.85
55	70	99.10	3.43	386.22	92.50	178.17	96.03	179.10
56	70	99.07	2.99	440.98	94.33	178.61	98.65	178.28
57	90	127.88	3.43	401.12	122.70	179.54	125.32	178.97
58	90	132.12	3.14	386.67	127.49	180.00	129.32	179.32
59	90	132.08	0.549	381.25	126.91	179.51	131.56	179.91
60	30	49.57	4.71	432.47	45.68	178.18	48.36	174.67
61	20	34.36	4.07	444.94	31.16	173.92	134.24	173.20
62	50	68.54	10.05	217.71	79.19	187.40	76.74	184.59
63	50	70.85	21.62	252.98	82.72	193.76	80.00	195.00
64*	50	69.01*	20.62	245.94	87.49	193.00	79.67*	193.67*
65	70	96.12	22.51	244.85	107.36	189.95	107.63	190.91
66	70	102.55	17.19	256.18	111.42	188.10	107.95	188.89
67	70	102.83	15.66	254.02	110.66	187.40	108.19	188.00
68	90	134.18	10.27	368.89	126.73	180.78	124.04	179.27
69	90	132.46	7.19	100.37	129.57	176.98	133.94	176.97
70	90	133.43	9.06	425.82	124.98	177.86	129.98	176.35

* Possibly erroneous data due to (i) incorrect average train speed measurement and/or (ii) incorrect onboard wind measurements.

† Measured relative to coordinate system in Figure 4-1a.

†† Measured relative to coordinate system in Figure 4-1b plus 180 degrees.

Table 4-1A (CONT)
Wind Speed and Direction Data - Configuration 1

Run No.	Nom. Train Speed	Avg. Train Speed	Wayside Wind		Onboard Relative Wind		Calculated Relative Wind	
			Speed	Dir.†	Speed	Dir.††	Speed	Dir.††
	mph	Ft/Sec	Ft/Sec	Degrees	Ft/Sec	Degrees	Ft/Sec	Degrees
71	50	75.92	11.04	395.58	62.85	177.20	67.25	174.52
72	50	74.76	11.11	412.50	63.72	175.20	68.57	172.61
73	50	75.43	16.70	406.89	58.75	173.10	65.17	169.22
74	50	77.23	3.88	461.40	76.18	179.33	78.08	177.21
75	50	76.58	3.81	370.59	72.17	179.85	72.84	179.45
76	50	76.88	5.83	413.67	71.73	179.56	73.58	176.34
77*	70	102.80	7.54	379.26	102.55*	180.25	95.71	178.51
78	70	100.68	10.14	287.18	102.59	183.30	98.16	185.66
79	70	100.04	15.32	284.79	103.01	189.02	97.26	188.76
80	90	132.17	9.37	240.97	134.50	183.37	135.96	183.42
81	90	133.56	7.22	254.99	134.33	183.11	135.61	182.95
82	90	132.46	11.52	251.33	142.01	184.94	136.58	184.58
83*	50	66.76*	9.79	186.99	81.78	181.11	76.49*	180.89*
84*	50	64.90*	5.83	182.40	79.99	179.60	70.73*	180.20*
85*	50	68.15*	12.58	148.71	83.03	174.47	79.17*	175.27*
86	70	101.85	6.42	211.41	104.36	180.10	107.38	181.79
87	70	101.82	1.45	187.17	101.24	181.47	103.26	180.10
88	70	99.31	0.844	297.75	100.28	181.70	99.92	180.43

* Possibly erroneous data due to (i) incorrect average train speed measurement and/or (ii) incorrect onboard wind measurements.

† Measured relative to coordinate system in Figure 4-1a.

†† Measured relative to coordinate system in Figure 4-1b plus 180 degrees.

Table 4-1A (CONT)
Wind Speed and Direction Data - Configuration 1

Run No.	Nom. Train Speed	Avg. Train Speed	Wayside Wind		Onboard Relative Wind		Calculated Relative Wind	
			Speed	Dir.†	Speed	Dir.††	Speed	Dir.††
	mph	Ft/Sec	Ft/Sec	Degrees	Ft/Sec	Degrees	Ft/Sec	Degrees
89*	90	133.80	19.53*	-474.64	131.98*	159.38*	143.05*	187.13*
90*	90	132.83	10.80	-	138.77	180.46	-	-
91	90	132.71	18.70	90.27	139.81	181.27	134.11	171.98
92	55	79.54	10.81	261.56	85.85	179.74	81.83	187.51
93	55	81.83	9.94	154.05	98.38	178.74	90.87	177.26
94*	70	92.31*	16.09	234.13	128.29	193.67	102.57*	187.30*
95	70	99.53	19.40	240.66	122.56	193.30	110.34	189.82
96	70	100.99	20.74	249.51	126.55	194.70	109.98	190.17
97	90	130.72	27.02	301.19	129.02	193.49	118.99	191.20
98	90	127.55	24.53	252.53	151.29	194.89	136.93	189.84
99	90	131.32	27.78	239.40	152.42	191.12	147.41	189.33
100	55	77.18	21.08	241.52	107.68	196.66	89.18	191.99
101*	55	78.72*	20.70	241.09	106.65	197.24	90.56*	191.54*
102	55	78.91	21.01	238.18	105.45	196.09	91.74	191.22

* Possibly erroneous data due to (i) incorrect average train speed measurement and/or (ii) incorrect onboard wind measurements.

† Measured relative to coordinate system in Figure 4-1a.

†† Measured relative to coordinate system in Figure 4-1b plus 180 degrees.

Table 4-1B
Wind Speed and Direction Data - Configuration 2

Run No.	Nom. Train Speed	Avg. Train Speed	Wayside Wind		Onboard Relative Wind		Calculated Relative Wind	
			Speed	Dir.+	Speed	Dir.++	Speed	Dir.++
	mph	Ft/Sec	Ft/Sec	Degrees	Ft/Sec	Degrees	Ft/Sec	Degrees
23	50	76.29	14.50	431.20	66.78	173.30	72.92	169.15
24	50	77.21	12.30	433.93	68.17	173.40	74.75	170.90
25	70	99.29	16.95	421.39	89.03	173.27	92.38	170.73
26	70	103.71	17.08	434.85	84.10	174.59	100.61	170.57
27*	90	125.10	14.05	420.92	SAT 118.9(CALC)	173.63	118.91	174.07
28*	90	126.65	16.10	445.45	SAT 125.4(CALC)	171.94	125.40	172.65
29	50	72.48	15.86	429.88	68.66	170.84	68.66	167.47
30	70	102.37	16.70	449.74	96.22	172.64	103.65	170.73
31*	90	123.69	18.97	444.28	SAT 123.3(CALC)	173.42	123.25	171.19
32	50	75.42	4.40	162.63	79.33	179.90	79.63	179.05
33	70	99.37	4.02	199.83	101.50	180.88	103.16	180.76
34*	90	127.93	6.31	140.44	SAT 132.9(CALC)	180.95	132.86	178.27
35*	90	128.98	0.97	149.58	SAT 129.8(CALC)	181.16	129.82	179.78
36	70	102.76	3.16	148.03	106.94	180.32	105.45	179.09
37	50	77.07	5.27	69.32	78.81	178.76	75.37	176.25
38	50	78.18	2.35	416.79	77.38	180.71	76.92	178.53
39	70	98.77	1.69	357.95	98.30	179.93	97.08	180.04
40*	90	137.58	2.92	68.86	SAT 136.6(CALC)	180.79	136.55	178.86

* Possibly erroneous data due to (i) incorrect average speed and/or (ii) incorrect onboard relative speed.
† Measured relative to coordinate system in Figure 4-1a.
++ Measured relative to coordinate system in Figure 4-1b plus 180°.
SAT Denotes saturation of the electrical output of the onboard wind speed and direction sensor.
(CALC) Relative wind speed and direction calculated by vectoring average train speed and wayside wind data. These values were used when onboard wind data was not available.

Table 4-1B (CONT)
Wind Speed and Direction Data - Configuration 2

Run No. @	Nom. Train Speed	Avg. Train Speed	Wayside Wind		Onboard Relative Wind		Calculated Relative Wind	
			Speed	Dir.+	Speed	Dir.++	Speed	Dir.++
	mph	Ft/Sec	Ft/Sec	Degrees	Ft/Sec	Degrees	Ft/Sec	Degrees
41	50	75.00	16.55	391.06	57.76	172.90	61.42	172.01
42	50	76.05	17.43	400.85	60.69	169.20	63.89	169.72
45	70	99.56	10.84	370.42	81.67	182.63	88.92	178.74
48	90	131.72	15.95	371.56	112.34	179.67	116.14	178.42
49	70	103.94	10.98	383.20	90.95	177.68	93.95	177.36
50	90	131.78	13.52	371.80	115.37	179.10	118.58	178.66
103	90	135.40	10.73	255.67	138.33	186.10	138.45	184.31
104	90	134.49	11.14	263.45	137.65	185.44	136.21	184.66
105	70	105.46	11.29	270.02	109.38	185.70	106.06	186.11
106	70	105.03	12.18	261.59	109.01	186.00	107.49	186.44
107	55	83.06	11.24	261.69	86.26	188.30	85.41	187.48
108*	55	78.78*	12.38	261.98	84.22	188.58	81.44*	188.60*

@ Run numbers 43, 44, 46 and 47 could not be processed due to ALD problems.

+ Measured relative to coordinate system in Figure 4-1a.

++ Measured relative to coordinate system in Figure 4-1b plus 180°.

* Possibly erroneous data due to (i) incorrect average speed and/or (iii) incorrect onboard relative speed.

Table 4-2A
Force Data for Configuration 1

Run No.	Drag Force			Side Force			Lift Force		
	A	B	A&B	A	B	A&B	A	B	A&B
	LBF	LBF	LBF	LBF	LBF	LBF	LBF	LBF	LBF
51	151	140	291	210	138	348	107	128	235
52	133	122	255	124	88	212	52	94	146
53*	185*	173*	358*	138	91	229	61	95	156
54	199	216	415	64	84	148	11	81	92
55	205	213	418	57	48	105	-8	81	73
56	227	254	481	40	40	80	-21	55	34
57	371	436	807	41	32	73	-54	78	24
58	418	477	895	32	14	46	-64	60	-4
59	378	440	818	43	56	99	-60	70	10
60	50	55	105	38	33	71	0	21	21
61*	11*	10*	21*	52	36	88	9	20	29
62*	107*	141*	248*	-95	-113	208	51	73	124
63	214	216	430	-377	-269	-646	246	256	502
64*	241*	248*	489*	-380	-285	-665	239	253	492
65	302	362	664	-445	-388	-833	265	310	575
66	267	375	642	-304	-357	-661	181	247	428
67	254	338	592	-268	-290	-558	147	202	349
68	340	402	742	5	-26	-21	5	104	109
69	336	344	680	112	159	271	36	157	193
70	332	449	781	65	111	176	-3	96	93

* Possibly erroneous data due to (i) unusually large momentum term contribution to drag force and/or (ii) unusually large side forces of opposite signs on trailers A and B and/or (iii) unusually large lift forces on the two trailers. Errors of type (i) may have resulted from incorrect initial and final train speed measurements. Errors (ii) and (iii) occurred because of hardware faults in data collection equipment.

Table 4-2A (CONT)
Force Data for Configuration 1

Run No.	Drag Force			Side Force			Lift Force		
	A	B	A&B	A	B	A&B	A	B	A&B
	LBF	LBF	LBF	LBF	LBF	LBF	LBF	LBF	LBF
71	78	82	160	60	70	130	24	45	69
72	84	81	165	114	87	201	49	64	113
73	90	86	176	150	98	248	67	78	145
74	110	122	232	55	70	125	26	59	85
75	110	127	237	47	54	101	17	45	62
76	99	111	210	39	65	104	10	36	46
77	193	227	420	-9	-12	-21	53	101	154
78	226	273	499	-52	-72	-124	110	156	266
79	257	330	587	-336	-332	-668	221	269	490
80	354	422	776	-59	-198	-257	15	109	124
81	379	458	837	-26	-197	-223	0	102	102
82	388	476	864	-140	-288	-428	55	150	205
83*	112*	135*	247*	31	24	55	-44	1	-43
84*	51*	75*	126*	45	47	92	-36	3	-31
85	146	145	291	185	133	318	53	77	130
86	235	274	509	31	11	42	-62	4	-58
87*	208	252	460	16*	-28*	-12	-52	11	-41
88*	198	246	444	21*	-18*	3	-48	10	-38

* Possibly erroneous data due to (i) unusually large momentum term contribution to drag force and/or (ii) unusually large side forces of opposite signs on trailers A and B and/or (iii) unusually large lift forces on the two trailers. Errors of type (i) may have resulted from incorrect initial and final train speed measurements. Errors (ii) and (iii) occurred because of hardware faults in data collection equipment.

Table 4-2A (CONT)
Force Data for Configuration 1

Run No.	Drag Force			Side Force			Lift Force		
	A	B	A&B	A	B	A&B	A	B	A&B
	LBF	LBF	LBF	LBF	LBF	LBF	LBF	LBF	LBF
89*	281*	157*	438*	594*	-1808*	-1214*	648*	1777*	2425*
90*	172*	167*	339*	427*	-835*	-408*	1973*	2003*	3976*
91*	169*	170*	339*	647*	-805*	-158*	2097*	2121*	4218*
92*	79*	63*	142*	546*	-472*	74*	1092*	1390*	2482*
93*	164	162	296	531*	-572*	-41*	681*	1075*	1756*
94*	694*	703*	1397*	-963	-720	-1693	632	651	1283
95	517	526	1043	-899	-680	-1579	599	630	1229
96	594	598	1192	-1080	-778	-1858	719	746	1465
97	599	579	1178	-1012	-733	-1745	642	686	1328
98	851	840	1691	-1589	-1177	-2766	1133	1123	2256
99	666	717	1383	-1001	-863	-1864	607	746	1353
100	420	441	861	-822	-728	-1550	618	644	1262
101	425	445	870	-872	-792	-1664	693	718	1411
102	416	427	843	-799	-657	-1456	591	613	1204

* Possibly erroneous data due to (i) unusually large momentum term contribution to drag force and/or (ii) unusually large side forces of opposite signs on trailers A and B and/or (iii) unusually large lift forces on the two trailers. Errors of type (i) may have resulted from incorrect initial and final train speed measurements. Errors (ii) and (iii) occurred because of hardware faults in data collection equipment.

Table 4-2B
Force Data for Configuration 2

Run No.	Drag Force			Side Force			Lift Force		
	A	B	A&B	A	B	A&B	A	B	A&B
	LBF	LBF	LBF	LBF	LBF	LBF	LBF	LBF	LBF
23	178	238	416	250	220	470	122	190	312
24	188	243	431	264	217	481	126	198	324
25	291	381	672	394	332	726	180	316	496
26	337	435	772	408	329	737	183	337	520
27	370	539	909	326	303	629	67	394	461
28	454	605	1059	491	360	851	158	468	626
29*	266 204 (EST)	341 319 (EST)	567 523 (EST)	332	395	727	223	253	476
30	361	485	846	495	430	925	248	390	638
31	514	665	1179	635	515	1150	281	530	811
32	144	218	362	83	61	144	-10	158	147
33	215	327	542	43	-1	42	-58	226	168
34	367	548	915	91	44	135	-111	376	265
35	363	565	928	79	28	107	-103	368	265
36	229	365	594	72	46	118	-60	247	187
37	148	220	368	92	87	179	-7	161	154
38	134	192	326	65	63	128	92	163	255
39	204	306	510	79	46	125	-44	211	167
40	381	612	993	96	67	163	-116	395	279

* Possibly erroneous data due to (i) incorrect initial train speed and/or (ii) final train speed data.

(EST) Value based on estimated initial or final train speed by assuming average train speed at the center of the test zone.

Table 4-2B (CONT)
Force Data for Configuration 2

Run No. @	Drag Force			Side Force			Lift Force		
	A	B	A&B	A	B	A&B	A	B	A&B
	LBF	LBF	LBF	LBF	LBF	LBF	LBF	LBF	LBF
41	137	185	322	206	193	399	98	157	255
42	164	249	413	284	322	606	176	221	397
45	156	239	395	10	-40	-30	-66	137	71
48	280	436	716	108	64	172	-113	266	153
49	188	292	480	102	105	207	-51	186	135
50	293	464	757	114	87	201	-117	271	154
103	429	742	1171	-300	-561	-861	36	559	595
104	421	705	1126	-250	-490	-740	-11	525	514
105	269	460	729	-170	-326	-496	20	346	366
106	285	475	760	-194	-345	-539	32	356	388
107	183	306	489	-147	-243	-390	37	230	267
108	178	294	472	-154	-241	-395	42	223	265

@ Run numbers 43, 44, 46 and 47 could not be processed due to ALD problems.

Table 4-3A
Force Area Data Based on
Onboard Relative Wind - Configuration 1

Run No.	Onboard Relative Wind		Dynamic Pressure LBF/Ft ²	Total Drag Force Area Ft ²	Total Side Force Area Ft ²	Total Lift Force Area Ft ²
	Speed	Dir. ††				
	Ft/Sec	Degrees				
51*	69.91	-6.85	5.43	52	57.5	43.0
52	71.98	-4.05	5.75	44	29.9	25.0
53*	70.16	-4.47	5.47	64*	35.6	28.0
54	91.62	-2.22	9.27	44	12.2	10.0
55	92.50	-1.83	9.45	43	7.3	7.0
56	94.33	-1.39	9.83	48	4.4	3.0
57	122.70	-0.46	16.51	48	1.9	1.0
58	127.49	0.00	17.83	49	0.025	0.0
59	126.91	-0.49	17.66	45	3.0	0.0
60	45.68	-1.82	2.28	46	15.6	9.0
61*	31.16	-6.08	1.06	21*	50.8	28.0
62*	79.19	7.40	6.16	40*	-38.7	20.0
63	82.72	13.76	6.73	63	-101.2	74.0
64*	87.49	13.00	7.53	65*	-92.7	65.0
65	107.36	9.95	11.40	57	-76.1	51.0
66	111.42	8.10	12.30	51	-55.9	34.0
67	110.66	7.40	12.13	47	-48.9	28.0
68	126.73	0.78	15.97	46	-3.2	6.0
69	129.57	-3.02	16.74	40	13.9	11.0
70	124.98	-2.14	15.57	43	8.7	5.0

* Possibly erroneous data due to incorrect values of drag, side or lift forces and/or dynamic pressure.

†† Measured relative to coordinate system in Figure

Table 4-3A (CONT)
 Force Area Data Based on
 Onboard Relative Wind Configuration 1

Run No.	Onboard Relative Wind		Dynamic Pressure LBF/Ft ²	Total Drag Force Area Ft ²	Total Side Force Area Ft ²	Total Lift Force Area Ft ²
	Speed	Dir. ††				
	Ft/Sec	Degrees				
71	62.85	-2.80	3.93	39	24.0	18.0
72	63.72	-4.80	4.04	40	41.3	28.0
73	58.75	-6.90	3.43	51	61.7	42.0
74	76.18	-0.67	5.69	40	15.8	15.0
75	72.17	-0.15	5.11	45	12.1	12.0
76	71.73	-0.44	5.05	41	13.0	1.0
77*	102.55*	0.25	10.24*	40*	-5.4*	15.0*
78	102.59	3.30	10.21	48	-15.4	26.0
79	103.01	9.02	10.39	55	-67.4	47.0
80	134.50	3.37	17.73	43	-16.0	7.0
81	134.33	3.11	17.68	46	-14.0	5.0
82	142.01	4.94	19.76	43	-22.8	10.0
83*	81.78	1.11	6.50	37*	2.6	-6.0
84*	79.99	-0.40	6.22	20*	8.3	-5.0
85	83.03	-5.53	6.70	42	42.0	19.0
86	104.36	0.10	10.50	48	0.65	-5.0
87*	101.24	1.47	9.88	46	†	-4.0
88	100.28	1.70	9.70	45	†	-3.0

* Possibly erroneous data due to incorrect values of drag, side or lift forces and/or dynamic pressure.

† Erroneous data due to hardware problems, hence not entered.

†† Measured relative to coordinate system in Figure 4-1b.

Table 4-3A (CONT)
Force Area Data Based on
Onboard Relative Wind - Configuration 1

Run No.	Onboard Relative Wind		Dynamic Pressure	Total Drag Force Area	Total Side Force Area	Total Lift Force Area
	Speed	Dir.††				
	Ft/Sec	Degrees	LBF/Ft ²	Ft ²	Ft ²	Ft ²
89*	131.98*	-20.62*	12.16*	36*	†	199.0*
90*	138.77	0.46	16.51	18*	†	214.0*
91*	139.81	1.27	18.78	18*	†	224.0*
92*	85.85	-0.26	7.07	20*	†	351.0*
93	98.38	-1.26	7.50	42	†	234.0*
94*	128.29	13.67	16.46	84*	-104	77.0
95	122.56	13.30	15.02	69	-107	81.0
96	126.55	14.70	16.03	74	-117	91.0
97	129.02	13.49	16.66	69	-106	79.0
98	151.29	14.89	22.90	73	-121.5	98.0
99	152.42	11.12	23.29	59	-81.5	58.0
100	107.68	16.66	11.65	73	-136.1	108.0
101	106.65	17.24	11.43	76	-148	123.0
102	105.45	16.09	11.18	75	-133	107.0

* Possibly erroneous data due to incorrect values of drag, side or lift forces and/or dynamic pressure.

† Erroneous data due to hardware problems, hence not entered.

†† Measured relative to coordinate system in Figure 4-1b.

Table 4-3B
Force Area Data Based on
Onboard Relative Wind - Configuration 2

Run No.	Onboard Relative Wind		Dynamic Pressure	Total Drag Force Area	Total Side Force Area	Total Lift Force Area
	Speed	Dir.†				
	Ft/Sec	Degrees				
23	66.78	-6.70	4.72	88	91.50	66.0
24	68.17	-6.60	4.92	87	90.80	66.0
25	89.03	-6.73	8.39	80	81.80	59.0
26	84.10	-5.41	9.38	82	74.25	55.0
27*	SAT * 118.9 (CALC)	-3.65	13.06*	69 * 60 (EST)	48 * 42 (EST)	35.0 * 30.7 (EST)
28*	SAT * 125.4 (CALC)	-4.97	13.17*	80 * 63 (EST)	64 * 51 (EST)	47.0 * 37.3 (EST)
29*	68.66	-10.16	4.99	113 * 105 (EST)	137.9	95.0
30	96.62	-7.36	9.89	85	89.4	64.0
31*	SAT * 123.3 (CALC)	-6.58	13.13*	89 * 73 (EST)	87 * 71 (EST)	61.0 * 30.0 (EST)
32	79.33	-0.10	6.76	53	15.8	21.0
33	101.50	0.88	11.07	49	-0.2	15.0
34*	SAT * 132.9 (CALC)	0.95	15.15*	60 * 48 (EST)	8.0 * 6.4 (EST)	17.0 * 13.6 (EST)
35*	SAT * 129.8 (CALC)	1.16	15.15*	61 * 51 (EST)	7.0 * 5.8 (EST)	17.0 * 14.2 (EST)
36	106.94	0.32	12.29	48	6.1	15.0
37	78.81	-1.24	6.67	55	21.7	23.0
38	77.38	0.71	6.35	51	14.5	40.0
39	98.30	-0.07	10.24	49	8.6	16.0
40*	SAT * 136.6 (CALC)	0.79	14.96*	65 * 43 (EST)	10.0 * 6.6 (EST)	18.0 * 12.0 (EST)

* Possibly erroneous data due to incorrect onboard relative wind speed.

† Measured relative to coordinate system in Figure 4-1b.

(EST) Force area estimated using calculated value of onboard relative wind speed (and hence dynamic pressure)

(CALC) Relative wind speed and direction calculated by vectoring average train speed and wayside wind data. These values were used when onboard wind data was not available.

Table 4-3B (CONT)
 Force Area Data Based on
 Onboard Relative Wind - Configuration 2

Run No. @	Onboard Relative Wind		Dynamic Pressure	Total Drag Force Area	Total Side Force Area	Total Lift Force Area
	Speed	Dir.†				
	Ft/Sec	Degrees	LBF/Ft ²	Ft ²	Ft ²	Ft ²
41	57.76	-8.10	3.55	91	102.1	72.0
42	60.69	-10.80	3.92	105	146.0	101.0
45	81.67	2.63	7.11	55	-9.0	9.0
48	112.34	-0.33	13.45	53	9.4	11.0
49	90.95	-2.32	8.81	54	19.0	15.0
50	115.37	-0.90	14.18	53	11.5	10.0
103	138.33	6.10	19.86	59	-44.8	29.0
104	137.65	5.44	19.66	57	-38.8	26.0
105	109.38	5.70	12.41	58	-42.8	29.0
106	109.01	6.00	12.33	61	-45.8	31.0
107	86.26	8.30	7.72	63	-54.6	34.0
108	84.22	8.60	7.36	64	-57.8	36.0

@ Run numbers 43, 44, 46 and 47 could not be processed due to ALD problems.

† Measured relative to coordinate system in Figure 4-1b.

Table 4-4A
Force Area Data Based on
Calculated Relative Wind - Configuration 1

Run No.	Calculated Relative Wind		Calc. Dynamic Pressure	Calculated Total Drag Area	Calculated Total Side Area	Calculated Total Lift Area
	Speed	Dir.††				
	Ft/Sec	Degrees	LBF/Ft ²	Ft ²	Ft ²	Ft ²
51*	72.95*	-5.71*	5.91*	47.76*	52.80*	39.5*
52	73.86	-5.18	6.05	41.78	28.40	23.8
53*	70.18	-5.54	5.47	63.96*	35.58	28.0
54	94.85	-4.15	9.94	41.05	11.38	9.3
55	96.03	-0.90	10.19	39.90	6.77	6.1
56	98.65	-1.72	10.75	43.89	4.02	2.7
57	125.32	-1.03	17.22	46.01	1.82	1.0
58	129.32	-0.68	18.35	47.50	0.024	0.0
59	131.56	-0.09	18.98	41.88	2.79	0.0
60	48.36	-5.33	2.55	41.04	13.92	8.0
61*	34.24	-6.80	1.28	17.39*	42.07	23.2
62*	76/74	4.59	5.78	42.59*	-41.21	21.3
63	80.00	15.00	6.29	67.36	-108.20	79.2
64*	79.67*	13.67*	6.24*	78.39*	-111.79*	78.4*
65	107.63	10.91	11.46	56.71	-75.72	50.7
66	107.95	8.89	11.55	54.33	-59.55	36.2
67	108.19	8.00	11.59	49.17	-51.16	29.3
68	124.04	-0.73	15.30	48.02	-3.34	6.3
69	133.94	-3.03	17.89	37.71	2.86	10.3
70	129.98	-3.65	16.84	39.76	8.04	4.6

* Possibly erroneous data due to (i) incorrect average train speed measurement resulting in incorrect calculated relative speed and direction and/or (ii) incorrect force measurement.

†† Measure relative to coordinate system in Figure 4-1b.

Table 4-4A (CONT)
Force Area Data Based on
Calculated Relative Wind - Configuration 1

Run No.	Calculated Relative Wind		Calc. Dynamic Pressure	Calculated Total Drag Area	Calculated Total Side Area	Calculated Total Lift Area
	Speed	Dir.††				
	Ft/Sec	Degrees				
71	67.25	-5.48	4.50	34.06	20.96	15.7
72	68.57	-7.39	4.68	34.54	35.66	24.2
73	65.17	-10.78	4.22	41.45	50.14	34.1
74	78.08	-2.79	5.98	38.08	15.04	14.3
75	72.84	-0.55	5.21	44.18	11.88	11.8
76	73.58	-3.66	5.32	38.96	12.35	0.9
77	95.71	-1.49	8.92	45.92	6.20	17.2
78	98.16	5.66	9.35	52.43	-16.82	28.4
79	97.26	8.76	9.26	61.70	-75.60	52.7
80	135.96	3.42	18.12	42.08	-15.66	6.8
81	135.61	2.95	18.02	45.14	-13.74	4.9
82	136.58	4.58	18.28	46.49	-24.65	10.8
83*	76.49*	0.89*	5.68*	42.29*	2.97*	-6.9*
84*	70.73*	0.20*	4.86*	25.58*	10.62*	-6.4*
85*	79.17*	-4.73*	6.09*	46.20*	46.21*	20.9*
86	107.38	1.79	11.12	45.23	0.61	-4.7
87	103.26	0.10	10.28	44.22	†	-3.8
88	99.92	0.43	9.63	45.32	†	-3.0

* Possibly erroneous data due to (i) incorrect average train speed measurement resulting in incorrect calculated relative speed and direction and/or (ii) incorrect force measurement.

† Erroneous data due to hardware problems, hence not entered.

†† Measured relative to coordinate system in Figure 4-1b.

Table 4-4A (CONT)
Force Area Data Based on
Calculated Relative Wind - Configuration 1

Run No.	Calculated Relative Wind		Calc. Dynamic Pressure	Calculated Total Drag Area	Calculated Total Side Area	Calculated Total Lift Area
	Speed	Dir.††				
	Ft/Sec	Degrees				
			LBF/Ft ²	Ft ²	Ft ²	Ft ²
89*	143.05*	7.13*	14.29*	†	†	169.3*
90*	†	†	†	†	†	†
91*	134.11	-8.02	17.28	†	†	243.4*
92*	81.83	7.51	6.42	†	†	385.4*
93*	90.87	-2.74	6.40	49.23	†	274.2*
94*	102.57*	7.3*	10.52	131.41*	-162.70	120.5
95	110.34	9.82	12.17	85.13	-132.00	100.0
96	109.98	10.17	12.11	97.98	-154.90	120.5
97	118.99	11.20	14.17	81.12	-124.60	92.9
98	136.93	9.84	18.76	89.11	-148.32	119.6
99	147.41	9.33	21.78	63.08	-87.13	62.0
100	89.18	11.99	7.99	106.43	-198.42	157.5
101*	90.56*	11.54*	8.24*	105.41*	-205.20*	170.6*
102	91.74	11.22	8.46	99.09	-175.70	141.4

* Possibly erroneous data due to (i) incorrect average train speed measurement resulting in incorrect calculated relative speed and direction and/or (ii) incorrect force measurement.

† Erroneous data due to hardware problems, hence not entered.

†† Measured relative to coordinate system in Figure 4-1b.

Table 4-4B
Force Area Data Based on
Calculated Relative Wind - Configuration 2

Run No.	Calculated Relative Wind		Calc. Dynamic Pressure LBF/Ft ²	Calculated Total Drag Area Ft ²	Calculated Total Side Area Ft ²	Calculated Total Lift Area Ft ²
	Speed	Dir. †				
	Ft/Sec	Degrees				
23	72.92	-10.85	5.63	73.8	76.7	55.30
24	74.75	-9.10	5.92	72.4	75.5	54.80
25	92.38	-9.27	9.03	74.3	76.0	54.80
26	100.61	-9.43	13.42	57.3	51.9	38.44
27	118.91	-5.93	15.09	60.2	41.9	30.55
28	125.40	-7.35	16.73	63.3	50.6	37.42
29	68.66	-12.53	4.99	104.8	137.9	95.00
30	103.65	-9.27	11.38	73.9	77.7	55.60
31	123.25	-8.81	16.24	72.6	71.0	49.94
32	79.63	-0.95	6.81	52.6	15.7	20.80
33	103.16	0.76	11.44	47.4	-0.19	14.50
34	132.86	-1.73	19.10	47.9	6.4	13.87
35	129.82	-0.22	18.20	51.0	5.9	14.56
36	105.45	-0.91	11.95	49.4	6.3	15.40
37	75.37	-3.75	6.10	60.1	23.7	25.10
38	76.92	-1.47	6.27	51.6	14.7	40.50
39	97.08	0.04	9.99	50.2	8.8	16.40
40	136.55	-1.14	23.20	42.8	6.6	12.03

† Measured relative to coordinate system in Figure 4-1b.

Table 4-4B (CONT)
 Force Area Data Based on
 Calculated Relative Wind - Configuration 2

Run No. @	Calculated Relative Wind		Calc. Dynamic Pressure LBF/Ft ²	Calculated Total Drag Area Ft ²	Calculated Total Side Area Ft ²	Calculated Total Lift Area Ft ²
	Speed	Dir.†				
	Ft/Sec	Degrees				
41	61.42	-7.99	4.01	80.5	90.3	63.7
42	63.89	-10.28	4.34	94.7	131.7	91.2
45	88.92	-1.26	8.43	46.4	-7.6	7.6
48	116.14	-1.58	14.38	49.6	8.8	10.3
49	93.95	-2.64	9.40	50.6	17.8	14.1
50	118.58	-1.34	14.98	50.2	10.9	9.5
103	138.45	4.31	19.89	58.9	-44.7	29.0
104	136.21	4.66	19.25	59.2	-39.6	26.6
105	106.06	6.11	11.67	61.7	-45.5	30.8
106	107.49	6.44	11.99	62.7	-47.1	31.9
107	85.41	7.48	7.57	64.3	-55.7	34.7
108*	81.44*	8.66*	6.88	68.4*	-61.81*	38.5

@ Run numbers 43, 44, 46 and 47 could not be processed due to ALD problems.

* Possibly erroneous data due to incorrect calculated relative wind speed.

† Measured relative to coordinate system in Figure 4-1b.

Table 4-5A

Rolling Resistance Data for Configuration 1

Run No.	Nom. Train Speed	Onboard Relative Wind Speed	Lead Coupler Force	Trail Coupler Force	Total Tractive Res.	Total Trailer Drag	Gravity Comp ^{††}	Rate of Momentum Change in Direction of Motion				Rolling Resist. [@]
								\bar{F}_{LC}	\bar{F}_{TC}	$\bar{F}_{LC} - \bar{F}_{TC}$	\bar{D}_{A+B}	
			mph	Ft/Sec	LBF	LBF	LBF	LBF	LBF	Ft/Sec	Ft/Sec	Sec
51	50	69.91	214	-199	413	291	267	71.15	73.56	55.04	-132	521
52	50	71.98	177	-179	356	255	267	74.77	75.98	53.35	-68	436
53*	50	70.16	207	-139	346	358*	267	60.30	71.15	54.63	-600	855*
54	70	91.62	430	-90	520	415	267	96.48	98.89	41.04	-177	549
55	70	92.50	510	-56	566	418	267	98.89	100.10	40.57	-90	505
56	70	94.33	580	-24	604	481	267	97.68	100.10	40.57	-180	570
57	90	122.70	1654	469	1185	807	267	127.84	126.63	31.42	116	529
58	90	127.49	1523	356	1167	895	267	131.45	132.66	30.41	-120	659
59	90	126.91	1451	393	1058	818	267	131.45	131.45	30.43	0	507
60	30	45.68	104	-110	214	105	267	49.44	47.03	80.89	90	286
61*	20	31.16	-12	-169	157	21*	267	36.18	25.32	116.68	281	122*
62*	50	79.16	84	-244	328	248*	267	71.15*	67.54*	55.26	197*	150*
63	50	82.72	479	-106	585	430	267	69.95	68.74	56.66	49	374
64*	50	87.49	223	-274	497	489*	267	69.95*	73.56*	55.87	-195*	470*
65	70	107.36	927	61	866	664	267	95.27	96.48	41.81	-87	556
66	70	111.42	1013	131	882	642	267	101.30	102.51	39.20	-93	600
67	70	110.66	717	6	711	592	267	102.51	103.71	39.01	-93	479
68	90	126.73	1895	654	1241	742	267	133.86	132.66	29.96	121	645
69	90	129.57	1257	237	1020	680	267	132.66	132.66	30.33	0	607
70	90	124.98	1481	397	1084	781	267	132.66	132.66	30.12	0	570

@ Includes aerodynamic drag force on instrumented TTX car.

* Possibly erroneous data due to incorrect measurement of (i) initial train speed and/or (ii) final train speed.

† Based on the total mass of two trailers and a TTX car with structural components of the force balance system = 3020 slugs

†† Based on a total mass = 3020 slugs as above and an average grade of 0.275 percent.

Table 4-5A (CONT)
Rolling Resistance Data for Configuration 1

Run No.	Nom. Train Speed	Onboard Relative Wind Speed	Lead Coupler Force	Trail Coupler Force	Total Tractive Res.	Total Trailer Drag	Gravity Comp ^{††}	Rate of Momentum Change in Direction of Motion				Rolling Resist. [@]
			\bar{F}_{LC}	\bar{F}_{TC}	$\bar{F}_{LC} - \bar{F}_{TC}$	\bar{D}_{A+B}	\bar{F}_{GR}	Final Speed	Init. Speed	Time Elapsed	Inertial Force [†]	
			LBF	LBF	LBF	LBF	LBF	Ft/Sec	Ft/Sec	Sec	LBF	LBF
71	50	62.85	121	-143	264	160	267	75.98	75.98	52.94	0	371
72	50	63.72	141	-151	292	165	267	74.77	73.56	53.78	68	326
73	50	58.75	167	-136	203	176	267	74.77	74.77	53.29	0	294
74	50	76.18	604	117	487	232	267	75.98	78.39	52.08	-140	662
75	50	72.17	542	103	439	237	267	75.98	77.18	52.50	-69	538
76	50	71.73	169	-107	276	210	267	75.98	75.98	52.42	0	333
77*	70	102.55*	266	-180	446	420	267	101.30	102.51	39.09	-93	386
78	70	102.59	256	-222	478	499	267	98.89	102.51	39.85	-274	520
79	70	103.01	404	-201	605	587	267	98.89	102.51	40.18	-272	557
80	90	134.50	1277	273	1004	776	267	131.45	132.66	30.41	-120	615
81	90	134.33	1461	368	1093	837	267	132.66	133.86	30.09	-120	643
82	90	142.01	1513	345	1168	864	267	131.45	132.66	30.34	-120	691
83*	50	81.78	119	-221	340	247*	267	71.15*	67.53*	55.10	198*	162*
84*	50	79.99	121	-182	303	126*	267	72.36*	59.09*			
85	50	83.03	98	-203	301	291	267	71.15	73.56	54.24	-134	411
86	70	104.36	110	-294	404	509	267	100.10	103.72	39.46	-277	439
87	70	101.24	171	-230	401	460	267	100.10	102.51	39.48	-184	392
88	70	100.28	807	149	658	444	267	100.10	97.89			

@ Includes aerodynamic drag force on instrumented TTX car.

* Possibly erroneous data due to incorrect measurement of (i) initial train speed and/or (ii) final train speed.

† Based on the total mass of two trailers and a TTX car with structural components of the force balance system = 3020 slugs

†† Based on a total mass = 3020 slugs as above and an average grade of 0.275 percent.

Table 4-5A (CONT)

Rolling Resistance Data for Configuration 1

Run No.	Nom. Train Speed	Onboard Relative Wind Speed	Lead Coupler Force	Trail Coupler Force	Total Tractive Res.	Total Trailer Drag	Gravity Comp ^{††}	Rate of Momentum Change in Direction of Motion				Rolling Resist. [@]
			\bar{F}_{LC}	\bar{F}_{TC}	$\bar{F}_{LC} - \bar{F}_{TC}$	\bar{D}_{A+B}	\bar{F}_{GR}	Final Speed	Init. Speed	Time Elapsed	Inertial Force [†]	
	mph	Ft/Sec	LBF	LBF	LBF	LBF	LBF	Ft/Sec	Ft/Sec	Sec	LBF	LBF
89*	90	131.98*	582	90	492	438*	267	133.86	132.66	30.04	121	200*
90*	90	138.77	698	-239	937	339*	267	132.66	132.66	30.26	0	865*
91*	90	139.81	642	-5	647*	339*	267	132.66	132.66	30.28	0	575*
92*	55	185.85	30	-111	141*	142*	267	78.39	79.60	50.58	-72	338*
93*	55	98.38	267	-143	410	296*	267	71.15*	83.21*	48.78	-746*	1127*
94*	70	128.29	1486	102	1384	1397*	267	73.56*	96.48*	42.70	-1621*	1875*
95	70	122.56	1387	65	1322	1043	267	97.69	101.30	40.37	-270	816
96	70	126.55	2034	378	1656	1192	267	100.10	102.51	39.80	-183	914
97	90	129.02	1963	319	1644	1178	267	129.04	131.45	30.75	-237	970
98	90	151.29	1881	-82	1963	1691	267	124.22	131.45	31.50	-693	1232
99	90	152.42	3032	894	2138	1383	267	130.25	131.45	30.59	-118	1140
100	55	107.68	1591	287	1304	861	267	77.98	77.18	52.10	46	664
101	55	106.65	1432	186	1246	870	267	78.39	79.59	50.66	-72	714
102	55	105.45	1386	181	1205	843	267	78.39	79.59	50.92	-71	700

@ Includes aerodynamic drag force on instrumented TTX car.

* Possibly erroneous data due to incorrect measurement of (i) initial train speed and/or (ii) final train speed.

† Based on the total mass of two trailers and a TTX car with structural components of the force balance system = 3020 slugs

†† Based on a total mass = 3020 slugs as above and an average grade of 0.275 percent.

Table 4-5B

Rolling Resistance Data for Configuration 2

Run No.	Nom. Train Speed	Onboard Relative Wind Speed	Lead Coupler Force	Trail Coupler Force	Total Tractive Res.	Total Trailer Drag	Gravity Comp ⁺⁺	Rate of Momentum Change in Direction of Motion				Rolling Resist. ξ
								F_{LC}	F_{TC}	$F_{LC} - F_{TC}$	D_{A+B}	
			mph	Ft/Sec	LBF	LBF	LBF	LBF	LBF	Ft/Sec	Ft/Sec	Sec
23	50	66.78	367	-157	524	416	267	74.77	77.18	52.72	-138	513
24	50	68.17	244	-227	451	431	267	75.98	78.39	52.10	-140	427
25	70	89.03	483	-247	730	672	267	97.68	100.10	40.50	-180	505
26	70	84.10	1372	278	1094	772	267	102.51	103.72	38.62	-95	684
27*	90	SAT 118.9(CALC)	944	-76	1020	909	267	123.01	126.63	32.12	-340	718
28	90	SAT 125.4(CALC)	1496	170	1326	1059	267	124.22	126.63	31.96	-228	762
29*	50	68.66	466	-114	580	567 * 523(EST)	267	66.33 * 70.20(EST)	74.77	54.28	-470 * -254(EST)	750 * 578(EST)
30	70	96.62	1404	238	1166	846	267	102.51	102.51	39.26	0	587
31	90	SAT 123.3(CALC)	1678	203	1475	1179	267	123.01	125.42	32.40	-225	788
32	50	79.33	316	-147	463	362	267	74.77	75.98	53.30	-69	436
33	70	101.50	546	-99	645	542	267	98.89	100.10	40.44	-90	460
34	90	SAT 132.9(CALC)	832	-162	994	915	267	126.63	129.04	31.41	-232	578
35	90	SAT 129.8(CALC)	1973	564	1409	928	267	129.04	127.84	31.13	116	632
36	70	106.94	1026	164	1062	594	267	103.72	102.51	38.55	95	640
37	50	78.81	332	-99	431	368	267	75.98	77.18	52.16	-69	399
38	50	77.38	246	-146	392	326	267	77.18	78.39	51.45	-71	404
39	70	98.30	761	67	694	510	267	98.89	98.89	40.70	0	451
40*	90	SAT 136.6(CALC)	2641	942	1699	993	267	138.69	136.28	29.22	249	724

* Possibly erroneous data due to (i) incorrect measurement of onboard relative wind speed and/or (ii) drag force (see Table IV.2B) and/or (iii) initial or final train speed.

† Based on the total mass of two trailers and a TTX car with structural components of the force balance system = **3020 slugs**

‡ Based on a total mass = **3020 slugs**

(SAT) Denotes saturation of the electrical output of the onboard wind speed and direction sensor.

(CALC) Relative wind speed and direction calculated by vectoring average train speed and wayside wind data. These values were used when onboard wind data was not available.

(EST) Value based on estimated initial or final train speed by assuming average train speed at the center of the test zone.

ξ Includes aerodynamic drag force on instrumented TTX car.

Table 4-5B (CONT)

Rolling Resistance Data for Configuration 2

Run No. e	Nom. Train Speed	Onboard Relative Wind Speed	Lead Coupler Force	Trail Coupler Force	Total Tractive Res.	Total Trailer Drag	Gravity Comp††	Rate of Momentum Change in Direction of Motion				Rolling Resist. §
			F _{LC}	F _{TC}	F _{LC} - F _{TC}	D _{A+B}	F _{GR}	Final Speed	Initial Speed	Time Elapsed	Inertia Force†	
	mph	Ft/Sec	LBF	LBF	LBF	LBF	LBF	Ft/Sec	Ft/Sec	Sec	LBF	LBF
41	50	57.76	339	-88	427	322	267	74.77	74.77	53.60	0	372
42	50	60.69	457	-108	565	413	267	74.77	75.98	52.84	-69	488
45	70	81.67	508	-100	608	395	267	98.89	100.40	40.37	-90	570
48	90	112.34	1956	598	1378	716	267	132.66	130.25	30.50	238	690
49	70	90.95	477	-153	630	480	267	103.72	104.92	38.53	-94	511
50	90	115.37	1977	578	1399	757	267	132.66	130.25	33.14	220	689
103	90	138.33	3215	1119	2096	1171	267	136.28	133.86	29.71	246	946
104	90	137.65	2085	439	1646	1126	267	133.86	133.86	29.91	0	787
105	70	109.38	515	-262	777	729	267	103.72	107.33	38.03	-287	602
106	70	109.01	1100	92	1008	760	267	103.72	104.92	38.20	-95	610
107	55	86.26	525	-110	635	489	267	82.01	83.21	48.44	-75	488
108	55	84.22	559	-81	640	472	267	80.80	80.80	49.66	0	435

Ⓔ Run numbers 43, 44, 46 and 47 could not be processed due to ALD problems.

* Possibly erroneous data due to (i) incorrect measurement of onboard relative wind speed and/or (i) drag force (see Table IV.2B) and/or (ii) initial or final train speed.

† Based on the total mass of two trailers and a TTX car with structural components of the force balance system = 3020 slugs

†† Based on a total mass = 3020 slugs

(SAT) Denotes saturation of the electrical output of the onboard wind speed and direction sensor.

(CALC) Relative wind speed and direction calculated by vectoring average train speed and wayside wind data. These values were used when onboard wind data was not available.

(EST) Value based on estimated initial or final train speed by assuming average train speed at the center of the test zone.

§ Includes aerodynamic drag force on instrumented TTX car.

Table 4-6A

Zero Changes of Measurement Transducers - Configuration 1

Test Date: 12/9/77

Test Series: 1

Transducer	Location	Zero Change*
F1 Load Cell	A Trailer Vertical Front	-17.6 lbs
F2 Load Cell	A Trailer Lateral Front	- 0.1 lbs
F3 Load Cell	A Trailer Longitudinal Front	- 8.1 lbs
F4 Load Cell	A Trailer Vertical Rear Left	- 5.8 lbs
F5 Load Cell	A Trailer Vertical Rear Right	- 0.8 lbs
F6 Load Cell	A Trailer Lateral Rear	0.1 lbs
F7 Load Cell	B Trailer Vertical Front	-12.2 lbs
F8 Load Cell	B Trailer Lateral Front	- 7.0 lbs
F9 Load Cell	B Trailer Longitudinal Front	- 5.6 lbs
F10 Load Cell	B Trailer Vertical Rear Left	- 3.1 lbs
F11 Load Cell	B Trailer Vertical Rear Right	- 3.8 lbs
F12 Load Cell	B Trailer Lateral Rear	- 1.1 lbs
F13 Load Cell	Leading Coupler Longitudinal	28.9 lbs
F14 Load Cell	Trailing Coupler Longitudinal	-122.2 lbs
D1 Displacement Transducer	A End Truck Right Side	-0.014 inch
D2 Displacement Transducer	A End Truck Left Side	-0.119 inch
D3 Displacement Transducer	B End Truck TTX Right Side	-0.020 inch
D4 Displacement Transducer	B End Truck TTX Left Side	-0.053 inch

*Zero change between beginning and end of a test series.

Table 4-6A (CONT)

Zero Changes of Measurement Transducers - Configuration 1

Test Date: 12/12/77
 Test Series: 2

Transducer	Location	Zero Change*
F1 Load Cell	A Trailer Vertical Front	4.1 lbs
F2 Load Cell	A Trailer Lateral Front	- 1.2 lbs
F3 Load Cell	A Trailer Longitudinal Front	- 0.2 lbs
F4 Load Cell	A Trailer Vertical Rear Left	0.7 lbs
F5 Load Cell	A Trailer Vertical Rear Right	3.8 lbs
F6 Load Cell	A Trailer Lateral Rear	- 2.2 lbs
F7 Load Cell	B Trailer Vertical Front	- 1.4 lbs
F8 Load Cell	B Trailer Lateral Front	- 0.4 lbs
F9 Load Cell	B Trailer Longitudinal Front	- 2.9 lbs
F10 Load Cell	B Trailer Vertical Rear Left	2.9 lbs
F11 Load Cell	B Trailer Vertical Rear Right	4.0 lbs
F12 Load Cell	B Trailer Lateral Rear	- 1.0 lbs
F13 Load Cell	Leading Coupler Longitudinal	17.1 lbs
F14 Load Cell	Trailing Coupler Longitudinal	-99.6 lbs
D1 Displacement Transducer	A End Truck Right Side	0.053 inch
D2 Displacement Transducer	A End Truck Left Side	0.034 inch
D3 Displacement Transducer	B End Truck TTX Right Side	0.022 inch
D4 Displacement Transducer	B End Truck TTX Left Side	0.048 inch

* Zero change between beginning and end of a test series.

Table 4-6A (CONT)

Zero Changes of Measurement Transducers - Configuration 1

Test Date: 12/14/77
 Test Series: 3

Transducer	Location	Zero Change*
F1 Load Cell	A Trailer Vertical Front	- 0.4 lbs
F2 Load Cell	A Trailer Lateral Front	- 0.3 lbs
F3 Load Cell	A Trailer Longitudinal Front	2.3 lbs
F4 Load Cell	A Trailer Vertical Rear Left	- 0.2 lbs
F5 Load Cell	A Trailer Vertical Rear Right	- 0.8 lbs
F6 Load Cell	A Trailer Lateral Rear	- 1.8 lbs
F7 Load Cell	B Trailer Vertical Front	- 0.6 lbs
F8 Load Cell	B Trailer Lateral Front	- 2.4 lbs
F9 Load Cell	B Trailer Longitudinal Front	- 0.9 lbs
F10 Load Cell	B Trailer Vertical Rear Left	- 2.9 lbs
F11 Load Cell	B Trailer Vertical Rear Right	- 7.3 lbs
F12 Load Cell	B Trailer Lateral Rear	- 1.1 lbs
F13 Load Cell	Leading Coupler Longitudinal	23.7 lbs
F14 Load Cell	Trailing Coupler Longitudinal	33.5 lbs
D1 Displacement Transducer	A End Truck Right Side	0.043 inch
D2 Displacement Transducer	A End Truck Left Side	0.008 inch
D3 Displacement Transducer	B End Truck TTX Right Side	-0.014 inch
D4 Displacement Transducer	B End Truck TTX Left Side	0.068 inch

* Zero change between beginning and end of a test series.

Table 4-6A (CONT)

Zero Changes of Measurement Transducers - Configuration 1

Test Date: 12/15/77

Test Series: 4

Transducer	Location	Zero Change*
F1 Load Cell	A Trailer Vertical Front	- 1.3 lbs
F2 Load Cell	A Trailer Lateral Front	6.2 lbs
F3 Load Cell	A Trailer Longitudinal Front	165.4 lbs [†]
F4 Load Cell	A Trailer Vertical Rear Left	0.4 lbs
F5 Load Cell	A Trailer Vertical Rear Right	911.2 lbs [†]
F6 Load Cell	A Trailer Lateral Rear	2.4 lbs
F7 Load Cell	B Trailer Vertical Front	129.5 lbs [†]
F8 Load Cell	B Trailer Lateral Front	5.0 lbs
F9 Load Cell	B Trailer Longitudinal Front	13.3 lbs
F10 Load Cell	B Trailer Vertical Rear Left	32.8 lbs
F11 Load Cell	B Trailer Vertical Rear Right	304.9 lbs [†]
F12 Load Cell	B Trailer Lateral Rear	13.7 lbs
F13 Load Cell	Leading Coupler Longitudinal	-18.8 lbs
F14 Load Cell	Trailing Coupler Longitudinal	423.5 lbs [†]
D1 Displacement Transducer	A End Truck Right Side	1.74 inch
D2 Displacement Transducer	A End Truck Left Side	-0.030 inch
D3 Displacement Transducer	B End Truck TTX Right Side	0.070 inch
D4 Displacement Transducer	B End Truck TTX Left Side	-0.009 inch

* Zero change between beginning and end of a test series.

[†] Unusually large zero shift in this test series were due to hardware problems.

Table 4-6A (CONT)

Zero Changes of Measurement Transducers - Configuration 1

Test Date: 12/16/77

Test Series: 5

Transducer	Location	Zero Change*
F1 Load Cell	A Trailer Vertical Front	-17.9 lbs
F2 Load Cell	A Trailer Lateral Front	- 8.4 lbs
F3 Load Cell	A Trailer Longitudinal Front	-11.9 lbs
F4 Load Cell	A Trailer Vertical Rear Left	- 0.9 lbs
F5 Load Cell	A Trailer Vertical Rear Right	- 0.7 lbs
F6 Load Cell	A Trailer Lateral Rear	- 8.1 lbs
F7 Load Cell	B Trailer Vertical Front	-14.8 lbs
F8 Load Cell	B Trailer Lateral Front	-10.0 lbs
F9 Load Cell	B Trailer Longitudinal Front	- 5.9 lbs
F10 Load Cell	B Trailer Vertical Rear Left	- 8.3 lbs
F11 Load Cell	B Trailer Vertical Rear Right	9.7 lbs
F12 Load Cell	B Trailer Lateral Rear	9.7 lbs
F13 Load Cell	Leading Coupler Longitudinal	14.6 lbs
F14 Load Cell	Trailing Coupler Longitudinal	-1641.9 lbs
D1 Displacement Transducer	A End Truck Right Side	-0.077 inch
D2 Displacement Transducer	A End Truck Left Side	-0.011 inch
D3 Displacement Transducer	B End Truck TTX Right Side	-0.049 inch
D4 Displacement Transducer	B End Truck TTX Left Side	0.076 inch

*Zero change between beginning and end of a test series.

Table 4-6B

Zero Changes of Measurement Transducers - Configuration 2

Test Date: 12/5/77

Test Series: 6

Transducer	Location	Zero Change*
F1 Load Cell	A Trailer Vertical Front	-13.0 lbs
F2 Load Cell	A Trailer Lateral Front	- 2.8 lbs
F3 Load Cell	A Trailer Longitudinal Front	- 4.3 lbs
F4 Load Cell	A Trailer Vertical Rear Left	- 5.8 lbs
F5 Load Cell	A Trailer Vertical Rear Right	- 1.3 lbs
F6 Load Cell	A Trailer Lateral Rear	0.0 lbs
F7 Load Cell	B Trailer Vertical Front	-14.8 lbs
F8 Load Cell	B Trailer Lateral Front	- 3.9 lbs
F9 Load Cell	B Trailer Longitudinal Front	- 2.6 lbs
F10 Load Cell	B Trailer Vertical Rear Left	- 0.2 lbs
F11 Load Cell	B Trailer Vertical Rear Right	0.0 lbs
F12 Load Cell	B Trailer Lateral Rear	- 3.8 lbs
F13 Load Cell	Leading Coupler Longitudinal	73.0 lbs
F14 Load Cell	Trailing Coupler Longitudinal	-2362.7 lbs
D1 Displacement Transducer	A End Truck Right Side	3.315 inch [†]
D2 Displacement Transducer	A End Truck Left Side	0.013 inch
D3 Displacement Transducer	B End Truck TTX Right Side	0.197 inch
D4 Displacement Transducer	B End Truck TTX Left Side	0.019 inch

* Zero change between beginning and end of a test series.

[†] Erroneous data.

Table 4-6B (CONT)

Zero Changes of Measurement Transducers - Configuration 2

Test Date: 12/6/77

Test Series: 7

Transducer	Location	Zero Change*
F1 Load Cell	A Trailer Vertical Front	- 1.6 lbs
F2 Load Cell	A Trailer Lateral Front	- 5.1 lbs
F3 Load Cell	A Trailer Longitudinal Front	- 9.8 lbs
F4 Load Cell	A Trailer Vertical Rear Left	3.3 lbs
F5 Load Cell	A Trailer Vertical Rear Right	9.8 lbs
F6 Load Cell	A Trailer Lateral Rear	- 6.9 lbs
F7 Load Cell	B Trailer Vertical Front	- 8.0 lbs
F8 Load Cell	B Trailer Lateral Front	- 5.1 lbs
F9 Load Cell	B Trailer Longitudinal Front	- 4.4 lbs
F10 Load Cell	B Trailer Vertical Rear Left	10.4 lbs
F11 Load Cell	B Trailer Vertical Rear Right	0.4 lbs
F12 Load Cell	B Trailer Lateral Rear	- 0.3 lbs
F13 Load Cell	Leading Coupler Longitudinal	- 4.8 lbs
F14 Load Cell	Trailing Coupler Longitudinal	4161.0 lbs
D1 Displacement Transducer	A End Truck Right Side	0.048 inch
D2 Displacement Transducer	A End Truck Left Side	0.057 inch
D3 Displacement Transducer	B End Truck TTX Right Side	-0.003 inch
D4 Displacement Transducer	B End Truck TTX Left Side	0.081 inch

*Zero change between beginning and end of a test series.

Table 4-6B (CONT)
Zero Changes of Measurement Transducers - Configuration 2

Test Date: 12/8/77

Test Series: 8

Transducer	Location	Zero Change*
F1 Load Cell	A Trailer Vertical Front	-22.2 lbs
F2 Load Cell	A Trailer Lateral Front	- 7.4 lbs
F3 Load Cell	A Trailer Longitudinal Front	-12.0 lbs
F4 Load Cell	A Trailer Vertical Rear Left	- 0.2 lbs
F5 Load Cell	A Trailer Vertical Rear Right	- 8.2 lbs
F6 Load Cell	A Trailer Lateral Rear	- 4.0 lbs
F7 Load Cell	B Trailer Vertical Front	-19.3 lbs
F8 Load Cell	B Trailer Lateral Front	- 9.0 lbs
F9 Load Cell	B Trailer Longitudinal Front	- 8.6 lbs
F10 Load Cell	B Trailer Vertical Rear Left	- 0.3 lbs
F11 Load Cell	B Trailer Vertical Rear Right	- 0.9 lbs
F12 Load Cell	B Trailer Lateral Rear	- 7.4 lbs
F13 Load Cell	Leading Coupler Longitudinal	26.4 lbs
F14 Load Cell	Trailing Coupler Longitudinal	-888.3 lbs
D1 Displacement Transducer	A End Truck Right Side	0.078 inch
D2 Displacement Transducer	A End Truck Left Side	0.074 inch
D3 Displacement Transducer	B End Truck TTX Right Side	0.034 inch
D4 Displacement Transducer	B End Truck TTX Left Side	3.590 inch

*Zero change between beginning and end of a test series.

Table 4-6B (CONT)

Zero Changes of Measurement Transducers - Configuration 2

Test Date: 12/16/77

Test Series: 9

Transducer	Location	Zero Change*
F1 Load Cell	A Trailer Vertical Front	-17.9 lbs
F2 Load Cell	A Trailer Lateral Front	- 8.4 lbs
F3 Load Cell	A Trailer Longitudinal Front	-11.9 lbs
F4 Load Cell	A Trailer Vertical Rear Left	- 0.9 lbs
F5 Load Cell	A Trailer Vertical Rear Right	- 0.7 lbs
F6 Load Cell	A Trailer Lateral Rear	0 8.1 lbs
F7 Load Cell	B Trailer Vertical Front	-14.8 lbs
F8 Load Cell	B Trailer Lateral Front	-10.0 lbs
F9 Load Cell	B Trailer Longitudinal Front	- 5.9 lbs
F10 Load Cell	B Trailer Vertical Rear Left	- 8.3 lbs
F11 Load Cell	B Trailer Vertical Rear Right	9.7 lbs
F12 Load Cell	B Trailer Lateral Rear	9.7 lbs
F13 Load Cell	Leading Coupler Longitudinal	14.6 lbs
F14 Load Cell	Trailing Coupler Longitudinal	-1641.9 lbs
D1 Displacement Transducer	A End Truck Right Side	-0.077 inch
D2 Displacement Transducer	A End Truck Left Side	-0.011 inch
D3 Displacement Transducer	B End Truck TTX Right Side	-0.049 inch
D4 Displacement Transducer	B End Truck TTX Left Side	0.076 inch

* Zero change between beginning and end of a test series.

Table 4-7
Changes in Carbody Attitude - Pitch and Roll

Test Date	Conf.	Carbody Displacements, † Inches				Change †† Attitude, Deg.		Component of Trailer Wt., lbs	
		D ₁	D ₂	D ₃	D ₄	Pitch	Roll	Long.	Lat.
12/5	2	3.315*	0.013	0.197	0.019	-0.113*	-0.857*	-19.4*	-147.3*
12/6	2	0.048	0.057	-0.003	0.081	-9.8x10 ⁻⁴	0.024	-0.168	4.15
12/8	2	0.078	0.074	0.034	3.590*	0.126*	0.922	21.6*	158.5*
12/9	1	-0.014	-0.119	-0.020	0.053	0.006	-0.008	1.03	-1.43
12/12	1	0.053	0.034	0.022	0.048	-6.2x10 ⁻⁴	0.002	-0.11	0.31
12/14	1	0.043	0.008	-0.014	0.068	1.1x10 ⁻⁴	0.012	0.02	2.10
12/15	1	1.740*	-0.030	0.070	-0.009	-0.060*	-0.480*	-10.3*	-82.5*
12/16	1&2	-0.077	-0.011	-0.049	0.076	0.004	0.050	0.72	8.52

† As defined in Figures 3-4 and 3-5. The displacements are changes between beginning and end of a test series (Tables 4.6A and 4.6B).

†† Change in attitude between beginning and end of a test series, calculated from Equations (3.28) and (3.33), respectively.

* Erroneous data due to incorrect displacement readings. Referring to Tables 4.6A and 4.6B it is observed that zero shifts of such magnitude were not read in the longitudinal and lateral load cells.

5.0 ANALYSIS OF TEST DATA

5.1 GENERAL

The reduced data presented in the previous chapter was analyzed in two steps. First, a preliminary examination was conducted onboard T-5 to determine the quality of the collected data using the following procedures:

- The distance travelled by the consist was computed from the number of samples collected and the sampling rate of 256 Hz. This value was compared with the nominal test zone length of 4000 feet. This check revealed the errors, if any, in average train speed due to loss of samples.
- Relative magnitudes of average, initial and final train speed were checked. Occasionally, errors were noticed in initial and/or final speeds due to loss of tachometer pulses. This led to unusually large momentum contributions in the drag force equation 3.27, resulting in erroneous drag areas. The tables in Section 4.0 reflect these incorrect values.
- For a few test runs selected at random, the onboard relative wind speed and direction were compared with the values calculated using average train speed and the wayside wind vector, Section 4.3.1. This check served to establish whether the onboard and wayside wind data were free of obvious errors. For instance, saturation of onboard speed sensor and drift problems associated with FM transmission of wayside data were discovered using this technique.
- The magnitudes of aerodynamic forces and force areas were checked for meaningfulness and were spot-compared against the wind tunnel results of References 1 and 2. This exercise was helpful in determining whether the aerodynamic data was reasonable. Thus, on a particular day of test (15 December 1977), it was found that the drag areas were too low and that the side forces on the two trailers had opposite signs. This problem was traced to some hardware faults developed in the T-5 data acquisition system and which were promptly corrected.

A post-test analysis of the AERO/TOFC (Series II) data was also performed and is the main subject of this section.

This phase consisted of selecting appropriate parameters to graphically display the data and fitting it analytically to describe its behavior. An analysis of the accuracy of the aerodynamic force data and the force area data is also presented.

5.2 FORCE AREA PLOTS BASED ON ONBOARD WIND DATA WITH OFFSET

Following Reference 1, the drag, side-force and lift areas (tabulated in Section 4.0) were selected as dependent variables and the onboard relative wind direction was chosen as the independent variable. As mentioned in Section 4.2, the force areas are obtained when the aerodynamic forces are divided by the dynamic pressure (Equation 4.6). Initially, onboard wind data corrected as discussed in Section 4.2 was used. Figures 5-1(a) and 5-1(b) show drag areas for Configurations 1 and 2 plotted against onboard relative wind direction. Similarly, Figures 5-2(a) and 5-2(b) show plots of side force areas versus onboard relative wind direction for Configurations 1 and 2, respectively. The data in these figures exclude any possibly erroneous values as identified in the tables in Section 4.0. The curves in Figures 5-1 and 5-2 were best fits obtained by performing a least squares polynomial regression of the force area against the wind direction. This procedure is described in Reference 14. The expressions for the curve-fits are:

Drag Area (Configuration 1)

$$y = 44.9195 + 9.7443 x - 24.1079 x^2 - 8.0378 \times 10^{-3} x^3 + 6.5679 \times 10^{-3} x^4 - 4.3765 \times 10^{-4} x^5 + 8.0866 \times 10^{-6} x^6$$

Drag Area (Configuration 2)

$$y = 54.50 - 1.89 x + 0.344 x^2$$

$$\begin{aligned} &\text{Side Force Area (Configuration 1)} \\ &y = 7.1973 - 6.4198 x + 0.0208 x^2 - 7.5834 x 10^{-3} x^3 \end{aligned}$$

$$\begin{aligned} &\text{Side Force Area (Configuration 2)} \\ &y = 22.0 - 1.03 x \end{aligned}$$

Where x denotes the wind angle in degrees and y is as defined for each of the preceding equations.

An interesting observation can be made from the curves in Figures 5-1(a), 5-1(b), 5-2(a) and 5-2(b). Ideally, the drag area should be symmetric about the zero wind direction (an even function) and the side force area plots should be antisymmetric, (an odd function). The curves in Figures 5-1(a) and 5-1(b) are nearly symmetric, but appear to be shifted to the right by 2.0 degrees for Configuration 1 and by 2.7 degrees for Configuration 2. Similarly, the side force area curves, while nearly antisymmetric, exhibit shifts to the right through 1.3 degrees for Configuration 1 and 2.1 degrees for Configuration 2. The consistency of these observations suggests that the onboard wind direction sensor may have suffered from a zero-offset. In other words, the indicated wind direction is slightly to the right of the true wind direction. Thus, a head wind at zero degrees (Figure 4-1(b)) is measured at +2 degrees approximately. In order to make certain that the offset was due to the instrument, it was decided to repeat the force area plots using relative wind data calculated according to Section 4.3.1. This is described in the next section.

5.3 FORCE AREA PLOTS BASED ON CALCULATED RELATIVE WIND DATA

The relative wind data generated by combining average train speed with the wayside wind vector is contained in Table 4-4A for Configuration 1 and in Table 4-4B for Configuration 2. The force areas based on calculated relative wind speed are also compiled in these tables. The tabulated data has been used in the drag area plots in Figures 5-3(a) and 5-3(b) for Configurations 1 and 2, respectively. Figures 5-4(a) and 5-4(b)

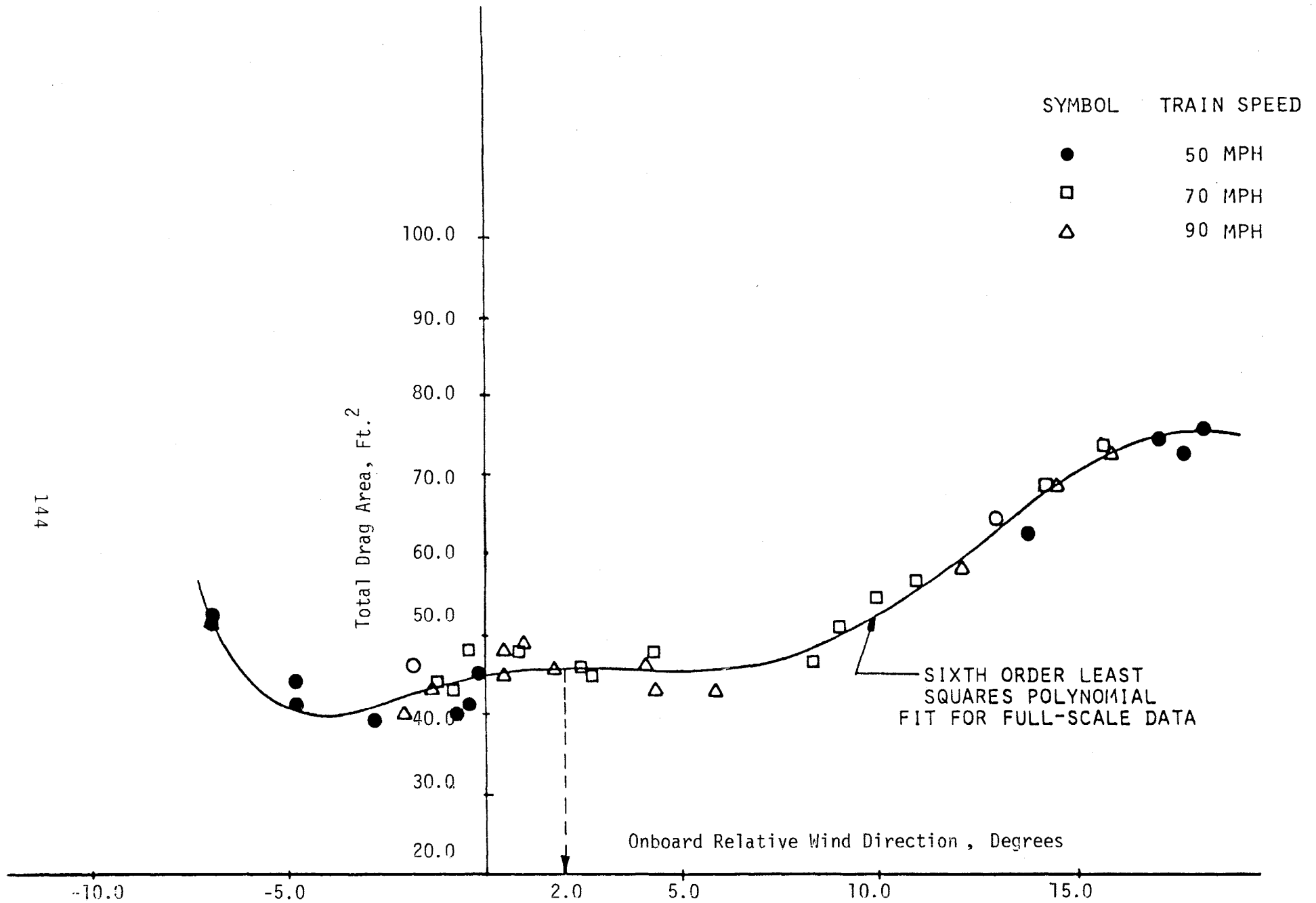


Figure 5-1(a). Total Drag Area Versus Onboard Relative Wind Direction with Offset - Configuration 1

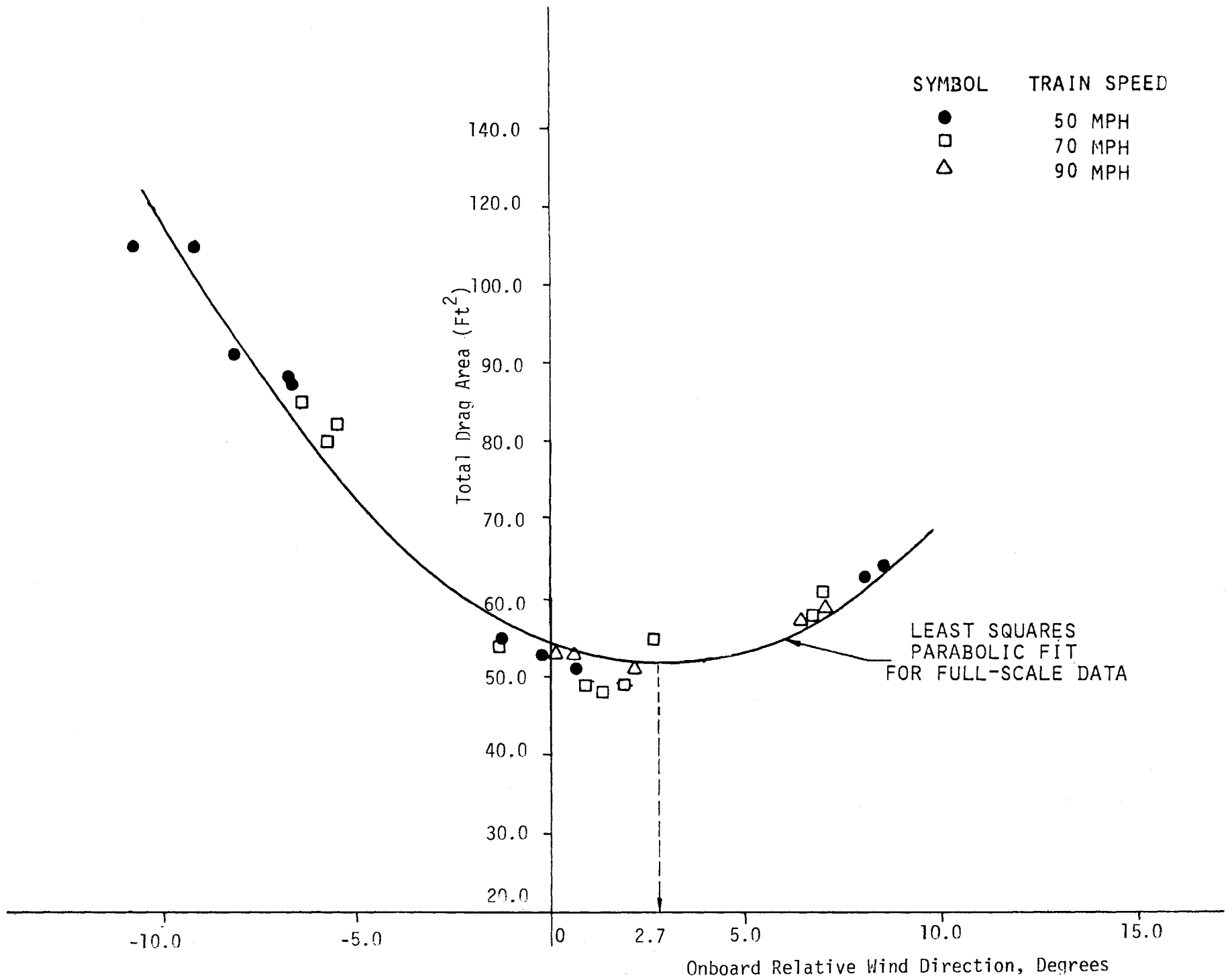


Figure 5-1(b). Total Drag Area versus Onboard Relative Wind Direction with Offset - Configuration 2

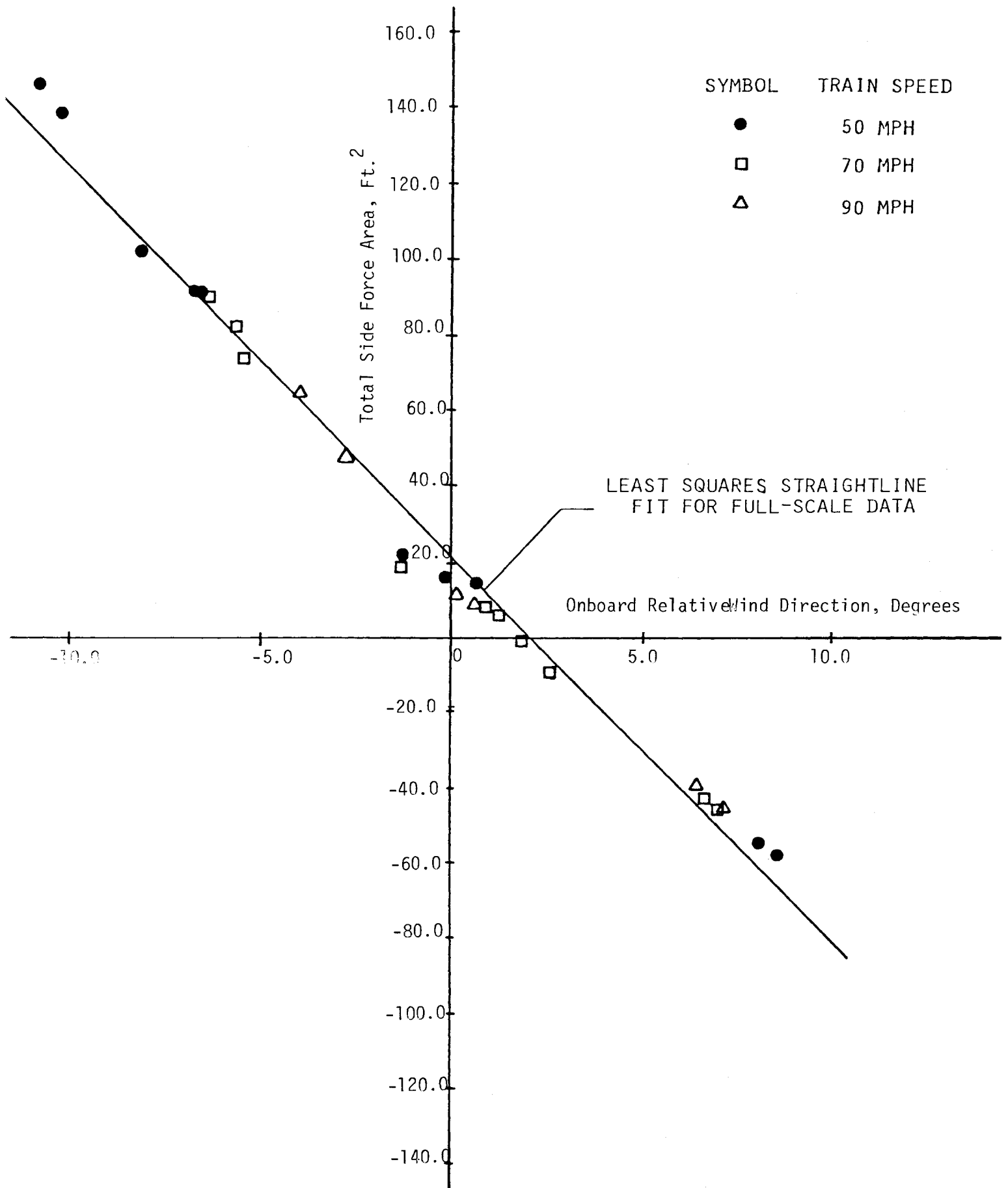


Figure 5-2(b). Total Side Force Area versus Onboard Relative Wind Direction with Offset - Configuration 2

display the corresponding side force area data. The curve-fits in the aforementioned figures are given by

Drag Area (Configuration 1)

$$y = 45.4456 + 5.9324 x - 0.3999 x^2 + 5.300 x 10^{-3} x^3 + 9.1025 x 10^{-3} x^4 + 6.3920 x 10^{-5} x^5 - 3.7211 x 10^{-5} x^6$$

Drag Area (Configuration 2)

$$y = 49.86 + 0.087 x + 0.288 x^2$$

Side Force Area (Configuration 1)

$$y = 1.9959 - 7.6801 x - 0.3316 x^2 + 6.1098 x 10^{-3} x^3$$

Side Force Area (Configuration 2)

$$y = 1.20 - 8.82 x$$

where x denotes the wind angle in degrees and y is as defined for each of the preceding equations.

A comparison should now be made between the force area plots based on on-board relative wind data and the force area plots based on calculated relative wind data. It reveals two significant differences. First, the calculated force area data (Figures 5-3(a), 5-3(b), 5-4(a) and 5-4(b)) exhibit considerably larger scatter than the on-board force area data (Figures 5-1(a), 5-1(b), 5-2(a) and 5-2(b)). More importantly, the curve-fits for calculated drag area data are very nearly symmetric about the zero relative wind direction. In addition, the side force area curve-fits are nearly antisymmetric and pass close to the origin.

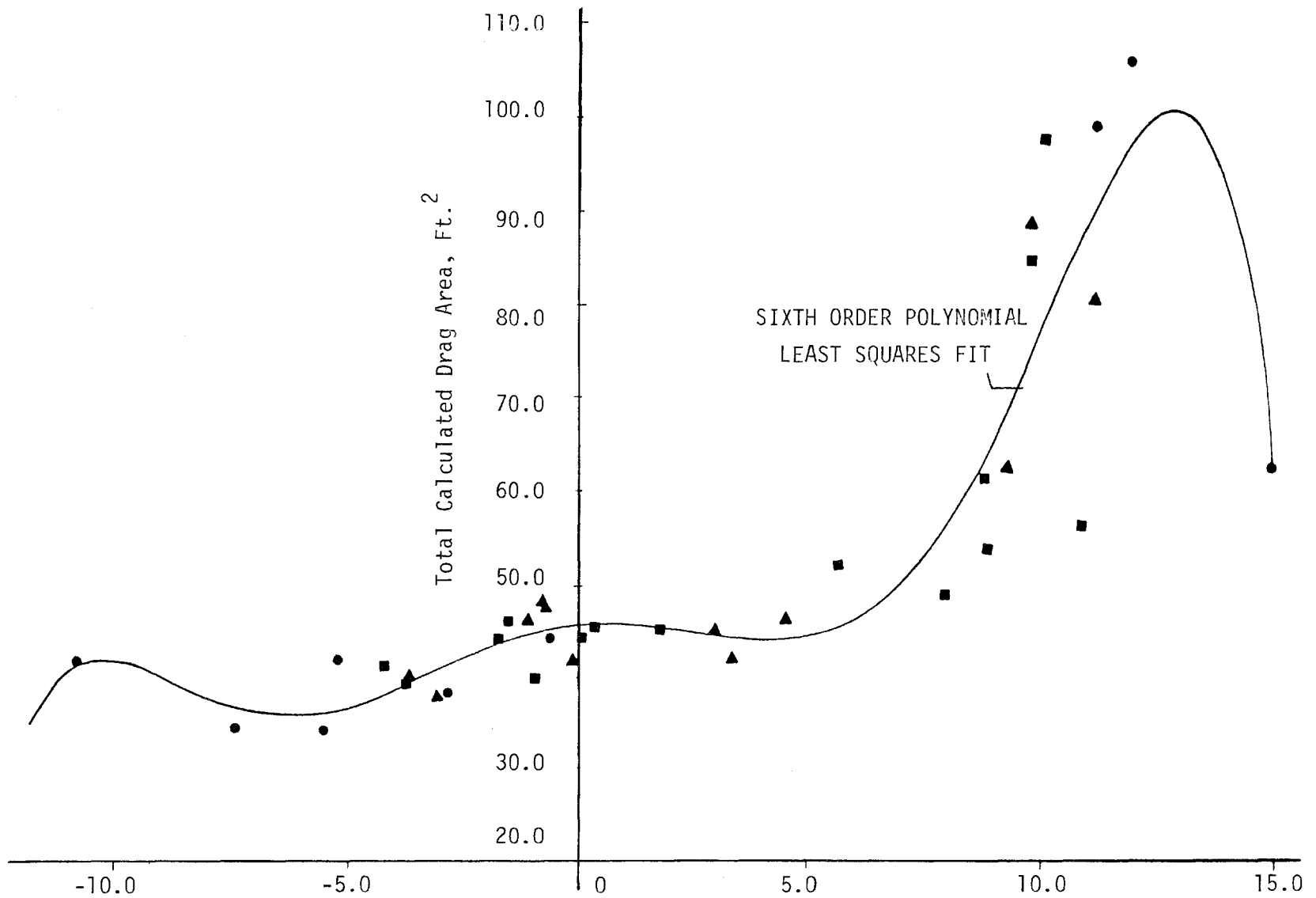


Figure 5-3(a) Total Calculated Drag Area Versus Calculated Relative Wind Direction - Configuration 1

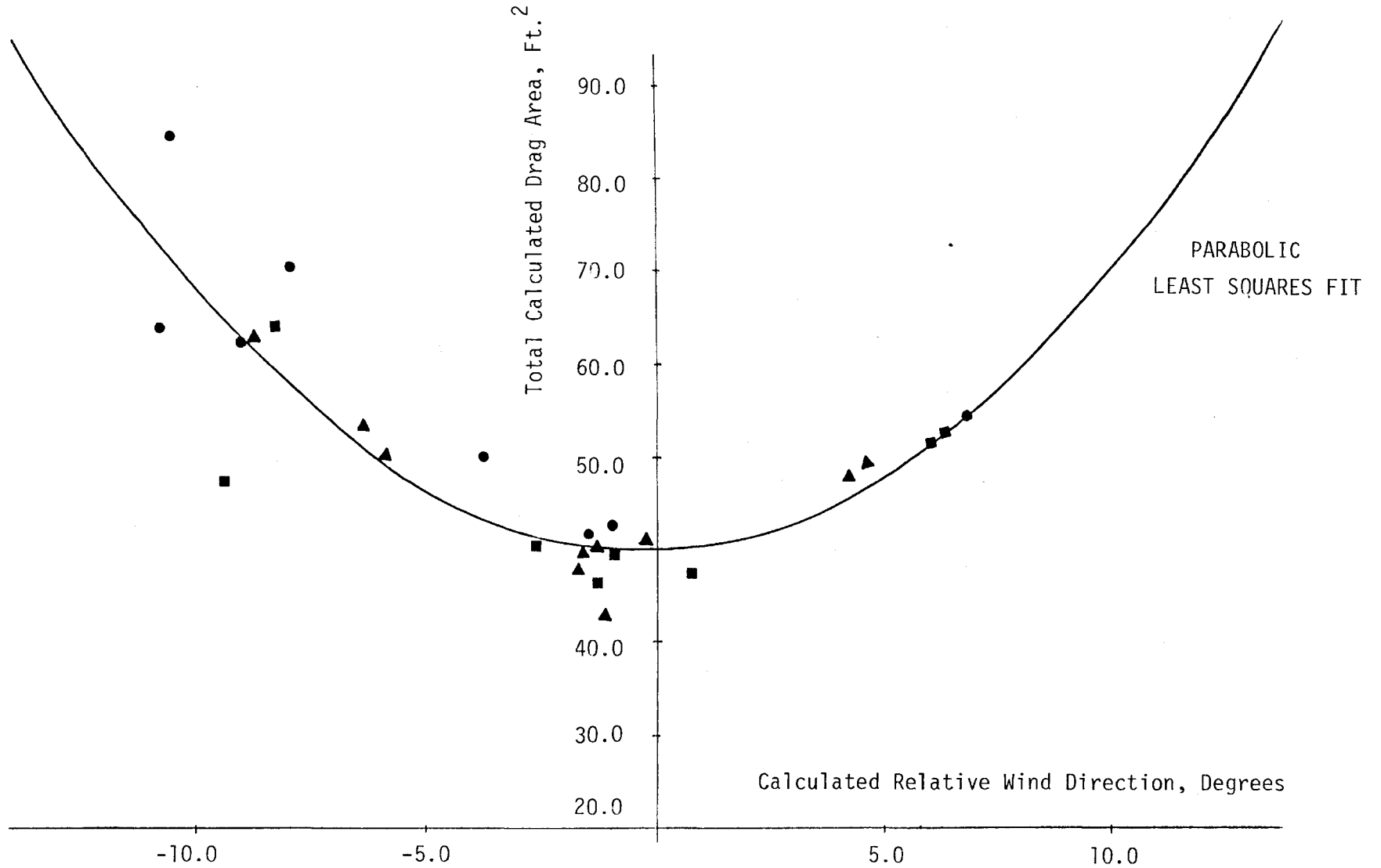


Figure 5-3(b). Total Calculated Drag Area Versus Calculated Relative Wind Direction - Configuration 2

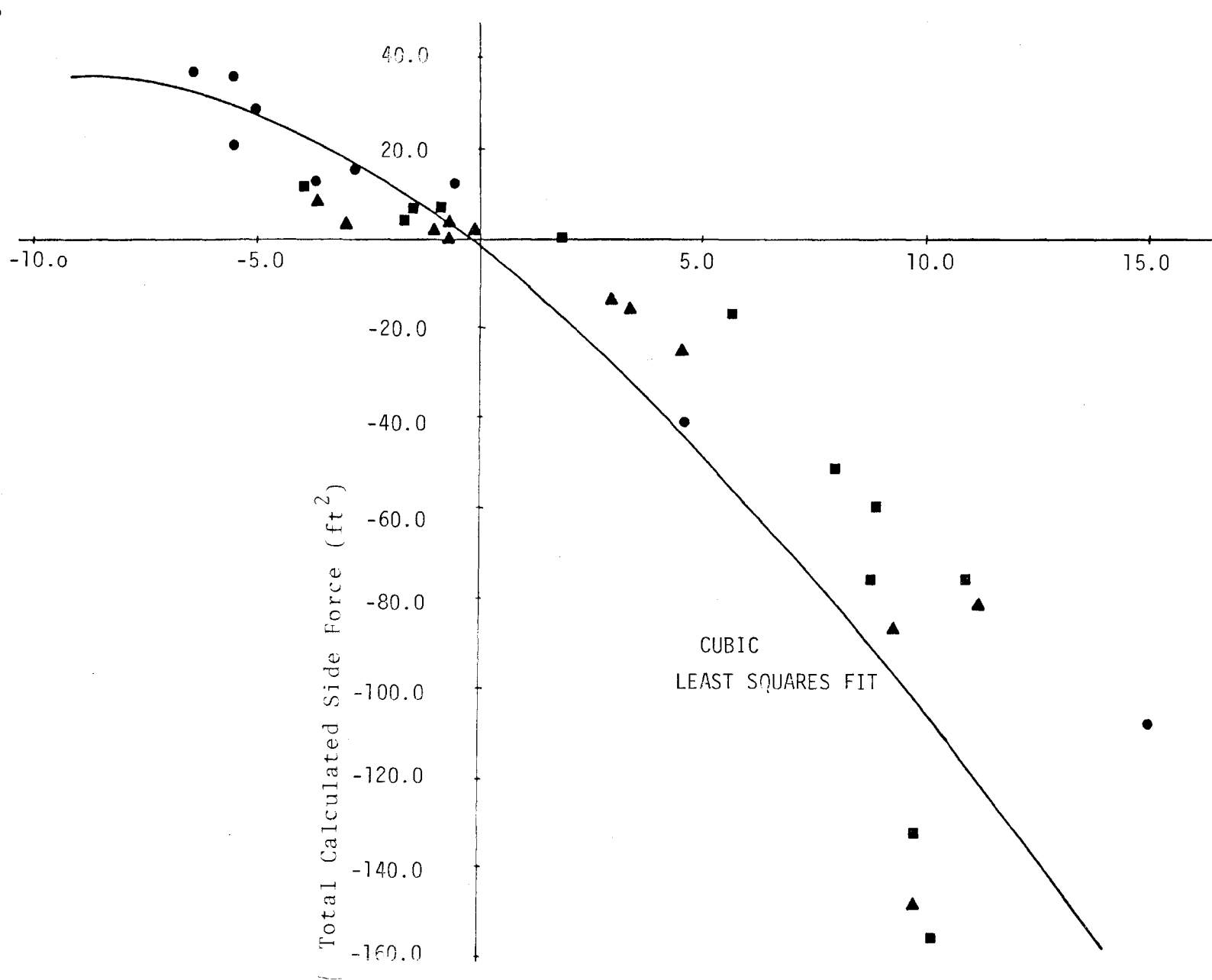


Figure 5-4(a). Total Calculated Side Force Area Versus
Calculated Relative Wind Direction - Configuration 1

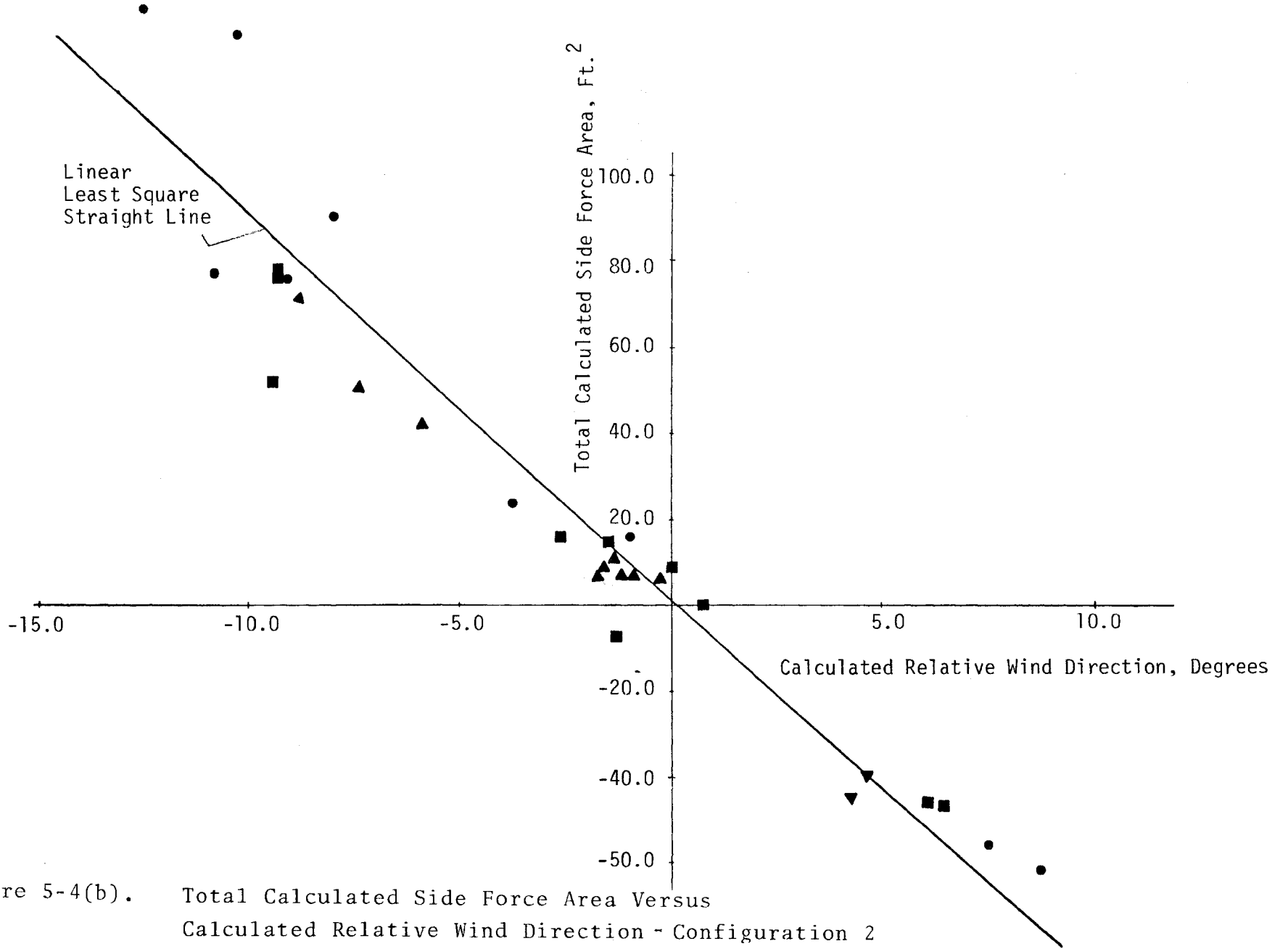


Figure 5-4(b). Total Calculated Side Force Area Versus Calculated Relative Wind Direction - Configuration 2

5.4 FORCE AREA DATA BASED ON ONBOARD WIND DATA CORRECTED FOR OFFSET

The observation in Section 5.3 regarding data scatter indicates that it is more appropriate to correlate the force areas using the onboard relative wind data rather than the calculated relative wind data. A possible explanation for the scatter is that the wayside wind measurement is affected by the passage of the test consist. For example, the consist tends to shield the weather station from winds coming at positive angles (Figure 4-1)b). Also, the wind direction at the weather station is influenced by mass entrainment into the train boundary layer and wake.

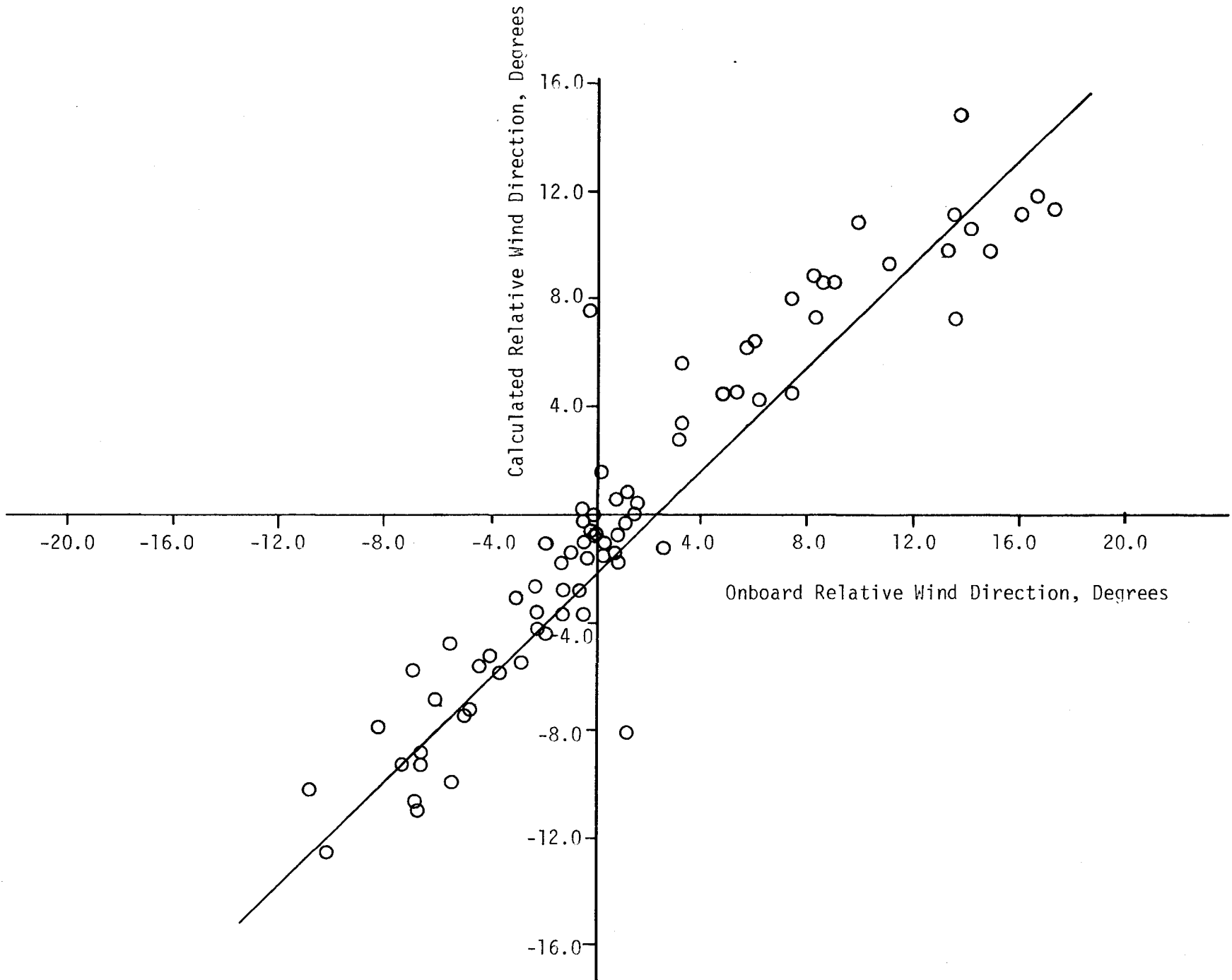
The near-absence of zero-offsets in the case of calculated force area data strengthens the conviction that the onboard wind direction measurement was slightly off. Further evidence supporting this assertion is provided by Figure 5-5 which shows the calculated relative wind direction plotted against onboard relative wind direction. The data used in these graphs was obtained from Tables 4-3A and 4-4A for Configuration 1, and from Tables 4-3B and 4-4B for Configuration 2. The equation of the linear least squares fit in Figure 5-5 is

$$y = -2.2 + 0.96x$$

where x and y represent the calculated and onboard wind directions in degrees.

Since the slope of this straight line is nearly unity, the two wind directions agree well with each other, except for a zero-offset of 2.2 degrees.

A visual examination of the onboard wind direction instrument (Figure 2-20) showed a small warp in its tail. A post-test calibration of the sensor was performed in a low-speed wind tunnel at Virginia Polytechnic Institute. These tests revealed the existence of an offset with respect to the true wind direction and in the sense expected (Section 5.3). However, the offset varied with airspeed and had to be averaged at



high speeds due to buffeting of the tail of the instrument. The results are listed in Table 5-1.

TABLE 5-1

ZERO OFFSETS OF ONBOARD WIND INSTRUMENT

AIR SPEED RANGE (MPH)	OFFSET W.R.T. TRUE WIND DIRECTION (DEGREES)
30 - 50	+1
50 - 60	0
60 - 100	+1

The offset corrections in Table 5-1 were applied to the onboard wind direction and are already incorporated into the AERO/TOFC (Series II) test data tables in Section 4.0. The drag, side force and lift-areas based on onboard wind data from Tables 4-3A and 4-3B have been plotted in Figures 5-6(a), 5-6(b), 5-7(a), 5-7(b), 5-8(a) and 5-8(b) for both Configurations 1 and 2. For convenience, the data points in these graphs are identified by the corresponding test run numbers. All possibly erroneous data in Tables 4-3A and 4-3B have been omitted from the aforementioned plots. The force area data points, taken as a whole on each plot, seem to have a slight shift to the right (approximately one degree) after the application of the offset correction. This may be due to (1) the fact that the onboard wind direction indicator is accurate within one degree as specified by the manufacturer; (2) such subtle factors as topography of the terrain near the test track (Figure 2-1(b)), which can result in the wind angle at the trailers being different from the wind angle at the locomotive.

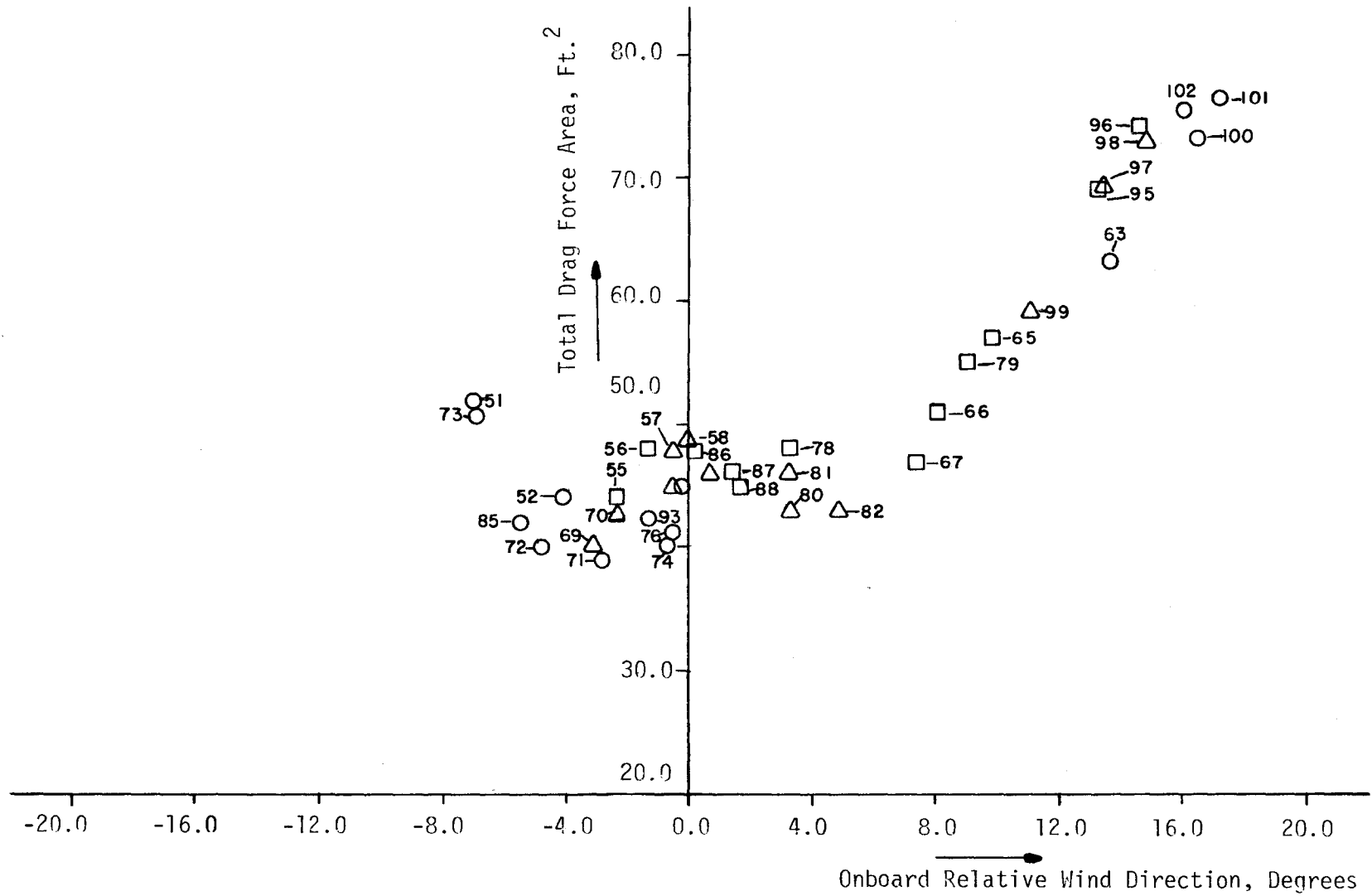


Figure 5-6(a). Total Drag Area vs Onboard Relative Wind Direction - Configuration 1

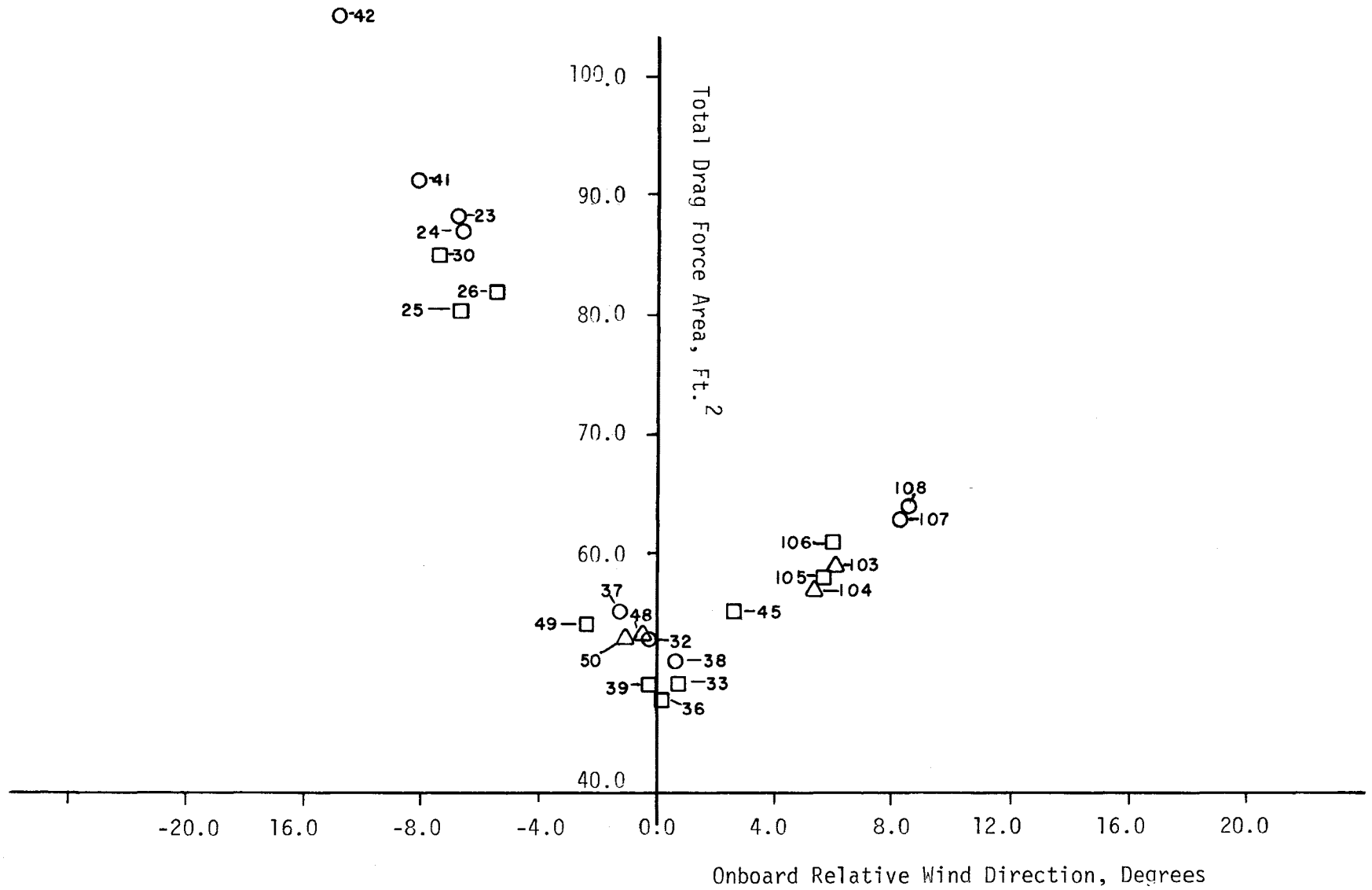


Figure 5-6(b). Total Drag Area vs Onboard Relative Wind Direction - Configuration 2

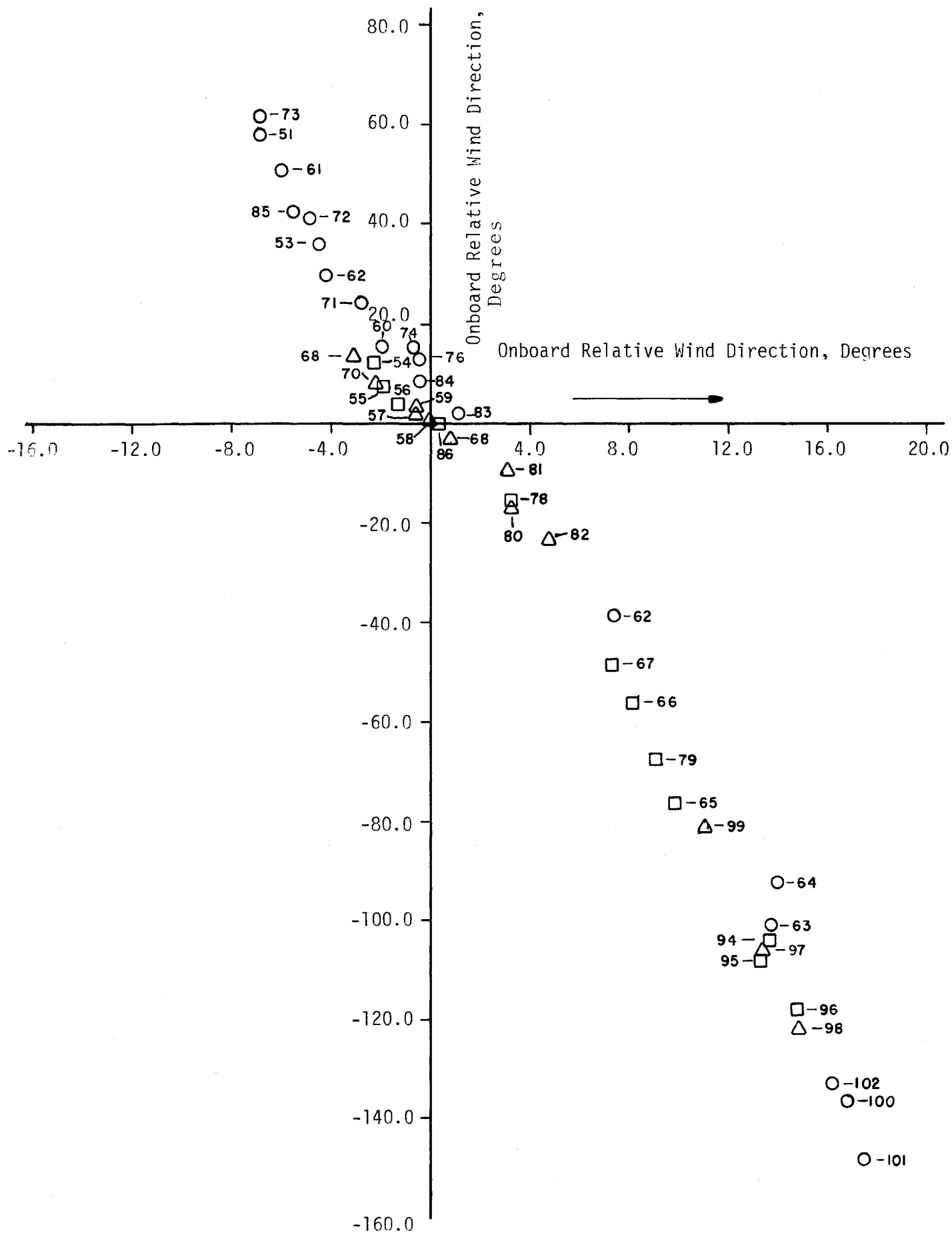


Figure 5-7(a). Total Side Force Area vs Onboard Relative Wind Direction - Configuration 1

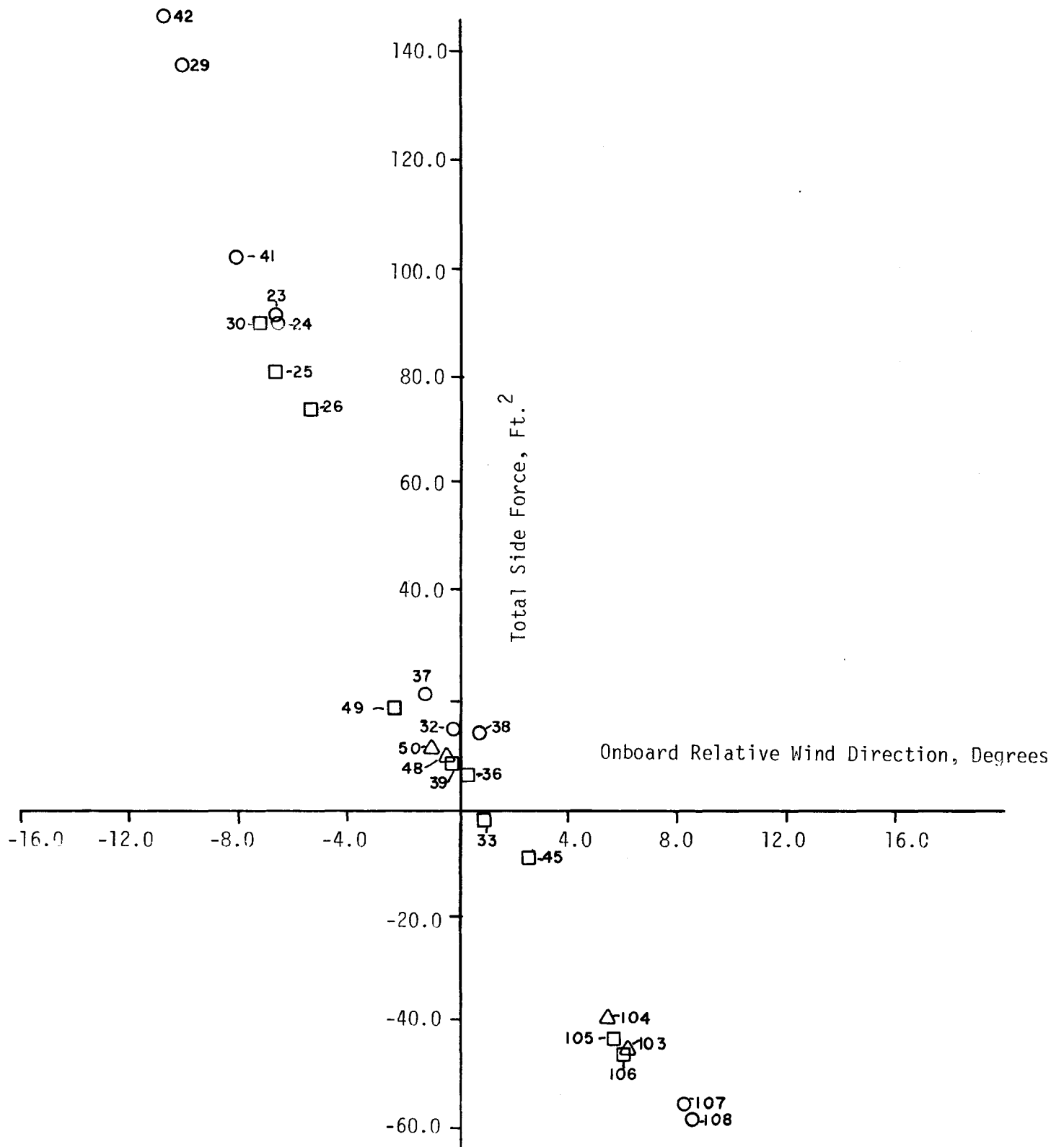


Figure 5-7(b). Total Side Force Area vs Onboard Relative Wind Direction- Configuration 2

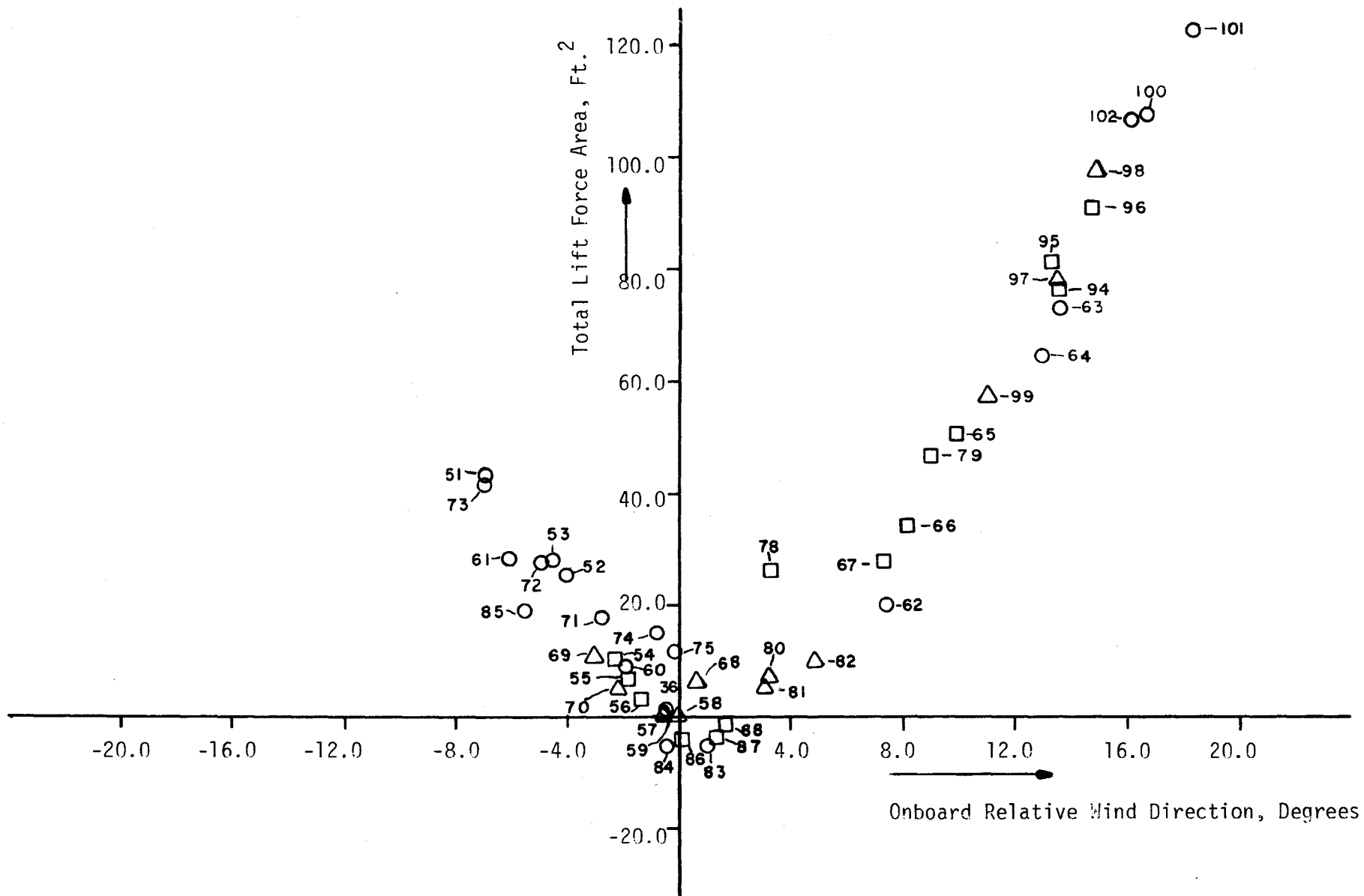


Figure 5-8(a). Total Lift Force Area vs Onboard Relative Wind Direction - Configuration 1

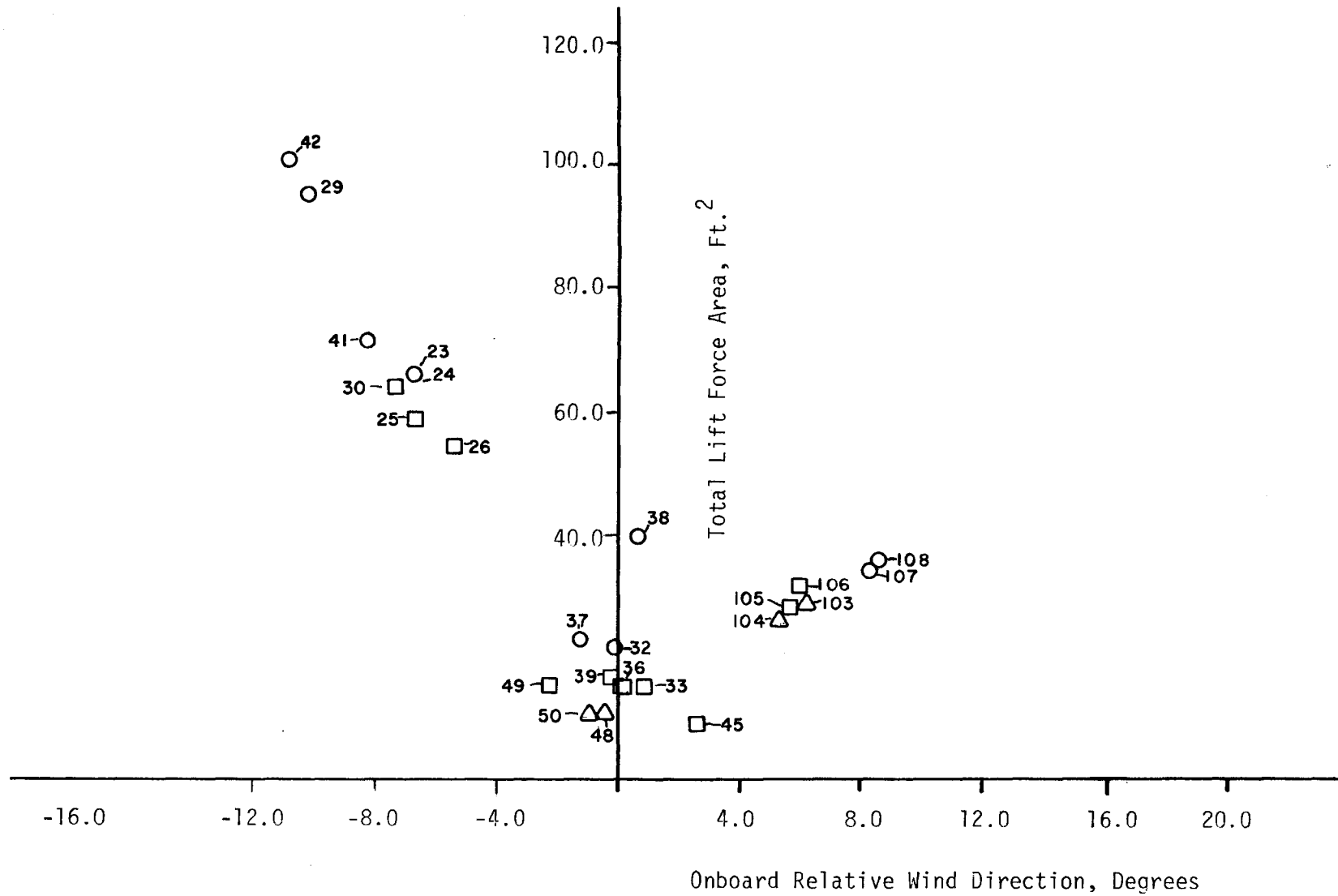


Figure 5-8(b). Total Lift Area vs Onboard Relative Wind Direction - Configuration 2

A comparison of Figures 5-6(a) and 5-6(b) shows that Configuration 2 experiences significantly larger drag than Configuration 1. The side forces for the two configurations are approximately the same from Figures 5-7(a) and 5-7(b).

5.5 ANALYSIS OF ROLLING RESISTANCE INFORMATION

The tractive resistance of the entire TOFC configuration consists of the rolling resistance and the aerodynamic drag as pointed out in Section 1.1. During the AERO/TOFC (Series II) tests, the tractive resistance was obtained as the difference between leading and trailing coupler forces and is listed in Tables 4-5A (Configuration 1) and 4-5B (Configuration 2). The rolling resistance information was computed using the procedure in Section 4.3.3 and is also contained in Tables 4-5A and 4-5B. It should be emphasized that this data contains the aerodynamic drag of the flat car.

Figures 5-9(a) and 5-9(b) show the total tractive resistance for Configurations 1 and 2 plotted against the onboard relative wind speed. The relative wind speed (V_{rel}) rather than average train speed was selected since the tractive resistance includes drag force, which is proportional to V_{rel}^2 . It is seen that the tractive resistance increases quite rapidly with the relative speed for both configurations. Configuration 2, however, generally experiences greater tractive resistance than Configuration 1 due to a larger aerodynamic drag contribution.

The following quadratic least squares fits apply to the tractive resistance data.

Configuration 1:

$$y = 306.7 - 8.05 x + 0.118 x^2$$

Configuration 2:

$$y = 1149 - 24.0 x + 0.213 x^2$$

where x and y represent relative wind speed (ft/sec) and total tractive resistance (lbs), respectively.

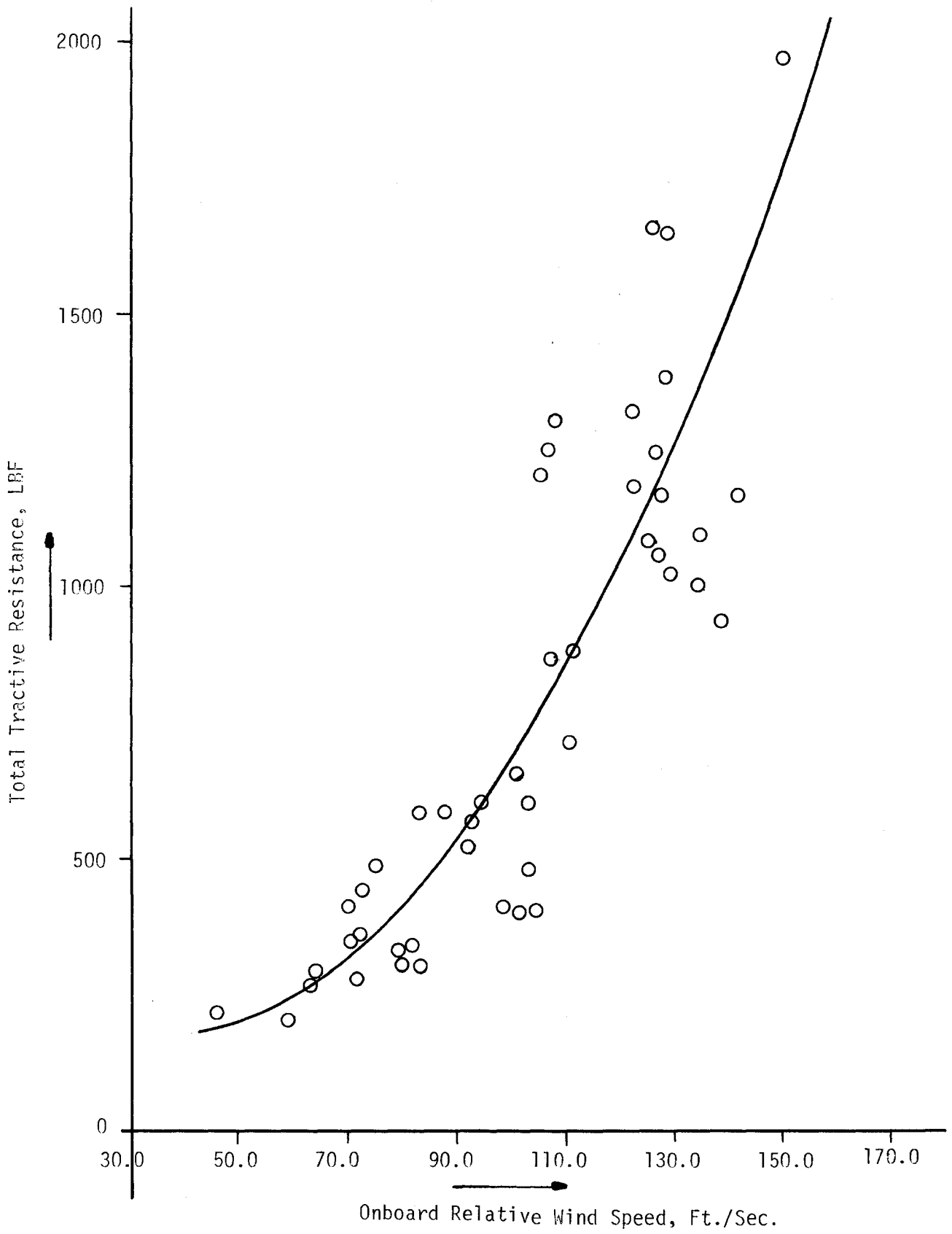


Figure 5-9(a). Total Tractive Resistance for Configuration 1.

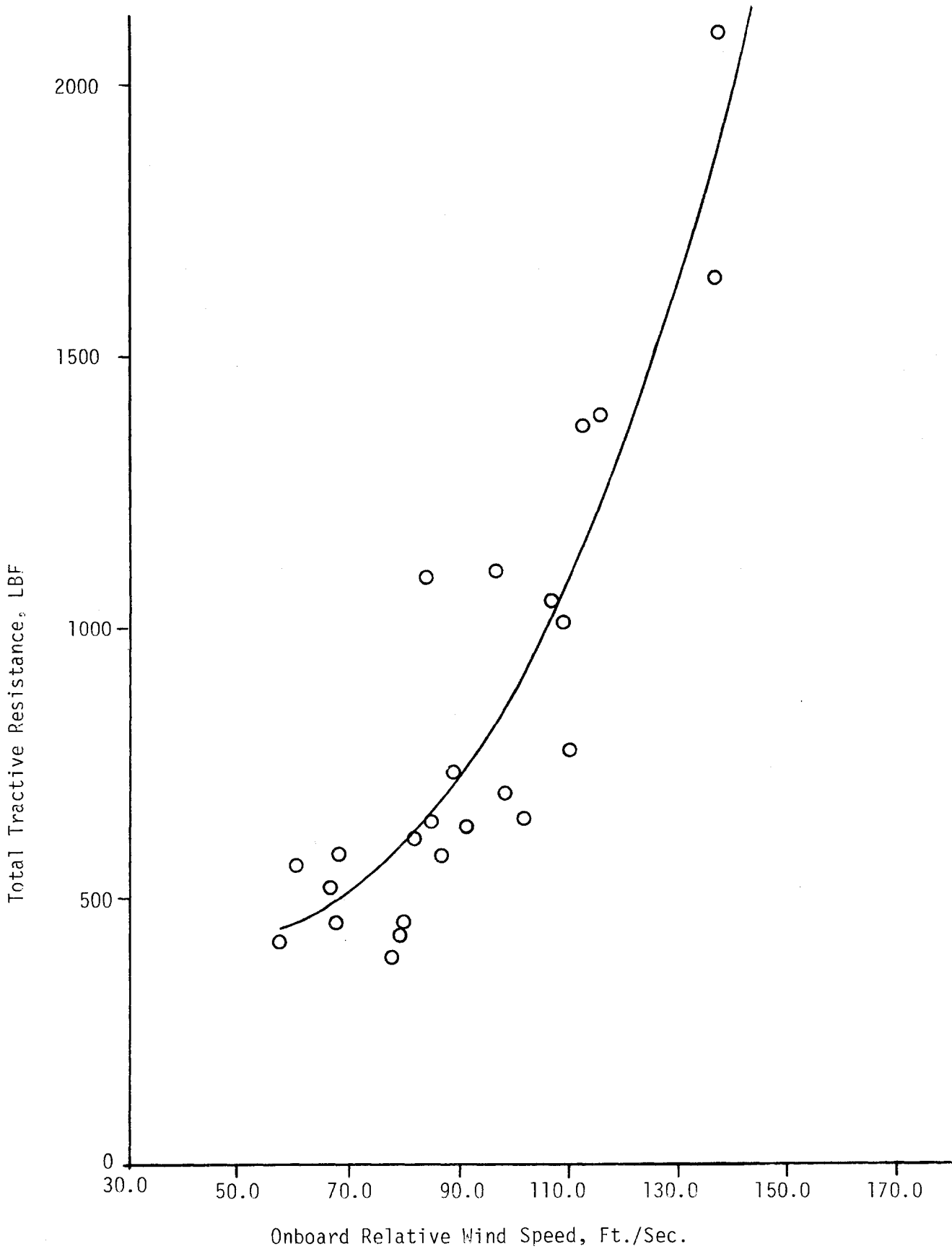


Figure 5-9(b). Total Tractive Resistance for Configuration 2

Since the rolling resistance data implies aerodynamic drag of the flat car, it is first displayed against onboard relative wind speed (Figures 5-10(a) and 5-10(b)). Both configurations are characterized by a gradual increase in rolling resistance (plus TTX drag) with wind speed. This slow increase indicates that the flat car drag amounts to a small share. It is expected that Configurations 1 and 2 should have the same rolling resistance and TTX drag. Comparing Figures 5-10(a) and 5-10(b) shows that this is indeed the case. In fact, the quadratic least squares fits for the two sets of data are close, as shown below.

Configuration 1:

$$y = 553.2 - 6.37x + 0.060x^2$$

Configuration 2:

$$y = 656.2 - 7.56x + 0.066x^2$$

where x denotes relative wind speed (ft/sec) and y the rolling resistance including TTX drag (lbs).

It may be useful to display the rolling resistance information against the average train speed (Tables 4-1A and 4-1B). This is done in Figure 5-11 (a) for Configuration 1 and in Figure 5-11(b) for Configuration 2. Although the data points are grouped about three values of average train speed, an interesting trend is evident. At low train speeds, when aerodynamic drag of the flat car is negligible, the data points are close together. As the train speed increases, the data points spread apart due to TTX drag contributions. Therefore, the envelopes of data points in Figures 5-11(a) and 5-11(b) tend to converge to purely rolling resistance when extrapolated to low train speeds. Also, as pointed out in Reference 1, it is generally assumed that the rolling resistance depends at most linearly on the train speed (after allowing for acceleration and gravitational forces).

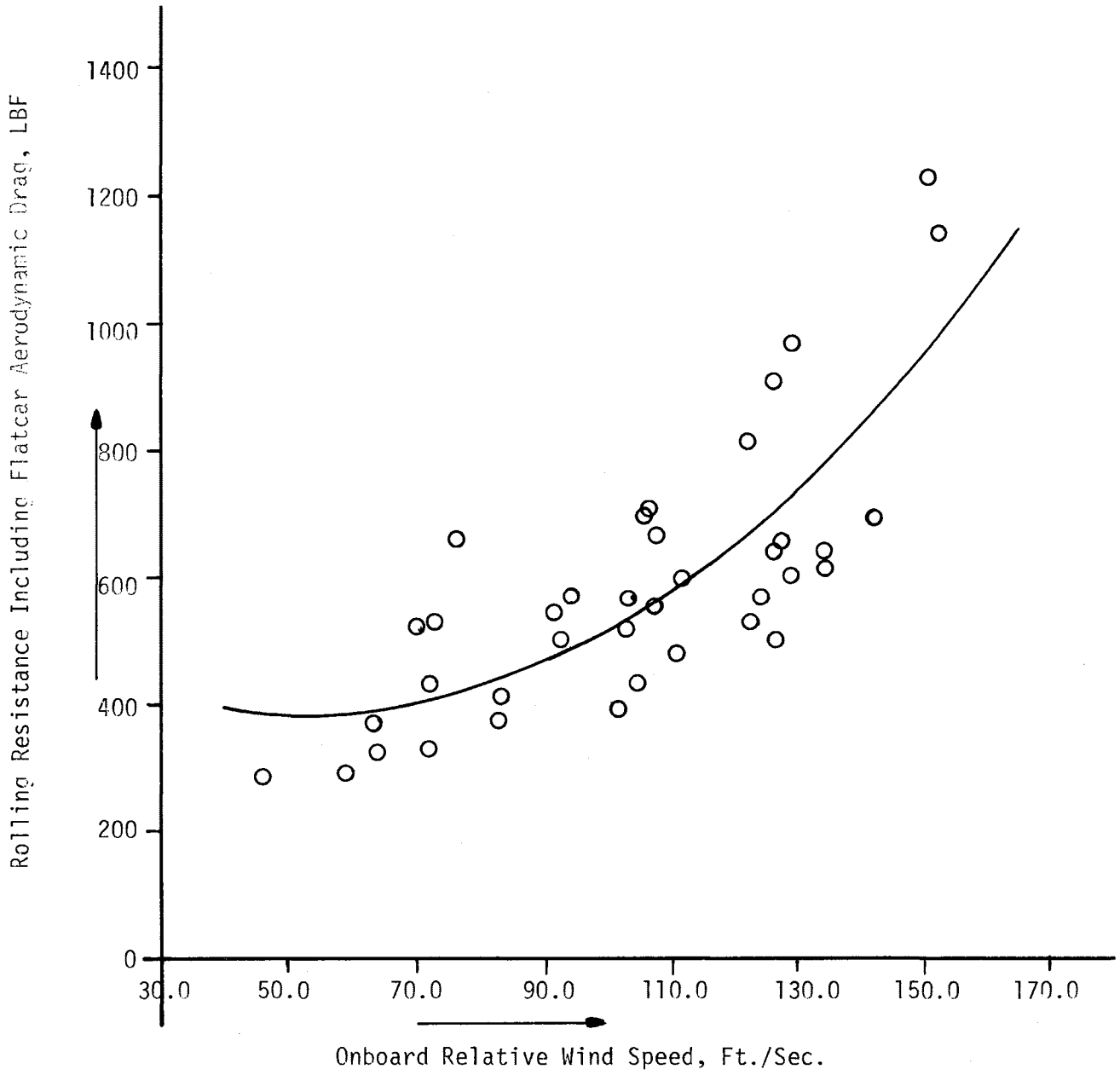


Figure 5-10(a). Rolling Resistance Information versus Onboard Relative Wind Speed - Configuration 1

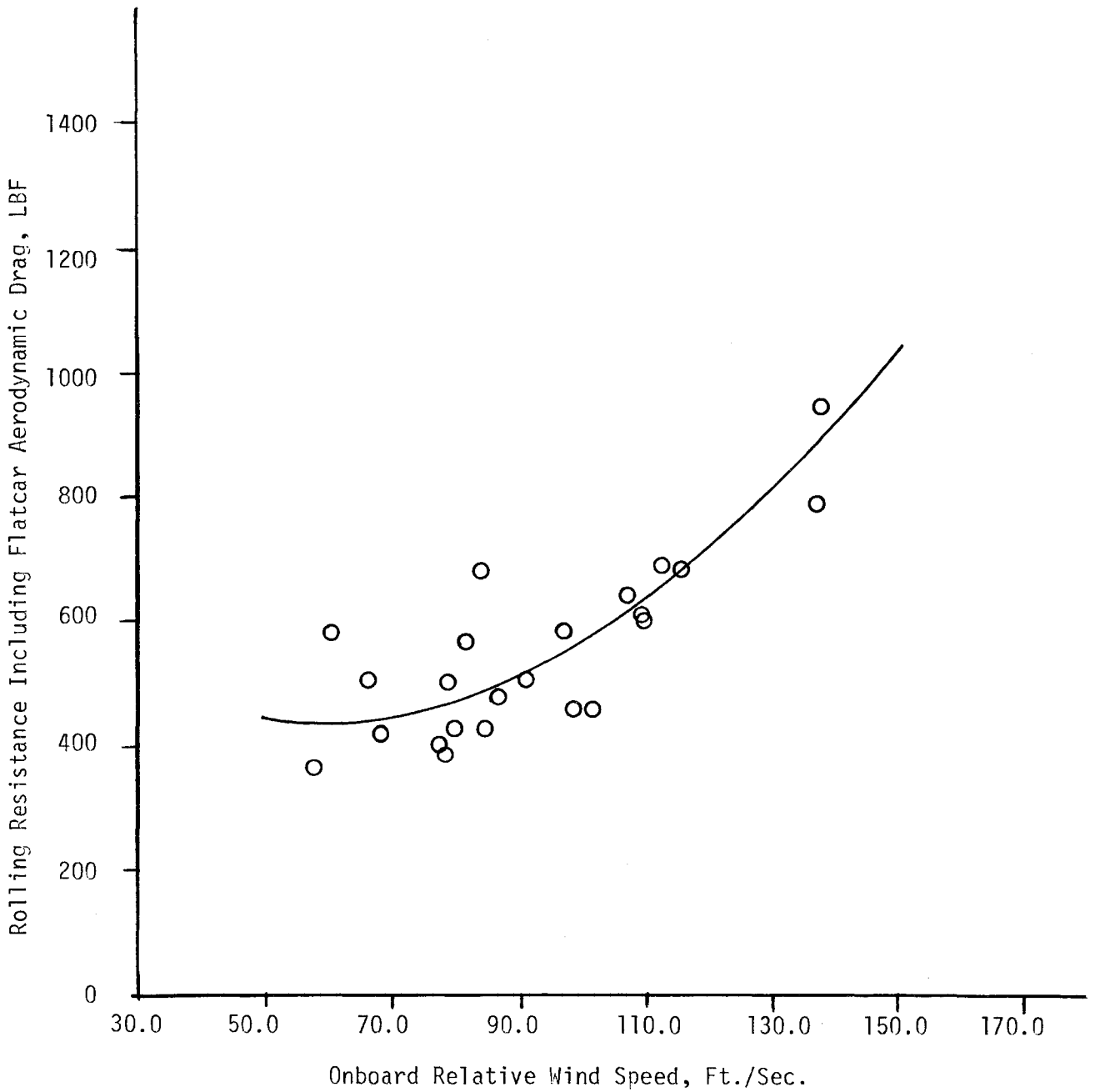


Figure 5-10(b). Rolling Resistance Information versus Onboard Relative Wind Speed - Configuration 2

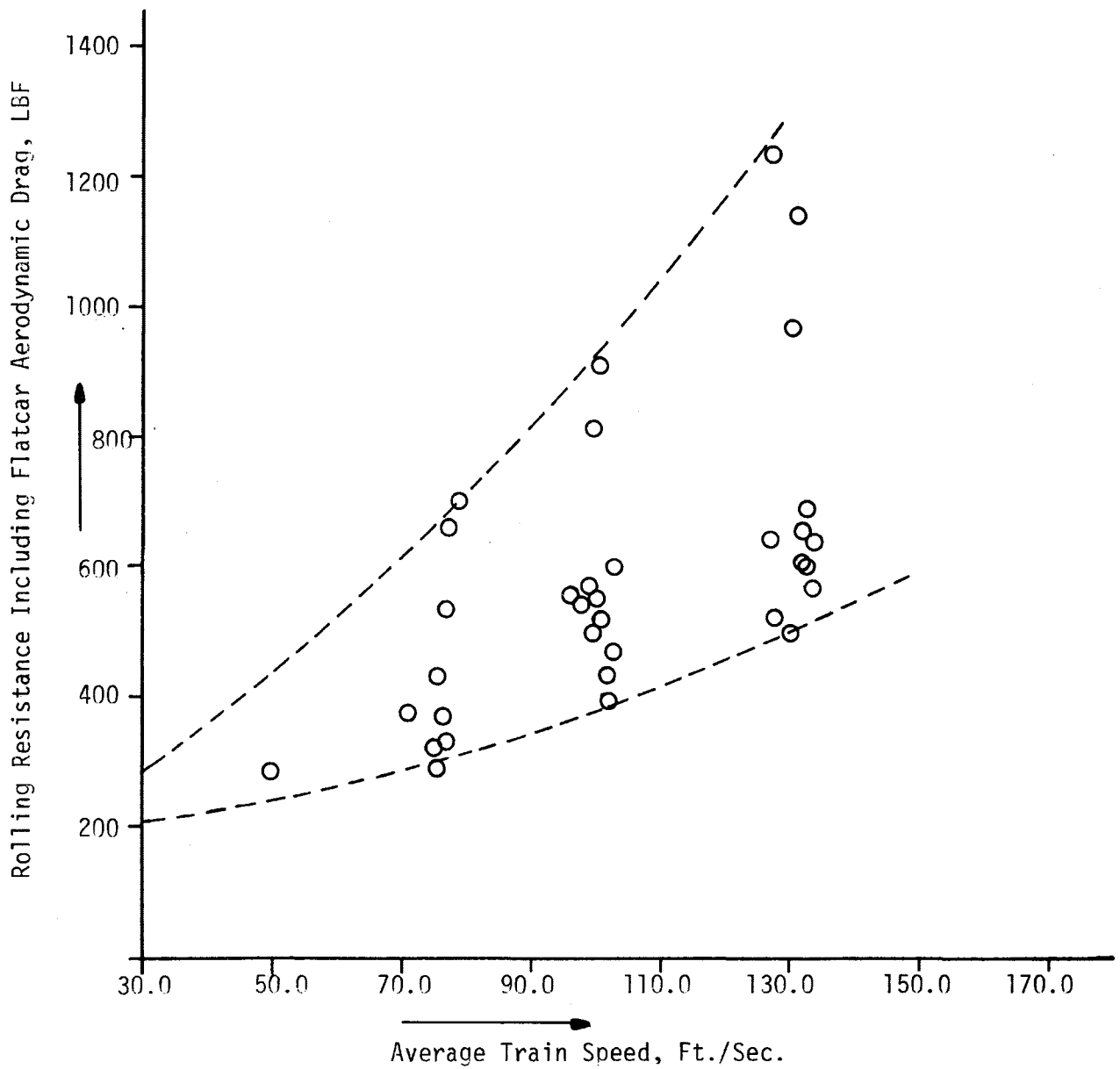


Figure 5-11(a). Rolling Resistance Information versus Average Train Speed - Configuration 1

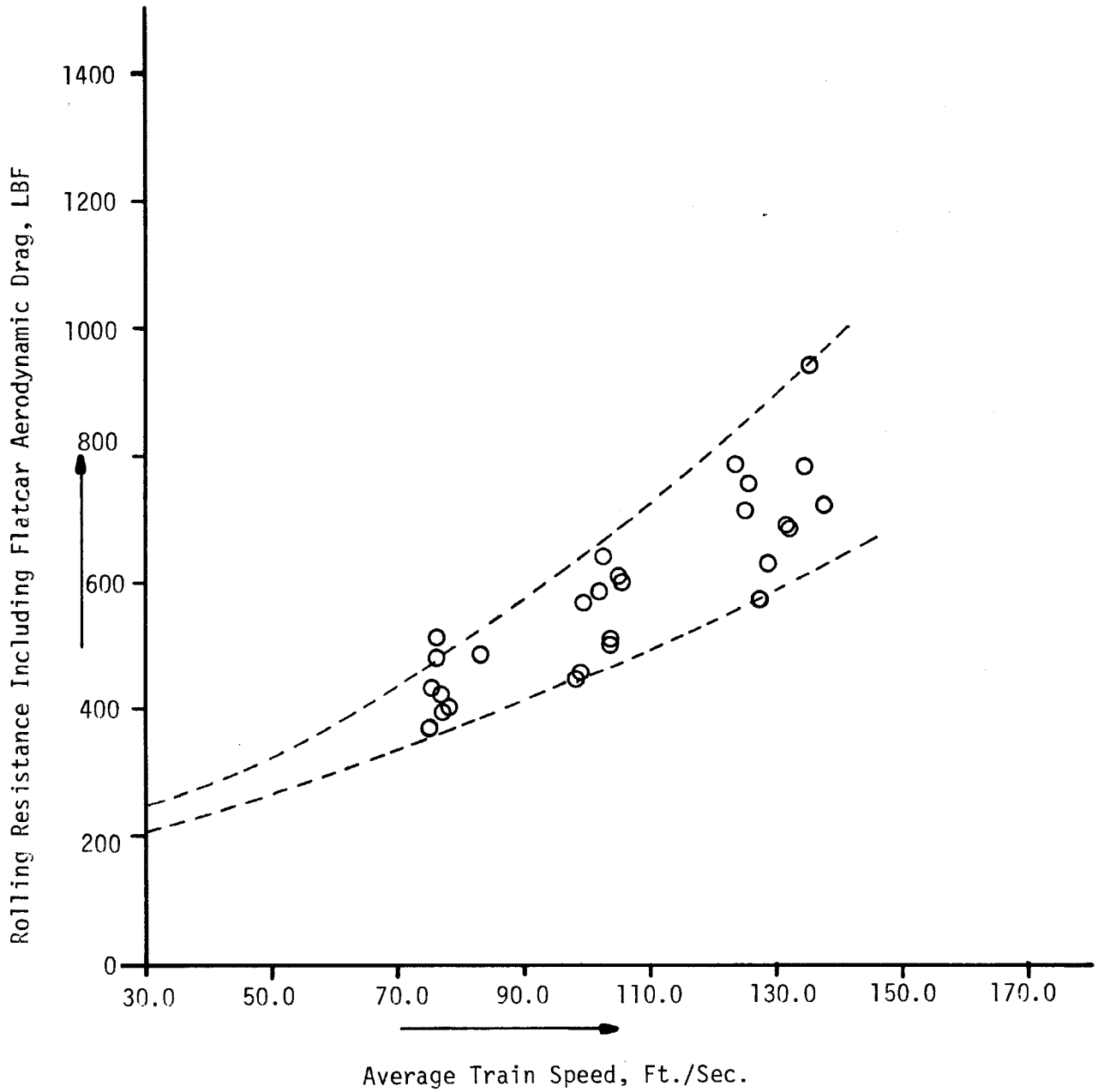


Figure 5-11(b). Rolling Resistance Information versus Average Train Speed - Configuration 2

Thus, the lower envelopes, which appear to be nearly linear and less sensitive to train speed, should yield approximate values of rolling resistance. The resistance values, obtained in this manner, are likely to be more accurate at low train speeds. Rough estimates of the rolling resistance of the TTX car as shown in Figures 5-1(a) and 5-1(b) are given in Table 5-2.

TABLE 5-2

APPROXIMATE RANGE OF TTX ROLLING RESISTANCE

TRAIN SPEED (MPH)	APPROXIMATE RANGE OF ROLLING RESISTANCE (LBS)
30	230 - 240
50	300 - 350
70	380 - 450
90	520 - 600

6.0 COMPARISON OF FULL-SCALE AND WIND TUNNEL DATA

6.1 GENERAL

It may be recalled that the primary objective of the AERO/TOFC (Series II) Tests was to obtain aerodynamic resistance data on full-scale TOFC configurations in order to validate the results of wind tunnel tests. As mentioned in Section 1.1, aerodynamic force measurements were made on 1/43-scale models of TOFC configurations in the wind tunnels of California Institute of Technology (Reference 1) and the Calspan Corporation (Reference 2): This chapter deals with the comparison of AERO/TOFC (Series II) aerodynamic force data with the wind tunnel results.

6.2 BRIEF DESCRIPTION OF WIND TUNNEL TESTS

The CIT tests employed a Reynolds number of 1.2×10^6 (1/20 of full-scale) based on trailer length. The ratio of boundary layer thickness to the model height was approximately 1/4. The Calspan experiments used a variable density tunnel and the Reynolds number ranged from 1/20 to 1/5 of full scale. The boundary layer thickness was reduced up to 1/5 of the model height. Both test programs simulated the ground plane by means of a stationary ground board.

A comparison of the results of the CIT and Calspan tests is given in Reference 8. While the Calspan data showed no trends in drag (or side force) with Reynolds number, it generally exhibited marked deviations from the CIT data, except at low Reynolds numbers. Figures 6-1(a), 6-1(b), 6-2(a) and 6-2(b) display the drag and side force areas for Configurations 1 and 2 as reproduced from Reference 2. It is obvious that the CIT results give larger drag and side forces (hence areas) than the Calspan results. Some significant differences between the two tests need to be pointed out here. First, the Calspan TOFC configurations were the same as the ones used in the full-scale AERO/TOFC (Series II) tests. Secondly, repeatability runs were

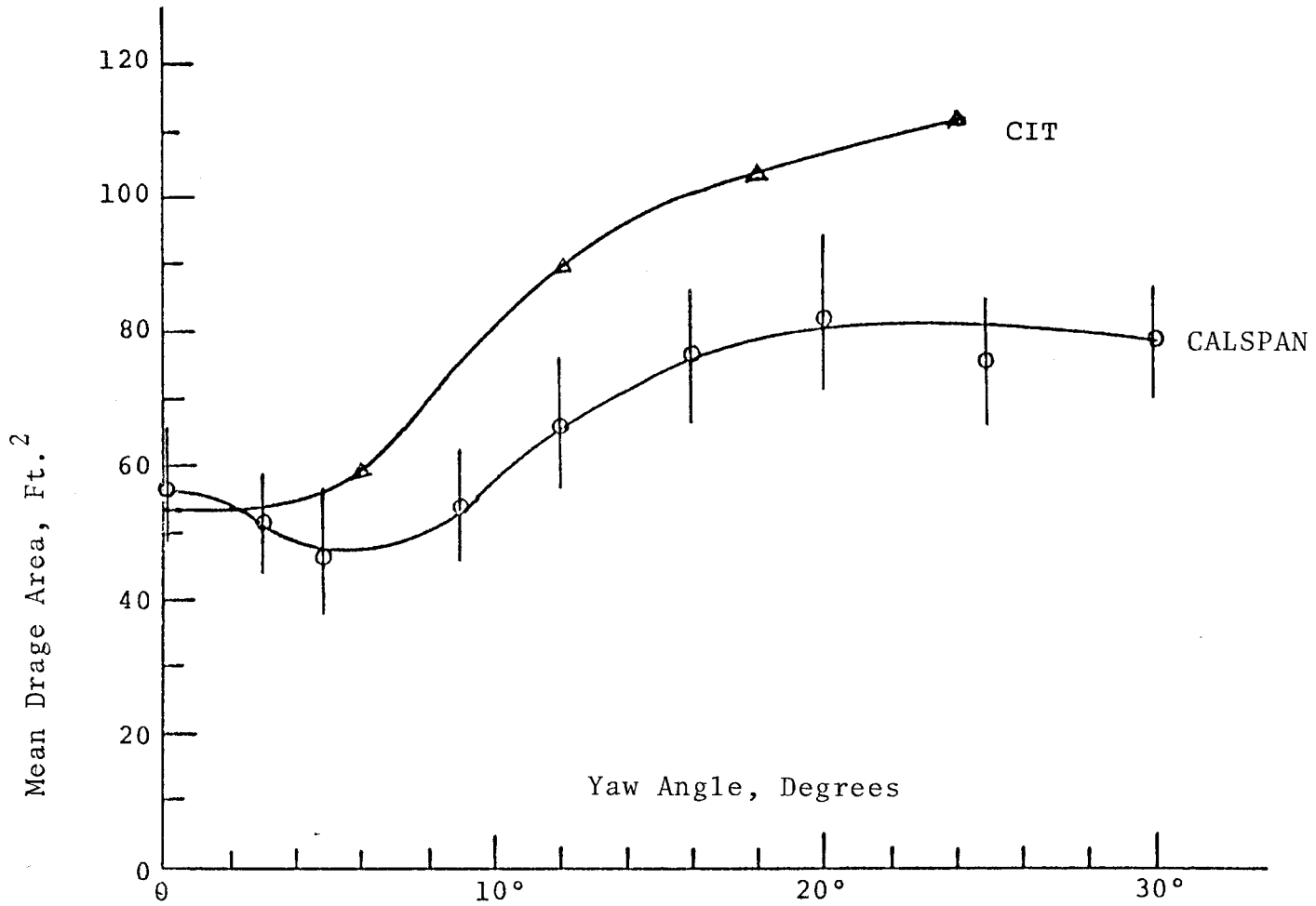


Figure 6-1(a). Mean Drag Area as a Function of Wind Angle - Configuration 1

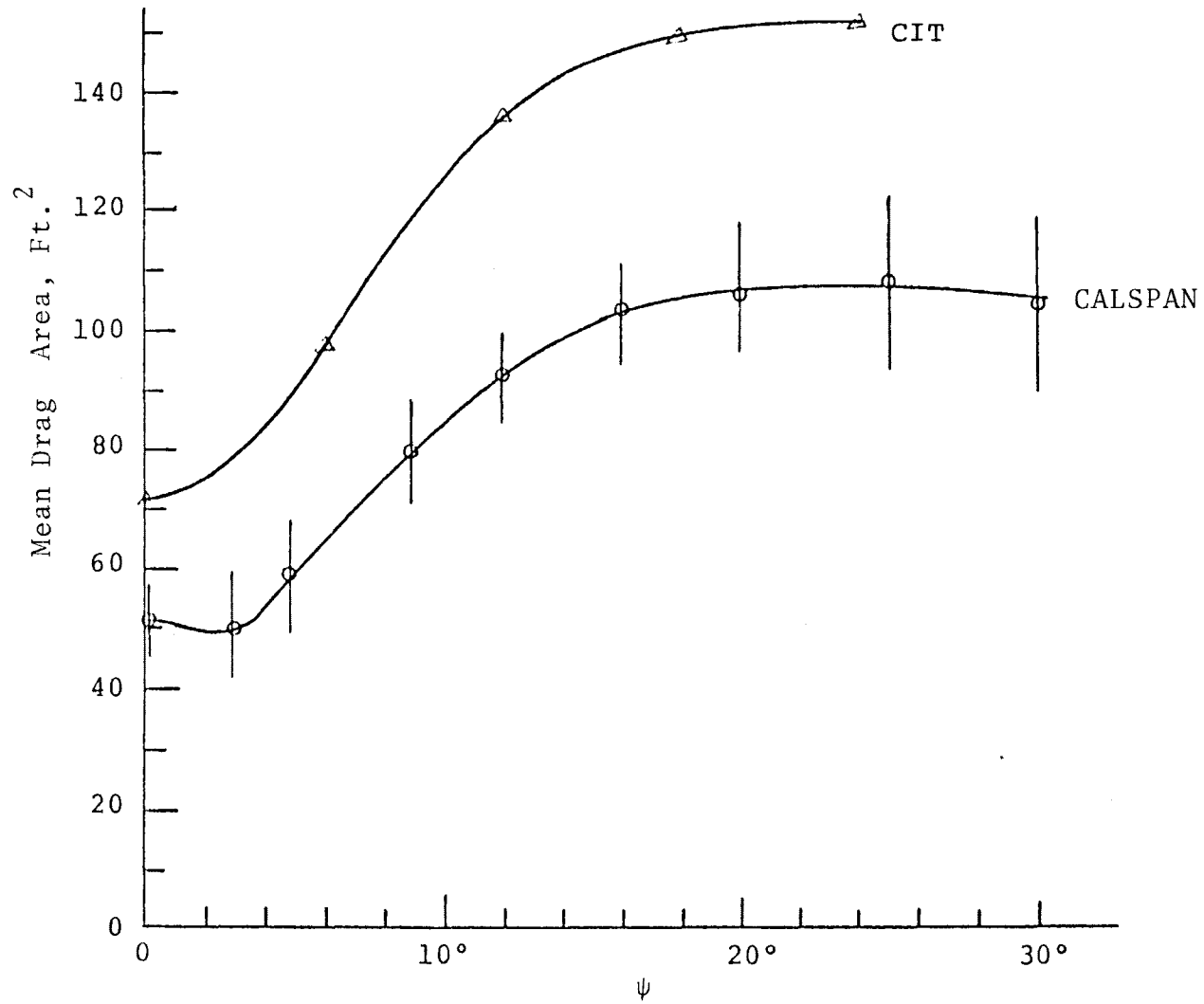


Figure 6-1(b). Mean Drag Area as a Function of Wind Angle - Configuration 2

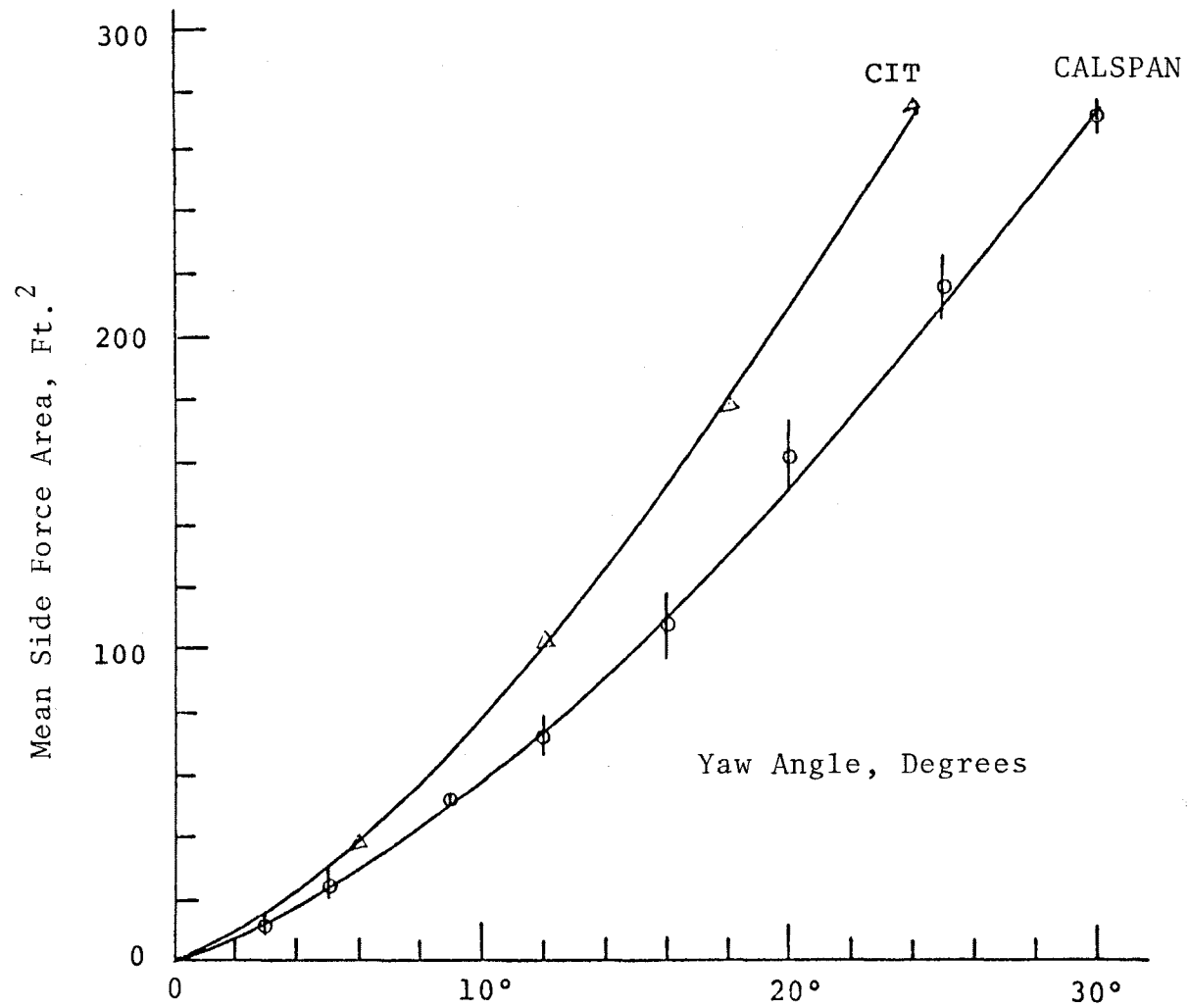


Figure 6-2(a). Mean Side Force Area as a Function of Wind Angle - Configuration 1

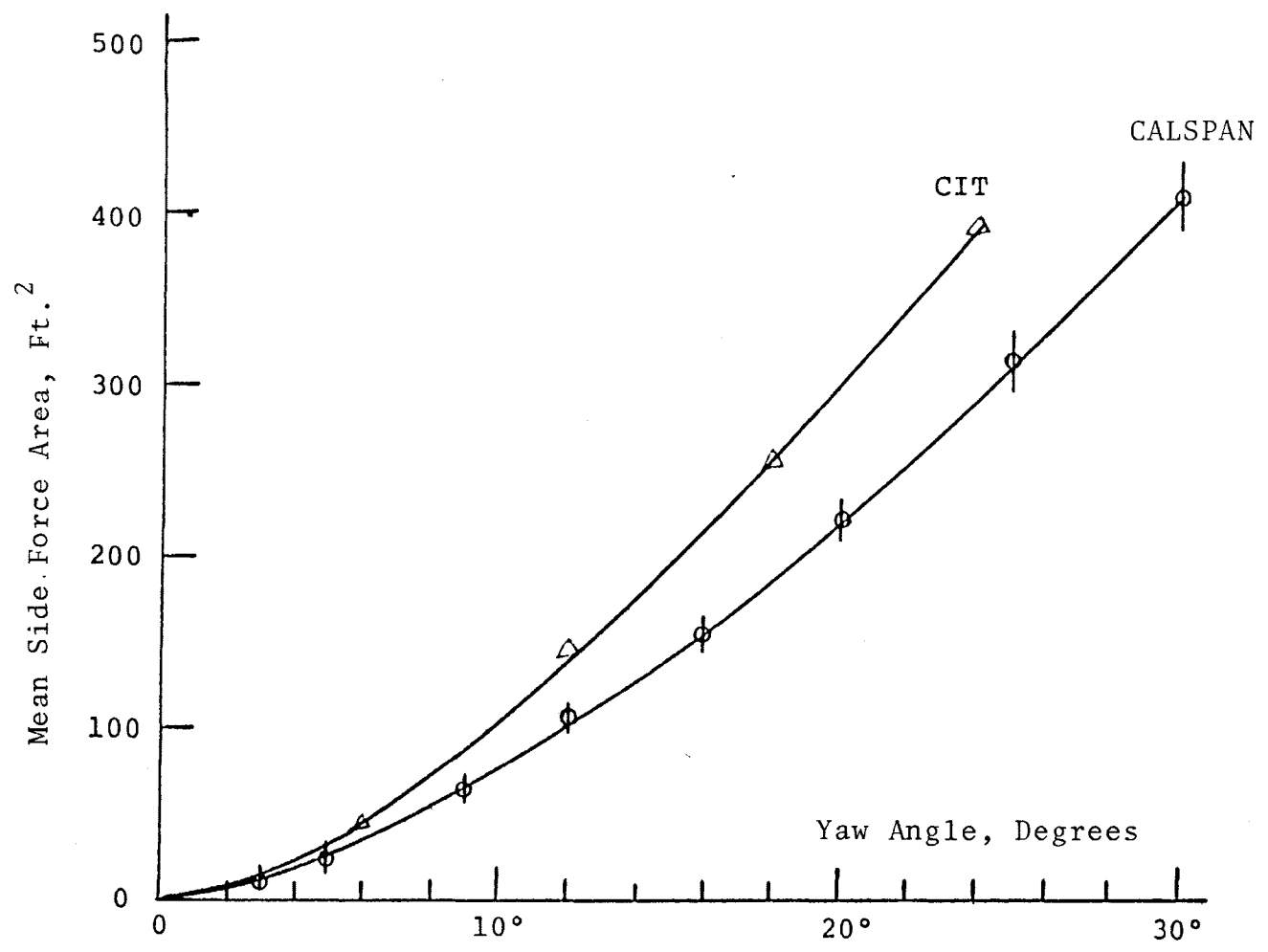


Figure 6-2(b). Mean Side Force Area as a Function of Wind Angle - Configuration 2

performed during the Calspan tests and a statistical analysis of the scatter in the data was made. It was found that the drag force data had a considerably larger scatter than the side force data. In the case of the CIT tests, no repeat runs were made to check consistency of the data. Reference 2 contains a detailed discussion attempting to explain the discrepancies between the results of the wind tunnel tests.

6.3 COMPARISON OF CONFIGURATION 1 DATA

6.3.1 Drag Area

Figure 6-3 shows the comparison between the total drag area for full-scale Configuration 1 (Figure 5-6(a)) and the wind tunnel results (Figure 6-1(a))* . It is seen that, in general, the full-scale values are closer to the Calspan curve and exhibit a similar trend with increasing wind angle. The agreement with the Calspan tests is especially good when the relative wind is from the right (Figure 4-1(b)) and at large angles.

The CIT wind tunnel results, on the other hand, do not follow the trend of the full-scale measurements and consistently overestimate the data. While the difference is small, near zero wind angle, deviations of as much as 150 percent occur at 10 degrees.

6.3.2 Side Force Area

Figure 6-4 shows the wind tunnel side force data of Figure 6-2(a) compared to the full-scale data of Figure 5-7(a). There appears to be a reasonable agreement between the wind tunnel and the full-scale values, and the differences are not as pronounced as in the case of drag area (Figure 6-3). For positive wind angles (i.e., head wind from the right as in Figure 4-1(b)), the full-scale measurements fall in between

*Wind tunnel drag area plots have been reproduced for both positive and negative wind angles, and are symmetric about zero wind angle.

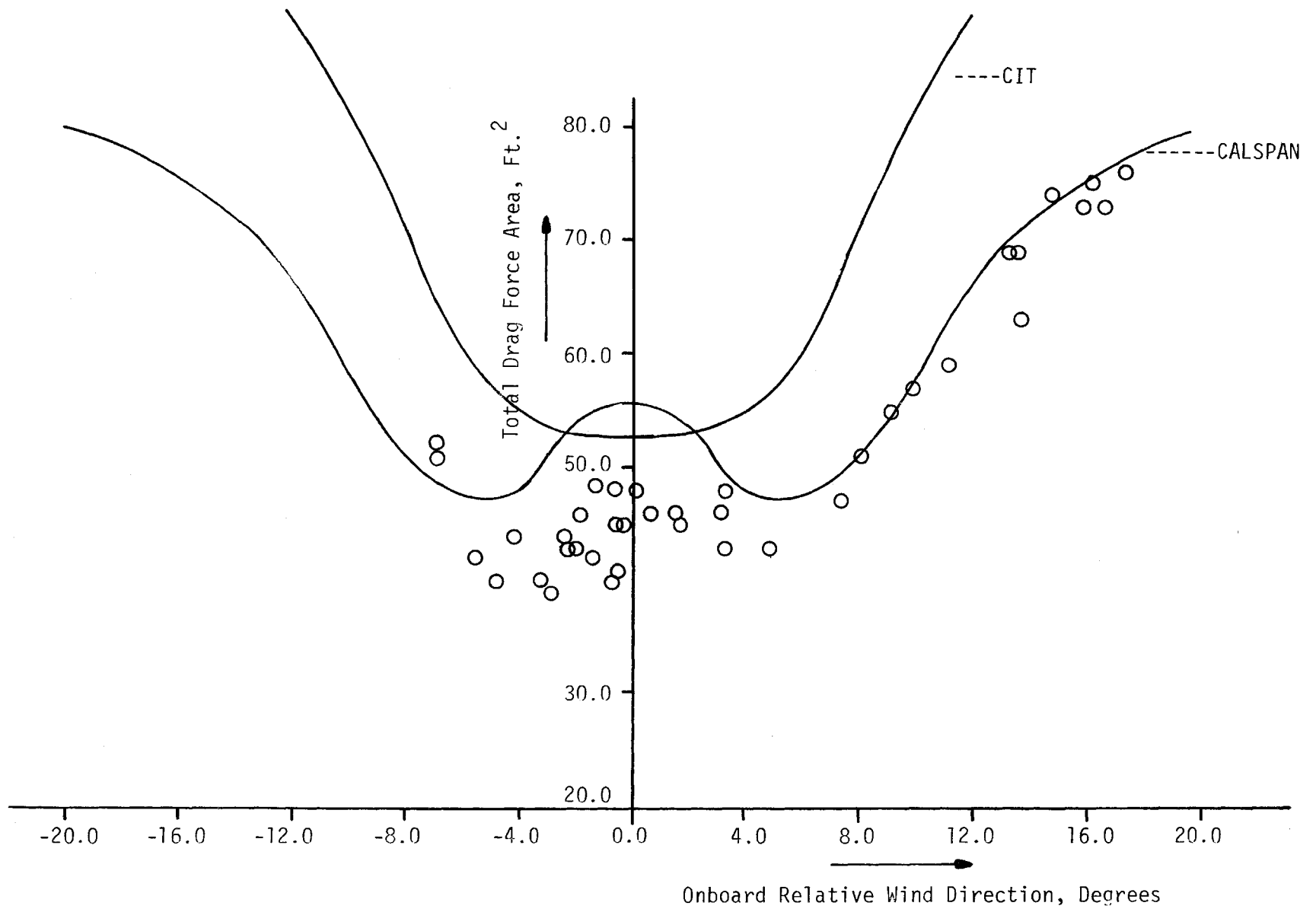


Figure 6-3. Comparison of Full-Scale Drag Area with Wind Tunnel Results - Configuration 1

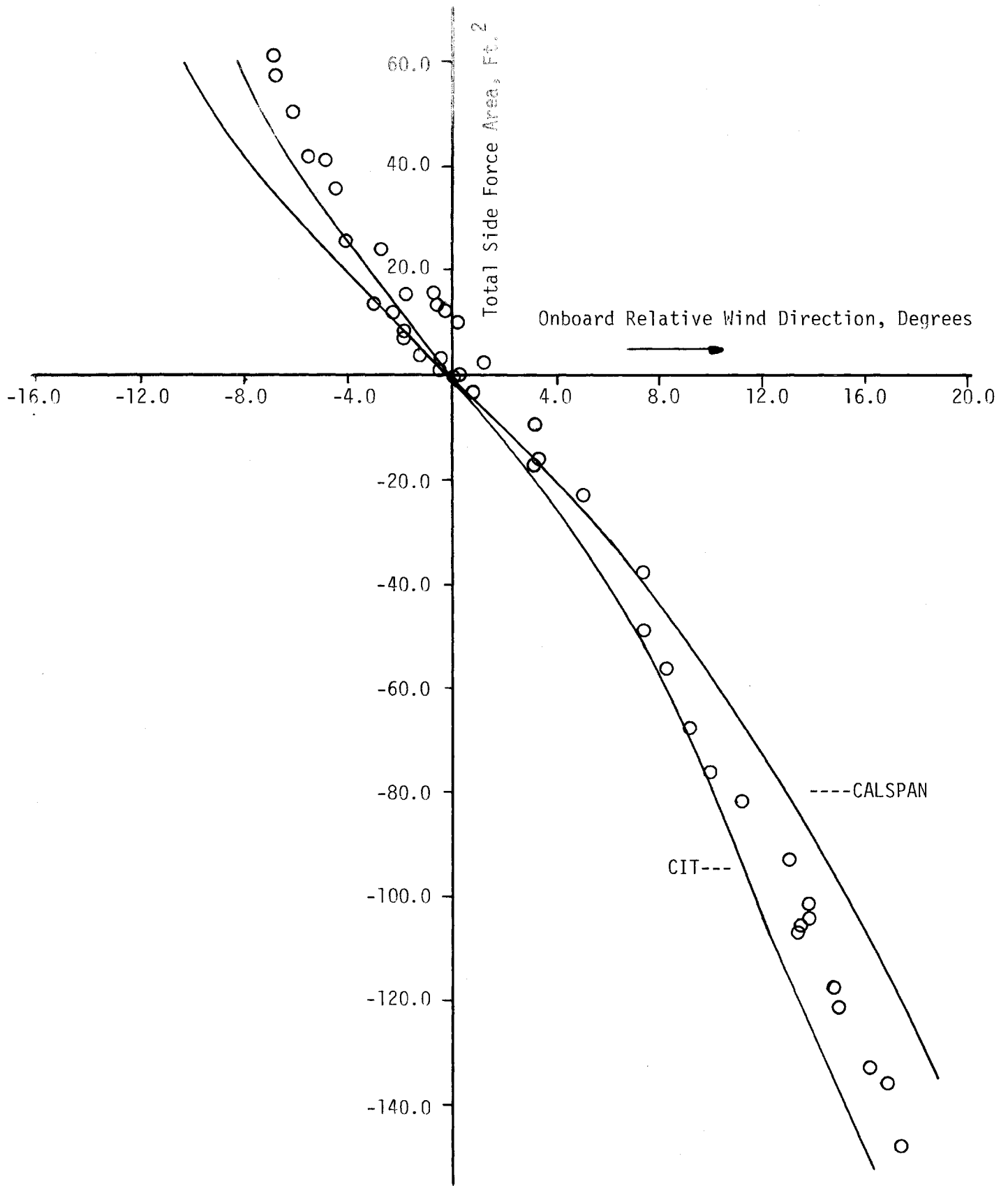


Figure 6-4. Comparison of Full-Scale Side Force Area with Wind Tunnel Results - Configuration 1

the results of the wind tunnel tests, somewhat closer to the CIT curve. When the incident wind is from the left, the full-scale values are clearly in better agreement with the CIT data than the Calspan data. Thus, the full-scale side force data displays a close overall agreement with the CIT experiments.

6.4 COMPARISON OF CONFIGURATION 2 DATA

6.4.1 Drag Area

Full-scale drag area data obtained from Figure 5-6(b) was compared with the wind tunnel data of Figure 6-2(b). The resulting plot is shown in Figure 6-5. As in the case of Configuration 1, the full-scale results are in better agreement with the Calspan curve for near-zero and positive wind angles. When the wind angle is negative, the two wind tunnel tests bracket the full-scale measurements. A more definitive comparison cannot be made for this configuration due to the relatively small number of full-scale data points.

6.4.2 Side Force Area

A comparison between the full-scale side force area of Figure 5-7(b) and the wind tunnel data of Figure 5-2(b) is shown in Figure 6-6. The CIT tests agree more closely with the full-scale data than the Calspan tests. The data points for positive wind angles are in slightly better agreement than negative wind angles. These observations are similar to those for Configuration 1.

6.5 DISCUSSION OF RESULTS

The foregoing comparison between the full-scale AERO/TOFC (Series II) tests and the wind tunnel tests at CIT and Calspan reveal the following general results.

The full-scale drag area data for both TOFC configurations is in good agreement with the Calspan tests. The CIT test results indicate significantly larger drag values than the full-scale measurements.

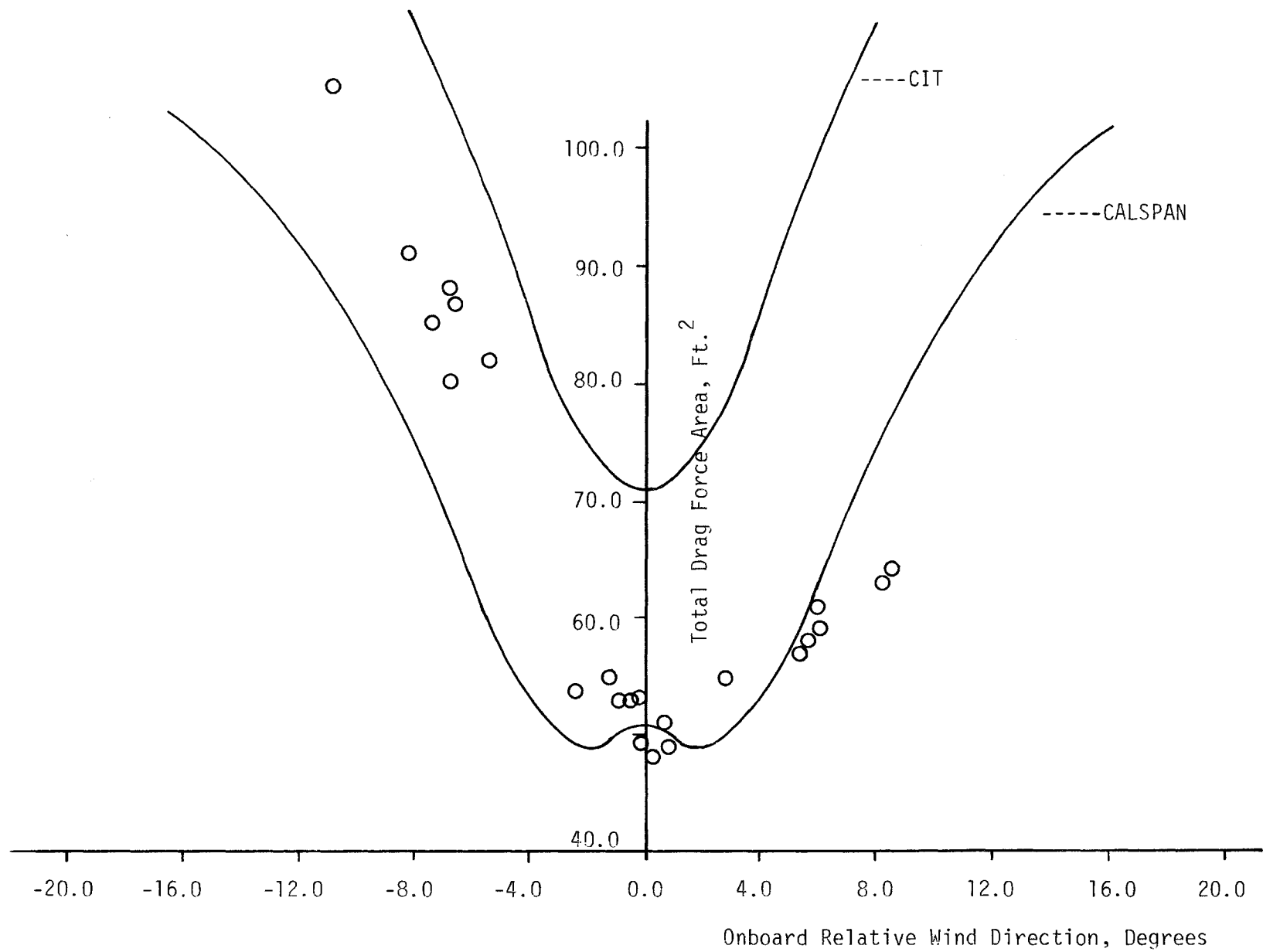


Figure 6-5. Comparison of Full-Scale Drag Area with Wind Tunnel Results - Configuration 2

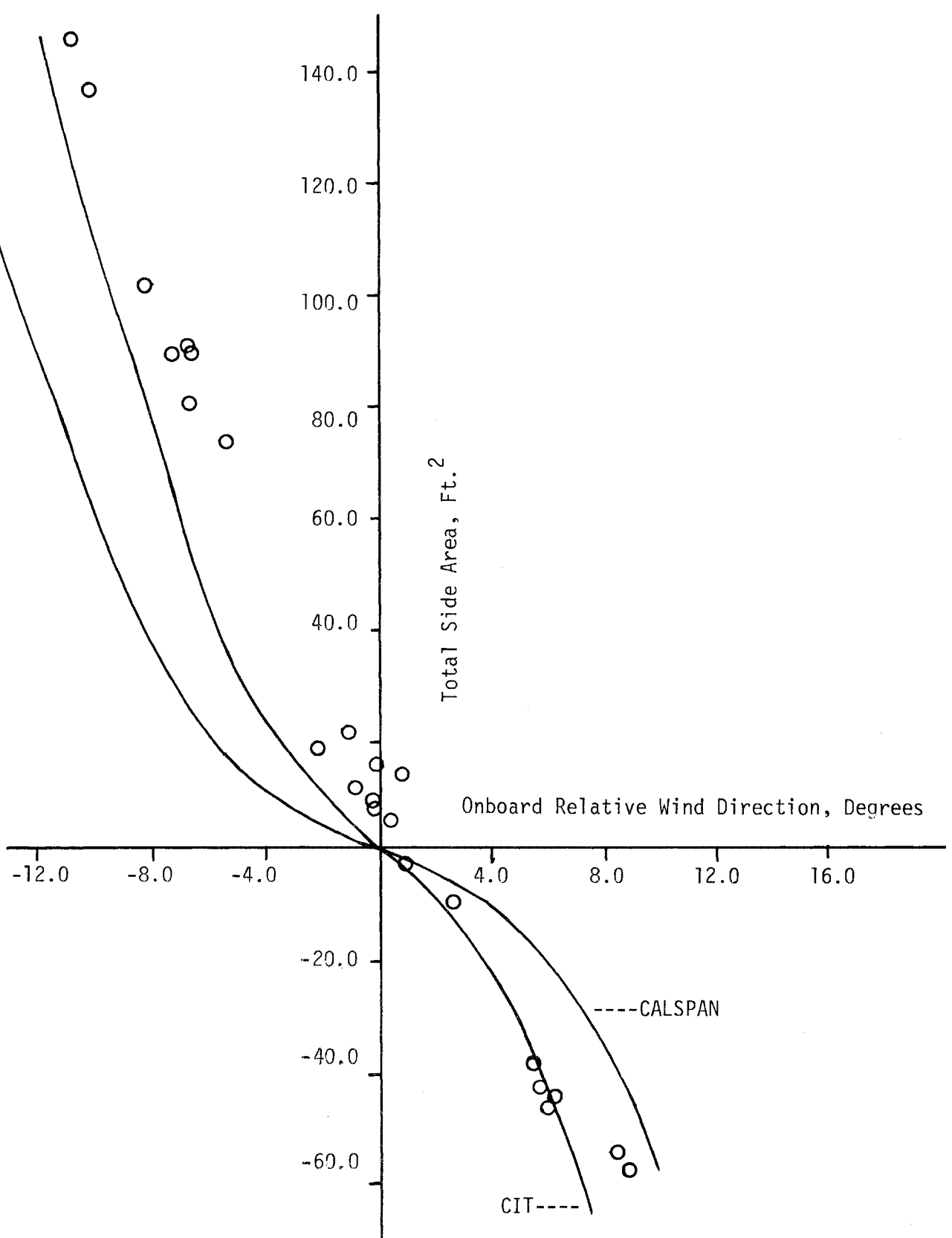


Figure 6-6. Comparison of Full-Scale Side Force Area with Wind Tunnel Results - Configuration 2

In contrast to the drag areas, the side force data is in reasonable agreement with the CIT wind tunnel results for both Configurations 1 and 2. The Calspan data gives relatively lower values of side force than the full-scale measurements.

An examination of the comparison plots in Figures 6-3 through 6-6 results in the quantitative estimate of the agreement between full-scale and wind tunnel tests as shown in Table 6-1.

It is of interest to compare the aerodynamic data for the two TOFC configurations with each other. Thus, it is seen from Figures 6-3 and 6-5 that Configuration 2 experiences consistently larger drag than Configuration 1. The side forces for the two configurations are not significantly different.

Table 6-1
 Approximate Percent Agreement Between
 Full-Scale and Wind Tunnel Results

Configura- tion	Param- eter	Approximate Percent Agreement of Full- Scale AERO/TOFC (Series II) Results With			
		Calspan Wind Tunnel Tests		CIT Wind Tunnel Tests	
		Percent	Wind Angle* Range, Deg.	Percent	Wind Angle Range, Deg.
1	Drag Area	20	$-8 < \alpha < 0$	40	$-8 < \alpha < -2$
		15	$0 < \alpha < 8$	15	$-2 < \alpha < 2$
		10	$8 < \alpha < 20$	20	$2 < \alpha < 6$
				>50	$2 > 6$
	Side† Force Area	>30	$-9 < \alpha < -4$	10	$-8 < \alpha < -2$
		10	$-4 < \alpha < -2$	10	$2 < \alpha < 4$
		20	$4 < \alpha < 12$	20	$4 < \alpha < 12$
		20	$\alpha > 12$	15	$\alpha > 12$
2	Drag Area	15	$-12 < \alpha < -6$	30	$-12 < \alpha < -4$
		10	$-6 < \alpha < 6$	>40	$\alpha > -4$
		15	$6 < \alpha < 12$		
	Side† Force Area	>40	$-12 < \alpha < 8$	20	$-12 < \alpha < -8$
				>30	$-8 < \alpha < 1$
				25	$1 < \alpha < 8$

* Wind Angle is denoted by α .

† Percent errors in side force are meaningless near zero wind angle since the side force itself goes to zero. In this case only the deviations from zero should be considered.

7.0 CONCLUSIONS

The AERO/TOFC (Series II) tests were conducted with the primary aim of obtaining reliable full-scale aerodynamic force data (mainly drag and side force) in order to validate the results of wind tunnel tests on scaled models. This task was accomplished by measuring wind forces via a specially designed mechanical force-balance system. It was also desired to derive rolling resistance of the TOFC configuration as a secondary objective of these tests. This information was obtained by measuring the total tractive resistance of the TOFC consist (using instrumented leading and trailing couplers) and subtracting the aerodynamic drag force. The following conclusions can be drawn from the successful completion of the AERO/TOFC (Series II) tests.

Average aerodynamic forces were measured effectively using a mechanical force-balance system. The resulting data was found to be reasonable and exhibited good repeatability. Analytical techniques were developed to accurately extract aerodynamic force information in a real dynamic environment. Also, errors in force determination were examined in detail and estimated accurately. The Trailer-on-a Flatcar system, which was modified extensively to improve structural integrity and to reduce the severity of dynamic forces, performed predictably and showed no significant changes in pitch and roll attitudes. The entire TOFC mechanical system and the associated electronics demonstrated excellent stability and consequently there were minimal zero shifts.

It can be concluded from the foregoing discussion that the AERO/TOFC (Series II) tests established a reliable data base for validation of the wind tunnel test programs. A comparison between the full-scale drag and side force data with the wind tunnel data of the CIT and Calspan tests revealed the following:

- For the two TOFC configurations which were tested, the full-scale drag area data agreed well (within 20 percent) with the Calspan tests. The CIT results indicate significantly larger (>40 percent) drag force than the full-scale measurements. This conclusion holds for all wind angles except a narrow range about the zero angle (-2 to 6 degrees).
- The side force data was generally in reasonable agreement (within 25 percent) with the CIT wind tunnel results for both configurations. The Calspan data gives relatively lower values of side forces than the full-scale measurements.
- A comparison between the full-scale results for the two TOFC configurations shows that Configuration 2 experiences consistently larger drag than Configuration 1 (10 percent for wind angles near zero and up to 20 percent at 6 degrees). The side forces are not significantly different for the two configurations.

The rolling resistance information was obtained by subtracting the drag force on the trailers from the total tractive resistance of the TOFC. This data included the aerodynamic resistance of the TTX car and must be interpreted carefully. Since the TTX drag is a small contribution, especially at low train speeds, it was possible to obtain rough estimates of the rolling resistance. For example, the AERO/TOFC (Series II) results indicate that at a train speed of 50 mph, the drag force for Configuration 2 ranged from 320 to 490 pounds and the rolling resistance was approximately 325 pounds. Thus, at 50 mph, the aerodynamic drag accounts for 50 to 60 percent of the total tractive resistance. At 90 mph, with 710 to 1,180 pounds of drag force and about 560 pounds of rolling resistance, the drag amounts to 55 to 70 percent of the total tractive resistance.

8.0 REFERENCES

1. Hammitt, A. G., "Aerodynamic Forces on Freight Trains", Volume 1 - Wind Tunnel Tests of Containers and Trailers on Flat Cars, Report No. FRA/ORD-76-295.I, December 1976.
2. Hammitt, A. G., "Wind Tunnel Tests of Trailers on Flat Cars at High Reynolds Numbers", Andrew G. Hammitt Associates, Report #11-001-78, January 1978.
3. "Test Results Report, TOFC Full-Scale Aerodynamic Validation Tests, CV-192, In Support of Test Request CV-192", Contractual Test Report, Contract DOT-FR-64113, March 1, 1977. Available Upon Request.
4. Local Climatological Data for Pueblo, Colorado, Environmental Data Service of NOAA, March 1977.
5. Plans for Proposed Project 4(4), FRA Conventional Rail Track at Transportation Test Center, U.S. Department of Transportation, May 1975.
6. Test Specifications, Aerodynamic TOFC Validation Tests-II, TTC Document TS-ATVT, November 9, 1977.
7. Operational Test Procedure, Aerodynamic TOFC Validation Tests-II, October 31, 1977.
8. Hammitt, A.G., "Instrumentation Requirements: TOFC Full-Scale Aerodynamic Validation Tests", Report #10-001-76, Andrew G. Hammitt Associates, February 27, 1976.
9. Scofield, R., "Test Requirements: TOFC Full-Scale Aerodynamic Validation Tests (II-Series)", ENSCO, Inc., June 24, 1977. Revised August 1, 1977.
10. Limaye, M., Project Engineer, Brewer Engineering Laboratories, Personal Communication on September 29, 1977.
11. Handbook of Chemistry and Physics, Chemical Rubber Company, 53rd Edition, 1972-73.
12. Operation Plan for Track Survey Between Track Stations 120 and 180 on East Tangent of Railroad Test Track, RG-293, September 15, 1977.
13. Test Results Report, Lightweight Flatcar Evaluation (Mode Shape), CV-128.2, prepared by ENSCO, Inc., for FRA, DOT, June 1977.
14. Ralston, A., "A First Course in Numerical Analysis", McGraw-Hill, 1965.

APPENDIX A
FULL-SCALE AERODYNAMIC LOAD MEASURING
SYSTEM FOR AERO/TOFC (SERIES II) TESTS

THIS REPORT PREPARED BY

BREWER ENGINEERING LABORATORIES INCORPORATED

BREWER ENGINEERING
LABORATORIES INCORPORATED

FULL-SCALE AERODYNAMIC
LOAD MEASURING SYSTEM
FOR AERO/TOFC-II

Written By

Hemant S. Limaye
Hemant S. Limaye

Approved By

LaVerne F. Wallace
LaVerne F. Wallace

March 7, 1978

- TABLE OF CONTENTS -

<u>ITEM</u>	<u>DESCRIPTION</u>
	ABSTRACT.
1.0	INTRODUCTION.
Figure A-1	Test Configurations.
2.0	PROCEDURE.
2.1	Force Balance System Design Review of AERO/ TOFC-I.
2.2	Force Balance System of AERO/TOFC-II.
Figure A-2	Flexural Assemblies.
2.3	Camber Test.
Figure A-3	Schematic of Force Balance System.
Table I	Force Balance System Design Summary.
2.4	Structural Stiffening of the Flatcar.
Figure A-4	Flatcar Transit Reading Locations.
Figure A-5	Flatcar Modifications.
2.5	Stiffening of the Trailers.
2.6	Installation of Support and Calibration Frames.
Figure A-6	Setup Used for Trailer Stiffening.
2.7	Installation of Flexural Assemblies.
2.8	Calibration and Alignment of Flexures.
2.9	Pluck Test.
2.10	Wind Load Simulation Jacking Test.
Figure A-7	Load Application Locations to Simulate Wind Loading.
2.11	Other Instrumentation Used.
Figure A-8	Setup for Wind Load Simulation Jacking Test.
2.12	Preliminary and Final Tests.
3.0	RESULTS AND CONCLUSIONS.
4.0	PERSONNEL.
4.1	Federal Railroad Administration/Department of Transportation.
4.2	ENSCO, Inc., Alexandria, Virginia.
4.3	ENSCO, Inc., Colorado Springs, Colorado.
4.4	ENSCO/Dynalectron, TTC.
4.5	Andrew G. Hammitt Associates.
4.6	Brewer Engineering Laboratories, Inc.

- TABLE OF CONTENTS -

<u>ITEM</u>	<u>DESCRIPTION</u>
5.0	REFERENCES.
6.0	BIBLIOGRAPHY.
Appendix A-1	Photographs of Test.
Appendix A-2	Jacking Calibration and Alignment Data.
Appendix A-3	Wind Load Simulation Trailer Jacking Data.
Appendix A-4	Preliminary and Final Test Log.
Appendix A-5	Results of Preliminary and Final Tests.
Appendix A-6	AERO/TOFC-II Equipment List.

ABSTRACT

ENSCO, Inc., issued a contract to Brewer Engineering Laboratories, Inc., to design, fabricate, and install a force balance system to measure the aerodynamic forces on trailer on flatcar (TOFC) consist. A series of TOFC tests were run at the Transportation Test Center (TTC), Pueblo, Colorado, to conduct a full-scale validation of wind tunnel tests.

BEL designed a force balance system using a flexural pivot concept to provide the system with better axial stiffness and low lateral stiffness at the same time. The system was also provided with the overload protection mechanism. BEL installed the entire system using an optical technique to minimize misalignment in flexural assemblies in the orthogonal planes.

The entire system was calibrated by applying known loads to the forward and lateral sides of both trailers to simulate the wind load. The calibration was very reliable and repeatable. BEL provided the engineering support during the actual testing. Throughout the testing period, the force balance system was very stable and experienced very small zero shifts.

Lateral and longitudinal aerodynamic drag forces were found in close agreement with values predicted from wind tunnel model tests.

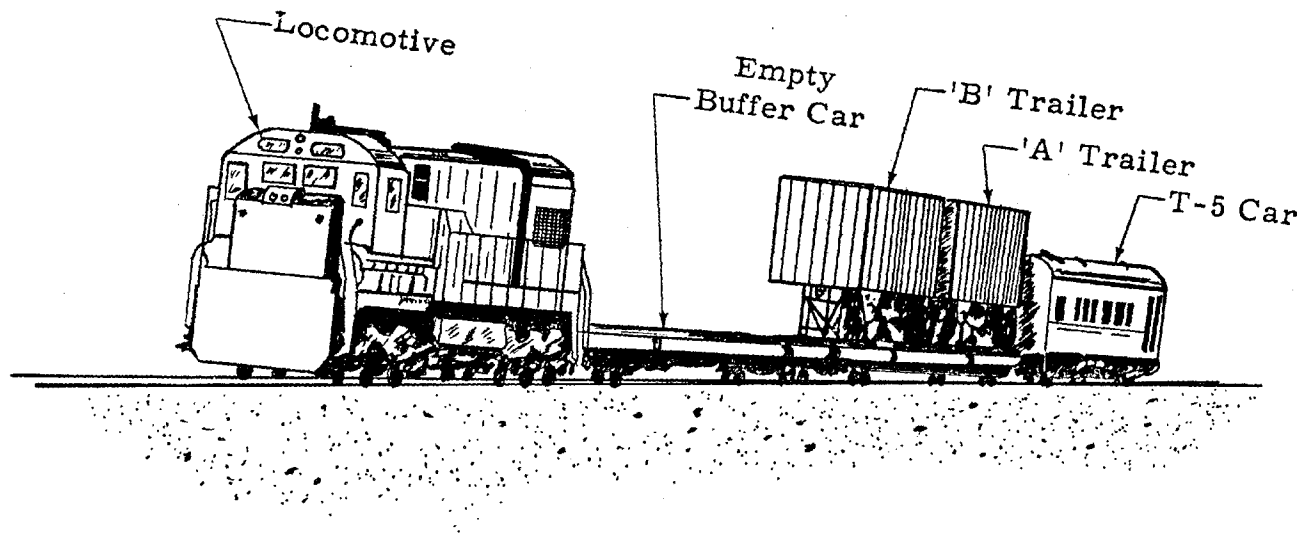
1.0 INTRODUCTION.

1.1 A series of tests of trailer on flatcar (TOFC) were run at the Transportation Test Center, Pueblo, Colorado, in October, 1976. The tests were run with two configurations of the train consist which are shown in Figure A-1. Configuration I included a locomotive, loaded buffer car, instrumented TTX car followed by an instrumentation car, T-5. The arrangement for Configuration II was the same except that an empty buffer car was used in place of a loaded buffer car.

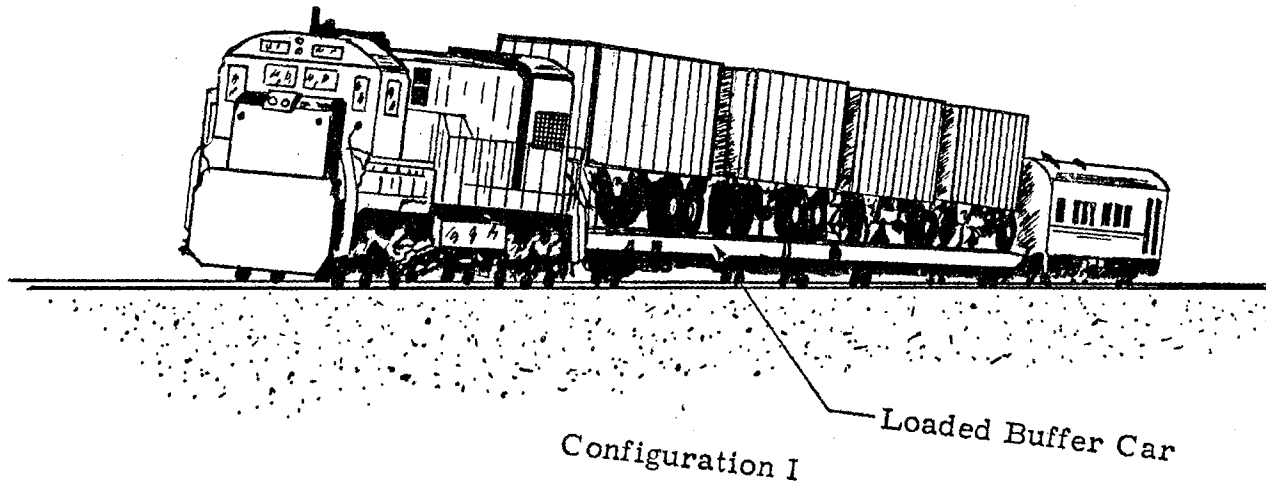
1.2 The objective of these tests was to conduct a full-scale validation of wind tunnel tests conducted by Andrew G. Hammitt Associates. The 10-foot diameter wind tunnel with a 12-foot ground plane and 1/43-scale models were used for the tests.

1.3 Experimental data from a prior series of full-scale TOFC tests¹ were inconsistent and experienced large zero shifts. As a result, the experimental data did not correlate well with the wind tunnel model data.² Some of the load cells used in the program were also damaged.

1.4 On February 14, 1977, the Federal Railroad Administration contracted Brewer Engineering Laboratories, Inc. (BEL), to review the procedures used in the AERO/TOFC-I tests and to assess the adequacy of the results. BEL did an on-site inspection of the full-scale test equipment and reviewed all available data in March, 1977. Analysis of the problems involved and the recommendations are presented in BEL Report 611.³



Configuration II



Configuration I

Figure A-1. Test Configurations.

1.5 On July 7, 1977, ENSCO, Inc., issued a contract to BEL to provide engineering support and materials to conduct a second series of full-scale tests to measure aerodynamic drag and side forces on the TOFC consist. The work statement required that BEL design a force balance system, facilitate calibration, and fabricate associated equipment necessary for proper implementation. The entire test program was designated as AERO/TOFC-II.

2.0 PROCEDURE.

2.1 Force Balance System Design Review of AERO/TOFC-I.

2.1.1 In the beginning of the AERO/TOFC-II program, BEL reviewed the force balance system design of AERO/TOFC-I. The instrumented TTX car included the two trailers supported on a force balance system. The drag force which was of primary interest was measured using a load cell in the longitudinal direction. The location and magnitude of the lateral force was determined by measuring the lateral force and resolving roll and yaw moments.

2.1.2 Each trailer on the flatcar was supported on two flexures under each side of the rear axle and one vertical flexure under the kingpin. Longitudinal flexure attached to the kingpin was used to measure the drag force; and the lateral force was measured by using two lateral flexures, one attached to the kingpin and one attached to the rear axle.

2.1.3 Instead of using external overload stops, larger capacity load cells were used to protect the system from excessive loads. These load cells had built-in overload protection in compression only. The trailers were fastened to the flatcar by means of metallic cables as a fail-safe restraint in case of an accident or if loads beyond the capacity of the system were applied.

2.2 Force Balance System of AERO/TOFC-II.

2.2.1 Since the force balance system was required to measure relatively small aerodynamic forces compared to the inertial forces, flexural pivot design was recommended by BEL.³ The analysis of this design is included in Reference 4. Flexural pivot design provides a system with better axial stiffness and low lateral stiffness at the same time. The design also allows the use of a simple but effective overload protection system with two-direction mechanical stops.

2.2.2 Figure A-2 shows the sketches of flexural assemblies for vertical, lateral, and longitudinal locations. Lateral and longitudinal flexural assemblies consisted of two flexures on each end with a load cell in between. One end of the flexure was threaded into the flexure bracket which had the oversized holes for adjustment. On the vertical flexure assembly, one flexure was threaded at each end of the stem rod, and the whole assembly was threaded into the load cell. The length or the height of the flexure assemblies could be varied with left- and right-handed threads provided on the flexures. The overload stop mechanism was provided only on the lateral and longitudinal flexures.

2.2.3 The accuracy of a force balance system depends upon its alignment in the orthogonal planes. Any misalignment in the flexural assemblies results in interaction forces. To minimize or eliminate these forces, it was necessary to apply externally applied loads to each of the flexural assemblies. To apply these loads, removable frames were designed to hold the jacking assembly.

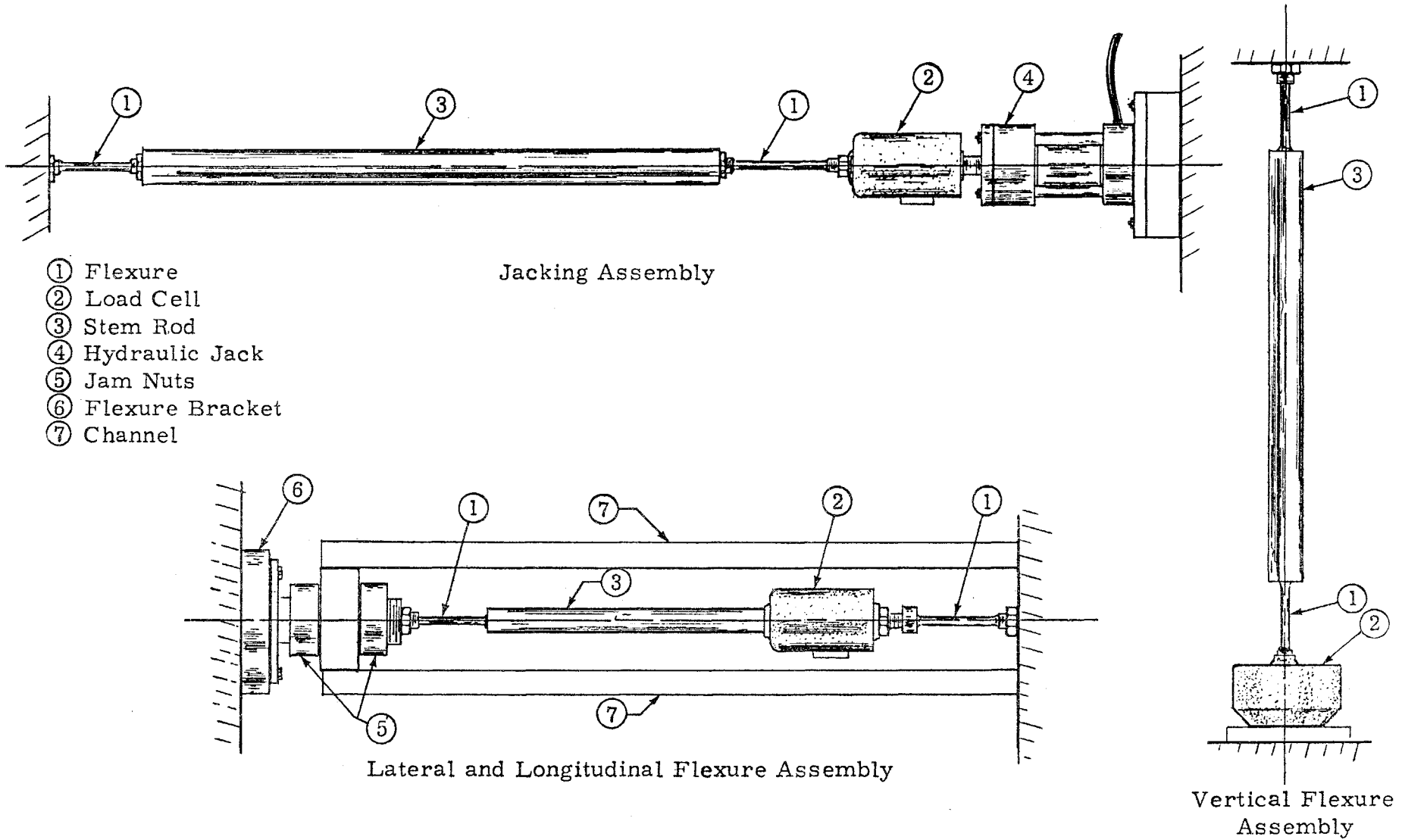


Figure A-2. Flexural Assemblies.

2.2.4 An entire balance system was designed to have the maximum possible sensitivity. The support frames, as well as the calibration frames, were designed to be very rigid so that the loads were carried by the load cells and not by the support frames. To increase the sensitivity and accuracy of the system, BEL also recommended the removal of the wheel bogie from the trailers and substitute a wooden assembly reducing the deadweight by 2,500 pounds to approximately 10,000 pounds but keeping the same aerodynamic profile.

2.2.5 The schematic of the force balance system designed by BEL is shown in Figure A-3. The forward flexural assemblies were attached to the kingpin in a similar manner to that of the AERO/TOFC-I program. The rear flexural assemblies were mounted to a 6" x 8" box beam 8 feet long which was welded to the rear bumper of the trailer. Since the dimensions of the flexural assemblies were very different (generally longer) from that of the AERO/TOFC-I program, BEL redesigned all the support frames and miscellaneous hardware. A flexural pivot design summary is included in Table I. Factor of safety is based on a buckling load. The detailed design philosophy is presented in References 3 and 4. All the framework used for the AERO/TOFC-I program was removed from the flatcar.

2.3 Camber Test.

2.3.1 The flatcar chosen for the test consist had a considerable camber in it. It was decided to place the two trailers on the same horizontal plane parallel to the rails. Therefore, it was necessary to find out the curvature of the camber to determine the metal pads required to put under the frames.

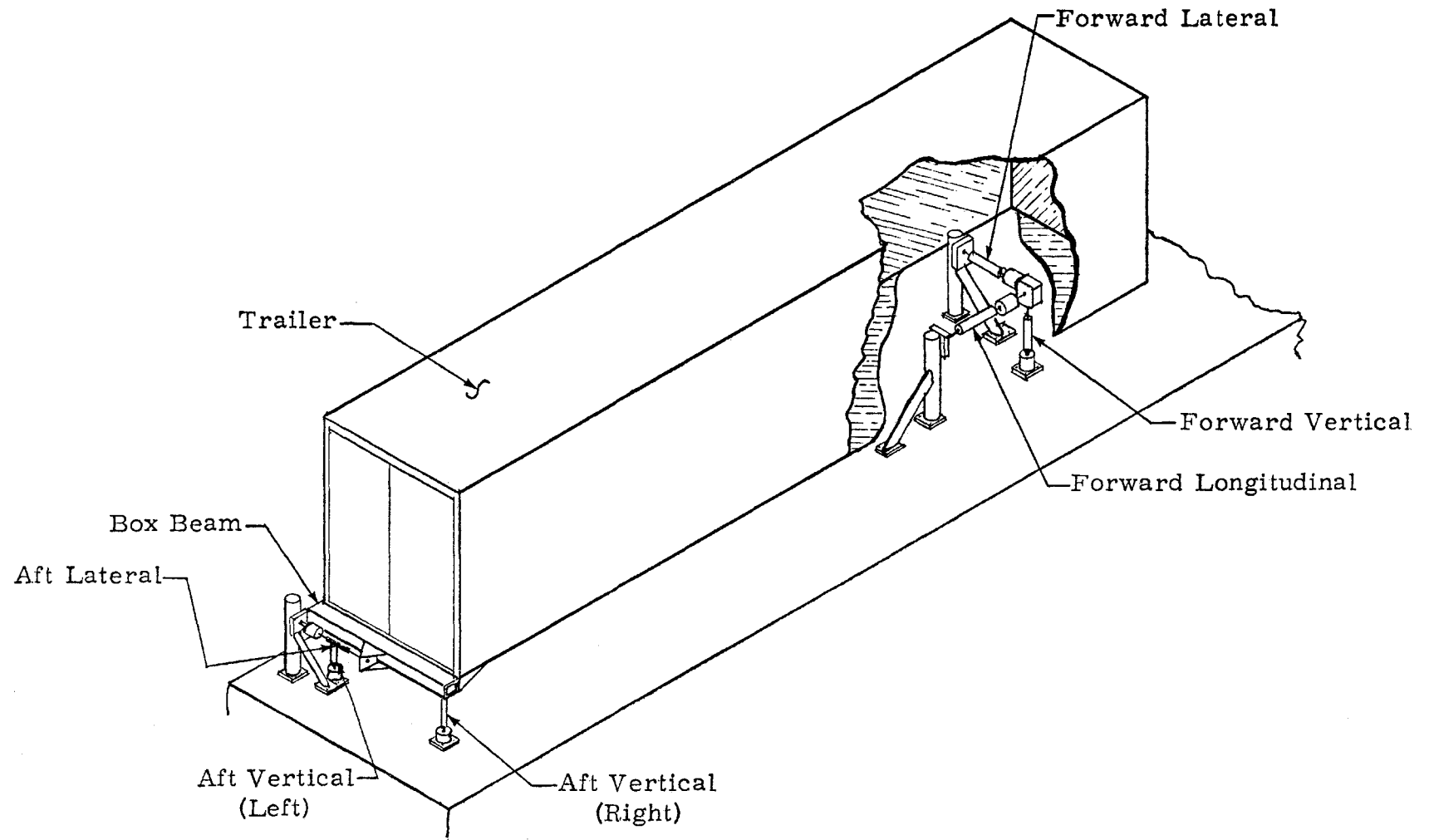
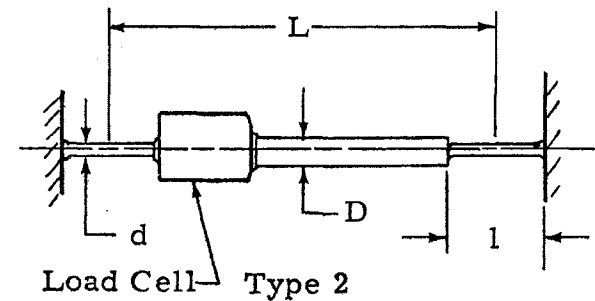
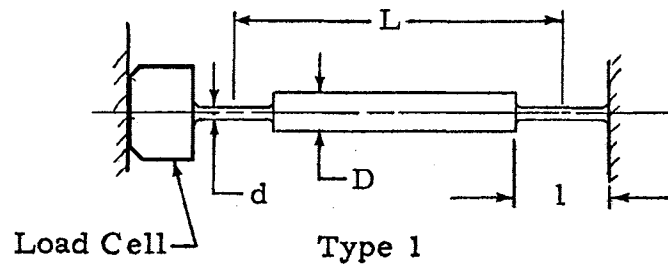


Figure A-3. Schematic of Force Balance System.

TABLE I
FORCE BALANCE SYSTEM DESIGN SUMMARY

Load Cell Strut	Type	Design Load (lbs)	L (in)	l (in)	d (in)	D (in)	Lateral Stiffness (lbs/in)	Allowable Lateral Deflection (in)	Bucking Load (lbs)	Factor of Safety	Axial Deflection (in)
Longitudinal	2	5,000	28	4	0.483	1½	51.20	0.272	66,800	13.0	0.0257
Forward Lateral	2	2,000	29	3	0.356	1½	18.90	0.430	34,900	17.5	0.0145
Forward Vertical	1	7,000	28	4	0.545	2½	82.90	0.241	108,100	15.0	0.0243
Aft Lateral	2	3,000	29	3	0.437	1½	42.65	0.350	79,400	26.0	0.0152
Aft Vertical	2	9,000	28	4	0.564	2½	95.30	0.163	123,951	13.8	0.0279



2.3.2 The unloaded TTX car was placed on Track No. 4 on the east side of the Central Services Building (CSB). With the surveyor's transit, readings were taken at the locations shown in Figure A-4. From the difference of these readings, the actual camber was determined. Then weight of 24,000 pounds in lead bricks was placed on the flatcar in a distributed manner to simulate the load of the two trailers. The readings were taken again at the same locations with the transit. From the difference of these readings, the camber in the loaded flatcar was found. Comparing the loaded and unloaded camber in the flatcar, it was concluded that the camber remained essentially the same even in the loaded condition indicating that most of the load was absorbed by the bolster springs.

2.3.3 Knowing the camber, the plates of proper size and thickness were cut to fit under the frames wherever required.

2.4 Structural Stiffening of the Flatcar.

2.4.1 To restrain buckling or warping of the deck plate due to rigid frames welded to it, it was necessary to stiffen the flatcar. At the aft vertical and lateral calibration frame locations, an 8" channel was used to mount the flexures and calibration frames; see Figure A-5.⁵ At the forward tower locations, a 3" angle iron was welded under the flatcar longitudinally. The drawings were approved by Trailer Train, the manufacturer of the flatcar.

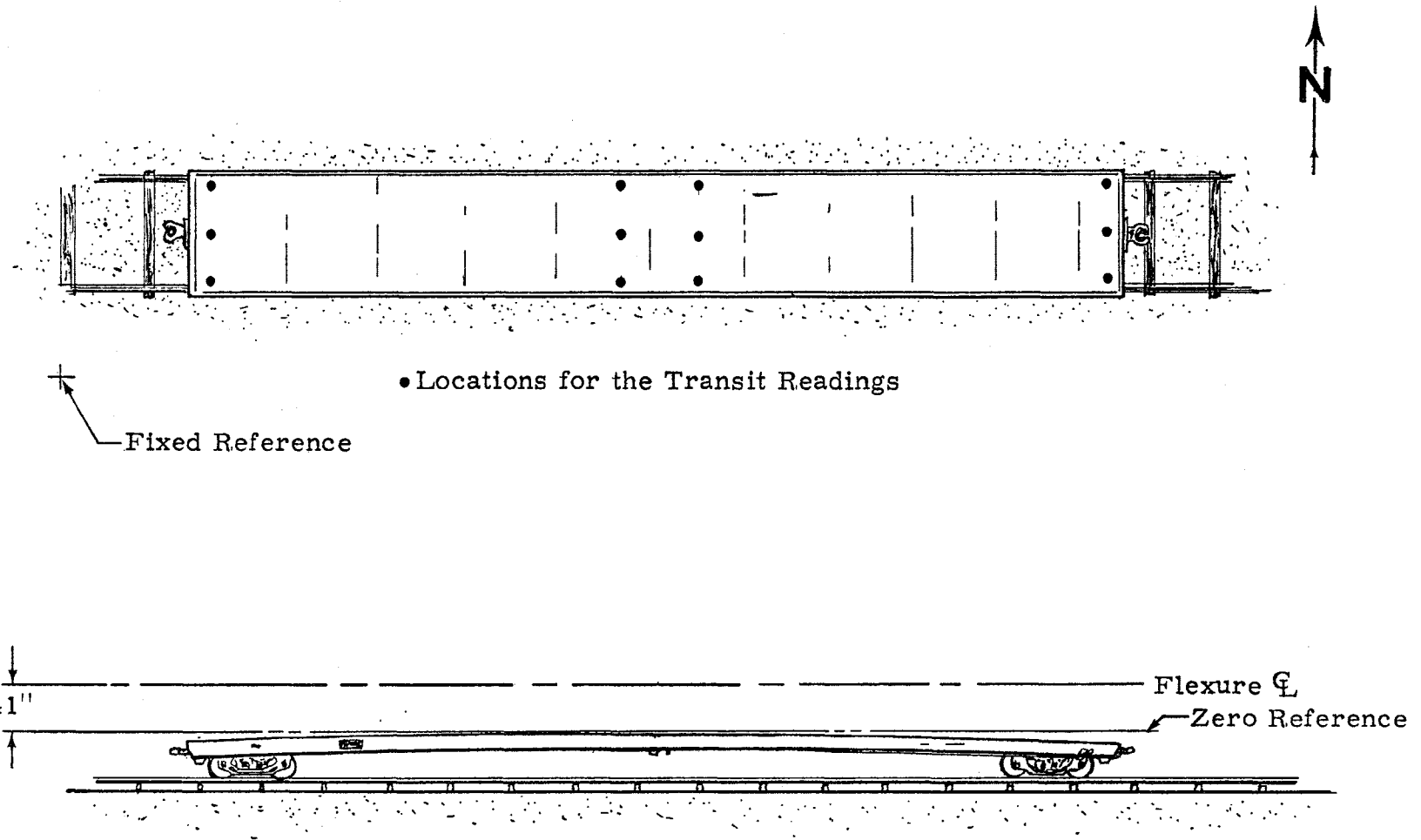


Figure A-4. Flatcar Transit Reading Locations.

2.5 Stiffening of the Trailers.

2.5.1 The AERO/TOFC-I test results seemed to indicate that there was a torsional distortion of the trailers which gave a false lateral wind loading. To avoid this it was decided to stiffen the trailers due to their weakness in torsion as well as in bending. Also these were used trailers, so most of the joints were loose adding to the structural weakness. It was decided to use the tension cables across the opposite corners of the trailers. Four such stations about 10 feet apart were chosen on each trailer.

2.5.2 At each corner of all the stations, holes were drilled to pass the eyebolts avoiding the structural member. After placing all the hardware together, wire ropes were loosely attached to the diagonally opposite eyebolts. Each trailer was brought into the CSB where an optical station was established with a transit. A scale was held at the top and bottom stations on one side, and optical readings were taken with the transit; see Figure A-6. Then the eyebolts were tightened just enough to get a good tension into the wire ropes keeping the original shape of the trailer body. This was verified by taking and comparing the optical readings at the same locations after the wire ropes were tensioned.

2.6 Installation of Support and Calibration Frames.

2.6.1 The empty flatcar was brought into CSB on Track No. 4. By measuring the width of the car both at 'A' (trailing) and 'B' (leading) ends (Figure A-5), center points were marked on the deck plate. A straight line passing through these two points was

A-18

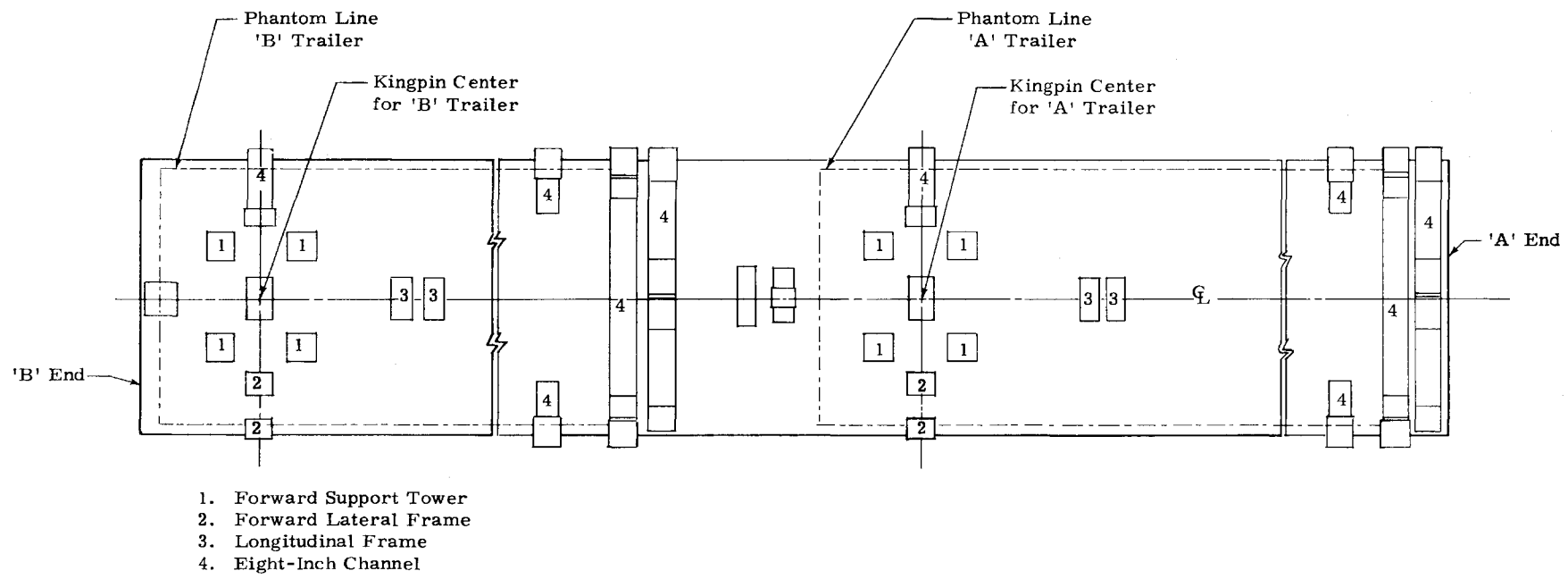


Figure A-5. Flatcar Modifications.

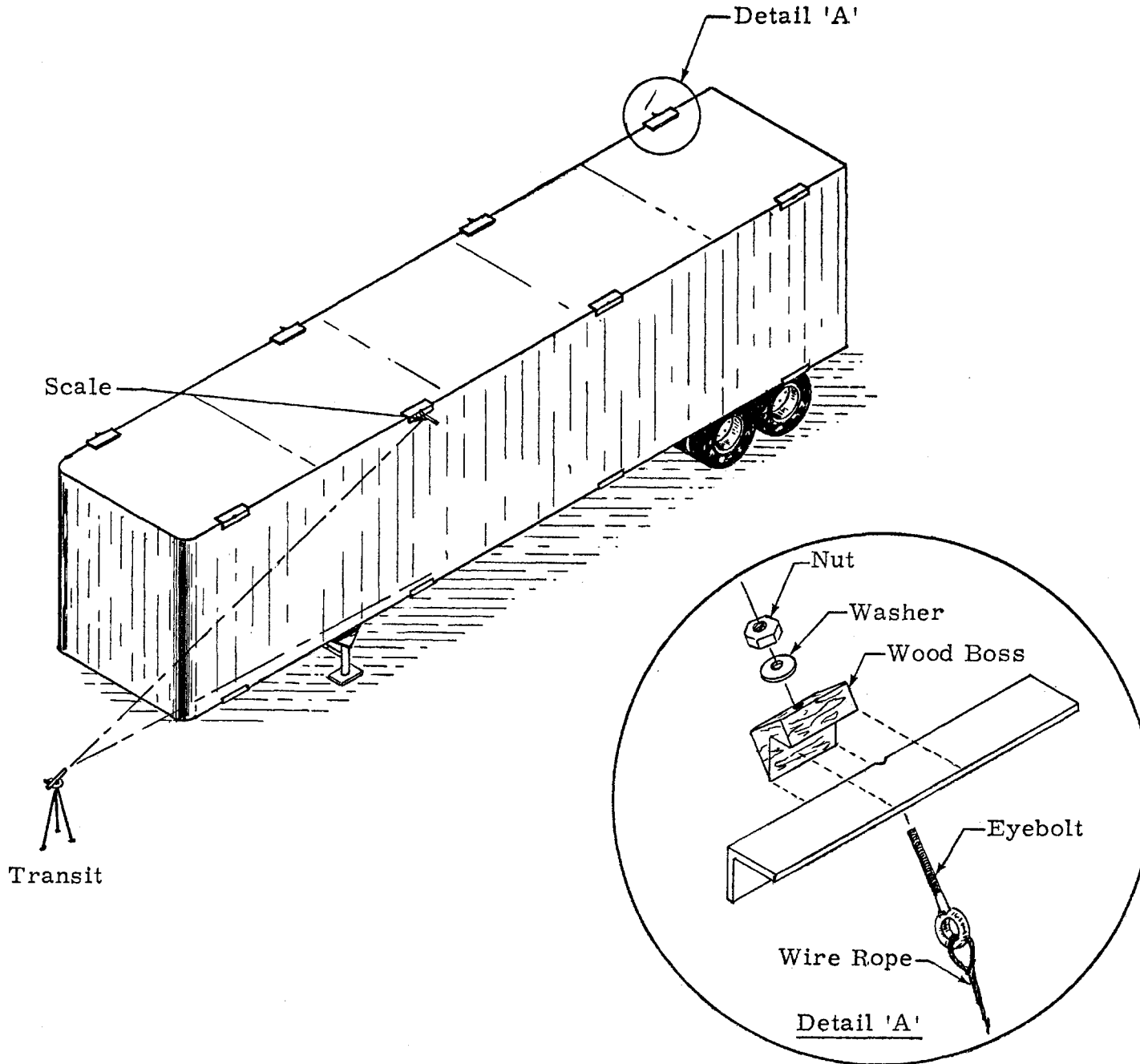


Figure A-6. Setup Used for Trailer Stiffening.

taken as the longitudinal centerline of the flatcar. This centerline was established on the flatcar by mounting a jig transit on the center at 'B' end and then aligning the scope on a target mounted at the center of 'A' end. Intermediate targets were mounted on the deck plate by plunging the scope. Then the kingpin location for each trailer was marked on this centerline establishing the reference points for each trailer. All the dimensions involved with a particular trailer were measured from the respective kingpin location.

2.6.2 To locate the positions of four forward frames on the 'B' end of the flatcar (one lateral support frame, one longitudinal support frame, and their respective calibration frames; Figure A-5), a jig transit was mounted on the kingpin location of the 'B' trailer; and the scope on the transit was aligned with the longitudinal centerline. Then the transit was turned 90° and locked, and a point was marked on the flatcar using the scope. By swinging the scope 180° , another point was marked establishing a line perpendicular to the longitudinal centerline through the kingpin location.

2.6.3 Knowing the two axes perpendicular to each other, pad areas of the frames were marked on the deck. Then each frame was placed in its location; and, using the transit mounted at the kingpin location, the frame was aligned in all directions within ± 0.030 ". To bring the center of the flexure pad 41" above the deck plate, shim pads were used under the frames. Once the frame was in proper position and aligned, it was tack welded to the deck plate.

2.6.4 After the four frames were tack welded to the deck plate, the vertical jacking frame was bolted to the support tower and was placed on the flatcar in its approximate location. Using the plumb bob from the center of the jacking pad, the frame position was adjusted until the jacking pad center and the kingpin center mark were aligned. Once the frame was aligned and leveled, it was tack welded to the deck plate and the jacking frame was removed.

2.6.5 The two 8" channels were located on the flat deck by measuring the proper distance from the kingpin location. By using the transit, channels were placed perpendicular to the longitudinal centerline and then tack welded.

2.6.6 The frames for the 'A' trailer were tack welded to the deck plate in a similar manner. Once all the frames and channels for both the trailers were tack welded, orthogonal alignment was rechecked and corrections were made wherever necessary. After this inspection, the frames were attached to the deck plate with full welds using proper welding practice.

2.6.7 The kingpin bracket was clamped to the kingpin, and the wheel bogie was removed from the trailer. With the overhead crane, the 'B' trailer was first lifted and was placed on the approximate position on the flatcar using pneumatic jacks and the forward landing gear. The trailer was moved around so that the kingpin was approximately in line with the kingpin location on the flatcar, and then the trailer was leveled using the jacks.

2.6.8 A permanent transit stand was welded on the longitudinal centerline just behind each longitudinal flexure support frame. Small holes were drilled through the center of the flexure pad and the support legs of these frames so that an optical sight could be taken at the kingpin location at 41" above the deck plate and the kingpin location on the deck plate. Then, using the transit, the kingpin bracket was aligned using see-through targets so that the longitudinal axis of the bracket was directly above the longitudinal centerline of the flatcar.

2.6.9 The fabricated box beam was then tack welded to the rear bumper of the trailer using temporary support legs. After making sure that the beam was in its position, leveled, and aligned, it was attached to the trailer using full welds.

2.7 Installation of Flexural Assemblies.

2.7.1 After assembling the flexures with their respective load cells, the forward vertical flexural assembly was installed first. The load cell was attached to the pad using the stud. Then by adjusting the height of the whole assembly using the left- and right-handed threads, the top flexure was threaded into the kingpin bracket. After installing all the assemblies in their respective positions, part of the trailer weight was put on the forward vertical and two aft vertical flexures by lowering the jacks and pulling the landing gear up.

2.7.2 The forward vertical flexure was aligned vertically using the leveling tool and by varying the length of the longitudinal and lateral flexures. Once the vertical flexure was aligned, the trailer position on the flatcar was fixed; and then the rest of the flexures were aligned using the leveling tool. All the assemblies were tightened, and then the whole trailer weight was taken by the vertical flexures by taking the landing gear all the way up and by further lowering the pneumatic jacks. The same procedure was used to install the flexures on 'A' trailer.

2.8 Calibration and Alignment of Flexures.

2.8.1 After assembling, the calibration load assembly (consisting of a flexured load column, precision load cell, and hydraulic jack) was mounted on the forward vertical calibration frame inside the trailer. Using the leveling tool, it was aligned so that it was exactly plumb and directly opposite the vertical force measuring flexure.

2.8.2 Using the hydraulic jack, compressive loads of 0 to 1500 pounds were applied in increments. The loads were monitored in each of the load cells by using the bridge switch box and the strain indicator. The results were analyzed in terms of the interactions; and the misalignments, if any, were corrected by adjusting the appropriate flexures. The calibration procedure was repeated until the interaction loads were reduced to less than 12 pounds.

2.8.3 An identical procedure was used to calibrate and align each of the load flexures on 'B' as well as on 'A' trailer.

2.9 Pluck Test.

2.9.1 A pluck test was performed to determine the natural frequency of the flatcar with the trailers mounted on the flexures. Two accelerometers were mounted, one on the flatcar and the second one on the trailer. The load was applied on the side of the trailer. Then the load was instantaneously removed, and the response of the accelerometers was recorded on the oscillograph.

2.10 Wind Load Simulation Jacking Test.

2.10.1 Each trailer was loaded up to 1000 pounds at the locations shown in Figure A-7 to simulate the wind load. The two trailers were loaded from the side on Track Nos. 1 and 2, and only the 'B' trailer was loaded on the forward face on Track No. 3.

During the pretest jacking test, the entire force balance system for each trailer was connected to a bridge balance switch box and the readings were taken on a strain indicator. The jacking test was also performed during the test and at the end of the test program to check the integrity of the force balance system. At this time the system was connected to the T-5 car.

2.10.2 The trailer jacking frame was fastened to the concrete floor in the CSB, and the flatcar was moved so that the jacking location on the trailer was in front of the frame. A 4" channel was placed on the trailer to protect the trailer jacking location from buckling. The transit was mounted between the flatcar

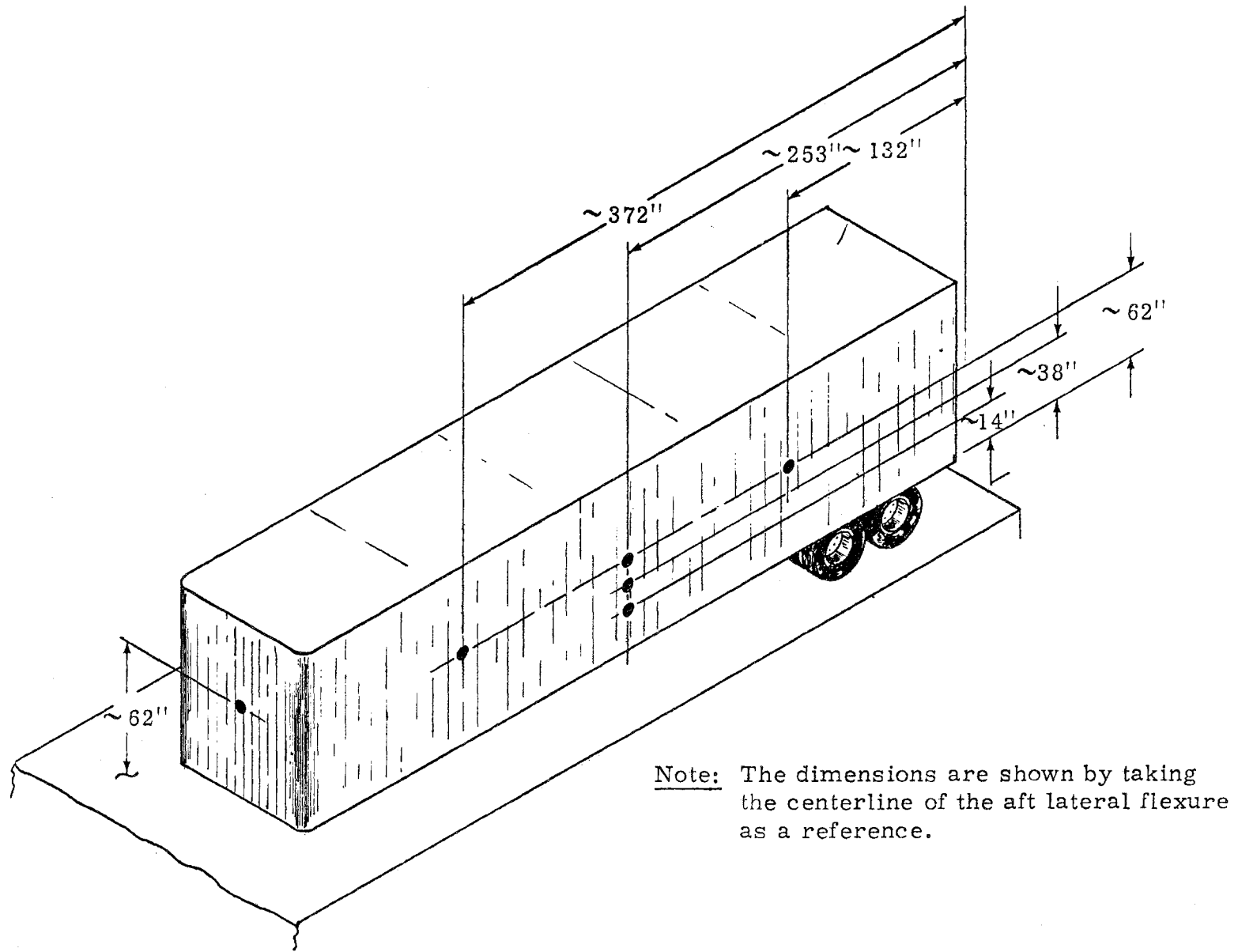


Figure A-7. Load Application Locations to Simulate Wind Loading.

and the frame to align the jacking flexure assembly so that it was perpendicular to the vertical plane of the trailer. The setup is shown in Figure A-8. The jacking flexure assembly was leveled using the level tool.

2.10.3 After zeroing all six channels, the loads were applied in increments by the hydraulic jack and the readings were noted. The procedure was repeated after dropping the load, and then the flatcar was moved to the next jacking location.

2.11 Other Instrumentation Used.

2.11.1 The wind velocity and direction was measured by using anemometers mounted at the weather station established in the test zone. The data were telemetered to the T-5 car. The wind relative to the train was sensed by an anemometer mounted 19½ feet ahead and 19½ feet above the locomotive.

2.11.2 Instrumented couplers designed by the TTC instrumentation group were used on each end of the TTX car to determine the combined aerodynamic and rolling resistance of the TOFC system.

2.11.3 Automatic location device (ALD) targets were mounted every 800 feet in the 4,000 feet of test zone to provide the data collection system with electrical markers.

2.11.4 The signal processing for all the transducers was performed by the signal conditioning amplifiers provided in the T-5 car. Each data channel was filtered at 1 Hz and 80 Hz using Bessel filters.

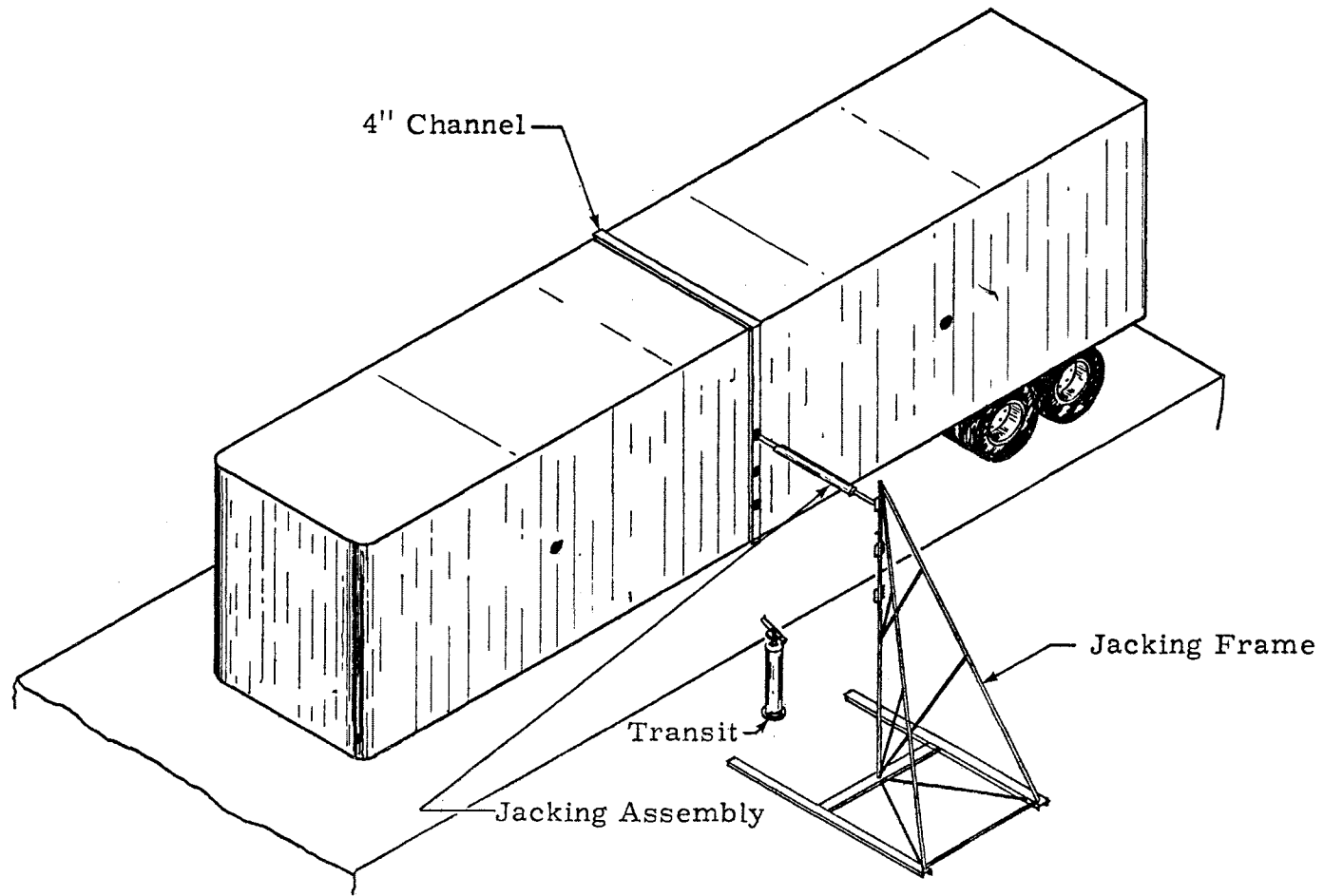


Figure A-8. Setup for Wind Load Simulation Jacking Test.

The data were digitized and recorded on a magnetic tape using a sample rate of 256 per second on the data acquisition system of T-5 car. A brush chart recorder was provided to display a limited number of channels in real time.

2.12 Preliminary and Final Tests.

2.12.1 Preliminary tests were conducted to evaluate the performance of the force balance system along with the data acquisition and data reduction systems. The primary purpose of these tests was to check the dynamic behavior of the total system under actual field conditions. The tests were also carried out to insure the zero repeatability and calibration stability.

2.12.2 To check the zero stability, it was important to spot the TTX car on the same location throughout the testing period. For this purpose, a target was marked on the floor adjacent to Track No. 3, and the location was determined from the plumb bob suspended from the flatcar. Also, two precision levels were mounted and leveled on the channel near the aft end of each trailer. Overload stops were set by measuring the gap of 0.006 inch between the jam nuts and a plate with feeler gages. All the channels were balanced, and the zero readings were taken.

2.12.3 After putting the whole consist (Configuration II) together (see Figure A-1), the test runs were performed at various train speeds. Force balance channels were monitored on a strip chart recorder. The weather data transmitted by the weather station alongside the test track were recorded for each test run. Each test run was repeated

at a constant speed, and the output on the recorder was compared for repeatability and consistency. After a few test runs, a data reduction program was loaded into the computer aboard T-5 and the data were processed for evaluation. After checking the total system operation, problem areas were identified and corrected. Once the engineering team was satisfied with the results, the next test condition was carried out.

2.12.4 At the end of each day's testing, the consist was disassembled and the flatcar with T-5 car was brought into the CSB on Track No. 3. The TTX car was spotted on the reference target, and the zeros were recorded on all the channels. These readings were compared to the pretest zeros. The entire force balance system was checked for any visual damage making sure the system, including overload jam nuts, was tight.

2.12.5 Actual testing began on December 5, 1977, and ended on December 16, 1977. The tests were conducted at the nominal train speeds of 50, 70, and 90 mph for both configurations following the same procedure for the preliminary tests.^{6,7}

3.0 RESULTS AND CONCLUSIONS.

3.1 Installation of all the framework on the flatcar was carried out without any major problems. More shim pads were required underneath the frames than what was originally anticipated because of the camber in the flatcar. The use of optics in aligning the frames was very helpful. Since the frames were installed accurately to begin with, it was easier to align and level the flexural assemblies with specially fabricated level tools. The photographs of the test program are presented in Appendix A-1.

3.2 Structural stiffening of the flatcar was adequate. There was no evidence of local buckling or warping of the deck plate throughout the test program.

3.3 Alignment/jacking calibration data are included in Appendix A-2. From these data, it can be seen that a very small amount of interaction (± 8 pounds at full load) was produced in the secondary channels when a primary channel was being loaded. In most cases, due to small interaction forces, it was not necessary to realign the flexural assemblies.

3.4 Wind load simulation jacking data are presented in Appendix A-3. The lateral load applied to the trailer correlated very well with the sum of the lateral loads measured by the forward and aft lateral flexures. The calibration was linear and repeatable. Roll, pitch, and yaw moments were calculated from the data and compared with the theoretical moments. Sample plots of applied load versus indicated yaw and roll moments are included in Appendix A-3.

3.5 From the pluck test data, the natural frequency of the trailer mounted on flexures was found to be approximately 3 Hz.

3.6 The log of preliminary and final tests is included as Appendix A-4. The dynamic response of the force balance system under actual field conditions was very reliable and repeatable. The zero return of the whole system was good and experienced very small zero shifts. The maximum zero shift experienced on vertical flexures was about ± 20 pounds and on lateral or longitudinal flexures was about ± 12 pounds. There was no indication of the system hitting the overload stops, and the mechanism seemed to be working well.

3.7 Throughout the testing period, the force balance system did not experience any unusual variations. The system was very stable, and the alignment of all the flexure assemblies remained orthogonal without introducing interaction forces of a serious nature. Overall, the performance of the system was better than what was required, and the procedures followed from the beginning of the program were helpful to achieve that performance.

3.8 The results of the preliminary and final tests are plotted in Appendix A-5. Drag force versus (velocity)² is plotted in Figure 1 for the preliminary test. The results of the final tests are plotted and compared with the wind tunnel model test results in Figures 2 and 3. From these results, it is seen that the aerodynamic forces predicted from the wind tunnel model tests correlate well with the measured full-scale values.

3.9 Appendix A-6 identifies all the equipment used by BEL in this test program.

4.0 PERSONNEL.

4.1 Federal Railroad Administration/Department of Transportation.

Mr. Arne Bang, Chief, Freight Service Division

Mr. John Koper, Research Manager, Freight Service Division

Mr. Lorin Staten, Test Controller, TTC

4.2 ENSCO, Inc., Alexandria, Virginia.

Mr. Thomas Jones

Mr. Robert Scofield

Mr. Robert Hendrickson

Mr. Prakash Joshi

Mr. John Berglund

4.3 ENSCO, Inc., Colorado Springs, Colorado.

Mr. Bryan Stewart

Mr. John Height

Mr. Donald Choffel

4.4 ENSCO/Dynalectron, TTC.

Mr. James Widger, Test Support Manager

Mr. Lane Maxwell, Test Support Engineer

Mr. Richard Peacock, Instrumentation Supervisor

Mr. Bruce Morrell, Design Engineer

Mr. Douglas Amaya, Test Support Engineer

Machine Shop Personnel

Rail Vehicle Maintenance Personnel

4.5 Andrew G. Hammitt Associates.

Mr. Andrew G. Hammitt, Consultant

4.6 Brewer Engineering Laboratories, Inc.

Mr. Given A. Brewer, Chief Engineer

Mr. LaVerne F. Wallace, Assistant Chief Engineer

Mr. Hemant S. Limaye, Project Engineer

Mr. George A. Leighton, Laboratory Superintendent

Mr. Jeffrey D. Tripp, Electromechanical Technician

Mr. Gilbert V. DeCouto, Electromechanical Technician

5.0 REFERENCES.

1. "Test Results Report TOFC Full-Scale Aerodynamic Validation Tests CV-192 in Support of Test Request CV-192; Test Dates: 10/18/1976 - 11/02/1976," Prepared by ENSCO, Inc., March 1, 1977.
2. Hammitt, Andrew G., "Investigation of the Aerodynamic Drag of Containers and Trailers on Flatcars: Full-Scale Tests," Final Report DOT-TSC-1002, May 5, 1977.
3. Brewer, Given A., "Assessment of Effectiveness of Full-Scale TOFC Aerodynamic Drag Tests in Performing Validation of Scale Model Wind Tunnel Tests Contract DOT-FR-74310," BEL Report 611, March 16, 1977.
4. Wallace, LaVerne F., Letter to Robert Scofield, "Straight Circular Flexures Versus Flexural Pivots," July 27, 1977.
5. Limaye, Hemant S., "Flatcar Modifications," BEL Drawing No. 10605-X, Revision B, August 22, 1977.
6. "TOFC II Full-Scale Aerodynamic Validations Tests," AERO/TOFC-II Test Plan, September 8, 1977.
7. "TOFC II Full-Scale Aerodynamic Validation Tests," AERO/TOFC-II Test Requirements, June 24, 1977.

6.0 BIBLIOGRAPHY.

1. "Preliminary Balance Design," By Andrew G. Hammitt Associates, November 7, 1975.
2. Hammitt, Andrew G., "Instrumentation Requirements - TOFC Full-Scale Aerodynamic Validation Tests," Report No. 10-001-76, Andrew G. Hammitt Associates, February 27, 1976.
3. Hammitt, Andrew G., "Scientific Test Plan - TOFC Full-Scale Aerodynamic Validation Tests," Report No. 10-002-76, Andrew G. Hammitt Associates, March 1, 1976.
4. Ross, W. H., "Test Plan/Specification/Procedure CV-192 TOFC Full-Scale Aerodynamic Validation Test in Support of Test Request CV-192," ENSCO, Inc., April 9, 1976.
5. "Test Specification Aerodynamic TOFC Validation Test No. 7128," Approved by E. E. Pazera, TTC, and J. Koper, FRA, and Concurred by L. Staten, TTC, July 23, 1976.
6. Hammitt, Andrew G., "Aerodynamic Forces on Freight Trains, Volume 1, Wind Tunnel Tests of Containers and Trailers on Flatcars," Report No. FRA-ORD-76-295-I, U. S. Department of Transportation, December, 1976.
7. Brewer, Given A., "Wind Tunnel Tests, 1/24 Scale Needles Reflector Model," BEL Report 196, May 26, 1960.
8. Vanstone, Robert A., "Wind Loading Millstone 84 Foot Radar Antenna," BEL Report 204, Appendix IV, November 30, 1960.
9. Brewer, Given A., "Calibrating the PBY-6A Airplane for Meteorological Purposes," "Aeronautical Engineering Review," February, 1954.
10. Brewer, Given A., "Flight and Ground Loads on Light Plane Wing Fittings," "Proceedings of the Society for Experimental Stress Analysis," Volume VIII, No. 1, 1950, Pages 93-102.

APPENDIX A-1
PHOTOGRAPHS OF TEST

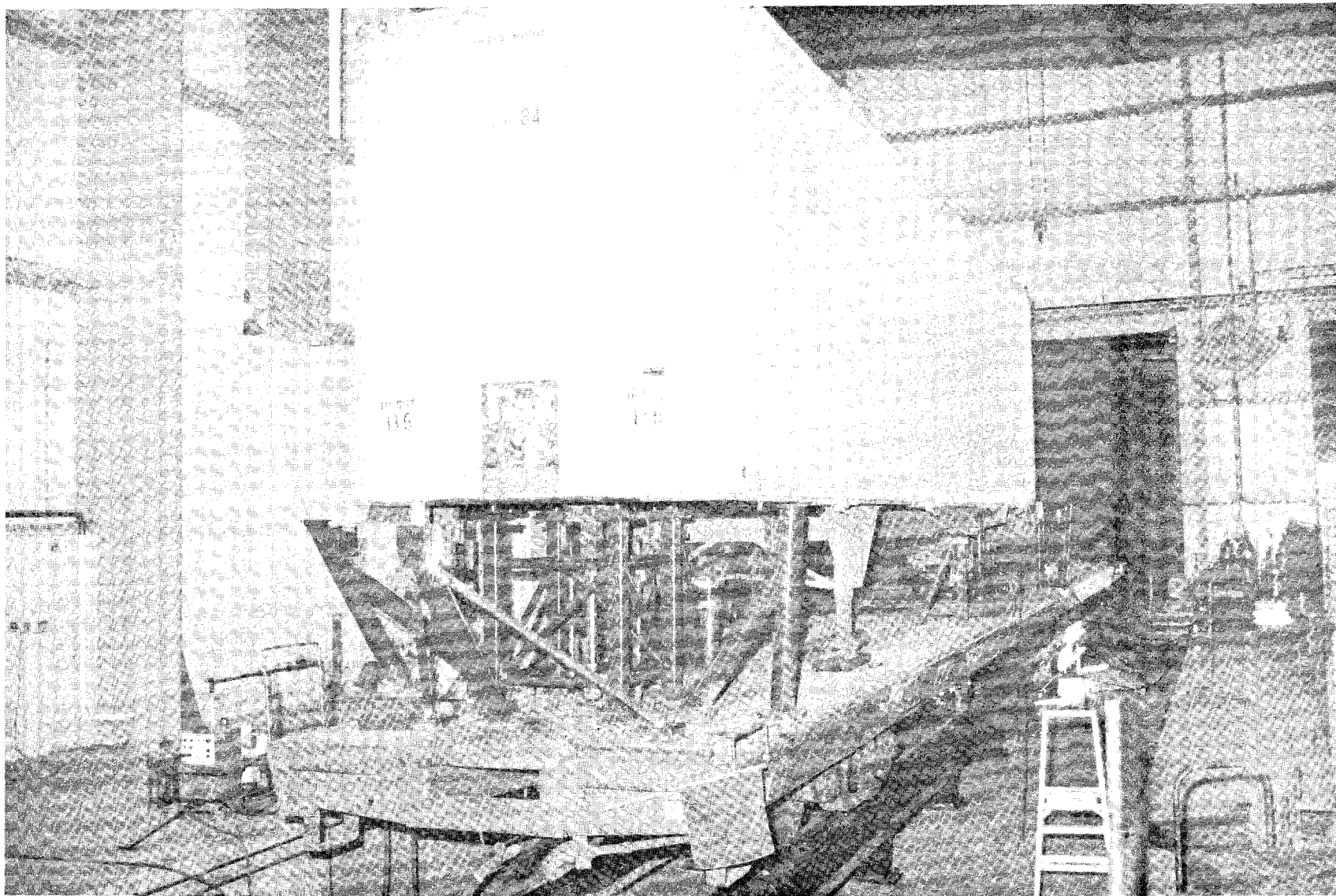


FIGURE 1. FORWARD TRAILER SUPPORTED ON A VERTICAL FLEXURE AND PNEUMATIC JACKS ON THE FLATCAR.

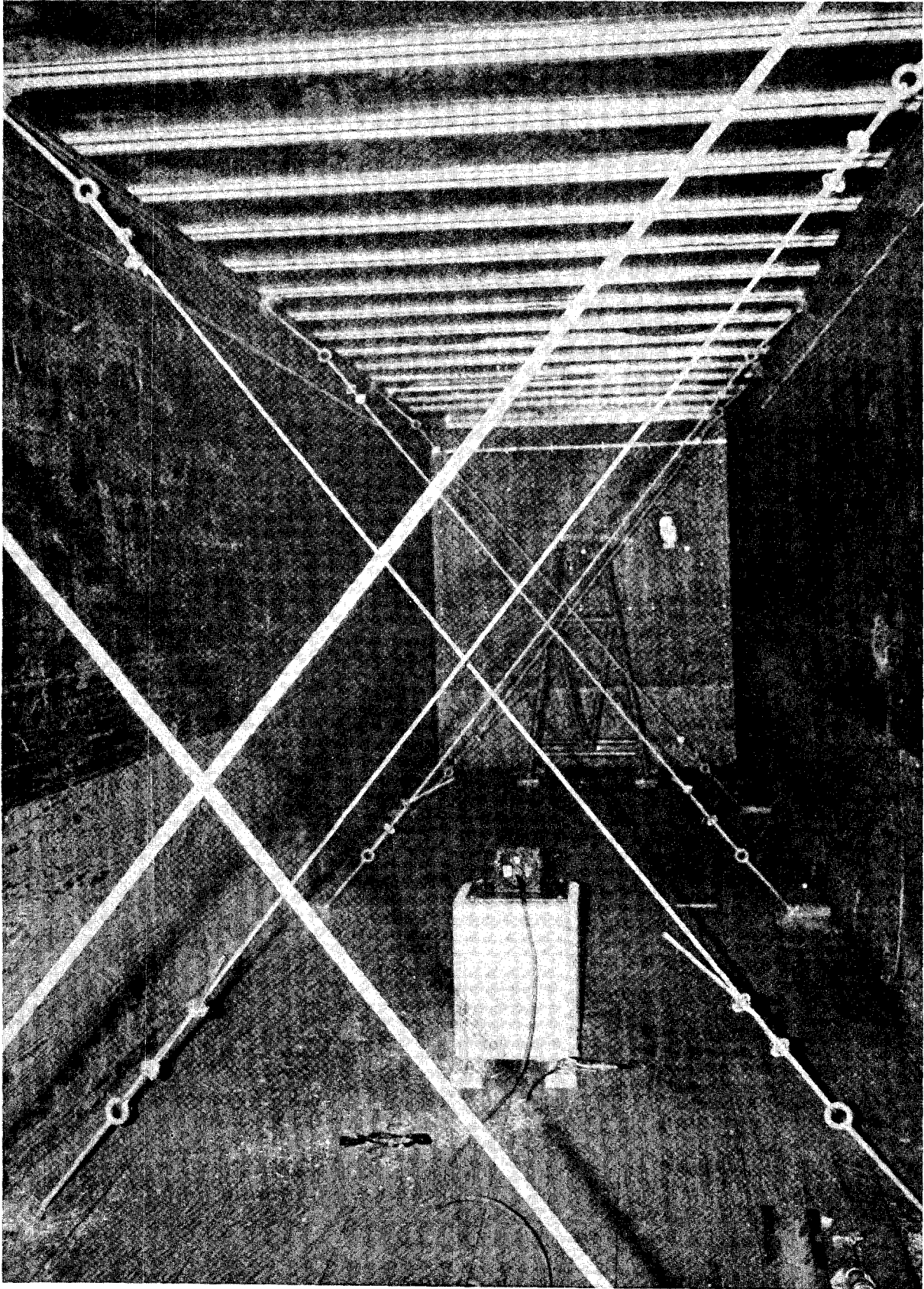


FIGURE 2. INSIDE VIEW OF THE TRAILER SHOWING TRAILER
STIFFENING WITH CABLES.
A-38

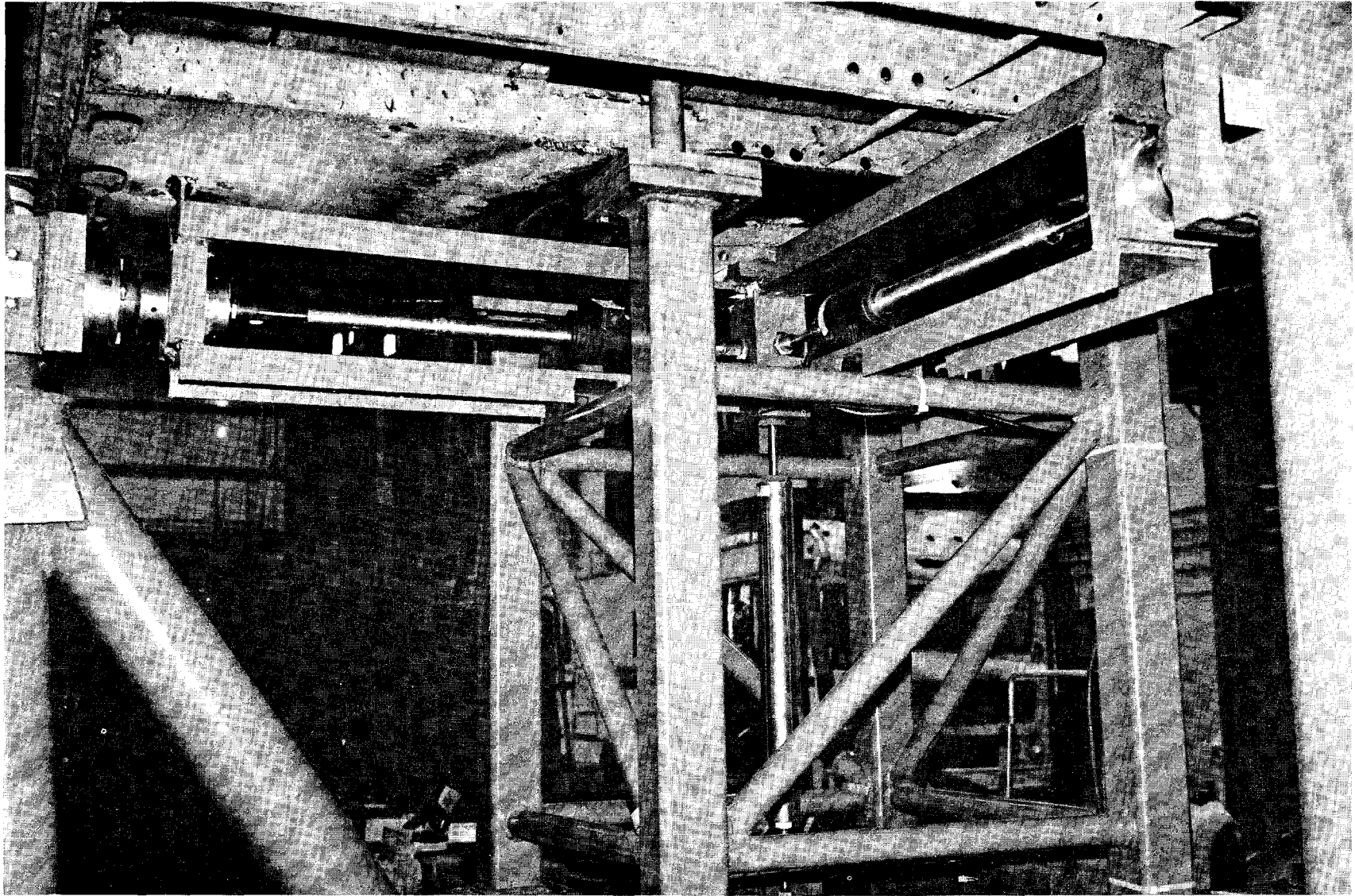


FIGURE 3. FORWARD END OF THE TRAILER SHOWING THE LATERAL, VERTICAL, AND LONGITUDINAL FLEXURES.

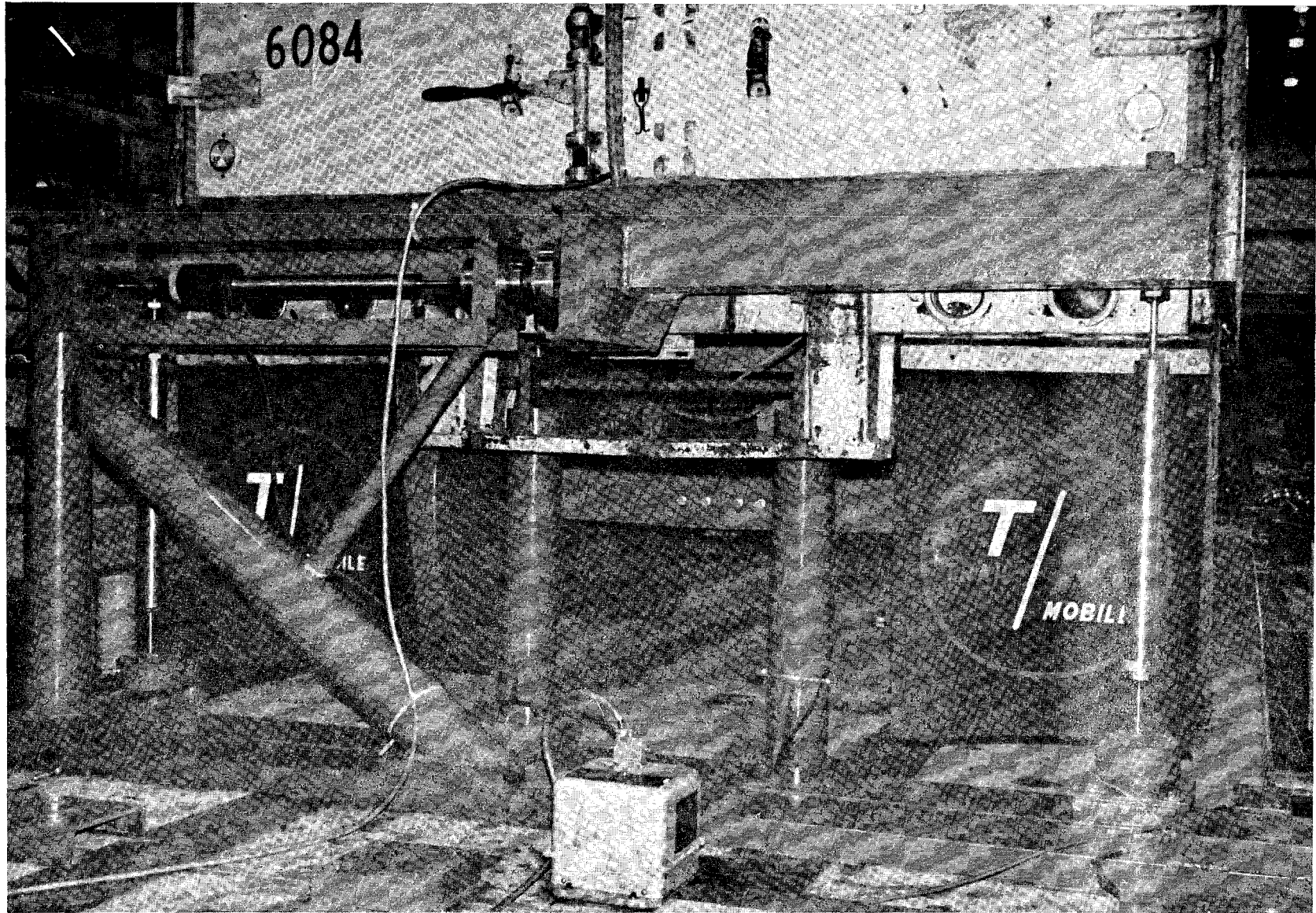


FIGURE 4. AFT END OF THE TRAILER WITH VERTICAL AND LATERAL FLEXURES.

A-41

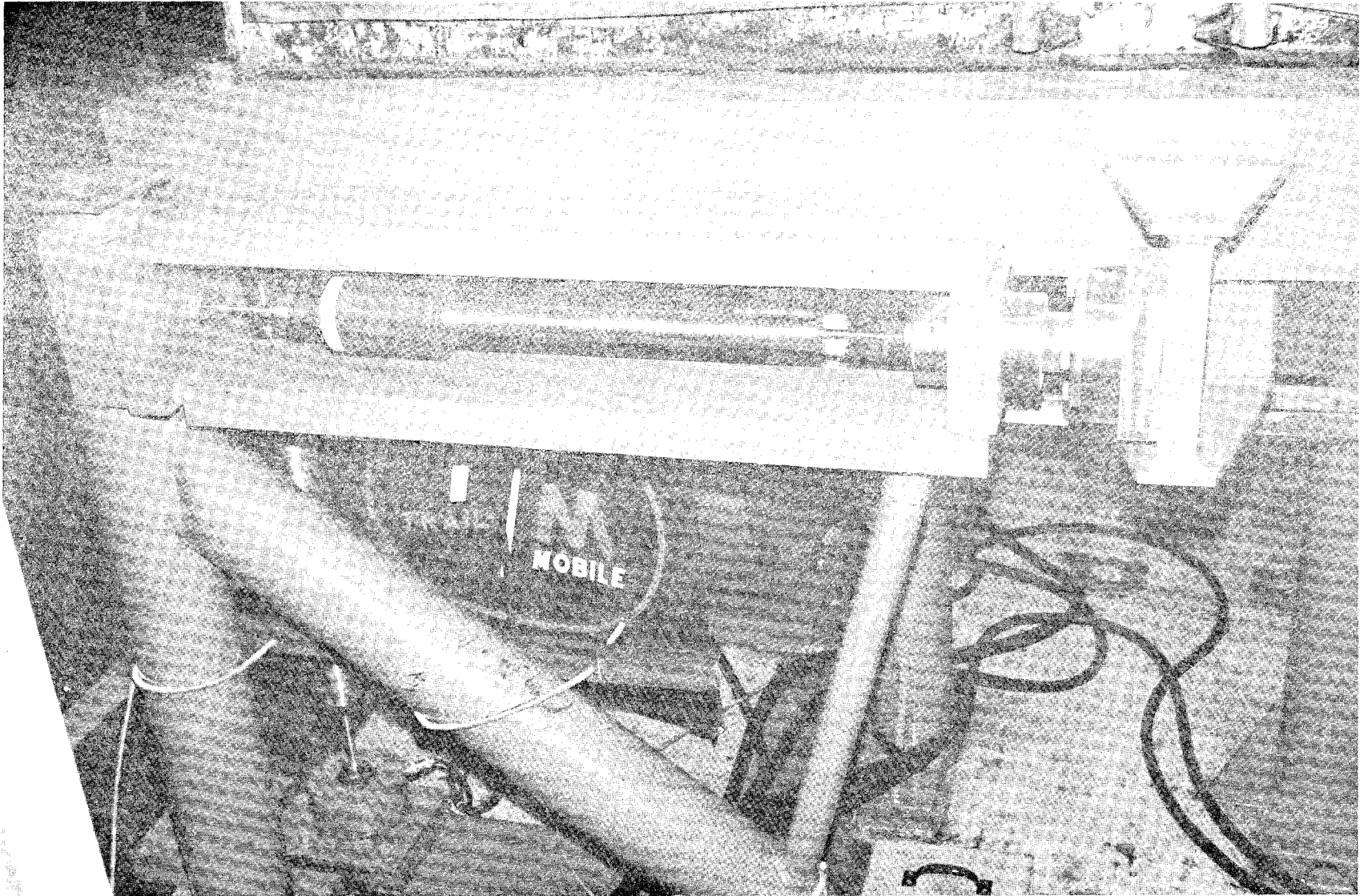


FIGURE 5. AFT LATERAL FLEXURE WITH OVERLOAD PROTECTION SYSTEM.

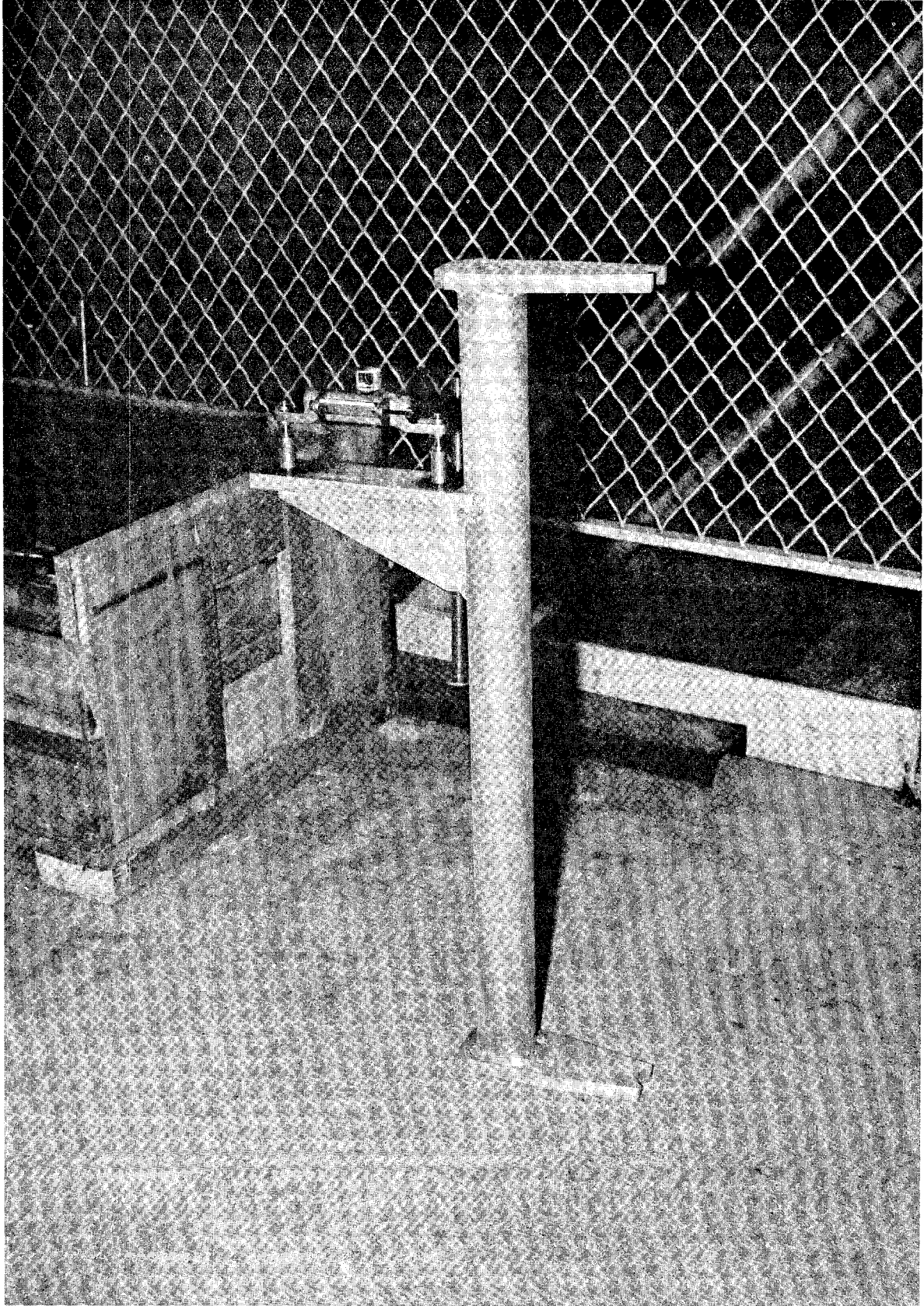


FIGURE 6. ALIGNMENT TOOL WITH PRECISION LEVEL.
A-42

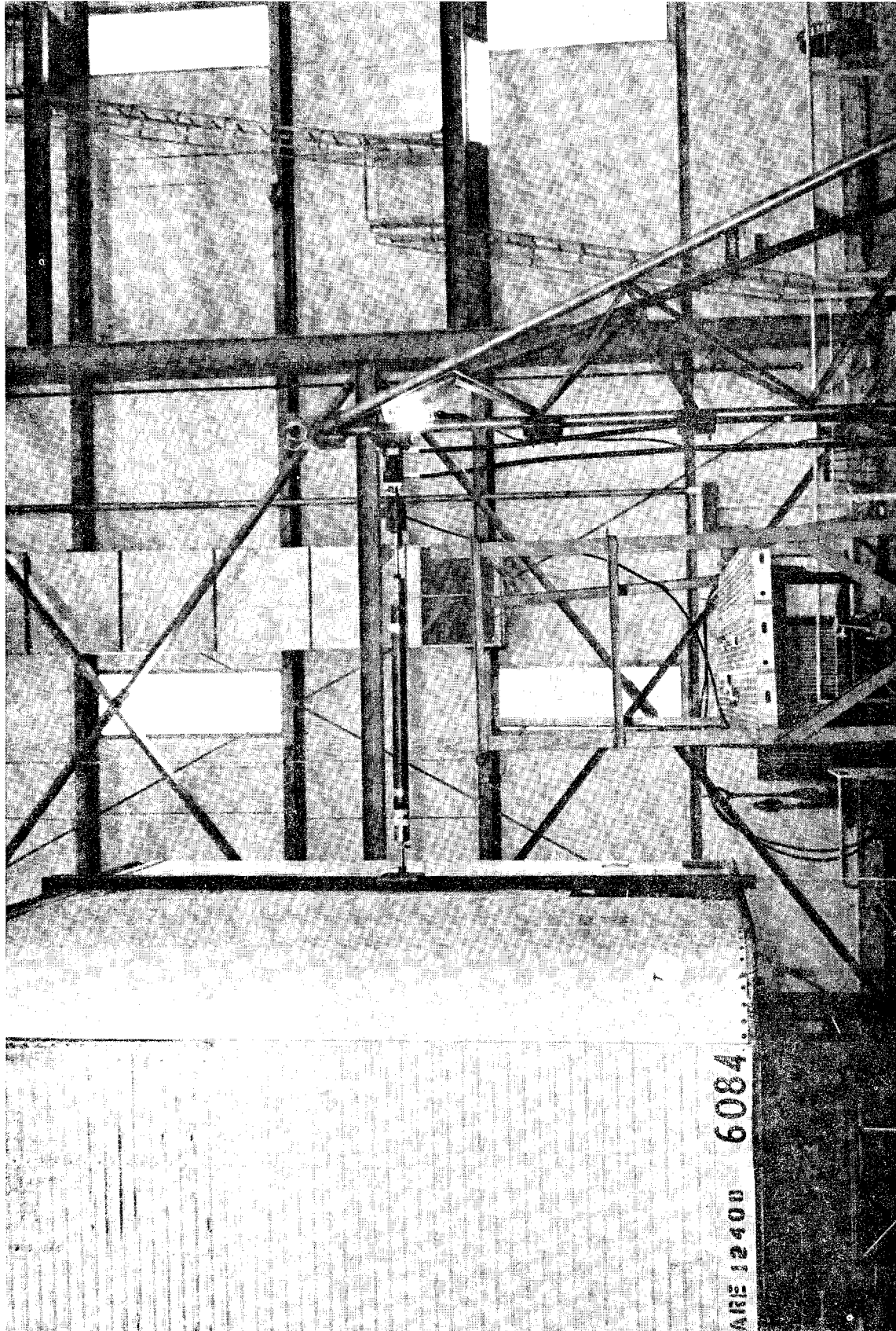


FIGURE 7. LONGITUDINAL JACKING CALIBRATION SYSTEM TO SIMULATE THE WIND LOAD.

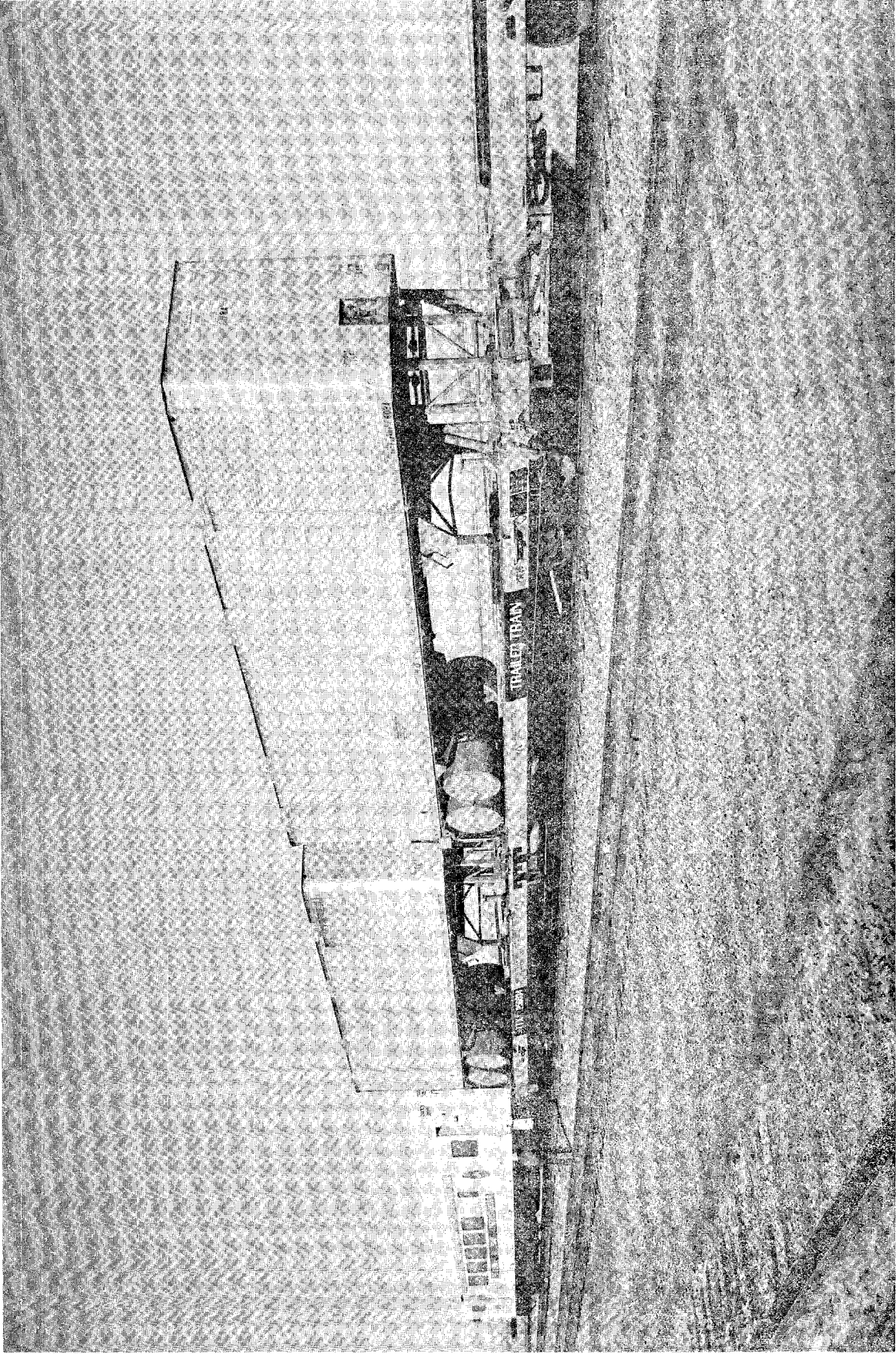


FIGURE 8. INSTRUMENTED TRAILERS COUPLED TO THE T-5 CAR.

APPENDIX A-2

JACKING CALIBRATION AND ALIGNMENT DATA

JACKING CALIBRATION DATA

Trailer: 'A' Aft
 Channel: Aft Right Vertical
 Run Nos.: 1 and 2
 Date: 11-10-77
 Time: 1840; 1852
 Standard: BLH 5000 Pound Load Cell

Applied Load (lbs)	Forward End			Aft End			Dial Gage (mils)
	Vertical (lbs)	Lateral (lbs)	Longitudinal (lbs)	Left Vertical (lbs)	Right Vertical (lbs)	Lateral (lbs)	
0	0	0	0	0	0	0	-
505	-3	-3	-4	3	521	-3	-
984	-3	-3	-3	-4	991	-3	-
1492	-3	-3	-3	-4	1482	-4	-
1984	-3	-3	-4	-3	1973	-3	-
1020	-3	-3	-3	-3	1030	-3	-
+5	-3	-3	-3	-4	+12	-4	-
0	0	0	0	0	0	0	-
500	0	0	0	0	506	0	-
996	0	0	0	0	997	0	-
1480	0	0	0	0	1464	0	-
1988	0	0	0	0	1964	0	-
973	0	0	0	0	976	0	-
-5	0	0	0	0	0	0	-

JACKING CALIBRATION DATA

Trailer: 'B' Forward
 Channel: Aft Left Vertical
 Run Nos.: 1 and 2
 Date: 11-9-77
 Time: 1345; 1358
 Standard: BLH 5000 Pound Load Cell

Applied Load (lbs)	Forward End			Aft End			Dial Gage (mils)
	Vertical (lbs)	Lateral (lbs)	Longitudinal (lbs)	Left Vertical (lbs)	Right Vertical (lbs)	Lateral (lbs)	
0	0	0	0	0	0	0	-
518	0	0	+3	-521	0	0	-
975	0	0	+3	-979	0	0	-
1472	0	0	+4	-1455	0	0	-
1957	+3	0	+4	-1935	0	-3	-
987	0	0	+4	-997	0	0	-
8	0	0	0	-12	0	0	-
0	0	0	0	0	0	0	-
+520	0	+3	0	-524	0	0	-
+1033	0	+3	0	-1023	0	0	-
+1470	0	+2	+3	-1452	0	-2	-
+1991	0	0	+3	-1982	+3	-2	-
1022	0	0	+3	-1023	0	-2	-
+4	0	+2	0	0	+2	0	-

JACKING CALIBRATION DATA

Trailer: 'A' Aft
 Channel: Aft Left Vertical
 Run Nos.: 1 and 2
 Date: 11-10-77
 Time: 1805; 1815
 Standard: BLH 5000 Pound Load Cell

Applied Load (lbs)	Forward End			Aft End			Dial Gage (mils)
	Vertical (lbs)	Lateral (lbs)	Longitudinal (lbs)	Left Vertical (lbs)	Right Vertical (lbs)	Lateral (lbs)	
0	0	0	0	0	0	0	-
477	0	0	0	481	0	0	-
985	0	0	0	971	0	3	-
1488	0	0	0	1455	0	3	-
1978	3	0	3	1960	0	3	-
996	0	0	0	980	0	+3	-
-5	0	0	0	0	0	0	-
0	0	0	0	0	0	0	-
503	3	0	0	508	0	2	-
985	3	0	0	971	0	2	-
1483	3	0	0	1458	0	3	-
1971	3	0	0	1939	0	2	-
994	3	0	0	995	0	0	-
0	0	0	0	0	0	0	-

JACKING CALIBRATION DATA

Trailer: 'B' Forward
 Channel: Longitudinal
 Run Nos.: 1 and 2
 Date: 11-2-77
 Time: 1353; 1404
 Standard: BLH 5000 Pound Load Cell

Applied Load (lbs)	Forward End			Aft End			Dial Gage (mils)
	Vertical (lbs)	Lateral (lbs)	Longitudinal (lbs)	Left Vertical (lbs)	Right Vertical (lbs)	Lateral (lbs)	
0	0	0	0	0	0	0	0
235	0	0	235	0	0	0	2
497	0	-4	496	0	0	0	4½
753	0	-8	755	0	0	0	6½
995	0	-8	998	0	0	0	9
497	0	5	500	0	0	0	4½
22	0	0	23	0	0	0	-½
20	0	0	21	0	0	0	0
263	0	0	260	0	0	0	3
503	0	-6	504	0	0	0	5
744	0	8	745	0	0	0	7½
1002	0	8	1001	0	0	0	10
535	0	5	535	0	0	0	5½
20	0	0	21	0	0	0	0

JACKING CALIBRATION DATA

Trailer: 'A' Aft
 Channel: Longitudinal
 Run Nos.: 1 and 2
 Date: 11-10-77
 Time: 1026; 1034
 Standard: BLH 5000 Pound Load Cell

Applied Load (lbs)	Forward End			Aft End			Dial Gage (mils)
	Vertical (lbs)	Lateral (lbs)	Longitudinal (lbs)	Left Vertical (lbs)	Right Vertical (lbs)	Lateral (lbs)	
0	0	0	0	0	0	0	0
255	0	0	253	0	0	0	1
525	0	0	524	0	0	0	1½
745	0	0	744	0	0	0	2
993	0	-2	992	0	0	0	3
492	0	0	493	0	0	0	1½
-20	0	0	-19	0	0	0	0
0	0	0	0	0	0	0	0
278	0	0	275	0	0	0	1
504	0	0	501	0	0	0	1½
764	0	0	761	0	0	0	2
994	0	0	991	0	0	0	3
527	0	0	527	0	0	0	1½
23	0	0	+23	0	0	0	0

JACKING CALIBRATION DATA

Trailer: 'B' Forward
 Channel: Forward Lateral
 Run Nos.: 1 and 2
 Date: 11-1-77; 11-2-77
 Time: 1600; 1613
 Standard: BLH 5000 Pound Load Cell

Applied Load (lbs)	Forward End			Aft End			Dial Gage (mils)
	Vertical (lbs)	Lateral (lbs)	Longitudinal (lbs)	Left Vertical (lbs)	Right Vertical (lbs)	Lateral (lbs)	
0	0	0	0	0	0	0	0
289	0	291	-4	0	0	0	3
504	0	508	7	0	0	0	6
779	0	783	8	0	0	0	10
1010	0	1013	8	0	0	0	14
524	0	528	7	0	0	0	7
4	0	7	0	0	0	0	-2
0	0	0	0	0	0	0	0
268	0	270	0	0	0	0	4
519	0	523	8	0	0	0	8
761	0	763	8	0	0	0	12
1041	0	1041	8	0	0	0	16
466	0	467	6	0	0	0	7
5	0	5	0	0	0	0	0

JACKING CALIBRATION DATA

Trailer: 'A' Aft
 Channel: Forward Lateral
 Run Nos.: 1 and 2
 Date: 11-9-77
 Time: 1842; 1850
 Standard: BLH 5000 Pound Load Cell

Applied Load (lbs)	Forward End			Aft End			Dial Gage (mils)
	Vertical (lbs)	Lateral (lbs)	Longitudinal (lbs)	Left Vertical (lbs)	Right Vertical (lbs)	Lateral (lbs)	
0	0	0	0	0	0	0	-
519	0	516	-2	0	0	0	-
983	0	980	-3	0	0	0	-
1485	0	1483	-6	0	0	0	-
2006	0	2007	-8	0	0	0	-
995	0	993	-3	0	0	0	-
5	0	4	0	0	0	0	-
0	0	0	0	0	0	0	-
503	0	498	0	0	0	0	-
1083	0	1080	-4	0	0	0	-
1513	0	1510	-7	0	0	0	-
1998	0	1997	-8	0	0	0	-
977	0	974	-3	0	0	0	-
3	0	3	0	0	0	0	-

JACKING CALIBRATION DATA

Trailer: 'B' Forward
 Channel: Aft Lateral
 Run Nos.: 1 and 2
 Date: 11-2-77
 Time: 1725; 1737
 Standard: BLH 5000 Pound Load Cell

Applied Load (lbs)	Forward End			Aft End			Dial Gage (mils)
	Vertical (lbs)	Lateral (lbs)	Longitudinal (lbs)	Left Vertical (lbs)	Right Vertical (lbs)	Lateral (lbs)	
0	0	0	0	0	0	0	0
258	0	0	0	0	0	258	1
511	0	0	0	0	0	513	1½
756	0	0	3	0	0	756	2½
1019	0	0	3	0	0	1024	3½
438	0	0	0	0	0	442	1½
-4	0	0	0	0	0	-4	0
0	0	0	0	0	0	0	0
252	0	0	0	0	0	250	1
529	0	0	0	0	0	528	2
764	0	0	2	0	0	765	2½
1008	0	0	2	0	0	1010	3½
522	0	0	0	0	0	523	2
0	0	0	0	0	0	6	0

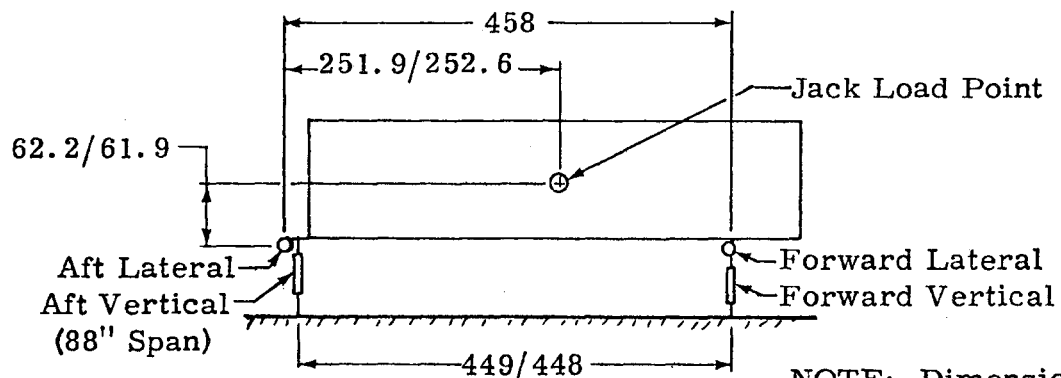
APPENDIX A-3

WIND LOAD SIMULATION TRAILER JACKING DATA

WIND LOAD SIMULATION - TRAILER JACKING DATA
TEST RUN NO. 5 FOR 'A' AND 'B' TRAILER

Applied Load (lbs)	Measured Load (lbs)						Trailer
	Forward End			Aft End			
	Vertical	Lateral	Longitudinal	Left Vertical	Right Vertical	Lateral	
0	0	0	0	0	0	0	A
303	0	-174	-5	-226	+238	-140	A
703	-3	-395	-5	-517	+527	-323	A
1082	-6	-606	-7	-790	+804	-495	A
1413	-6	-790	-8	-1030	+1045	-648	A
0	0	0	0	0	0	0	B
437	0	-250	-4	-330	+289	-201	B
660	-3	-372	-5	-482	+429	-298	B
923	-3	-523	-6	-670	+616	-418	B
1168	-3	-662	-7	-842	+795	-530	B
1418	-3	-803	-8	-1027	+973	-644	B

NOTE: The test data are corrected for flatcar lateral tilt error.

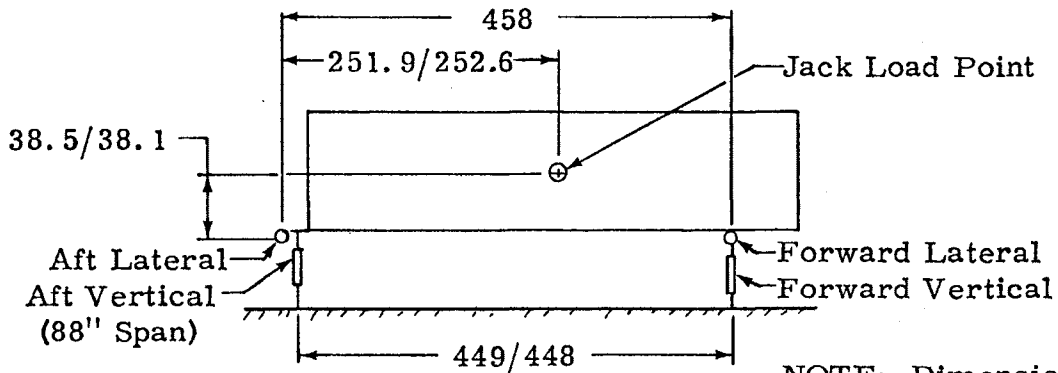


NOTE: Dimensions shown are for A/B trailer.

TEST RUN NOS. 9 AND 7 RESPECTIVELY
FOR TRAILERS 'A' AND 'B'

Applied Load (lbs)	Measured Load (lbs)						Trailer
	Forward End			Aft End			
	Vertical	Lateral	Longitudinal	Left Vertical	Right Vertical	Lateral	
0	0	0	0	0	0	0	A
291	-3	-168	-1	-128	+143	-134	A
703	-12	-396	0	-315	+330	-320	A
1129	-15	-635	0	-511	+524	-513	A
1414	-12	-792	-2	-635	+655	-645	A
0	0	0	0	0	0	0	B
400	-6	-227	-3	-193	+158	-182	B
636	-6	-359	-3	-298	+247	-288	B
892	-6	-503	-6	-411	+351	-401	B
1137	-6	-642	-6	-518	+455	-513	B

NOTE: The test data are corrected for flatcar lateral tilt error.

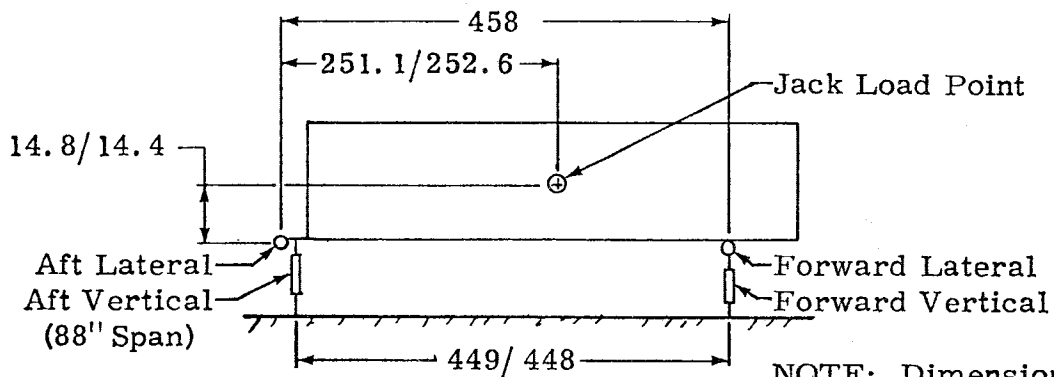


NOTE: Dimensions shown are for A/B trailer.

TEST RUN NOS. 11 AND 9 RESPECTIVELY
FOR TRAILERS 'A' AND 'B'

Applied Load (lbs)	Measured Load (lbs)						Trailer
	Forward End			Aft End			
	Vertical	Lateral	Longitudinal	Left Vertical	Right Vertical	Lateral	
0	0	0	0	0	0	0	A
347	+6	-200	0	-74	+68	-159	A
773	0	-432	-2	-157	+143	-351	A
1085	-3	-608	-1	-220	+202	-488	A
1430	-3	-797	-2	-285	+271	-648	A
0	0	0	0	0	0	0	B
376	-6	-214	+1	-68	+45	-172	B
734	0	-415	0	-137	+107	-333	B
978	0	-554	0	-182	+149	-440	B
1238	-6	-702	+1	-229	+188	-558	B
1501	-3	-851	0	-277	+226	-677	B

NOTE: The test data are corrected for flatcar lateral tilt error.

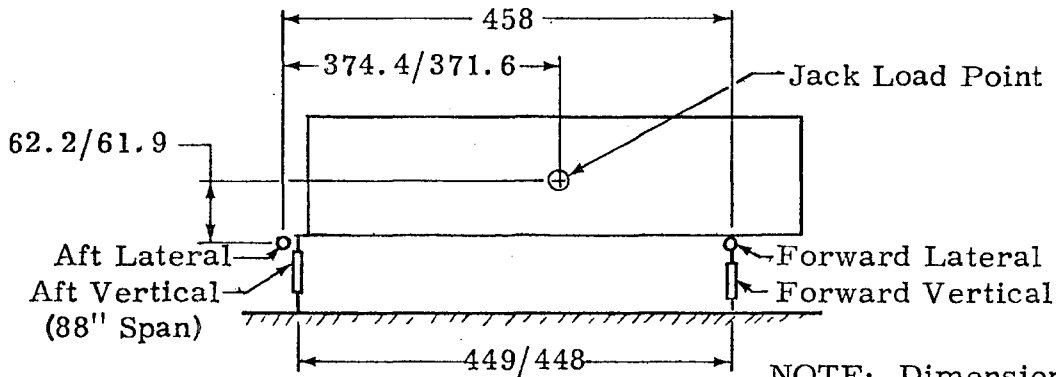


NOTE: Dimensions shown are for A/B trailer.

TEST RUN NOS. 5 AND 11 RESPECTIVELY
FOR TRAILERS 'A' AND 'B'

Applied Load (lbs)	Measured Load (lbs)						Trailer
	Forward End			Aft End			
	Vertical	Lateral	Longitudinal	Left Vertical	Right Vertical	Lateral	
0	0	0	0	0	0	0	A
287	-6	-238	-3	-220	+220	-58	A
744	-15	-610	-11	-546	+548	-143	A
1165	-18	-958	-12	-849	+851	-223	A
1420	-18	-1170	-14	-1027	+1030	-273	A
0	0	0	0	0	0	0	B
339	-9	-287	-4	-262	+217	-73	B
585	-18	-484	-8	-435	+369	-120	B
883	-12	-733	-12	-643	+574	-178	B
1138	-12	-944	-16	-830	+756	-227	B
1390	-9	-1155	-18	-1015	+938	-276	B

NOTE: The test data are corrected for flatcar lateral tilt error.

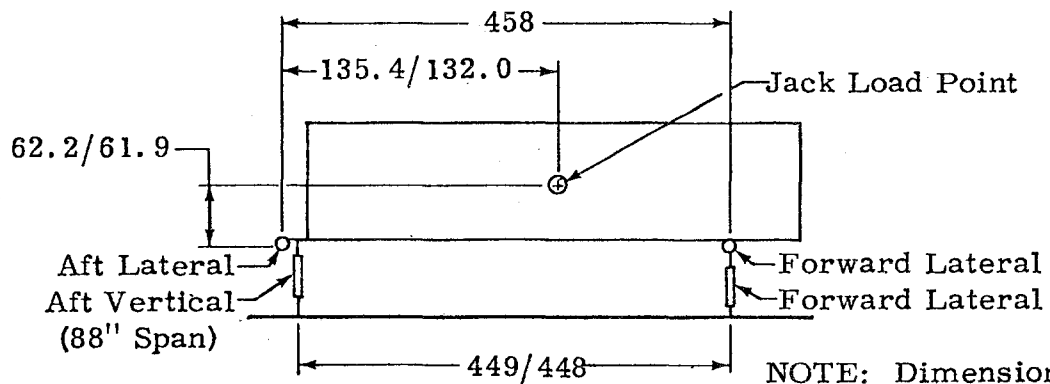


NOTE: Dimensions shown are for A/B trailer.

TEST RUN NO. 13 FOR TRAILERS 'A' AND 'B'

Applied Load (lbs)	Measured Load (lbs)						Trailer
	Forward End			Aft End			
	Vertical	Lateral	Longitudinal	Left Vertical	Right Vertical	Lateral	
0	0	0	0	0	0	0	A
340	+3	-108	0	-258	+259	-242	A
744	+3	-233	-1	-555	+560	-533	A
1152	0	-356	-8	-846	+857	-825	A
1486	+3	-454	-11	-1093	+1098	-1065	A
0	0	0	0	0	0	0	B
276	0	-89	-1	-220	+188	-204	B
527	0	-165	0	-405	+348	-301	B
1065	0	-327	-2	-786	+723	-768	B
1421	0	-434	-5	-1036	+967	-1025	B

NOTE: The test data are corrected for flatcar lateral tilt error.



NOTE: Dimensions shown are for A/B trailer.

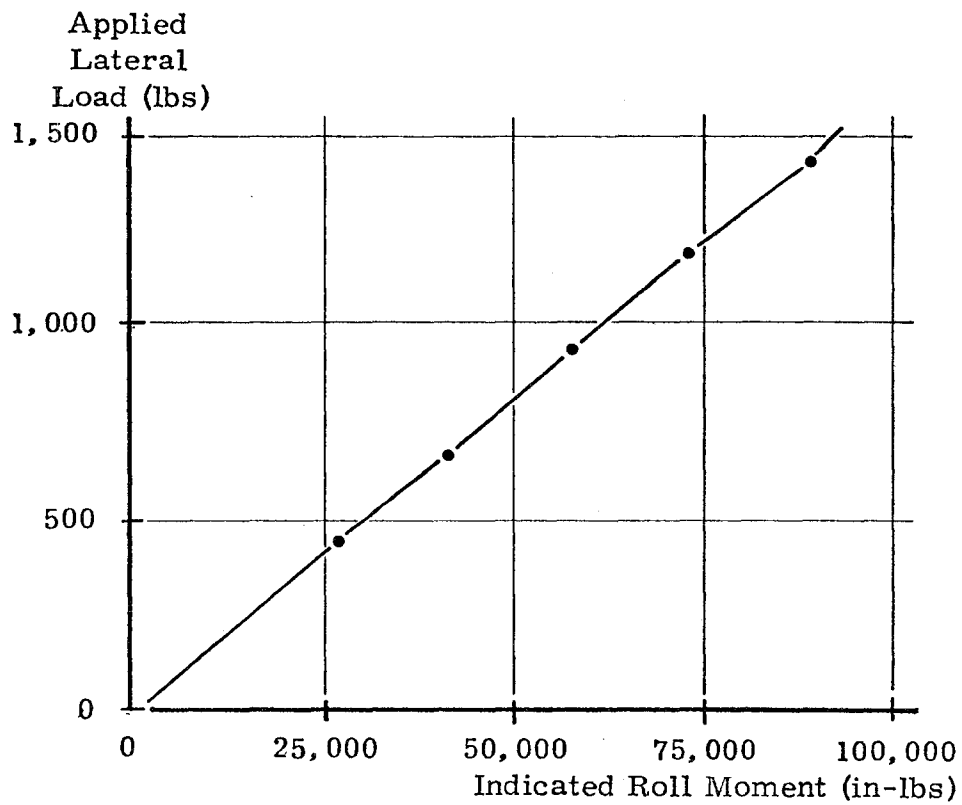
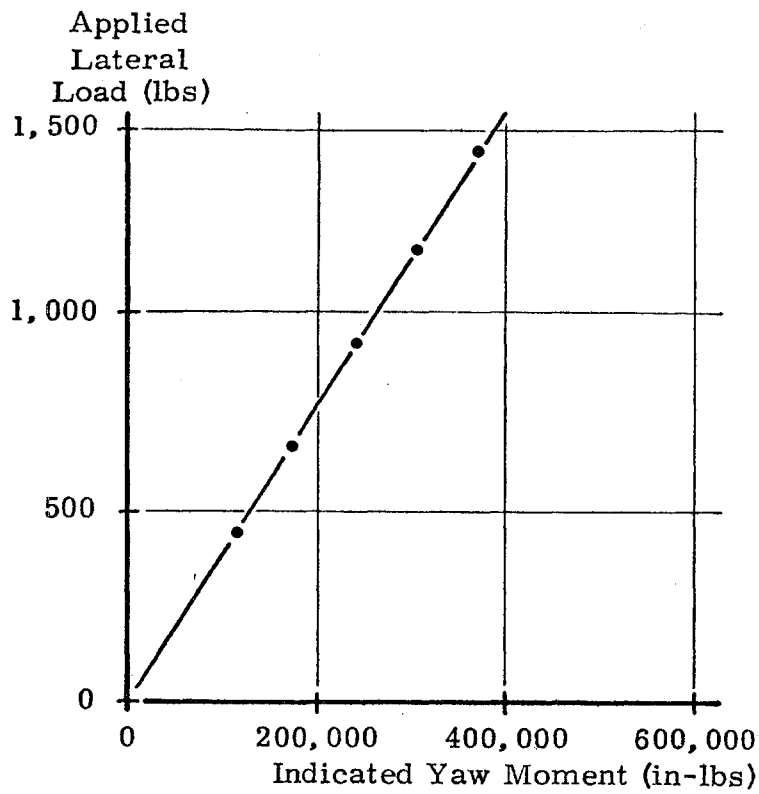


Figure 1. Applied Lateral Load Versus Indicated Yaw and Roll Moments for 'B' Trailer.

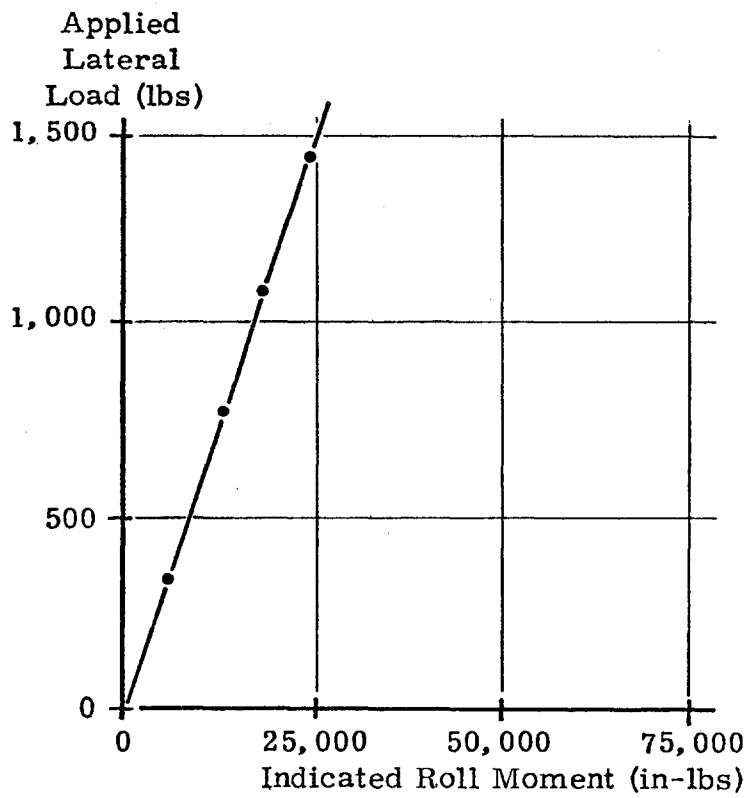
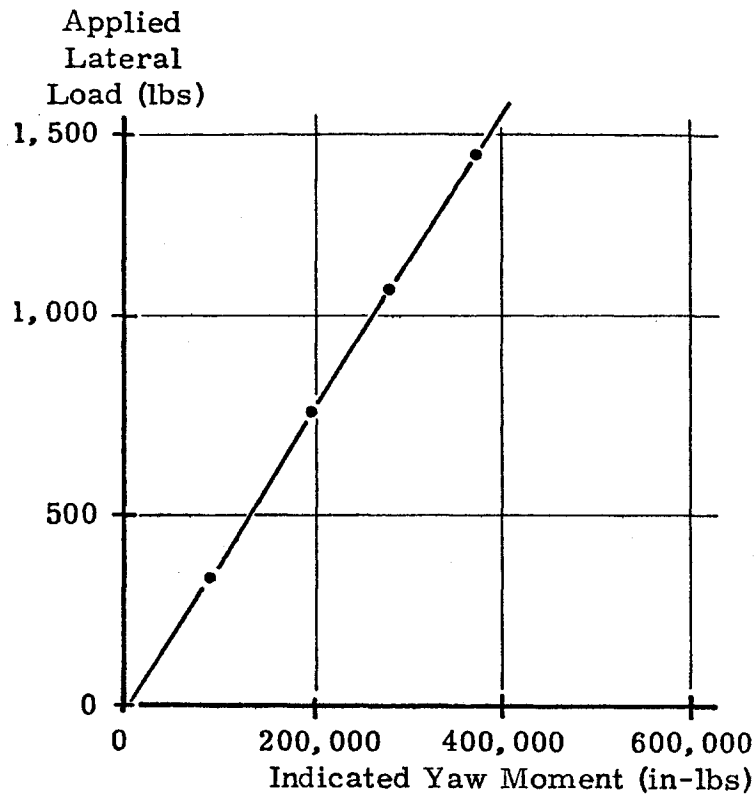


Figure 2. Applied Lateral Load Versus Indicated Yaw and Roll Moments for 'A' Trailer.

APPENDIX A-4
PRELIMINARY AND FINAL TEST LOG

TABLE I
TEST LOG

Date	Run No.	Time	Nominal Train Speed (mph)	Wind		Barometric Pressure Inches of Hg	Relative Humidity (%)	Temperature (°F)	Type of Configuration	Remarks
				Speed (mph)	Direction (°)					
12-01-77	5	1252	76/69	6	NE	24.85	13.0	37	II	
12-01-77	6	1305	73/71	6	NE	24.85	13.0	37	II	
12-01-77	7	1347	71/65	3	200	24.85	16.0	36	II	
12-01-77	8	1401	72/70	5	200	24.85	16.0	36	II	
12-01-77	9	1407	84/81	8	90	24.85	16.0	36	II	
12-01-77	10	1427	87/86	3	100	24.85	16.0	36	II	
12-01-77	11	1440	87/86	5	120	24.85	16.0	38	II	
12-01-77	12	1456	90/89	5	120	24.85	16.0	38	II	
12-01-77	13	1519	60/59	5	70	24.85	16.0	36	II	
12-01-77	14	1529	62/60	4	90	24.85	17.0	36	II	
12-02-77	15	1108	65	10	250	24.80	33.0	56	II	Not recorded on computer completely
12-02-77	16	1125	65/63	10	290	24.80	30.0	56	II	
12-02-77	17	1137	65/62	10	280	24.80	30.0	56	II	
12-02-77	18	1147	65/63	12	250	24.72	28.0	56	II	
12-02-77	19	1252	77/77	2	260	24.72	28.0	58	II	
12-02-77	20	1304	77/77	2	300	24.72	27.0	58	II	ALD problem - computer did not trigger
12-02-77	21	1338	77/77	4	280	24.70	27.0	59	II	
12-02-77	22	1425	75/73	17	250	24.70	27.0	59	II	
12-05-77	23	1230	52/51	10	70	25.02	80.0	26	II	
12-05-77	24	1241	53/52	8	70	25.02	80.0	26	II	Missed one ALD
12-05-77	25	1309	69/67	9	70	25.02	80.0	26	II	
12-05-77	26	1326	71/70	11	70	25.02	79.0	26	II	Missed one ALD, Lost D-4 string pot
12-05-77	27	1352	86/85	11	80	25.00	76.0	27	II	Lost D-1 and D-3 string pots
12-05-77	28	1404	86/85	9	80	25.00	74.0	27	II	
12-05-77	29	1418	51/50	10	90	25.02	75.0	27	II	
12-05-77	30	1430	70/70	10	80	25.02	76.0	27	II	
12-05-77	31	1441	85/84	10	80	25.06	78.0	26	II	
12-06-77	32	1038	52/51	3	90	25.02	81.0	19	II	
12-06-77	33	1042	68/67	2	170	25.02	81.0	19	II	
12-06-77	34	1055	89/86	2	200	25.02	80.0	19	II	
12-06-77	35	1110	88/88	4	140	25.10	73.0	22	II	
12-06-77	36	1122	71/71	Calm		25.10	76.0	20	II	
12-06-77	37	1138	52/52	2	160	25.10	76.0	21	II	
12-06-77	38	1249	53/53	3	30	25.02	66.0	25	II	
12-06-77	39	1300	67/68	1	90	25.02	64.0	26	II	
12-06-77	40	1312	93/94	Calm		25.02	63.0	26	II	

A-63

TABLE I (CONTINUED)

TEST LOG

Date	Run No.	Time	Nominal Train Speed (mph)	Wind		Barometric Pressure Inches of H _g	Relative Humidity (%)	Temperature (°F)	Type of Configuration	Remarks
				Speed (mph)	Direction (°)					
12-08-77	41	1226	51/51	10	40	24.85	81.0	24	II	
12-08-77	42	1233	52/51	10	0	24.90	81.0	23	II	
12-08-77	43	1249	69/69	10	40	24.95	78.0	22	II	ALD problem
12-08-77	44	1314	69/68	15	45	24.90	73.0	22	II	ALD problem
12-08-77	45	1352	68/68	10	10	24.90	70.0	21	II	
12-08-77	46	1403	67/69	7	10	24.95	69.0	20	II	ALD problem
12-08-77	47	1415	89/90	8	10	24.90	68.0	20	II	ALD problem
12-08-77	48	1430	89/90	9	10	25.00	66.0	20	II	
12-08-77	49	1442	72/71	10	0	25.00	66.0	20	II	
12-08-77	50	1452	89/90	7	30	25.00	65.0	20	II	
12-09-77	51	1321	50/49	5	90	25.30	77.0	8	I	Installed new ALD system
12-09-77	52	1332	52/51	5	100	25.30	77.0	8	I	
12-09-77	53	1343	50/50	5	70	25.30	77.0	8	I	
12-09-77	54	1400	67/67	5	100	25.30	76.0	10	I	
12-09-77	55	1411	68/67	5	70	25.28	75.0	10	I	
12-09-77	56	1422	68/67	2	20	25.28	76.0	11	I	
12-09-77	57	1439	87/87	3	80	25.28	75.0	13	I	
12-09-77	58	1451	90/90	2	50	25.25	74.0	13	I	
12-09-77	59	1508	90/90	2	30	25.25	72.0	14	I	
12-09-77	60	1524	32/32	Calm		25.25	70.0	16	I	
12-09-77	61	1537	22/24	4	50	25.10	71.0	15	I	
12-12-77	62	1218	50/49	5	270	24.75	23.0	58	I	Speed measurement error
12-12-77	63	1228	49/48	5	210	24.75	23.0	59	I	Speed measurement error
12-12-77	64	1250	50/48	15	270	24.75	23.0	58	I	Speed measurement error
12-12-77	65	1314	66/65	14	260	24.80	25.0	57	I	
12-12-77	66	1328	70/70	13	260	24.80	30.0	56	I	
12-12-77	67	1339	71/70	11	260	24.80	31.0	55	I	
12-12-77	68	1351	90/92	10	250	24.85	31.0	53	I	
12-12-77	69	1413	91/90	6	10	24.85	33.0	53	I	
12-12-77	70	1421	91/91	5	90	24.80	34.0	53	I	
12-12-77	71	1435	51/52	6	70	24.80	34.0	52	I	
12-12-77	72	1446	51/51	7	40	24.80	34.0	52	I	
12-12-77	73	1456	51/51	7	50	24.50	34.0	52	I	
12-14-77	74	1225	52/53	2	90	24.90	29.0	63	I	
12-14-77	75	1239	51/53	1	220	24.90	28.5	62	I	
12-14-77	76	1249	52/53	2	360	24.90	31.0	60	I	

A-64

TABLE I (CONTINUED)

TEST LOG

Date	Run No.	Time	Nominal Train Speed (mph)	Wind		Barometric Pressure Inches of H _g	Relative Humidity (%)	Temperature (°F)	Type of Configuration	Remarks
				Speed (mph)	Direction (°)					
12-14-77	77	1333	70/69	3	380	24.90	31.0	61	I	
12-14-77	78	1343	70/68	5	370	24.90	31.0	62	I	
12-14-77	79	1349	70/68	7	300	24.90	30.0	62	I	
12-14-77	80	1422	90/90	5	280	25.00	30.0	62	I	
12-14-77	81	1433	91/91	5	210	24.80	32.0	61	I	
12-14-77	82	1458	91/90	5	210	24.80	32.0	61	I	
12-15-77	83	1239	50/49	7	220	24.65	33.0	58	I	Speed measurement problem
12-15-77	84	1244	50/49	6	180	24.60	33.0	59	I	Speed measurement problem
12-15-77	85	1253	50/49	5	180	24.65	32.5	59	I	Speed measurement problem
12-15-77	86	1331	71/69	3	160	24.55	32.0	59	I	
12-15-77	87	1342	70/69	4	190	24.60	31.0	62	I	
12-15-77	88	1352	68/68	1	160	24.60	30.0	61	I	
12-15-77	89	1424	91/91	1	75	24.50	28.0	62	I	
12-15-77	90	1437	90/91	1	170	24.60	28.0	62	I	Wayside weather station data questionable
12-15-77	91	1448	90/91	Calm		24.60	27.0	65	I	
12-15-77	92	1522	54/54	1	460	24.50	26.0	63	I	Tape header indicates Run No. 91
12-15-77	93	1538	56/55	3	130	24.50	26.0	63	I	Tape header indicates Run No. 92
12-16-77	94	1311	66/63	15	210	24.55	18.0	41	I	Speed measurement problem
12-16-77	95	1321	69/67	20	230	24.60	17.0	42	I	
12-16-77	96	1332	70/68	15	230	24.60	17.0	42	I	
12-16-77	97	1358	90/88	18	270	24.60	17.0	42	I	
12-16-77	98	1414	90/85	15	250	24.60	17.0	42	I	
12-16-77	99	1426	90/90	20	220	24.60	16.0	42	I	
12-16-77	100	1448	53/52	15	240	24.60	16.0	42	I	
12-16-77	101	1458	55/54	15	230	24.60	19.0	40	I	
12-16-77	102	1512	55/54	12	220	24.00	18.0	40	I	
12-16-77	103	1809	91/93	6	250	24.60	26.0	32	II	
12-16-77	104	1822	92/91	7	260	24.60	26.0	32	II	Radio interference
12-16-77	105	1839	73/71	6	260	24.60	26.0	32	II	
12-16-77	106	1842	72/71	7	260	24.70	26.0	30	II	
12-16-77	107	1901	57/56	7	250	24.70	27.0	29	II	
12-16-77	108	1909	55/55	9	250	24.70	27.0	30	II	

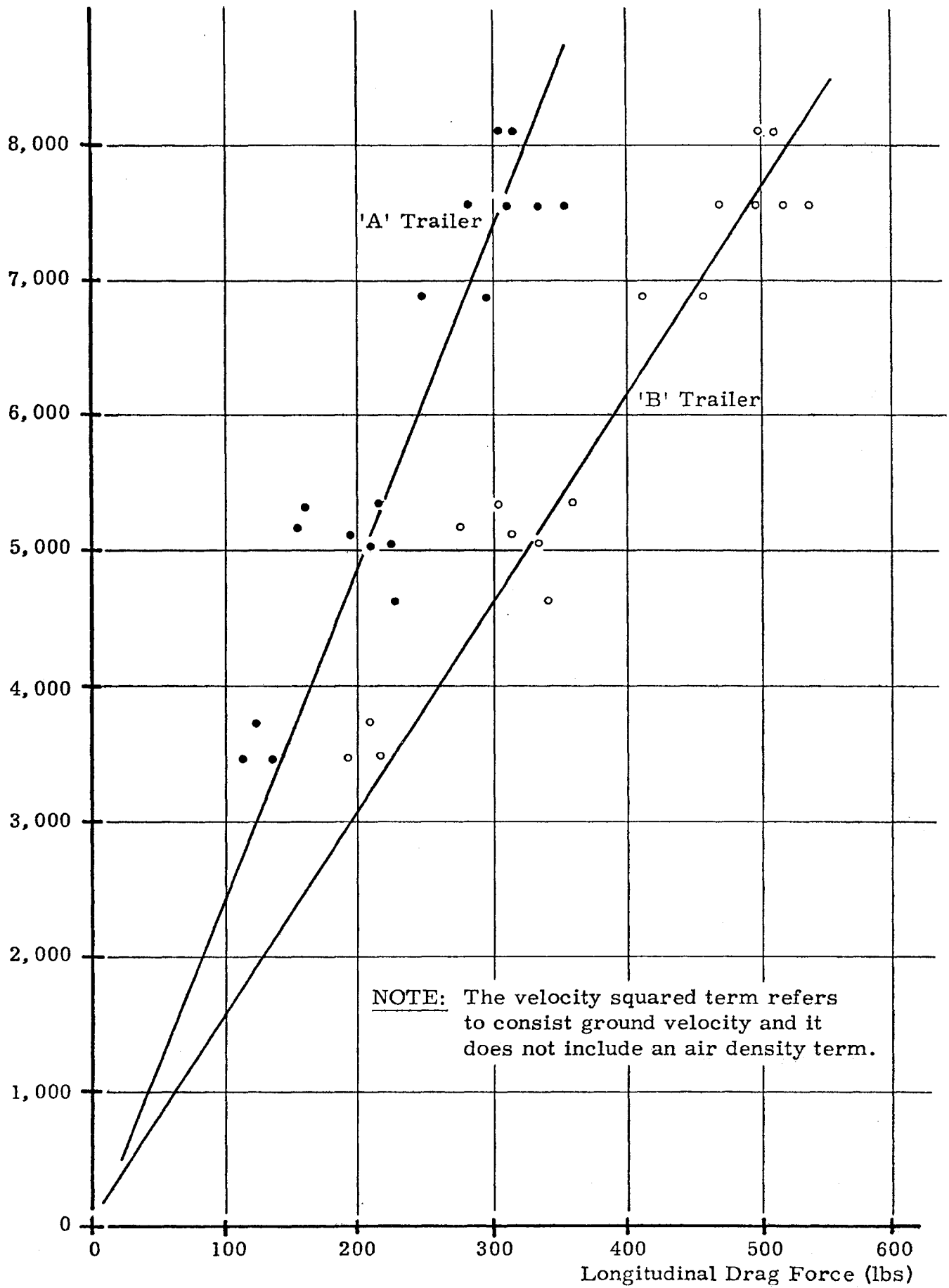
A-65

NOTE: 1. Run Nos. 5 through 22 were preliminary test runs.

APPENDIX A-5

RESULTS OF PRELIMINARY AND FINAL TESTS

(Velocity)², mph²



NOTE: The velocity squared term refers to consist ground velocity and it does not include an air density term.

Figure 1. Drag Force Versus (Velocity)².

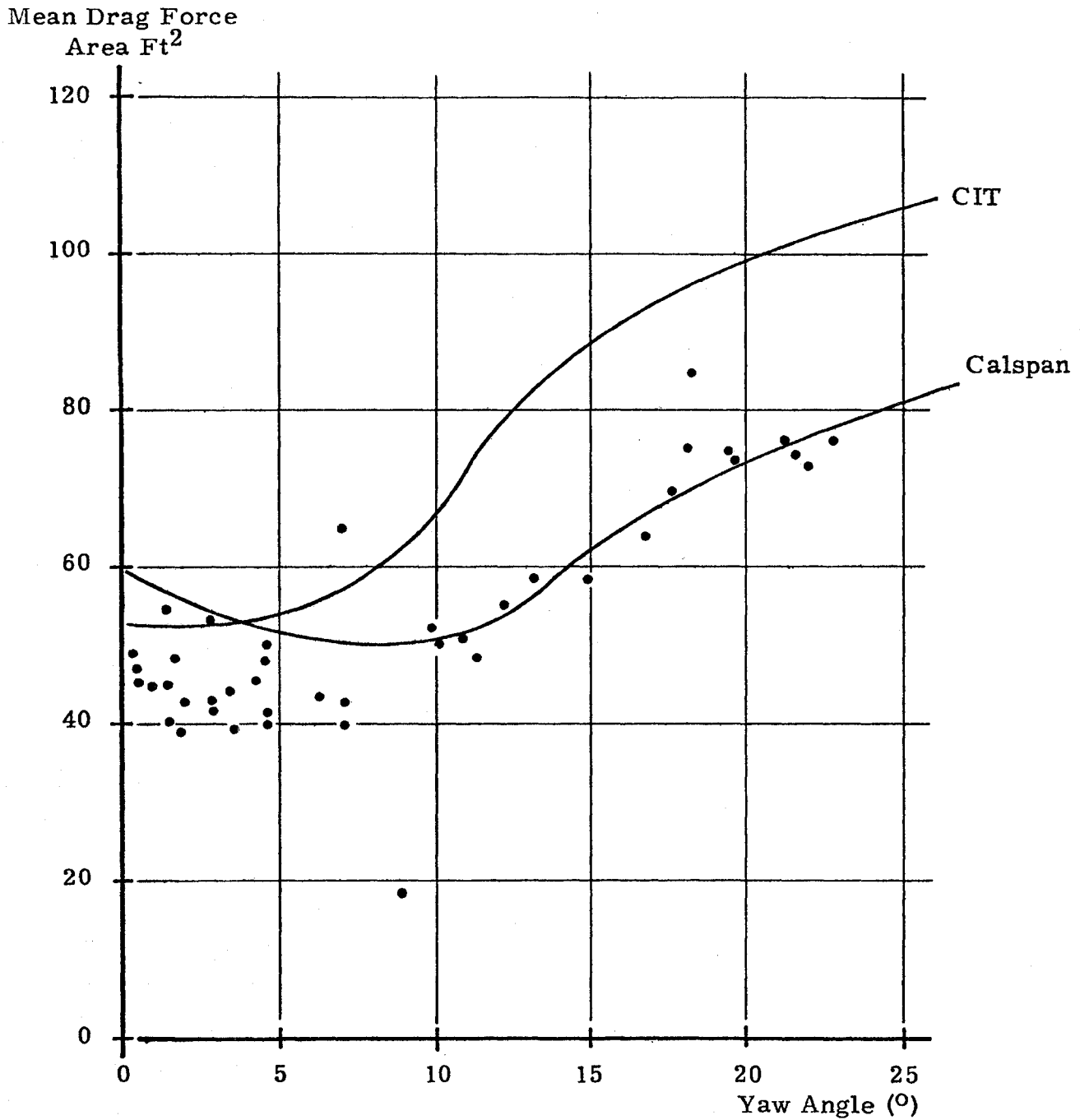


Figure 2. Mean Drag Force Area Versus Wind Angle for Configuration I.

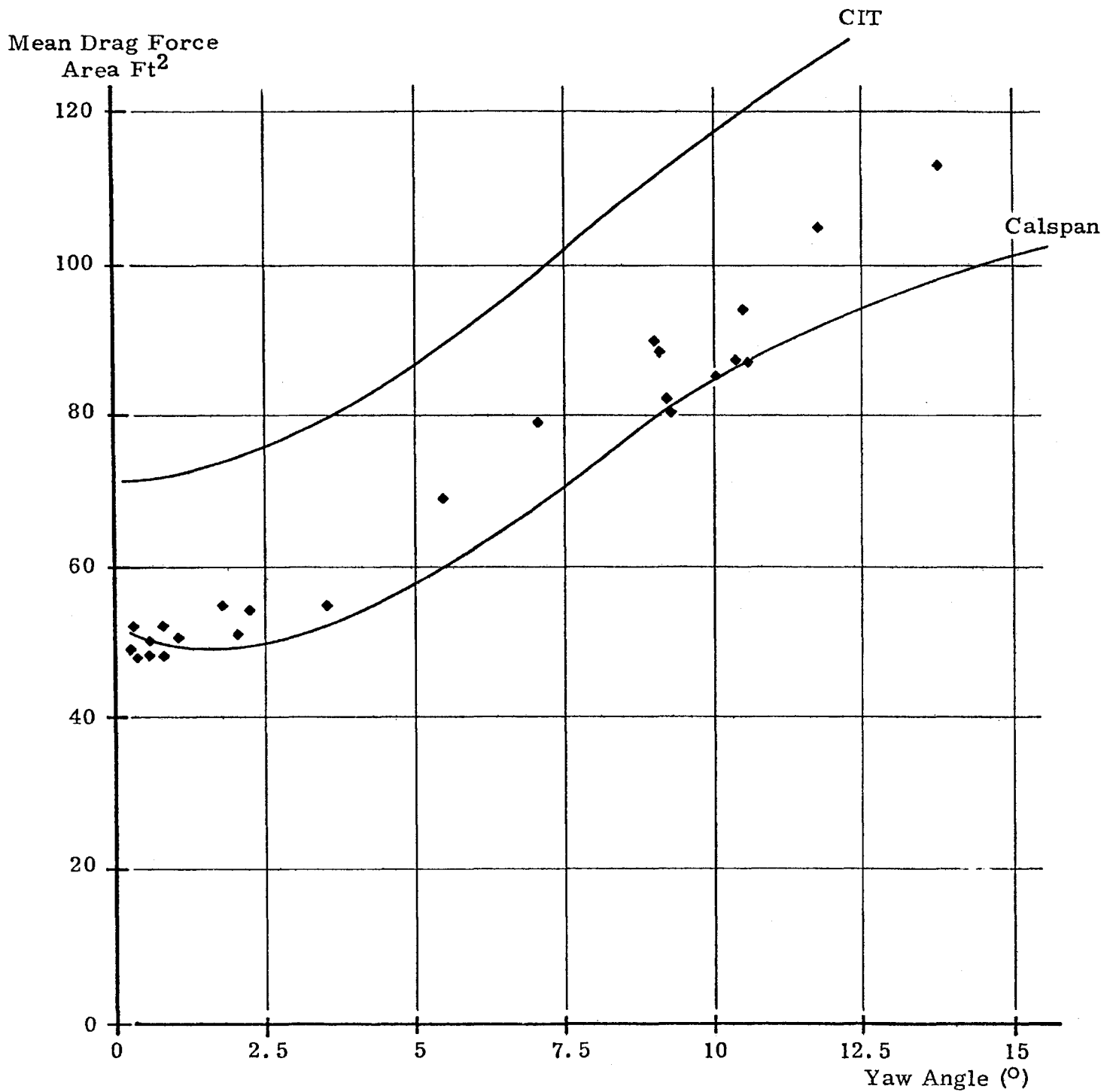


Figure 3. Mean Drag Force Area Versus Wind Angle for Configuration II.

APPENDIX A-6
AERO/TOFC-II EQUIPMENT LIST

AERO/TOFC-II EQUIPMENT LIST

<u>Equipment</u>	<u>Manufacturer</u>
Locomotive DOT 001	General Electric
Buffer Car and Test Car	Pullman Standard
Trailers	Trailmobile
Transit	Brunson
Precision Levels	Brunson
Strain Indicator	Vishay
Oscillograph	Bell & Howell 5-134 with CEC 7-316 Galvanometers
Signal Conditioners	Bell & Howell 1-115

TABLE I
IDENTIFICATION OF THE LOAD CELLS

Location	Manufacturer	Capacity	Type	Serial Number	Trailer
Forward Lateral	BLH	5K	U3G1	32993 32899	B A
Forward Longitudinal	BLH	5K	U3G1	33002 32881	B A
Forward Vertical	Interface	10K	1210-AF	3959 4014	B A
Aft Lateral	BLH	5K	U3G1	29851A 36312	B A
Aft Vertical Right Side	Interface	25K	1220-11	6487 6486	B A
Aft Vertical Left Side	Interface	25K	1220-11	6485 6488	B A

APPENDIX B
TEST EVENTS REPORT

Prepared by

TRANSPORTATION TEST CENTER
PUEBLO, COLORADO

TABLE OF CONTENTS

APPENDIX	TITLE
B-1	Calibration Procedure for Instrumented Couplers
B-2	AERO/TOFC (Series II) Weather Station Calibration Procedures
B-3	AERO/TOFC (Series II) Weather Station Logs
B-4	AERO/TOFC (Series II) Test Logs

APPENDIX B-1
CALIBRATION PROCEDURE FOR
INSTRUMENTED COUPLERS

NOVEMBER, 1977

PREPARED BY: TTC INSTRUMENTATION GROUP

B.1.0 PURPOSE

B.1.1 GENERAL

The TTC Instrumentation Group has built three instrumented couplers. The purpose of this document is to outline a procedure for the initial calibration and periodic checkout of these devices.

B.1.2 PROCEDURE

1. With the instrumented coupler installed on the railcar, position the end of the railcar with the coupler near an end of track bumper of the type used in the CSB or CSB yard.
2. Assemble load cell/jack/modified coupler assembly to bumper post fixture.
3. Mount yoke assembly on bumper post.
4. Move the railcar so that the modified coupler on the fixture attached to the bumper post mates and locks with the instrumented coupler.
5. Block couplers so that very little relative motion can occur.
6. Shim fixtured coupler so that it is level and aligned with the one on the railcar.
7. Chock all the wheels on the railcar so it will not roll.
8. Set up signal conditioning and recording equipment to record output from both load cells as directed in Section B.3 of this appendix.
9. Using the hydraulic jack, exercise the coupler system at least three times to near full load in both tension and compression.
10. Remove all load from the system and zero the outputs of both load cells. Record a minimum of 20 seconds each 0, positive, negative cal.
11. Record 5 data runs as follows with a calibration between each run:
 - A. While monitoring output of standard load cell, apply compressive force to the system. Hold the following forces (+10%) and record load cells outputs on log sheet: 0-100-500-1000-2000-5000 pounds.
 - B. Slowly release applied force and record final outputs.

- C. Repeat A and B, applying tensile force.
12. Perform overload system check as described in Section B.5 of this Appendix.
 13. Process the data as described in Section B.4 of this Appendix.

B.1.3 SETUP OF SIGNAL CONDITIONING AND RECORDING EQUIPMENT

1. Set analog tape system so that band edge is 2.000v.
2. Determine values of shunt cal resistors for each load cell and install on mode cards. Cal should be equal to full scale on load cell.
3. Install mode cards in signal conditioners.
4. Connect the load cells to the signal conditioners.
5. Set the excitation of the signal conditioners to 10.00 volts \pm 10 mv.
6. Balance the signal conditioners with no load applied, 0.00v \pm 10 mv.
7. Set the conditioner gains to give 1.500 volts on the galvo output when in the cal position.
8. Set the tape output of the standard load cell's conditioner to (CAL/100) volts. Connect this output to the DVM placed near the hydraulic jack. This meter provides the operator with a direct reading of the applied force in pounds.
9. Patch equipment as follows:

TO FROM	TAPE CHANNEL	BRUSH CHANNEL	X-Y RECORDER
Std. L.C.	1	2	X
Coup. L.C.	2	3	Y
Tape Repo	1	4	
Tape Repo	2	5	
IRIG B	14		
Slow Code		1	

B.1.4 DATA PROCESSING

The data from the coupler calibration was processed as follows:

1. Time histories in engineering units (lbs.) vs time were produced for each load cell.
2. The output of the coupler load cell in E.U. will be plotted as a function of the standard load cell in E.U. The slope and intercept was found using a least squares fit for a straight line. The standard deviation was computed for both the slope and the intercept.
3. The output of the standard load cell in E.U. was plotted vs the output of the coupler load cell in corrected millivolts (equals actual output voltage divided by the amplifier gain). The slope and intercept of this line was computed using a least squares fit. The standard deviation of both the slope and intercept was also computed.

B.1.5 OVERLOAD PROTECTION CHECKOUT

The purpose of this test is to check the operation of the overload protection system.

1. Replace the 5klb. standard load cell with a 10 klb. load cell. Install new mode card in signal conditioner and set up as described in Section B.4 .
2. Apply a tensile force of 5,000 lbs. Note output of load cell in coupler. Increase force to 7,500 lbs. Overload protection should come into play and an increase in applied force should cause no additional change in coupler output. If protection does not occur by 7,500 lbs., stop test.
3. Continue increasing applied force until 10,000 lbs. is reached to check continued operation of overload protection.
4. Repeat steps 1 through 3 using a compressive load.
5. Release the applied force, replace the 5k load cell and repeat the calibration procedure.

B.1.6 PRELIMINARY CALIBRATION VALUES FOR INSTRUMENTED COUPLERS

Tests were made on instrumented couplers numbers 10 and 15 on November 15-30, 1977 and January 6-9, 1978, to determine their operating characteristics.

Since both couplers exhibited rather large (about 300 pounds) hysteresis loops, the curves were separated into sections and a

least-squares straight line fitted to each section. The equation has the form $y = a_0 + a_1x$ where y was the output in mv, x the input in pounds, a_0 is the zero offset in mv, a_1 is the sensitivity in mv with 10v excitation, and r is a coefficient of fit for the least-squares line. The sections used were:

- A. 0 to 5000 pounds increasing tension
- B. 5000 to 0 pounds decreasing tension
- C. 0 to 5000 pounds increasing compression
- D. 5000 to 0 pounds decreasing compression

The results of this analysis are shown in Table B-1. The data used in the analysis was read from a strip chart produced at the time the test was run and is at best accurate to $\pm 2\%$ (the accuracy of the recorder). Therefore, the results will not be more accurate than 2%.

TABLE B-1
COUPLER CALIBRATION DATA

COUPLER NUMBER	SECTION	a_0	a_1	r^2	SENSITIVITY mv/v
10 (B End) Load Cell S/N 6472 Sensitivity: 4.066 $\frac{mv}{v}$	A	-.1957	.0082	.9664	4.10
	B	-.0572	.00778	.9996	3.89
	C	-0.294	.00797	.9991	3.895
	D	1.849	.00845	.9997	4.225
15 (A End) Load Cell S/N 8904 Sensitivity: 4.008 $\frac{mv}{v}$	A	-.0482	.0079	.9999	3.95
	B	2.183	.0078	.9966	3.90
	C	-1.624	.0077	.9995	3.85
	D	-.40	.00768	.9975	3.84

It is suggested that coupler data taken on AERO/TOFC (Series II) be handled as follows:

If all collected data is reduced enmass, the original load cell sensitivity may be used. This provides data accurate to approximately 5% Full Scale (250 pounds).

If more accurate values are required, the line equations for each section must be used. The loading history of the

coupler prior to and during the period of interest must be examined. To determine which equation to use, examine the loading curve to determine the direction and slope of the load vs time. The slope of the loading curve must not change direction just before and during the period; that is, if an increasing compressive load is applied, there should be no decreases in compressive load during the period of interest and the equation for Section C would then apply.

As previously stated, the source data is only accurate to $\pm 2\%$ and therefore, using the equations in the manner described will provide load values limited to $\pm 2\%$ accuracy.

Experiments performed after the calibration data was taken indicate that the hysteresis of the couplers can be decreased by heating and that applying a vertical dither to the coupler has no noticeable effect. Copies of the original X-Y plots are shown in Figures B-1(a), B-1(b) and B-2. Since heating the coupler did reduce the hysteresis, it is suspected that the grease used on the coupler caused most of the problem. A study has been undertaken to find a more suitable lubricant.

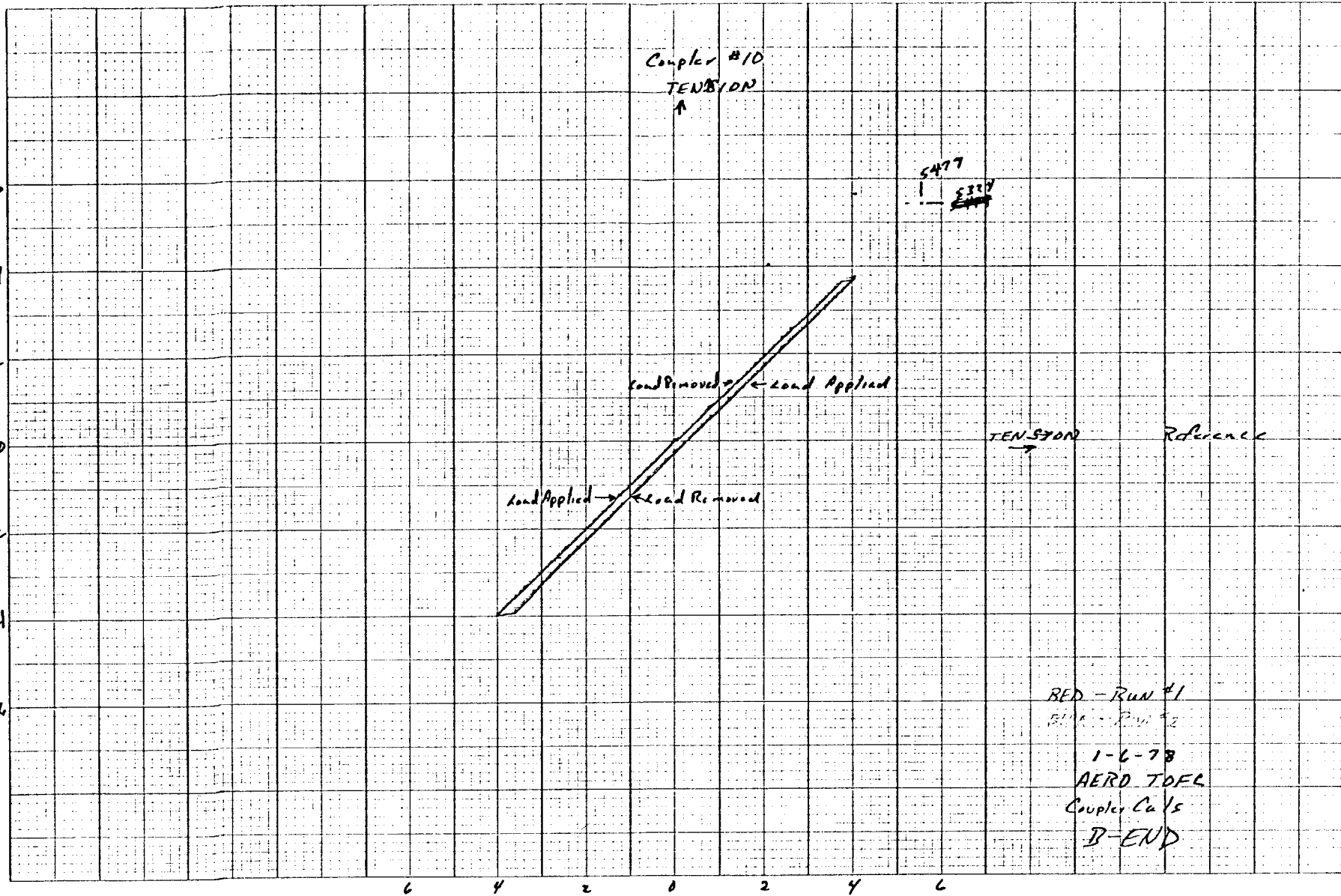


Figure B-1.1(a). B-End Coupler Calibration Data Without Dither

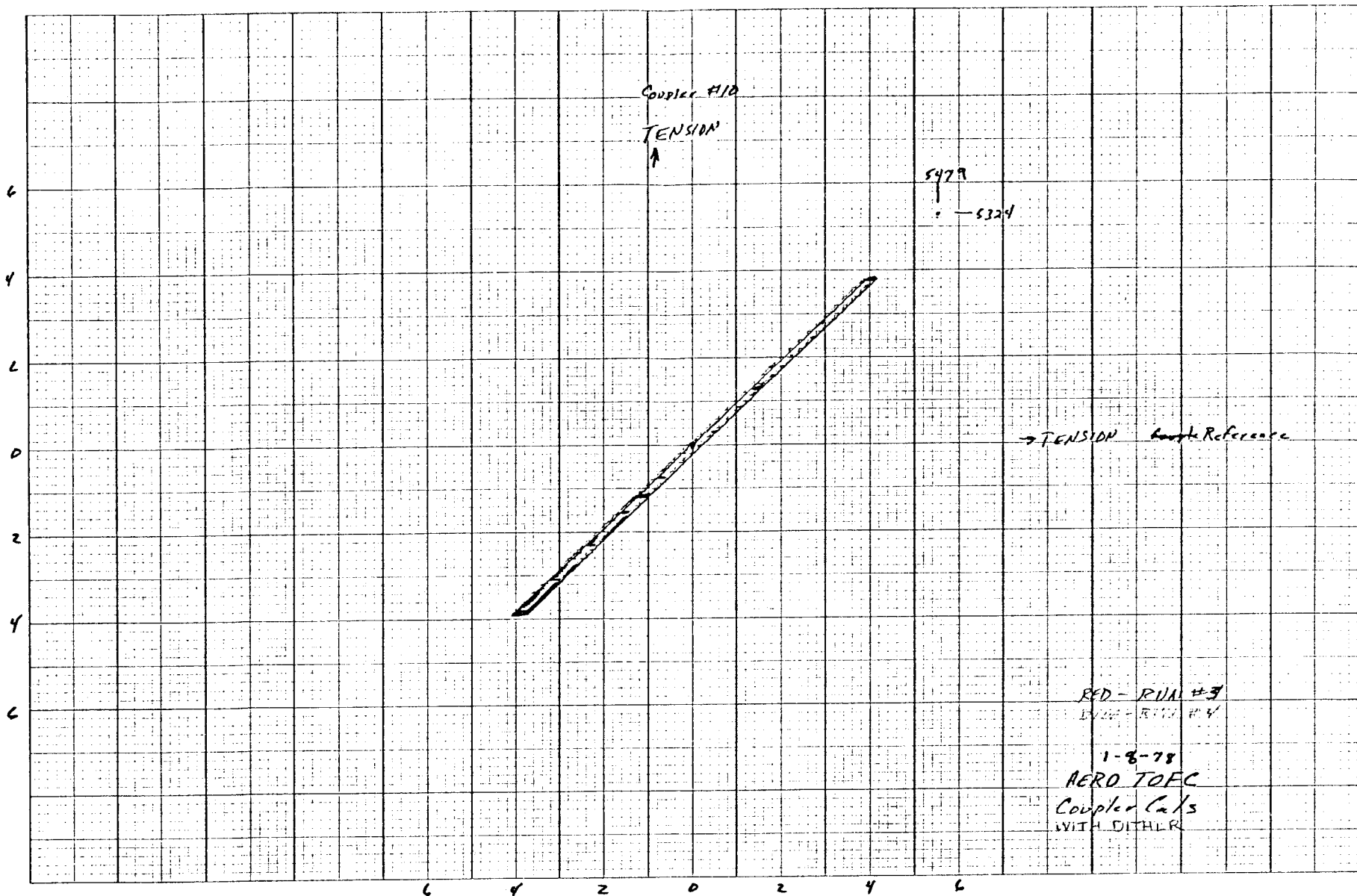


Figure B-1.1(b). B-End Coupler Calibration Data With Dither

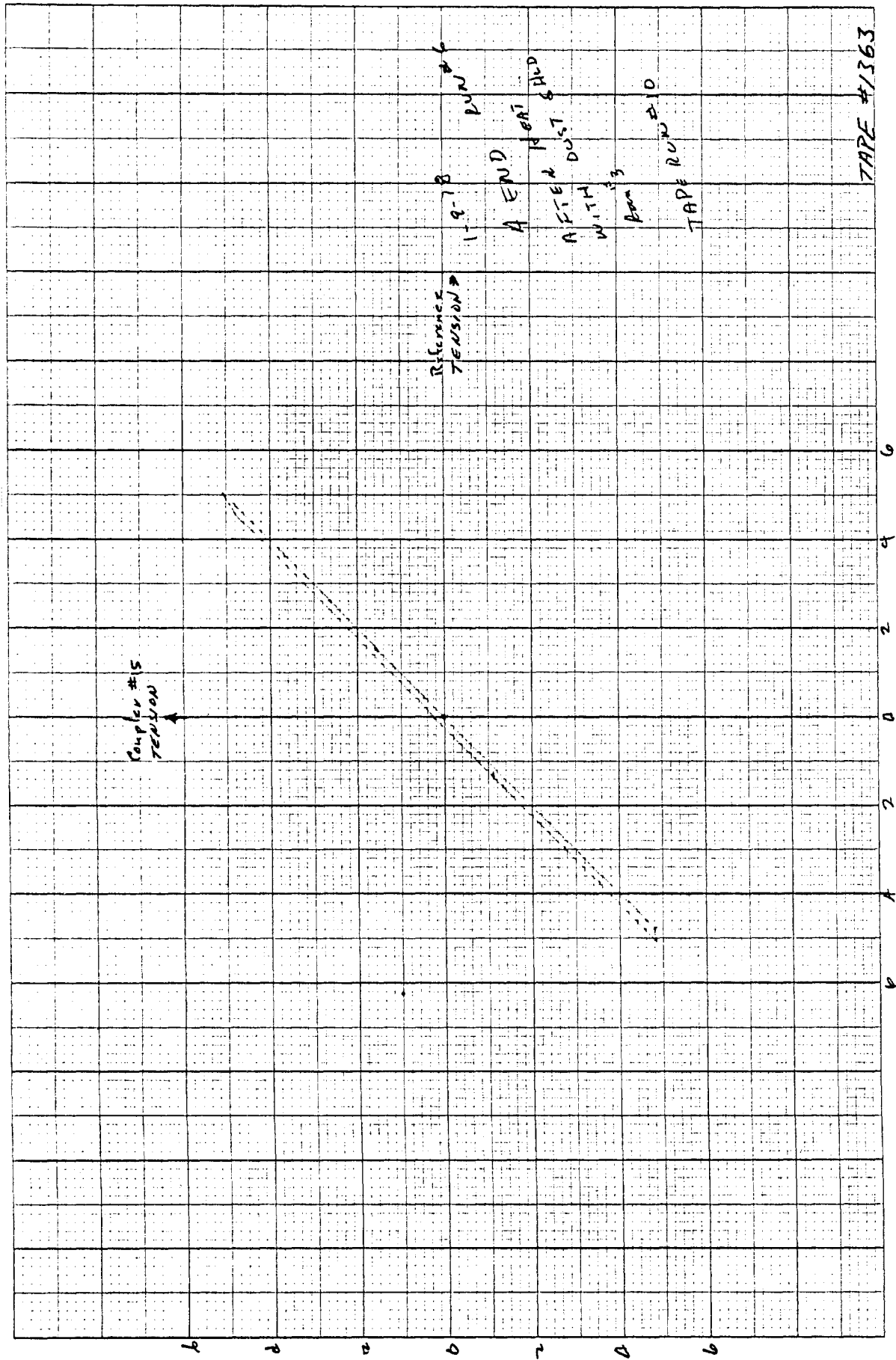


Figure B-1.2. End Coupler Calibration Data

APPENDIX B-2

TEST EVENTS REPORT

AERO/TOFC (SERIES II) WEATHER STATION CALIBRATION

DECEMBER, 1977

PREPARED BY: TECHNICAL SERVICES/INSTRUMENTATION
TRANSPORTATION TEST CENTER

B.2.0 DESCRIPTION

B.2.1 GENERAL

A weather station consisting of two Climatronics weather sensors, with their related electronics, was set up at Station 160 on the east tangent of the RTT at the Transportation Test Center. The weather recorders, a Brush 481 8-channel strip chart and a FM-FM telemetry system, were housed in an all-weather trailer which is electrically heated and air conditioned. A 10kw diesel set provided 110 volt A.C. power to the trailer. A mast attached to the trailer was used to mount one weather unit consisting of a wind speed sensor and a wind direction sensor at a height of 20 feet above the top of the rail (ATR). A tripod was positioned about 50 feet northeast of the trailer and another sensor set was mounted 8 feet ATR. Both sensor sets were aligned parallel* with the RTT and their heights were adjusted by optical surveying techniques. The alignment was considered good to $\pm 1^\circ$ and the heights to $\pm .25$ inches. A post test survey was made to confirm that these tolerances did not change during the test.

Due to drift problems associated with the FM-FM system, an overall long-term accuracy of 2% is about the best that can be expected. The direction transducer is a 540° device and the velocity transducer was set up to measure speeds of 50 mph maximum; so, the error in direction is, at best, about 11° and the error in the speed is about 1 mph. Errors of this magnitude were seen during the test.

The direction transducer was aligned so that a wind from north to south parallel with the RTT would cause a 0° or 360° reading.

*A post-test verification revealed that the actual alignments were slightly off (+ 5 degrees for the 8-foot mast and - 6 degrees for the 20-foot mast). The sign convention for the wayside wind direction is given in Figure 4-1(a).

A rotation of the sensor in the clockwise direction results in a more positive output. The direction sensor resets to 180° when it goes through 540° . The sensors were set up to output scale factors of $210.8^\circ/\text{volt}$ and $20 \text{ mph}/\text{volt}$ for the direction and speed respectively.

The two wind speeds and directions, along with Slow Code #3 giving the approximate time of day, were FM-modulated and transmitted to DOT railcar T-5 where the data was demodulated and recorded as analog inputs by the digital data system.

The weather equipment and telemetry link were calibrated every day before testing and then after each speed series (3 runs usually) during the test. Drifts of as much as 45mv were noted between calibrations. 45mv corresponds to about 9.5° and .9 mph.

The calibration procedure for the weather station is in Section B.2.2.

A strip chart was made of the wind speed and direction and time code for each test run and was annotated with the run number and speed. These strip charts were given to the Chief Test Engineer following each day's testing since the data was analyzed each night after the test.

The strip chart channels from left to right were: lower wind speed, lower wind direction, upper wind speed, upper wind direction, not used, and the time slow code. All the Brush chart gains were set at 50mv/small division at all times. Zero corresponds to 2.5 volts. The forementioned scale factors hold for this recording as well as for the T-5 analog input.

Logs indicating the time of day, wind speed, wind direction, temperature, relative humidity, and barometric pressure were kept for each test run. The wind speeds and directions are those taken from the upper sensor at the weather station. Therefore, the direction is relative to the RTT with the forementioned convention.

The barometric pressure was measured locally by an absolute barometer. The temperature and relative humidity values were those measured by equipment in the Office of Central Control (OCC) and were radioed to the weather station operator after each test run. These logs appear in Section B.3.

B.2.2 CALIBRATION PROCEDURE CLIMATRONICS WEATHER STATION AND TELEMETRY SYSTEM

B.2.2.1 Setup

Remove the orange wire coming from the weather transducer to terminal strip lug 4 on the back of the signal conditioner/recorder. Attach an oscillator producing a 433 Hz square wave with a signal amplitude of from 1 volt to 10 volts peak to lug 4 on the terminal strip. Note: The rest of the wires to the transducer must remain connected. Open the front of the recorder. There are three toggle switches in the lower right hand corner of the circuit board. The first two of these switches viewed from left to right are the calibrate speed and calibrate direction switches. Each of these switches have three positions. The up position is the operate position. The center position is the zero position. And the bottom position is the cal position. The third switch controls the range full scale of the wind speed. In the up position, full scale equals 50 mph. In the down position, full scale equals 100 mph.

The voltage outputs of the wind speed and direction electronics are voltage divided by a factor of two to give 2.5 volts maximum output for each parameter. This is done so that the input to the VCOs in the telemetry system do not become saturated. These voltage-divided outputs are displayed on a Brush 481 chart recorder for monitoring in real time. When calibrating a 1% or better volt meter should be used to monitor the signal at the VCO input.

B.2.2.2 Performing Calibration

Since the receiving half of the system is mounted on the DOT test car, calibration requires two people: one on the ground and one on the test car. Both persons must be radio equipped in order to facilitate the calibration. Note: To avoid the problem of the radio talking into the telemetry equipment, a remote outside antenna should be used in both locations.

PROCEDURE:

1. With the volt meter monitoring the wind speed input to the VCO, place both calibrate switches to the center or zero position. The voltage should be zero volts. The chart recorder and Brush chart recorder should read zero volts. The person on the test car should verify that the demodulator output reads zero volts. The zero adjustment of that demodulator output reads zero volts. The zero adjustment of that demodulator channel should be adjusted if it does not.
2. Repeat step 1 for the wind direction.
3. Make sure that oscillator output is set to 344 Hz. Place the wind speed cal switch in the bottom position.
4. Observe the wind speed output. It should be 1.25 volts. The reading on the chart recorder should be 25 mph. Adjust the output adjustment on the demodulator until its output also reads 1.25 volts.
5. Observe the wind direction output. It should read 1.62 volts. The direction output on the chart recorder should read 350 degrees. Adjust the output adjustment on the demodulator until its output reads 1.62 volts.
6. Place the wind speed cal switch in the middle position and place the direction switch in the bottom position. The direction output should read 1.66 volts. The direction as shown on the chart recorder should read 360 degrees. The demodulator output should also be 1.66 volts.
7. Place both cal switches in the up or operate position. The system is now operational. Disconnect pulse generator and reconnect orange wire.
8. Observe the approximate wind direction and confirm that the system is working properly. Check with T-car personnel that data is being received.

NOTE:

Since the wind sensor is a tachometer type device producing some undocumented number of pulses per revolution, a sensor calibration would be difficult to perform without a wind tunnel or some way of measuring the actual wind speed.

APPENDIX B-3

AERO/TOFC (Series II)

WEATHER STATION LOGS

TTC WEATHER STATION LOG

Station 160

LOCATION RFT EAST TANGENT

DATE 12/2/77

ENG/TECH G. GOSWAMI

TIME HR/MIN	WIND SPEED MPH	WIND DIRECTION DEGREES	TEMPERATURE °F	HUMIDITY %	PRESSURE INCHES Hg
10:40 am	30	W	58°	33%	24.5 in
10:55 am	20-40	250° relative	56°	30%	24.5 in
11:16	10	290° "	56°	30%	24.5 in
11:29	10-13-15	290 "	56°	30%	
11:41	12	250 "	56	28%	24.72
11:51	8	240	56	28%	24.72
12:50	2	260	58	28%	24.72
12:55	2	300	58.5	27%	24.72
13:08	2	200 300	59	27%	
13:34	4	280	59	27%	24.7
13:50	15	260	59	26%	
14:23	17	250	59	27%	24.7
14:29	15	250			

B-17

Run 15

Run 21

TTC WEATHER STATION LOG

LOCATION EAST PIT STATION 160 DATE 12/5/77 ENG/TECH GOOSMAN

TIME HR/MIN	WIND SPEED MPH	WIND DIRECTION DEGREES	TEMPERATURE °F/°C	HUMIDITY %	PRESSURE INCHES Hg
10/43	10 mph	050°	25/-4 ^{3.88}	80	25.05
12/20	10 mph	070°	26/-3.33	80	25.02
12/13	8 mph	070°	26/-3.33	80	25.02
12/45	9 mph	070	26/-3.33	80	25.02
13/11	11 mph	070	26/-3.33	79	25.02
13/30	11 mph	080	27/-2.77	76	25.00
13/56	9 mph	080	27/-2.77	74	25.00
14/16	10 mph	090	27/-2.77	75	25.02
14/21	10	080	27/-2.77	76	25.00
14/32	10	080	26/-3.33	78	25.06
14/45	13	090	26/-3.33	57	25.06

p.0684
p.0682
p.0682
p.0682
.0682
.0681
.0681
.0681
.0682
.0682

B-18

TTC WEATHER STATION LOG

LOCATION Station 160 EAST RTT

DATE 12/06/77

ENG/TECH Grossman

TIME HR/MIN	WIND SPEED MPH	WIND DIRECTION DEGREES	TEMPERATURE °F	HUMIDITY %	PRESSURE INCHES Hg
9:40	3 mph	90° relative	20° F / 6.66	79%	25.02 p = .0691
10:20	3 mph	90° to	19° F - 7.22	81%	25.02 p = .0692
10:35	2	170° RTT	19° F - 7.22	81%	25.02 p = .0692
10:45	2	200°	19° F - 7.22	80%	25.02 p = .0692
11:01	4	140°	22° F - 5.55	73%	25.12 p = .0690
11:13	calm	180°	20° F - 6.66	76%	25.12 p = .06925
11:25	2	160°	21° F - 6.11	76%	25.1 p = .0691
11:37	3	70°	21° F - 6.11	75%	25.1 p = .0691
12:32	3	30°	25° F - 3.88	66%	25.02 p = .0682
12:52	1	90°	26° F - 3.33	64%	25.02 p = .0683
13:05	0	180°	26° F - 3.33	63%	25.00 p = .0681
13:14	2	60°	26° F - 3.33	66%	25.00 p = .0681

B-19

TTC WEATHER STATION LOG

Reproduced from
best available copy.

LOCATION Station 160 E2 + ATT

DATE 12/8/77

ENG/TECH CRONSON

TIME HR/MIN	WIND SPEED MPH	WIND DIRECTION DEGREES	TEMPERATURE °F	HUMIDITY %	PRESSURE INCHES Hg
09:44	4	NE	26°F	85%	24.85 abs
10:33	13	060	25°F/-35	86%	25.000
11:25	10	040	24°F/-44	81%	24.85
12:15					
12:24	10	0°	23°F/-50	81%	24.90
12:42	10	040	22°F/-55	78%	24.95
13:10	15	045	22°F/-55	73%	24.90
13:42	10	010	21°F/-6.1	70%	24.95
13:55	7	010	20°F/-6.6	69%	24.95
14:08	8	010	20°F/-6.6	68%	24.95
14:19	9	010	20°F/-6.6	66%	25.00
14:33	10	0°	20°F/-6.6	66%	25.00
14:43	7	30°	20°F/-6.6	65%	25.00
14:57	7	10°	21°F/-6.1	62%	25.00

B-20

45/70

46/70

47/90

48/90

49/70

50/90

B
col

-0.001	-0.003	-0.002	1.001	-0.008	4.006	.007	.006	PAGE 10
1.25	1.66	1.25	1.66	1.25	1.25	1.25	1.25	

TTC WEATHER STATION LOG

LOCATION RTT EAST

DATE 12/9/77

ENG/TECH COOSMICH

TIME HR/MIN	WIND SPEED MPH	WIND DIRECTION DEGREES	TEMPERATURE °F	HUMIDITY %	PRESSURE INCHES Hg	
11/14	5 mph	SE	6	77	25.2	
51/50	13/11	5 mph	090 rel RTT	8	77	25.3
52/50	13/24	5 mph	100 rel	8	77	25.3 p = .07
53/50	13/35	5 mph	70 rel	8	77	25.3 p = .0710
54/70	13/45	5 mph	100 rel	10	76	25.28 p = .0712
55/70	13/51	5 mph	20° rel	10	75	25.28 p = .0712
56/70	14/08	2 mph	20° rel	11	76	25.28 p = .0711
7/90	14/19	3 mph	80° rel	13	75	25.28 p = .0707
8/90	15/41 - 14/41	2 mph	50° rel.	13	74	25.25 p = .0707
9/90	15/53 - 14/53	2 mph	30° rel.	14	72	25.25 p = .0706
0/30	15/10	calm	10° rel	16	70	25.25 p = .0702
1/20	15/25	1-4	30-100°	15	71	25.10 p = .0704
	15/41	2-3	90°	14	74	25.10 p = .0705

B-21

0 - .006 .000 -.003 -.002 .011 -.003 .007 .004 PAGE 1 OF 1
 1.00 1.15 1.25 1.66 1.650 1.665

TTC WEATHER STATION LOG

Station 160
 LOCATION East DTT Tangent DATE 12/12/77 ENG/TECH Grossman

TIME HR/MIN	WIND SPEED MPH	WIND DIRECTION DEGREES	TEMPERATURE °F	HUMIDITY %	PRESSURE INCHES Hg
10:40	12	42 N.W.	52/11	21%	24.7 p = .06
12:00	5	270° col to DTT	58/14.4	23%	24.75 p = .06
12:20	5	210°	59/15	23%	24.75 p = .06
12:33	15	270°	58/14.4	23%	24.75 p = .06
12:52	14	260°	57/13.8	25%	24.80 p = .06
13:15	13	260°	56/13.3	30%	24.80 p = .06
13:29	11	260°	55/12.7	31%	24.80 p = .06
13:46	10	250°	53/11.7	31%	24.85 p = .06
13:57	6	100°	53/11.7	33%	24.85 p = .06
14:10	5	90°	53/11.7	34%	24.85 p = .064
14:22	6	70°	52/11.1	34%	24.85 p = .064
14:42	7	40°	52/11.1	34%	24.85 p = .064
14:53	7	50°	52/11.1	34%	24.85 p = .064
15:04	10	50°	51/10.5	35%	24.85 p = .064

62/50
 65/50
 B-22
 66/70
 67/70
 68/90
 69/90
 70/90
 71/50
 72/50
 73/50

.000 .001 -.003 .002
 1.235 1.663 1.236 1.660

TTC WEATHER STATION LOG

Reproduced from
best available copy.

LOCATION East TTC Station 160

DATE 12/14/77

ENG/TECH CRASMAN

TIME HR/MIN	WIND SPEED MPH	WIND DIRECTION DEGREES	TEMPERATURE °F	HUMIDITY %	PRESSURE INCHES Hg
10:20			54	37	24.92
12:17	2 MPH	(270°) 90°	63°	29%	24.9
12:28	1 MPH	220°	62	28.5	24.9
12:42	2 MPH	360°	60/116	31	24.9 .0670 1.0591
12:50	4 MPH	400°	61/116	30	24.9 } = .06
13:27	3 MPH	380°	61°	31	24.9 } (=0.01
13:33	5 MPH	370°	62	31	24.9
13:44	7 MPH	300°	62	30	24.9
13:54	10 MPH	250°	62	30	25.00
13:16	5 MPH	280°	61	32	24.80
14:24	5 MPH	210°	61	32	24.80
14:35	5 MPH	210°	61	32	24.80
14:45	9 MPH	220°	61	32	24.80

B-23

MPH RW

70/78

70/79

90/80

90/81

90/82

001 +.000 003 -.002

TTC WEATHER STATION LOG

LOCATION East tangent RTT DATE 12/15/77 ENG/TECH Goodman

TIME HR/MIN	WIND SPEED MPH	WIND DIRECTION DEGREES	TEMPERATURE °F	HUMIDITY %	PRESSURE INCHES Hg	
12:21	7 mph	220°	58°F	33%	24.65	P.061
12:44	6	180°	59	33	24.6	P.062
12:48	5	180°	59	32.5	24.65	P.062
12:56	10	160°	59	32.5	24.70	P.062
13:32	3	160°	59	32	24.55	P.062
13:33	4	190°	62	31	24.60	P.0619
13:45	1	160	61	30	24.60	P.062
13:56	0	*	62	29.5	24.5	P.061
14:19	1	175°	62	28	24.5	P.061
14:28	1	175° 170°	62	28	24.6	P.0619
14:39	0	*	65	27	24.6	P.0618
14:51	3	200°	64	37	24.6	P.061
15:05	1 MPH	130°	63°F	26%	24.5 in Hg	
15:23	1 MPH	460	63	26	24.5	
	7	130°	63	26		

B-24

TTC WEATHER STATION LOG

Station 160

LOCATION EAST RTY Tangent

DATE 12/16/77

ENG/TECH Goosman

TIME HR/MIN	WIND SPEED MPH	WIND DIRECTION DEGREES	TEMPERATURE °F	HUMIDITY %	PRESSURE INCHES Hg
10:40			42°F	42%	24.5
11:34	27-30				
12:33	21	270	41°F	20%	24.6
12:55	10-18	210°	41°	18%	24.55
13:12	5-15 ²⁰	210°	42°F	17%	24.6
13:23	20	230°	42°	17%	24.6
13:55	15	230°	42	17%	24.6
14:03	18	270°	42	17%	24.6
14:16	15	250°	41	16%	24.6
14:27	20	270°	42	16%	24.6
14:50	15	240°	40	17%	24.6
14:59	15	230°	40	19%	24.6
15:08	12	220°	40	18%	24.6
17:15	6	250°	32	26%	24.6
18:12	6	250°	32	26%	24.6
18:23	7	260	32	26%	24.6

B-25

40 shift
40 shift
10-20

.06
.06
.06
.06
.06
.06
.06
.06
.06

TTC WEATHER STATION LOG

LOCATION _____

DATE 16TH Dec 77

ENG/TECH _____

TIME HR/MIN	WIND SPEED MPH	WIND DIRECTION DEGREES	TEMPERATURE °F	HUMIDITY %	PRESSURE INCHES Hg
18:33	6	260	30	26	24.7
18:43	7	260	30	27	24.7
18:55-	8	240	26	28	24.7
19:01	7	250	27	29	24.7
19:09	9	250	27	30	24.7

B-26

APPENDIX B-4

AERO/TOFC (SERIES II) TEST LOGS

TEST LOG

PROGRAM Aerotofc

DATE 11/22/77

PRE-TEST MEETING ATTENDEES:

<u>SIGNATURE</u>	<u>ORGANIZATION</u>	<u>DUTY</u>
<u>Jay Amey</u>	<u>Enr</u>	<u>TEST CONTROLLER</u>
<u>Tom Jones</u>	<u>ENSCO</u>	<u>TEST DIRECTOR</u>
<u>Peck</u>	<u>Dyn</u>	<u>CHIEF TEST ENGINEER</u>
<u>Derman</u>	<u>✓</u>	<u>TEST SUPPORT ENGINEER</u>
<u>R.L. Maxwell</u>	<u>ENSCO</u>	<u>VEHICLE OPERATOR</u>
		<u>VEHICLE OPERATOR</u>
		<u>TRACK SECURITY OFFICE</u>
		<u>Asst. Test Contol.</u>

PASSENGER LIST: 10-2

<u>J. Gorman</u>	<u>ENSCO TTC</u>
<u>Andy Hamitt</u>	<u>ART Ass</u>
<u>H. Owens</u>	<u>ENSCO, TTC</u>
<u>John S. Hight</u>	<u>Enesco</u>
<u>Byron Howard</u>	
<u>LOW BERGLUND</u>	<u>ENSCO</u>
<u>Don Choffel</u>	<u>ENSCO</u>

TEST CONDITIONS:

WEATHER: 60°F, Windy (gusts to 45 mph,)

TRACK: RTT Lower Sta T14 - T18

Checkout runs

6-28

TEST CONTROLLER R.L. Maxwell

TEST SUPPORT ENGINEER

TIME	EVENT	REMARKS
1000	Consist Formed	Ready for Briefing
1115	Discovered Damaged ALD sensor. Replaced it	
1215	Adjusted height of new ALD to clear Sta 5 crossing.	ALD's in test zone will have to be raised to get them closer to the sensor now that it has been raised. Will use 2x4's under them.
1445	First Data run through test zone complete. We had a false ALD blip near the weather sta.	ALD Blip turned out to be weather Sta Telemetry Xmtr. Will use a lower power system.
1552	Completed three good 70 mph runs through the test zone	

Reproduced from
best available copy.



B-29

TEST LOG

PROGRAM AERO/TOFC checkout

DATE 1 Dec 77

PRE-TEST MEETING ATTENDEES:

<u>SIGNATURE</u>	<u>ORGANIZATION</u>	<u>DUTY</u>
<u>R. Maxwell</u>	_____	<u>TEST CONTROLLER</u>
<u>[Signature]</u>	_____	<u>TEST DIRECTOR</u>
_____	_____	<u>CHIEF TEST ENGINEER</u>
<u>[Signature]</u>	<u>Brewer</u>	<u>TEST SUPPORT ENGINEER</u>
<u>Peeli</u>	_____	<u>VEHICLE OPERATOR</u>
<u>Pennman</u>	_____	<u>VEHICLE OPERATOR</u>
_____	_____	<u>TRACK SECURITY OFFICER</u>
_____	_____	_____

PASSENGER LIST:

<u>Hemant S. Limaye</u>	<u>Brewer Eng. Labs.</u>
<u>J. E. [Signature]</u>	<u>TTC. O&M</u>
<u>[Signature]</u>	<u>ENSCC</u>
<u>Palmer J. Walling</u>	<u>BREWER ENG. LABS.</u>
<u>[Signature]</u>	<u>[Signature]</u>
_____	_____
_____	_____

TEST CONDITIONS:

WEATHER: 35°F, calm

TRACK: RTT

OTHER:

PROGRAM AERO/TCFC II cont.

Date 1 Dec 77

EST CONTROLLER R.F. Maxwell

TEST SUPPORT ENGINEER D. Amaya

TIME	EVENT	REMARKS
0900	Delay	Instrumentation had to connect wires left off by FAST Data Van Yesterday L. Station required Deviation to OTP allowing B. Stewart and T Jones to be Test Directors Also had to resolve schedule interface with NOVATEK
1015	Pretest Briefing	
1030	Ready to move to RTE	
1120	Surveillance/Cond Run compl.	
1152	Completed weather Sta Cals.	
1157	Stopped N of Sta 7	Lunch, and to allow DOT 018 to cross test zone
1247	Ready for 70 mph run #5	
1305	Ready for 70 mph run #6	
1320	Ready for 70 mph run #7	#7 did not go on tape, lost a word in the program
1331	Checking & reducing data	
1345	Ready for 70 mph run #7 (repeat)	good
1356	Cal at weather Sta	
1403	Ready for #8 - 70 mph.	
1416	Ready for #9 - 90 mph	Actual 84 mph
1429	Ready for #10 - 90 mph	Actual 87 mph
1444	Ready for #11 - 90 mph	Actual 87 mph
1457	Ready for #12 - 90 mph	Actual 90 mph
1507	Reducing Data	
1516	Ready for #13 - 50 mph	Actual 60 mph
1531	Ready for #14 - 60 mph (same speed as #13)	
1545	Completed testing & exited RTT	Excellent Day! B-21

TEST LOG

PROGRAM AERO/TOFC II ct

DATE 2 Dec 77

PRE-TEST MEETING ATTENDEES:

<u>SIGNATURE</u>	<u>ORGANIZATION</u>	<u>DUTY</u>
<u>Rob Maxwell</u>	<u>ENSCO</u>	<u>TEST CONTROLLER</u>
<u>[Signature]</u>	<u>Enscoc</u>	<u>TEST DIRECTOR</u>
<u>[Signature]</u>	<u>BEL</u>	<u>CHIEF TEST ENGINEER</u>
<u>[Signature]</u>	<u>Enscoc</u>	<u>TEST SUPPORT ENGINEER</u>
<u>[Signature]</u>	<u>_____</u>	<u>VEHICLE OPERATOR</u>
<u>[Signature]</u>	<u>_____</u>	<u>VEHICLE OPERATOR</u>
<u>_____</u>	<u>_____</u>	<u>TRACK SECURITY OFFICE</u>
<u>_____</u>	<u>_____</u>	<u>_____</u>

PASSENGER LIST:

<u>[Signature]</u>	<u>TTC - Int</u>
<u>[Signature]</u>	<u>ENSCO INC.</u>
<u>[Signature]</u>	<u>Enscoc</u>
<u>[Signature]</u>	<u>BEL</u>
<u>_____</u>	<u>_____</u>

TEST CONDITIONS:

WEATHER: 53° F 30 mph wind W

TRACK: RTT Lowet

OTHER:

TEST CONTROLLER R.L. Maxwell

TEST SUPPORT ENGINEER _____

TIME	EVENT	REMARKS
0900	Pretest - Delay for log moves	TSO ..Informs that due to log moves, switches must be reverified.
1000	Moving on to RTT	
1034	Surv. / Cond. Run Complete	
1042	Stopped @ Weather Sta	Zero Cals & Adjust ALD Sensor
1105	Ready for run #15 65 mph	Lost part of the data
1120	Ready for run #16	
1137	Ready for run #17	
1148	" " " #18	
1205	Break for lunch	
1250	Ready for run #19 78 mph	
1305	" " " 20	Too many ALD marks - Adjusted Sensor
1337	" " " 21	
1357	Readjusted ALD sensor	
1425	Run #22	
1430	More ALD problems	Decision to go back to CSB to rework ALD

TEST LOG

PROGRAM AERO / TOFC II

DATE 5 Dec 77

PRE-TEST MEETING ATTENDEES:

<u>SIGNATURE</u>	<u>ORGANIZATION</u>	<u>DUTY</u>
<u>R. L. Maxwell</u>	<u></u>	<u>TEST CONTROLLER</u>
<u>C. T. Jones</u>	<u></u>	<u>TEST DIRECTOR</u>
<u></u>	<u></u>	<u>CHIEF TEST ENGINEER</u>
<u>John H. [unclear]</u>	<u>Enscow</u>	<u>TEST SUPPORT ENGINEER</u>
<u>[unclear]</u>	<u></u>	<u>VEHICLE OPERATOR</u>
<u>[unclear]</u>	<u></u>	<u>VEHICLE OPERATOR</u>
<u></u>	<u></u>	<u>TRACK SECURITY OFFICER</u>
<u></u>	<u></u>	<u></u>

PASSENGER LIST:

<u>Con Chappel</u>	<u>ENSCO INC -</u>
<u>Hemant M. Limaye</u>	<u>Brewer Eng. Labs.</u>
<u>A. B. Hamilton</u>	<u>AGH AOS.</u>
<u>[unclear]</u>	<u></u>
<u>John S. Hight</u>	<u>Enscow</u>
<u>J. E. [unclear]</u>	<u>TTC. Trust</u>
<u></u>	<u></u>
<u></u>	<u></u>

TEST CONDITIONS:

WEATHER: 25°F cloudy, calm

OTHER:

TRACK: RTT
(Abbreviated test zone per Deviation 5 Dec.)

AERO/TOFC II

Date 5 Dec 77

EST CONTRACTOR R.L. Maxwell

TEST SUPPORT ENGINEER

1st Day of actual Testing

TIME	EVENT	REMARKS
0900	Delay	Could not make log moves due to blue flag. Removed
0930	Pretest	
1025	Begin Surveillance Run	
1051	Surveillance Run complete	Back to weather Sta for Cals
1140	Still at weather Sta. Breaking for lunch.	
1230	Ready for Run #23	Good
1245	Run #24	50 mph
1315	Run #25	50 mph
1330	Run #26	70 mph
1345	Run #27	70 mph
1405	Run #28	90 mph
1420	Run #29	90 mph
1430	Run #30	50 mph
1445	Run #31	70 mph
1450	Conclude Testing	90 mph
1501	Escorted to OCC	

string pot lost on N side (troublehead) replaced.

String pots lost on N side, Jones decided not to replace.

TEST LOG

PROGRAM _____

DATE 12/6/77

PRE-TEST MEETING ATTENDEES:

<u>SIGNATURE</u>	<u>ORGANIZATION</u>	<u>DUTY</u>
<i>[Signature]</i>	<i>Enaco</i>	<u>TEST CONTROLLER</u>
<i>[Signature]</i>	<i>Enaco</i>	<u>TEST DIRECTOR</u>
_____	_____	<u>CHIEF TEST ENGINEER</u>
_____	_____	<u>TEST SUPPORT ENGINEER</u>
<i>Dezman</i>	<i>Pgn</i>	<u>VEHICLE OPERATOR</u>
<i>Picke</i>	<i>Dyn</i>	<u>VEHICLE OPERATOR</u>
<i>Sullivan</i>	<i>✓</i>	<u>TRACK SECURITY OFFICE</u>
<i>[Signature]</i>	<i>PRA</i>	_____

PASSENGER LIST:

8-2

<i>A. G. Hammett</i>	<i>AGH Ops</i>
<i>Don Choffel</i>	<i>ENSCO INC</i>
<i>[Signature]</i>	<i>TTC-Inst</i>
<i>[Signature]</i>	<i>Ensed</i>
<i>[Signature]</i>	<i>Power Labs.</i>
_____	_____
_____	_____

TEST CONDITIONS:

WEATHER:

TRACK:

OTHER:

6:30 AM

Aero

Date

12/6/77

1st CONTROLLER

OFF

TEST SUPPORT ENGINEER

TIME	EVENT	REMARKS
951	Custody from OCC	
1035	Run #32	50 mph Wind 2-3 mph steady @ 90°
1045	#33	70
1100	#34	90
1110	35	90
1125	36	70
1135	37	50
1145	Break for lunch	
1235	38	50
1300	39	70
1315	40	90
1400	Custody to OCC	

B-37

TEST LOG

PROGRAM _____

DATE 12/8

PRE-TEST MEETING ATTENDEES:

<u>SIGNATURE</u>	<u>ORGANIZATION</u>	<u>DUTY</u>
<u>[Signature]</u>	<u>Enso</u>	<u>TEST CONTROLLER</u>
<u>[Signature]</u>	<u>Enso</u>	<u>TEST DIRECTOR</u>
<u>[Signature]</u>	<u>Enso</u>	<u>CHIEF TEST ENGINEER</u>
<u>[Signature]</u>	<u>Enso</u>	<u>TEST SUPPORT ENGINEER</u>
<u>[Signature]</u>	<u>Enso</u>	<u>VEHICLE OPERATOR</u>
<u>[Signature]</u>	<u>Enso</u>	<u>VEHICLE OPERATOR</u>
<u>[Signature]</u>	<u>FRA</u>	<u>TRACK SECURITY OFFICER</u>
<u>[Signature]</u>	<u>FRA</u>	<u>TEST CONTROL</u>

PASSENGER LIST:

11-2

<u>[Signature]</u>	<u>Enso</u>
<u>[Signature]</u>	<u>TTC Inst</u>
<u>[Signature]</u>	<u>Brewer Eng. Labs.</u>
<u>[Signature]</u>	<u>Brewer Eng. Labs Inc.</u>
<u>[Signature]</u>	<u>ENSCO, INC</u>
<u>[Signature]</u>	<u>FRA/OREP</u>
<u>[Signature]</u>	<u>Ab H Co</u>

TEST CONDITIONS:

WEATHER:

TRACK:

OTHER:

TIME	EVENT	REMARKS
		T-11 gate left open by DOT 018, delay of 15 min. Switch point lock missing from 602.
1005	Custody from OCC	
1015- 1215	Calibrating wind vane on DOT 001	
1220	Run # 41	50 mph
1235	# 42	50
1250	43	70
1315	44	70
1355	45	70
1400	46	70
1415	47	90
1430	48	90
1445	49	70
1455	50	90
1514	Custody to OCC	

2-39

TEST LOG

PROGRAM _____

DATE 12/9/77

PRE-TEST MEETING ATTENDEES:

<u>SIGNATURE</u>	<u>ORGANIZATION</u>	<u>DUTY</u>
<u>J. Holt</u>	<u>FRA</u>	<u>TEST CONTROLLER</u>
<u>Bryan J. Howard</u>	<u>EnSCO</u>	<u>TEST DIRECTOR</u>
<u>Bryan J. Howard</u>		<u>CHIEF TEST ENGINEER</u>
<u>Donny Amey</u>	<u>EnSCO</u>	<u>TEST SUPPORT ENGINEER</u>
<u>D.L. Hammer</u>		<u>VEHICLE OPERATOR</u>
<u>R.F. Peelle's</u>		<u>VEHICLE OPERATOR</u>
<u>Larry L. Inaba</u>	<u>DYN.</u>	<u>TRACK SECURITY OFFICER</u>
_____	_____	_____

PASSENGER LIST:

8-2

<u>A. B. Hammit</u>	<u>AGH Ass</u>
<u>Bryan J. Howard</u>	<u>EnSCO</u>
<u>Herman S. Dimayeg</u>	<u>Brewer Eng. Labs.</u>
<u>John J. Hajek</u>	<u>EnSCO</u>
<u>Don Chaffin</u>	<u>ENSCO INC</u>
<u>J. E. Roseman</u>	<u>TTC-Inst</u>
_____	_____
_____	_____

TEST CONDITIONS:

WEATHER:

TRACK:

OTHER:

B-40

TIME	EVENT	REMARKS
9:00	~ 1 hr delay - change ALD targets + load buffer cal	
10:45	Start reassembly of circuit	
11:10	Pre Test	
11:30	Ready for surveillance surveillance run	~ 25 min delay - DTD13 move.
11:52	Custody from OCC	
12:15	Break for lunch / calibration of weather cone	
13:10	Ready to position for test	
13:20	Run # 51	50 mph
13:30	52	50
13:40	53	50
14:00	54	70
14:10	55	70
14:20	56	70
14:40	57	90
14:50	58	90
15:10	59	90
15:25	60	30
15:35	61	20
15:52	Custody to OCC	B-41

TEST LOG

PROGRAM ATUT

DATE 12/12

PRE-TEST MEETING ATTENDEES:

<u>SIGNATURE</u>	<u>ORGANIZATION</u>	<u>DUTY</u>
<u>[Signature]</u>	<u>FRA</u>	<u>TEST CONTROLLER</u>
<u>[Signature]</u>	<u>Ensec</u>	<u>TEST DIRECTOR</u>
<u>[Signature]</u>	<u>Ensec</u>	<u>CHIEF TEST ENGINEER</u>
<u>[Signature]</u>	<u>Ensec</u>	<u>TEST SUPPORT ENGINEER</u>
<u>[Signature]</u>	<u>Dyn</u>	<u>VEHICLE OPERATOR</u>
<u>[Signature]</u>	<u>V</u>	<u>VEHICLE OPERATOR</u>
<u>[Signature]</u>	<u>Dyn</u>	<u>TRACK SECURITY OFFICER</u>
<u> </u>	<u> </u>	<u> </u>

PASSENGER LIST:

6-2

<u>Hemant S. Limaye</u>	<u>Brewer Eng. Labs</u>
<u>[Signature]</u>	<u>ENSCO INC</u>
<u>[Signature]</u>	<u>AGH Am.</u>
<u>[Signature]</u>	<u>Ensec</u>
<u> </u>	<u> </u>

TEST CONDITIONS:

WEATHER:

TRACK:

OTHER:

TIME	EVENT	REMARKS
1050	Custody to CC	5th day of actual test
1115	Corylate ^{swallow} swallow ₂ tracks for lunch + mit. Call.	<u>runs.</u>
1200	Start set-up for 50 mph run	
1215	Run 62	50 mph wind speed
1230	Run 63	50 2-15 mph
1245	64	50 270°-10°
1310	65	70
1325	66	70
1340	67	70
1355	68	90
1410	69	90
1420	70	90
1435	71	50
1445	72	50
1505	73	50
1532	Custody to CC	

43

TEST LOG

PROGRAM _____

DATE 12/14/77

PRE-TEST MEETING ATTENDEES:

<u>SIGNATURE</u>	<u>ORGANIZATION</u>	<u>DUTY</u>
<u>[Signature]</u>	<u>FRA</u>	<u>TEST CONTROLLER</u>
<u>[Signature]</u>	} <u>ENSCO</u>	<u>TEST DIRECTOR</u>
<u>[Signature]</u>		<u>CHIEF TEST ENGINEER</u>
<u>[Signature]</u>	<u>ENSCO</u>	<u>TEST SUPPORT ENGINEER</u>
<u>[Signature]</u>	_____	<u>VEHICLE OPERATOR</u>
<u>[Signature]</u>	_____	<u>VEHICLE OPERATOR</u>
<u>[Signature]</u>	<u>DYN.</u>	<u>TRACK SECURITY OFFICER</u>
<u>[Signature]</u>	<u>ENSCO</u>	_____

PASSENGER LIST:

<u>[Signature]</u>	<u>ARTI</u>
<u>[Signature]</u>	<u>ENSCO</u>
<u>[Signature]</u>	<u>Brewer Eng. Labs.</u>
<u>[Signature]</u>	<u>TTC Inst.</u>
<u>[Signature]</u>	<u>ENSCO</u>
_____	_____
_____	_____
_____	_____

TEST CONDITIONS:

WEATHER:

TRACK:

OTHER:

B-44

Date 12/14/77

ST CONTROLLER

TEST SUPPORT ENGINEER D. Amaya

TIME	EVENT	REMARKS
1035	Custody from OCC	~ 1 hr. delay due to DOT 015 work, replacement of ALO targets & EMT moves.
1055	Tried down @ weather sta. - calcs.	
1130	Assemble for lunch & weather calcs.	
1220	Start setup for 1st run	
1225	Run # 74	50 mph Wind 2 mph @ 90°
1235	75	50
1250	76	50 ~ 5 min delay - power outage on 7-5 (engine shut off)
1330	77	70 Wind 3 mph
1340	78	70 @ 380°
1350	79	70
1420	80	90
1430	81	90
1455	82	90 Wind 9 mph @ 220°
1527	Custody to OCC	8-45

TEST LOG

PROGRAM _____

DATE 12/15

PRE-TEST MEETING ATTENDEES:

<u>SIGNATURE</u>	<u>ORGANIZATION</u>	<u>DUTY</u>
<u>[Signature]</u>	<u>KRA</u>	<u>TEST CONTROLLER</u>
<u>[Signature]</u>	_____	<u>TEST DIRECTOR</u>
<u>[Signature]</u>	_____	<u>CHIEF TEST ENGINEER</u>
<u>[Signature]</u>	<u>Ensc</u>	<u>TEST SUPPORT ENGINEER</u>
<u>[Signature]</u>	_____	<u>VEHICLE OPERATOR</u>
<u>[Signature]</u>	_____	<u>VEHICLE OPERATOR</u>
<u>[Signature]</u>	<u>Dyn</u>	<u>TRACK SECURITY OFFICER</u>
_____	_____	_____

8-2

PASSENGER LIST:

<u>Hemant S. Limaye</u>	<u>Brewer Eng. Labs.</u>
<u>Prakash B. Joshi</u>	<u>ENSCO</u>
<u>J. E. [Signature]</u>	<u>TTC. Inst</u>
<u>[Signature]</u>	<u>APV Ass</u>
<u>Don Chappel.</u>	<u>ENSCO INC.</u>
<u>John Hight</u>	_____
_____	_____
_____	_____

TEST CONDITIONS:

WEATHER:

TRACK:

OTHER:

GRAM

Date 12/15/77

EST CONTROLLER

TEST SUPPORT ENGINEER D. Amaya

TIME	EVENT	REMARKS
1005	Ready for control R TT	~ 1 hr delay due to inaccurate zeroes (necessitated reentering CSB on track #3)
1136	Custody from OCC	
1145	Break for lunch, calls.	
1230	Run # 83	50 mph
1240	84	50
1250	85	50
1330	86	70
1340	87	70
1350	88	70
1420	89	90
1430	90	90
1445	91	90
1510	92	55
1535	93	55
1603	Custody to OCC	Wind 0-10 mph @ 130° - 220°

B-47

TEST LOG

PROGRAM _____

DATE 12/16/77

PRE-TEST MEETING ATTENDEES:

<u>SIGNATURE</u>	<u>ORGANIZATION</u>	<u>DUTY</u>
<u>[Signature]</u>	<u>FRA</u>	<u>TEST CONTROLLER</u>
<u>[Signature]</u>	} <u>ENSCO</u>	<u>TEST DIRECTOR</u>
<u>[Signature]</u>		<u>CHIEF TEST ENGINEER</u>
<u>[Signature]</u>	<u>Enso</u>	<u>TEST SUPPORT ENGINEER</u>
<u>[Signature]</u>		<u>VEHICLE OPERATOR</u>
<u>[Signature]</u>		<u>VEHICLE OPERATOR</u>
<u>[Signature]</u>	<u>[Signature]</u>	<u>TRACK SECURITY OFFICER</u>

8-2

PASSENGER LIST:

Hemant S. Limaye
Prakash B. Joshi
[Signature]
[Signature]
[Signature]
[Signature]

Brewer Eng. Labs
ENSCO
TTC. Inct.
ALH Ass.
Enso
ENSCO

TEST CONDITIONS:

WEATHER:

TRACK:

OTHER:

GRAM

Date 12/16/77

TEST CONTROLLER

TEST SUPPORT ENGINEER D. Amaya

TIME	EVENT	REMARKS
1075	Pre Test - Start w/70 mph runs, then 90's + 50's.	
		~1 hr. delay due to brake shoe replacement on test car & cal's.
1145	Break for lunch, cal's.	
1255	Back from lunch.	
1305	Run # 94	70 mph
	95	70
1315	96	70
1325	97	90
1355	98	90
1415	99	90
1425	100	55
1440	101	55
1455	102	55
3:30 - 4:30 P	Awaiting more cars to dock from in front of CSB	
1810	103	90
1820	104	90
1830	105	70
1840	106	70
1855	107	55
1905	108 — End of Test!	55
1920	Custody to OCC	B-49

APPENDIX C

MATHEMATICAL DERIVATIONS

APPENDIX C

Table of Contents

- C.1 Calculation of Radius of Curvature
- C.2 Examination of the Approximation $\dot{r}_L(t) \approx \dot{R}_X(t)$
- C.3 Evaluation of Drag Force in Energy Method
- C.4 Determination of Errors in Gravitational Force Computation
- C.5 Error in Averaging A Sinusoidal Signal
- C.6 Determination of Error in Measurement of Instantaneous Train Speed
- C.7 Errors in Side Force Due to Decoupling Between Translational and Rotational Motions
- C.8 Computation of Acceleration Due to Gravity
- C.9 Deviation of Rolling Resistance Information

APPENDIX C.1
CALCULATION OF RADIUS OF CURVATURE

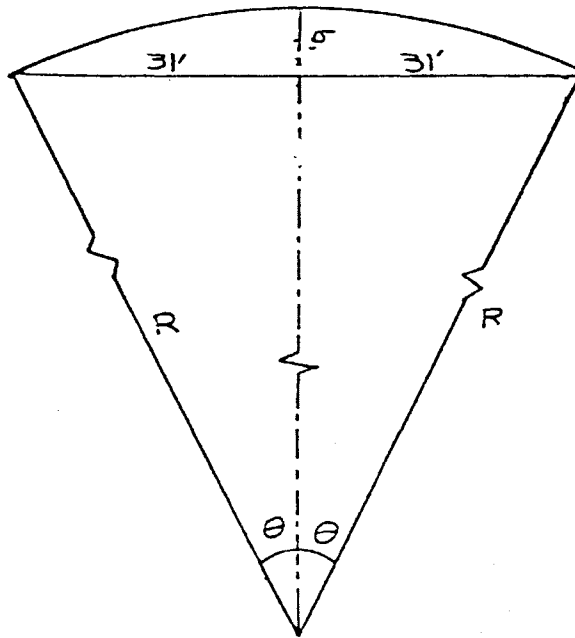


Figure C.1. Radius of Curvature

From Figure C.1,

$$\begin{aligned}\sigma &= R - R\cos\theta \\ &= R(1 - \cos\theta)\end{aligned}$$

Since $R\sin\theta = 31$ feet

$$\begin{aligned}\sigma &= R\left[1 - \sqrt{1 - \sin^2\theta}\right] \\ &= R\left[1 - \sqrt{1 - (31/R)^2}\right]\end{aligned}$$

where σ is in ft.

Hence,

$$\left(1 - \frac{\sigma}{R}\right)^2 = 1 - \left(\frac{31}{R}\right)^2$$

or

$$-\frac{2\sigma}{R} + \frac{\sigma^2}{R^2} = -\left(\frac{31}{R}\right)^2$$

Solving for R ,

$$R = \frac{(31)^2 + \sigma^2}{2\sigma} \text{ ft} \quad (\text{C.1})$$

Extending line $O\tilde{O}$ in $\Delta O\tilde{O}P$ to point Q, it may be verified that

$$\tan \eta = \frac{|\bar{\rho}| \sin(\phi - \alpha + \nu)}{|\bar{R}| + |\bar{\rho}| \cos(\phi - \alpha + \nu)} \quad (C.5)$$

$$\therefore \eta = \tan^{-1} \left[\frac{|\bar{\rho}| \sin(\phi - \alpha + \nu)}{|\bar{R}| + |\bar{\rho}| \cos(\phi - \alpha + \nu)} \right] \quad (C.6)$$

Substituting for η in Equation (C.4),

$$\beta = \alpha - \nu + \tan^{-1} \left[\frac{|\bar{\rho}| \sin(\phi - \alpha + \nu)}{|\bar{R}| + |\bar{\rho}| \cos(\phi - \alpha + \nu)} \right] \quad (C.7)$$

In view of the assumptions listed in Section 3.4 the angles α , ν and ϕ are small. Therefore,

$$(\phi - \alpha + \nu) \ll 1 \quad (C.8)$$

When sufficient time has elapsed from the start of motion,

$$|\bar{R}| \gg |\bar{\rho}|$$

or

$$\frac{|\bar{\rho}|}{|\bar{R}|} \ll 1 \quad (C.9)$$

Equation (C.7) may be written as

$$\beta = \alpha - \nu + \tan^{-1} \left[\frac{\frac{|\bar{\rho}|}{|\bar{R}|} \sin(\phi - \alpha + \nu)}{1 + \frac{|\bar{\rho}|}{|\bar{R}|} \cos(\phi - \alpha + \nu)} \right] \quad (C.10)$$

Noting that the sine and cosine functions are bounded between ± 1 and using the approximations (C.8) and (C.9) one obtains,

$$\beta = \alpha - \nu + \tan^{-1} \left[\frac{|\bar{\rho}|}{|\bar{R}|} (\phi - \alpha + \nu) \right] \quad (C.11)$$

where the result $\sin(x) \approx x$ for $x \ll 1$ has been used. Further, since the argument of \tan^{-1} in (C.9) is small due to (C.8) and (C.9), Equation (C.2) reduces to

$$\beta = \alpha - \nu + (\phi - \alpha + \nu) \frac{|\bar{\rho}|}{|\bar{R}|} \quad (C.12)$$

where the result $\tan^{-1}(x) \approx x$ for $x \ll 1$ has been employed. Equation (C.12) can be put in the form

$$\beta = \alpha \left(1 - \frac{|\bar{\rho}|}{|\bar{R}|}\right) - \nu \left(1 - \frac{|\bar{\rho}|}{|\bar{R}|}\right) + \phi \frac{|\bar{\rho}|}{|\bar{R}|}$$

which yields the following relation when the approximation (C.8) is invoked.

$$\beta = \alpha - \nu + \phi \frac{|\bar{\rho}|}{|\bar{R}|} \quad (C.13)$$

Recalling that the angles α , ν and ϕ are themselves very small and since (C.9) holds, to the leading order Equation (C.13) becomes

$$\beta \approx \alpha - \nu \quad (C.14)$$

As seen from Figure (C.2), this result implies that $r_L \parallel \bar{R}$, and from Equation (C.4) $\eta = 0$, which means that \bar{r} and \bar{R} are collinear. This proves that the motion along r_L can be approximated very closely by the motion along \bar{R} .

The next task is to show that

$$\dot{r}_L(t) \approx \dot{R}_x(t) \quad (C.15)$$

is a valid approximation and to examine its accuracy.

In Figure (3-6) the velocity of the center of gravity of the trailer (point C) relative to the inertial reference is given by

$$\dot{\vec{r}} = \dot{\vec{R}} + \dot{\vec{\rho}} + \vec{\omega} \times \vec{\rho} \quad (\text{C.16})$$

Splitting the vector $\dot{\vec{r}}$ into its components one gets

$$\dot{r}_x = \dot{R}_x + \dot{\tilde{x}} + (\omega_y \tilde{z} - \omega_z \tilde{y}) \quad (\text{C.17a})$$

$$\dot{r}_y = \dot{R}_y + \dot{\tilde{y}} + (\omega_z \tilde{x} - \omega_x \tilde{z}) \quad (\text{C.17b})$$

$$\dot{r}_z = \dot{R}_z + \dot{\tilde{z}} + (\omega_x \tilde{y} - \omega_y \tilde{x}) \quad (\text{C.17c})$$

where $\dot{\tilde{x}}$, $\dot{\tilde{y}}$, $\dot{\tilde{z}}$ are components of trailer velocity relative to the carbody. An order of magnitude estimation of various terms in Equations (C.17) is performed as follows. Assume that

$$\begin{aligned} \dot{R}_x &= 0(1) \\ \dot{R}_y, \dot{R}_z &= 0(\lambda) \\ \dot{\tilde{x}}, \dot{\tilde{y}}, \dot{\tilde{z}} &= 0(\lambda) \end{aligned} \quad (\text{C.18})$$

$$\omega_x, \omega_y, \omega_z = 0(\lambda)$$

$$\tilde{x}, \tilde{y} = 0(1)$$

$$\tilde{z} = 0(\lambda)$$

where $\lambda \ll 1$

Now,

$$|\dot{\vec{r}}| = \sqrt{\dot{r}_x^2 + \dot{r}_y^2 + \dot{r}_z^2} \quad (\text{C.19})$$

Substituting Equations (C.17) into Equation (C.19), simplifying and keeping terms only up to $O(\lambda)$,

$$\dot{\vec{r}} = \dot{r}_x + \dot{\tilde{x}} + \omega_y \tilde{z} + O(\lambda^2) \quad (C.20)$$

where the last term represents contribution to the longitudinal velocity due to pitching (ω_y) of the carbody. As shown in Section 3.5 the momentum of the carbody results in the force contribution

$$M_F = \frac{m}{T} [\dot{r}_L(T) - \dot{r}_L(0)] \quad (C.21)$$

If the approximation

$$M_F \approx \frac{m}{T} [\dot{R}_x(T) - \dot{R}_x(0)] \quad (C.22)$$

is used then the terms

$$\Delta M_F = \frac{m}{T} [\dot{\tilde{x}}(T) - \dot{\tilde{x}}(0)] + \frac{m}{T} [\omega_y(T) - \omega_y(0)] \tilde{z} \quad (C.23)$$

are ignored. Relative magnitudes of M_F and ΔM_F are computed as follows. At 90 mph the test duration T over 4000 feet is 30.3 seconds. If the train speed can be maintained within 3 percent (3.95 ft/sec) as indicated by AERO/TOFC-II test data,

$$\begin{aligned} M_{F_{\max}} &= \frac{9850}{32.2} \frac{1}{30.3} \quad 2 \quad (3.96) \\ &= 80.0 \text{ lb at 90 mph} \end{aligned}$$

and at 50 mph with $T = 54.5$ seconds

$$\begin{aligned} M_{F_{\max}} &= \frac{9850}{32.2} \frac{1}{54.5} \quad 2 \quad (2.19) \\ &= 24.6 \text{ lb at 50 mph} \end{aligned}$$

Since the trailer motions relative to the carbody are expected to be very small, let $\tilde{x} = 0.01$ ft/sec (about 0.1 inch/sec). Then in Equation (C.23).

$$\begin{aligned}
\frac{m}{T} [\ddot{x}(T) - \ddot{x}(0)] &= \frac{9850}{32.2} \frac{1}{30.3} 2(0.01) \\
&= 0.20 \text{ lbs at 90 mph} \\
&= 0.11 \text{ lbs at 50 mph}
\end{aligned}$$

The frequency of pitch oscillations is typically 3Hz and the maximum amplitude is approximately 2 inches over the carbody wheelbase of 60 feet.

Therefore,

$$\theta_y = \pm \frac{2}{60 \times 12} \sin 2\pi(3)t$$

or

$$\theta_y = \pm \frac{1}{360} \sin 6\pi t$$

Hence,

$$(\omega_y)_{\max} = \left(\frac{d\theta_y}{dt} \right)_{\max} = \pm \frac{\pi}{60} = \frac{\pi}{60}$$

The distance of the center of gravity of the trailer above the carbody deck plate is $\tilde{z} = 54$ inches, therefore, the last term in Equation (C.23) has the value

$$\begin{aligned}
\frac{m}{T} [\omega_y(T) - \omega_y(0)] \tilde{z}_{\max} &= \frac{9850}{32.2} \frac{1}{30.3} \frac{2\pi}{60} \cdot \frac{54}{12} \\
&= 4.8 \text{ lbs at 90 mph} \\
&= 2.6 \text{ lbs at 50 mph}
\end{aligned}$$

It can therefore be concluded that the approximation

$$\dot{r}_L(t) \approx \dot{R}_X(t) \tag{C.24}$$

can be introduced provided the errors computed above are taken into account. Equation (C.24) states that the longitudinal motion of the trailer can be approximated by the average rectilinear motion of the carbody.

A corollary of this result is that the transverse direction 'n' in Figure 3-8 can be approximated by the lateral direction y in Figure 3-6. A similar exercise can be carried out in the y direction.

APPENDIX C.3

EVALUATION OF DRAG FORCE IN ENERGY METHOD

The energy approach yields the average value of the drag power

$$\bar{P} = \frac{1}{T} \int_0^T \dot{R}_X(t) D(t) dt \quad (C.25)$$

from which it is necessary to evaluate the average drag force.

$$\bar{D} = \frac{1}{T} \int_0^T D(t) dt \quad (C.26)$$

Let the instantaneous speed $R_X(t)$ and the drag $D(t)$ be written as

$$\dot{R}_X(t) = \dot{R}_{X_{ave}} + \Delta \dot{R}_X(t) \quad (C.27)$$

$$D(t) = \bar{D} + \Delta D(t) \quad (C.28)$$

where $\dot{R}_{X_{ave}}$ and \bar{D} are time independent, with $\Delta \dot{R}_X(t)$ and $\Delta D(t)$ satisfying the following zero average conditions

$$\int_0^T \Delta \dot{R}_X(t) dt = 0 \quad (C.29)$$

and

$$\int_0^T \Delta D(t) dt = 0 \quad (C.30)$$

Substituting Equations (C.27) and (C.28) into Equation (C.25).

$$\begin{aligned} \bar{P} &= \frac{1}{T} \int_0^T \dot{R}_{X_{ave}} \bar{D} dt + \frac{1}{T} \int_0^T \dot{R}_{X_{ave}} \Delta D dt + \frac{1}{T} \int_0^T \bar{D} \Delta \dot{R}_X dt + \frac{1}{T} \int_0^T \Delta \dot{R}_X \Delta D dt \\ \text{or,} \\ \bar{P} &= \dot{R}_{X_{ave}} \bar{D} + \frac{1}{T} \int_0^T \Delta \dot{R}_X \Delta D dt \end{aligned} \quad (C.31)$$

where Equations (C.29) and (C.30) have been used along with the fact that $\dot{R}_{x\text{ave}}$ and \bar{D} do not depend on time. From Equation (C.30),

$$\bar{D} = \frac{1}{\dot{R}_{x\text{ave}}} \left[\bar{P} - \frac{1}{T} \int_0^T \Delta \dot{R}_x \Delta D dt \right] \quad (\text{C.32})$$

Assuming that the drag force to follow a square law variation for each time instant t ,

$$D(t) = K \dot{R}_x^2(t) \quad (\text{C.33})$$

where K is a constant of proportionality. Introducing Equations (C.27) and (C.28) in Equation (C.33),

$$\bar{D} + \Delta D = K \left[\dot{R}_{x\text{ave}}^2 + 2\dot{R}_{x\text{ave}} \Delta \dot{R}_x + \Delta \dot{R}_x^2 \right]$$

or

$$\bar{D} + \Delta D = K \dot{R}_{x\text{ave}}^2 \left[1 + 2 \frac{\Delta \dot{R}_x}{\dot{R}_{x\text{ave}}} + \left(\frac{\Delta \dot{R}_x}{\dot{R}_{x\text{ave}}} \right)^2 \right] \quad (\text{C.34})$$

Assuming that the fluctuation $\Delta \dot{R}_x$ from the average speed $\dot{R}_{x\text{ave}}$ are small compared to the average speed, i.e.,

$$\frac{\Delta \dot{R}_x}{\dot{R}_{x\text{ave}}} \ll 1 \quad (\text{C.35})$$

Equation (C.34) becomes, up to first order,

$$\bar{D} + \Delta D = K \dot{R}_{x\text{ave}}^2 \left[1 + \frac{2\Delta \dot{R}_x}{\dot{R}_{x\text{ave}}} \right] \quad (\text{C.36})$$

Assuming now that the average drag force also follows a square law variation

$$\bar{D} = K \dot{R}_{x\text{ave}}^2 \quad (\text{C.37})$$

Equation (C.36) takes the form,

$$\Delta D = \frac{2\dot{\bar{R}}_x}{\dot{R}_{x\text{ave}}} \bar{D} \quad (\text{C.38})$$

Eliminating ΔD between Equations (C.32) and (C.38) one obtains,

$$\bar{D} = \frac{1}{\dot{R}_{x\text{ave}}} \left[\bar{P} - \frac{2\bar{D}}{\dot{R}_{x\text{ave}} T} \int_0^T (\dot{\bar{R}}_x)^2 dt \right]$$

or

$$\bar{D} = \frac{1}{\dot{R}_{x\text{ave}}} \left[\bar{P} - \frac{2\bar{D}}{\dot{R}_{x\text{ave}} T} \int_0^T (\dot{R}_x(t) - \dot{R}_{x\text{ave}})^2 dt \right] \quad (\text{C.39})$$

where Equation (C.27) has been employed.

Equation (C.39) can be used to determine the average drag force iteratively as described below.

- (i) Since the instantaneous speed $\dot{R}_x(t)$ is recorded during the test and averaged to yield $\dot{R}_{x\text{ave}}$, the following integral in Equation (C.39) can be computed once and for all.

$$I = \frac{1}{T} \int_0^T (\dot{R}_x(t) - \dot{R}_{x\text{ave}})^2 dt \quad (\text{C.40})$$

- (ii) Assume an initial estimation for \bar{D} ,

$$\bar{D}_0 = \bar{P} / \dot{R}_{x\text{ave}} \quad (\text{C.41})$$

(iii) Compute an improved value for average drag force.

$$\bar{D}_1 = \frac{1}{\dot{R}_{x\text{ave}}} \left[\bar{P} - \frac{2\bar{D}_0}{\dot{R}_{x\text{ave}}} I \right] \quad (\text{C.32})$$

(iv) Compare \bar{D}_0 and \bar{D}_1 to check whether their values agree within a prescribed limit, typically 1%.

(v) Repeat steps (ii) through (iv) until the required convergence is obtained.

APPENDIX C.4
 DETERMINATION OF ERRORS IN
 GRAVITATIONAL FORCE COMPUTATION

The average gravitational force over the test zone is given by

$$\hat{m}g\bar{\theta}_g = \hat{m}g \frac{1}{T} \int_0^T \bar{\theta}_g(t) dt \quad (C.43)$$

where the symbol \hat{m} (instead of m) is used to denote trailer mass in order to differentiate it from the integer counter m used subsequently.

Using the time-distance transformation

$$t = t(x)$$

and $T = t(\Lambda)$, the above integral becomes

$$\hat{m}g\bar{\theta}_g = \frac{\hat{m}g}{T} \int_0^\Lambda \bar{\theta}_g(x) \frac{dt}{dx} dx \quad (C.44)$$

where $\theta_g(x)$ is the slope of the locus of trailer center of gravity in the x - h (or y) plane. Since the track is made up of 39 feet length welded rail with a maximum profile deviation of 1/8-inch as per the requirement in Reference 9, the rail can be approximated by a half sinusoid of base $\lambda/2$ (=39 feet) and height A (= 1/8-inch). The profile may be continued as an odd periodic function of wavelength 2λ , resulting in an odd half range expansion in $\pm x$ direction as shown in Figure C-3.

The rail profile is then given by

$$h' = A \sin \frac{2\pi x'}{\lambda} \quad (C.45)$$

The reason for using primed variables x' and h' will become clear very shortly. The actual AERO/TOFC-II test zone has an average grade on which the sinusoidal variations of Figure C-3 are superimposed. This situation is depicted in Figure C-4 in which Λ is the length of the test zone and ΔH is the change in ground elevation (final elevation minus initial elevation). Typical values are $\Delta H = 11$ feet and $\Lambda = 4,000$ feet.

In the present analysis the h - x system has been employed and therefore a coordinate transformation is necessary. For a rotation of coordinate axes through an angle θ , the following relations apply

$$\begin{aligned} h' &= -x \sin\theta + h \cos\theta \\ x' &= x \cos\theta + h \sin\theta \end{aligned} \tag{C.46}$$

When the average slope $\Delta H/\Lambda$ is small,

$$\begin{aligned} \tan\theta &= \frac{\Delta H}{\Lambda} \\ &\approx \sin\theta \approx \theta \end{aligned}$$

and $\cos\theta \approx 1$

thus,

$$\begin{aligned} h' &= -x \frac{\Delta H}{\Lambda} + h \\ x' &= x + h \frac{\Delta H}{\Lambda} \end{aligned} \tag{C.47}$$

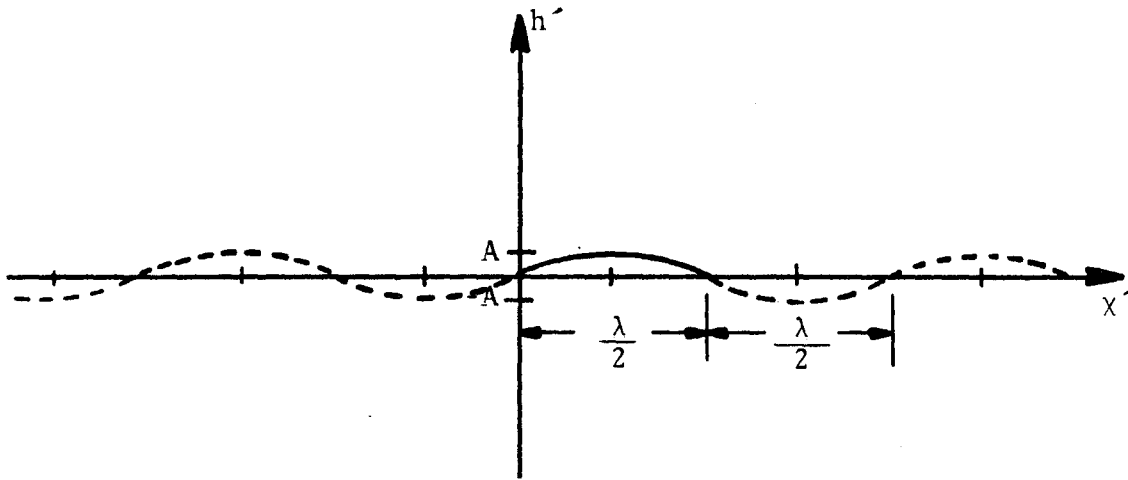


Figure C-3. Odd Half Range Expansion of Rail Profile

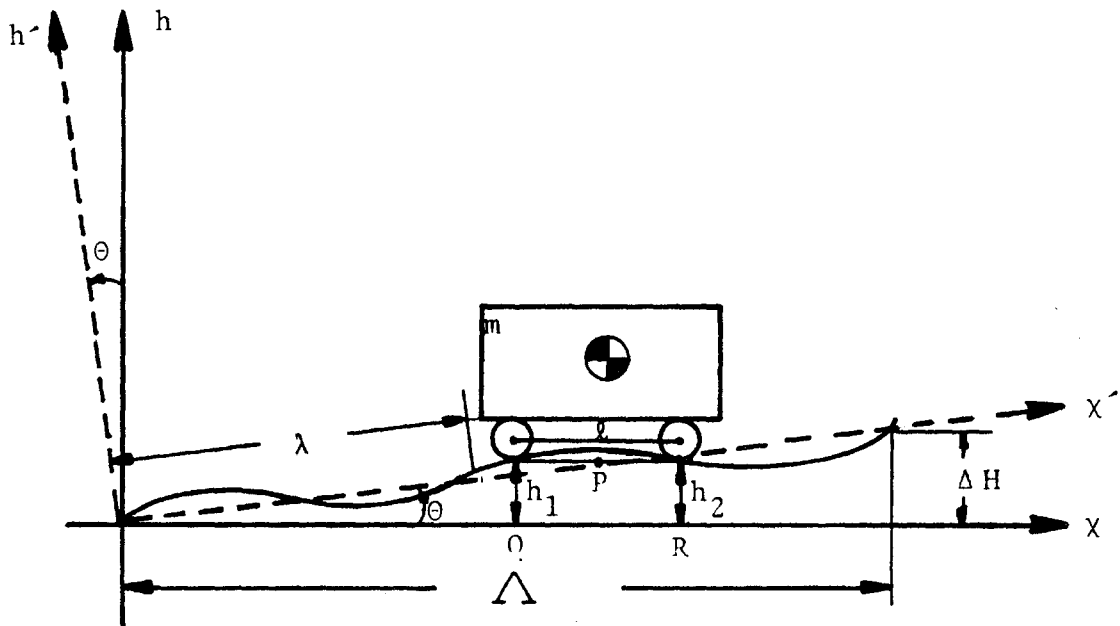


Figure C-4. Transformation of Coordinates

Substituting Equations (C.47) into (C.46)

$$-\frac{\Delta H}{\Lambda} x + h = A \sin \left\{ \frac{2\pi}{\lambda} \left(x + h \frac{\Delta H}{\Lambda} \right) \right\} \quad (C.48)$$

or

$$h = \frac{\Delta H}{\Lambda} x + A \sin \left\{ \frac{2\pi x}{\lambda} + \frac{h}{\lambda} \frac{\Delta H}{\Lambda} \right\}$$

This is an implicit relation for h and further simplification is necessary. The largest value h can have is approximately $(\Delta H + A)$ and hence

$$\left| \frac{h}{\lambda} \frac{\Delta H}{\Lambda} \right|_{\max} = \frac{(\Delta H + A)}{\lambda} \cdot \frac{\Delta H}{\Lambda}$$

Furthermore, the amplitude $A \ll \Delta H$ (1/8-inch compared to 11 feet for the present test zone) and thus

$$\begin{aligned} \left| \frac{h}{\lambda} \frac{\Delta H}{\Lambda} \right|_{\max} &= \frac{\Delta H}{\lambda} \frac{\Delta H}{\Lambda} \\ &= \frac{10}{39} \frac{10}{4,000} \\ &= 6.4 \times 10^{-4} \end{aligned}$$

On the other hand, the term $\frac{2\pi x}{\lambda}$ in Equation (BB.6) is considerably larger than the above estimate, except for extremely small values (less than 1/2-inch) of x which are not of practical interest. Therefore,

$$\frac{h}{\lambda} \frac{\Delta H}{\Lambda} \ll \frac{2\pi x}{\lambda} \quad (C.49)$$

and Equation (BB.6) reduces to

$$h = \frac{\Delta H}{\Lambda} x + A \sin \frac{2\pi x}{\lambda} \quad (C.50)$$

which is a simple superposition of a ramp and a sinusoid.

Consider the carbody riding on the track as shown in Figure C-4. ' ℓ ' is the distance between front and aft bolsters and h_1 and h_2 are coordinates of the wheel-rail contact points.

The length of the straight line joining these points is also ℓ and its projection on the x axis (QR) is very nearly ' ℓ ', provided

$$\frac{A}{\lambda} \ll 1 \quad (C.51)$$

This condition is well satisfied in the present problem. Only one trailer is shown for simplicity in Figure C-4 and it is assumed to be rigidly fastened to the carbody. In addition, the carbody is assumed to be rigidly connected to the wheels. These simplifications are appropriate for analysis of gravitational force corrections. The rigidity of the vehicle insures absence of any relative motion between the center of gravity and point P, the midpoint of the line joining the contact points. Thus, it is sufficient to consider the slope of the locus of point P, rather than the slope of the locus of the center of gravity, in Equation (C.44). Let x be the coordinate of Point Q so that the Point R is located at (x + ℓ). Then, from Equation (C.50).

$$h_1 = \frac{\Delta H}{\Lambda} x + A \sin \frac{2\pi x}{\lambda}$$

$$h_2 = \frac{\Delta H}{\Lambda} (x + \ell) + A \sin \frac{2\pi(x + \ell)}{\lambda}$$

and the Point P is given by

$$\begin{aligned}
 h &= \frac{1}{2} (h_1 + h_2) \\
 &= \frac{1}{2} \frac{\Delta H}{\Lambda} (2x + \ell) + \frac{A}{2} \left[\sin \frac{2\pi x}{\lambda} + \sin \frac{2\pi(x + \ell)}{\lambda} \right] \\
 &= \frac{\Delta H}{\Lambda} \left(x + \frac{\ell}{2}\right) + \frac{A}{2} \left[2 \sin \frac{1}{2} \left\{ \frac{4\pi x}{\lambda} + \frac{2\pi \ell}{\lambda} \right\} \cos \frac{1}{2} \left\{ \frac{2\pi \ell}{\lambda} \right\} \right]
 \end{aligned}$$

or

$$h(x) = \frac{\Delta H}{\Lambda} \left(x + \frac{\ell}{2}\right) + A \cos \frac{\pi \ell}{\lambda} \sin \left(\frac{2\pi x}{\lambda} + \frac{\pi \ell}{\lambda}\right) \quad (C.52)$$

Notice that if $\ell = n\lambda$, where $n = 0, 1, 2 \dots$, the sinusoidal part of the preceding equation becomes

$$\begin{aligned}
 &A \cos (n\pi) \sin \left(n\pi + \frac{2\pi x}{\lambda}\right) \\
 &= A (-1)^n (-1)^n \sin \left(\frac{2\pi x}{\lambda}\right) \\
 &= A \sin \left(\frac{2\pi x}{\lambda}\right)
 \end{aligned}$$

Thus, the carbody 'sees' the entire amplitude A of the sinusoidal track disturbance. On the other hand if $\ell = (2n + 1)\frac{\lambda}{2}$ with $n=0, 1, 2 \dots$; $\cos \left[(2n + 1)\frac{\pi}{2}\right] = 0$, and the sinusoidal term disappears. Thus, the factor $\cos \frac{\pi \ell}{\lambda}$ serves as an attenuation factor multiplying the disturbance amplitude A.

Returning to Equation (C.44), let

$$I = \frac{1}{T} \int_0^{\Lambda} \theta(x) \frac{dt}{dx} dx \quad (C.53)$$

where

$$\theta(x) = \frac{dh}{dx}$$

Also, let

$$\frac{dt}{dx} = \frac{1}{dx/dt} = \frac{1}{\dot{R}_{x\text{ave}} + \Delta\dot{R}_x} \quad (\text{C.54})$$

where $\dot{R}_{x\text{ave}}$ is the average speed over the test zone, so that by definition,

$$\int_0^\Lambda \Delta\dot{R}_x dx = 0 \quad (\text{C.55})$$

and $\dot{R}_{x\text{ave}} T = \Lambda$. With the foregoing substitutions Equation (C.53) becomes

$$I = \frac{1}{T\dot{R}_{x\text{ave}}} \int_0^\Lambda \frac{dh}{dx} \left(1 + \frac{\Delta\dot{R}_x}{\dot{R}_{x\text{ave}}} \right)^{-1} dx$$

Assuming that the fluctuations $\Delta\dot{R}_x$ about $\dot{R}_{x\text{ave}}$ are small, i.e.,

$$\frac{\Delta\dot{R}_x}{\dot{R}_{x\text{avg}}} \ll 1$$

$$\left(1 + \frac{\Delta\dot{R}_x}{\dot{R}_{x\text{ave}}} \right)^{-1} \approx 1 - \frac{\Delta\dot{R}_x}{\dot{R}_{x\text{ave}}}$$

Hence,

$$I = \frac{1}{\Lambda} \int_0^\Lambda \frac{dh}{dx} \left(1 - \frac{\Delta\dot{R}_x}{\dot{R}_{x\text{ave}}} \right) dx$$

Substituting for $\frac{dh}{dx}$ obtained from Equation (C.52)

$$\frac{dh}{dx} = \frac{\Delta H}{\Lambda} + \frac{2\pi A}{\lambda} \cos \frac{\pi \ell}{\lambda} \cos \left(\frac{2\pi x}{\lambda} + \frac{\pi \ell}{\lambda} \right)$$

One gets

$$\begin{aligned} \Delta I &= \frac{\Delta H}{\Lambda} \int_0^{\Lambda} dx + \frac{2\pi A}{\lambda} \cos \frac{\pi \ell}{\lambda} \int_0^{\Lambda} \cos \left(\frac{2\pi x}{\lambda} + \frac{\pi \ell}{\lambda} \right) dx \\ &- \frac{\Delta H}{\Lambda} \int_0^{\Lambda} \Delta \dot{R}_x dx - \frac{2\pi A}{\lambda} \cos \frac{\pi \ell}{\lambda} \int_0^{\Lambda} \cos \left(\frac{2\pi x}{\lambda} + \frac{\pi \ell}{\lambda} \right) \frac{\Delta \dot{R}_x}{\dot{R}_{x_{ave}}} dx \end{aligned} \quad (C.56)$$

The third integral in (C.56) is zero by virtue of the definition (C.55). Consistent with this relation, it may be assumed that the track profile variations about the mean slope $\frac{\Delta H}{\Lambda}$ average out to zero. Thus, the second integral in (C.56) is zero or

$$\int_0^{\Lambda} \cos \left(\frac{2\pi x}{\lambda} + \frac{\pi \ell}{\lambda} \right) dx = 0$$

or

$$\frac{\lambda}{2\pi} \sin \left(\frac{2\pi x}{\lambda} + \frac{\pi \ell}{\lambda} \right) \Big|_0^{\Lambda} = 0$$

$$\sin \left(\frac{2\pi \Lambda}{\lambda} + \frac{\pi \ell}{\lambda} \right) = \sin \frac{\pi \ell}{\lambda}$$

or

$$\frac{2\pi \Lambda}{\lambda} + \frac{\pi \ell}{\lambda} = \frac{\pi \ell}{\lambda} + 2n\pi \quad n=0,1,2,\dots$$

or

$$\frac{\Lambda}{\lambda} = n \quad n=0,1,2,\dots \quad (\text{C.57})$$

Assume now that the velocity fluctuations $\Delta \dot{R}_x$ are of the form

$$\Delta \dot{R}_x = B \sin (2\pi f x + \phi) \quad (\text{C.58})$$

Then (C.55) requires that

$$\begin{aligned} B \int_0^{\Lambda} \sin (2\pi f x + \phi) dx &= 0 \\ - \frac{B}{2\pi f} \cos (2\pi f x + \phi) \Big|_0^{\Lambda} &= 0 \end{aligned}$$

or

$$\cos (2\pi f \Lambda + \phi) = \cos \phi$$

$$2\pi f \Lambda + \phi = \phi + 2m\pi \quad m = 0,1,2,\dots$$

or

$$f \Lambda = m \quad m = 0,1,2,\dots \quad (\text{C.59})$$

Finally, Equation (C.56) reduces to,

$$\Delta I = \frac{\Delta H}{\Lambda} \Lambda - \frac{2\pi AB}{\lambda \dot{R}_{x \text{ ave}}} \cos \frac{\pi \ell}{\lambda} \int_0^{\Lambda} \cos \left(\frac{2\pi x}{\lambda} + \frac{\pi \ell}{\lambda} \right) \sin (2\pi f x + \phi) dx$$

or

$$\Delta I = \Delta H - 2\pi \frac{A}{\lambda} \frac{B}{\dot{R}_{x_{ave}}} \cos \frac{\pi \ell}{\lambda} \int_0^{\Lambda} \cos \left(\frac{2\pi x}{\lambda} + \frac{\pi \ell}{\lambda} \right) \sin (2\pi f x + \phi) dx = \Delta H + J \quad (C.60)$$

where,

$$J = -2\pi \frac{A}{\lambda} \frac{B}{\dot{R}_{x_{ave}}} \cos \frac{\pi \ell}{\lambda} \int_0^{\Lambda} \cos \left(\frac{2\pi x}{\lambda} + \frac{\pi \ell}{\lambda} \right) \sin (2\pi f x + \phi) dx$$

Consider,

$$\begin{aligned} J &= - \frac{2\pi AB}{\lambda \dot{R}_{x_{ave}}} \cos \frac{\pi \ell}{\lambda} \left[\frac{1}{2} \int_0^{\Lambda} \sin \left\{ 2\pi x \left(f + \frac{1}{\lambda} \right) + \left(\phi + \frac{\pi \ell}{\lambda} \right) \right\} dx \right. \\ &\quad \left. + \frac{1}{2} \int_0^{\Lambda} \sin \left\{ 2\pi x \left(f - \frac{1}{\lambda} \right) + \left(\phi - \frac{\pi \ell}{\lambda} \right) \right\} dx \right] \\ &= - \frac{\pi AB}{\lambda \dot{R}_{x_{ave}}} \cos \frac{\pi \ell}{\lambda} \left[\frac{-1}{2\pi \left(f + \frac{1}{\lambda} \right)} \cos \left\{ 2\pi x \left(f + \frac{1}{\lambda} \right) + \left(\phi + \frac{\pi \ell}{\lambda} \right) \right\} \Big|_0^{\Lambda} \right. \\ &\quad \left. - \frac{1}{2\pi \left(f - \frac{1}{\lambda} \right)} \cos \left\{ 2\pi x \left(f - \frac{1}{\lambda} \right) + \left(\phi - \frac{\pi \ell}{\lambda} \right) \right\} \Big|_0^{\Lambda} \right] \\ &\quad + \left(\phi - \frac{\pi \ell}{\lambda} \right) \Big|_0^{\Lambda} \end{aligned}$$

$$\begin{aligned}
&= \frac{1}{2} \frac{AB}{R_x} \cos \frac{\pi \ell}{\lambda} \left[\frac{1}{(f\lambda + 1)} \cos \left\{ 2\pi \Lambda \left(f + \frac{1}{\lambda} \right) \right. \right. \\
&\quad \left. \left. + \left(\phi + \frac{\pi \ell}{\lambda} \right) \right\} - \frac{1}{(f\lambda + 1)} \cos \left(\phi + \frac{\pi \ell}{\lambda} \right) \right. \\
&\quad \left. + \frac{1}{(f\lambda - 1)} \cos \left\{ 2\pi \Lambda \left(f - \frac{1}{\lambda} \right) + \left(\phi + \frac{\pi \ell}{\lambda} \right) \right\} - \frac{1}{(f\lambda - 1)} \cos \left(\phi - \frac{\pi \ell}{\lambda} \right) \right]
\end{aligned}
\tag{C.61}$$

In Equation (C.61) consider,

$$\begin{aligned}
&\cos \left\{ 2\pi \Lambda f + \frac{1}{\lambda} + \left(\phi + \frac{\pi \ell}{\lambda} \right) \right\} \\
&= \cos \left\{ 2\pi f \Lambda + 2\pi \frac{\Lambda}{\lambda} + \phi + \frac{\pi \ell}{\lambda} \right\}
\end{aligned}$$

Using Equations (C.57) and (C.59),

$$\begin{aligned}
&= \cos \left\{ 2\pi m + 2\pi n + \phi + \frac{\pi \ell}{\lambda} \right\} \\
&= \cos \left\{ 2\pi (m + n) + \left(\phi + \frac{\pi \ell}{\lambda} \right) \right\}
\end{aligned}$$

and similarly,

$$\begin{aligned}
&\cos \left\{ 2\pi \left(f - \frac{1}{\lambda} \right) + \left(\phi - \frac{\pi \ell}{\lambda} \right) \right\} \\
&= \cos \left\{ 2\pi (m - n) + \left(\phi - \frac{\pi \ell}{\lambda} \right) \right\}
\end{aligned}$$

Thus, Equation (C.61) simplifies to

$$\begin{aligned}
 J = \frac{1}{2} \frac{AB}{R_{x_{ave}}} \cos \frac{\pi \ell}{\lambda} & \left[\frac{1}{(f\lambda + 1)} \right\} \cos [2\pi(m + n) \\
 & + \left(\phi + \frac{\pi \ell}{\lambda} \right) \left. \right\} - \cos \left(\phi + \frac{\pi \ell}{\lambda} \right) \left. \right\} \\
 & + \frac{1}{(f\lambda - 1)} \left\{ \cos [2\pi(m - n) + \left(\phi - \frac{\pi \ell}{\lambda} \right)] \right. \\
 & \left. - \cos \phi - \frac{\pi \ell}{\lambda} \right.
 \end{aligned}$$

Recall from (C.57) and (C.59) that

$$f\lambda = \frac{f\Lambda}{\lambda} = \frac{m}{n}$$

Therefore,

$$\begin{aligned}
 J = \frac{1}{2} \frac{AB}{R_{x_{ave}}} \cos \frac{\pi \ell}{\lambda} & \left[\frac{n}{(m + n)} \left\{ -2 \sin [\pi(m + n) \right. \right. \\
 & \left. \left. + \left(\phi + \frac{\pi \ell}{\lambda} \right)] \sin [\pi(m + n)] \right\} + \frac{n}{m - n} \right. \\
 & \left. \left\{ -2 \sin [\pi(m - n) + \left(\phi - \frac{\pi \ell}{\lambda} \right)] \sin [\pi(m - n)] \right\} \right]
 \end{aligned}$$

Finally,

$$\begin{aligned}
 J = - \frac{AB}{\dot{R}_{x_{ave}}} \cos \frac{\pi \ell}{\lambda} & \left[\frac{n}{(m+n)} \sin \left\{ \pi(m+n) \right\} \sin \right. \\
 & \left. \left\{ \pi(m+n) + \left(\phi + \frac{\pi \ell}{\lambda} \right) \right\} + \frac{n}{(m-n)} \sin \left\{ \pi(m-n) \right\} \right. \\
 & \left. \sin \left\{ \pi(m-n) + \left(\phi - \frac{\pi \ell}{\lambda} \right) \right\} \right] \quad (C.62)
 \end{aligned}$$

The following possible cases are considered next.

Case I: $m \neq n$

Physically, this means that the track variations do not occur at the same frequency as the speed variations. An example in practice would be the variations in train speed due to train handling (i.e., coordination between the throttle and the brake performed by the locomotive engineer). These variations are expected to occur at much slower frequencies than the track variations.

When $m \neq n$, and since m and n are integers,

$$\frac{\sin \{ \pi(m-n) \}}{(m-n)} \equiv 0$$

Also,

$$\sin \{ \pi(m+n) \} \equiv 0$$

Hence, $J \equiv 0$ in Equation (C.62). Thus in Equation (C.60),

$$I = \frac{\Delta H}{\Lambda}$$

and using (C.53) and (C.44) the gravitational term is

$$\hat{m}g\bar{\theta} = \hat{m}g \frac{\Delta H}{\Lambda}, \quad m \neq n$$

and there is no error due to track and train speed variations.

Case II: $m = n$

That is, the variations in track and in train speed occur at the same frequency. In practice, such fluctuations can occur due to an exchange between potential and kinetic energy when the carbody traverses the peaks and valleys in the track profile. The amplitude of these fluctuations, as pointed out earlier, is attenuated by a factor which depends upon the carbody bolster spacing.

When $m=n$, and since m and n are integers,

$$\sin \{\pi(m + n)\} \equiv 0$$

whereas,

$$\frac{\sin \{\pi(m - n)\}}{(m - n)} = \pi$$

Therefore, in Equation (C.62),

$$J = - \frac{\pi n AB}{\dot{R}_{x_{ave}}} \cos \frac{\pi \ell}{\lambda} \sin \left(\phi - \frac{\pi \ell}{\lambda} \right)$$

Substituting for n from (C.57),

$$J = - \frac{\Lambda}{\lambda} \frac{\pi AB}{\dot{R}_{x_{ave}}} \cos \frac{\pi \ell}{\lambda} \sin \left(\phi - \frac{\pi \ell}{\lambda} \right)$$

Substituting the above expression for J into Equation (C.60),

$$I = \frac{\Delta H}{\Lambda} - \pi \frac{A}{\lambda} \frac{B}{\dot{R}_{x_{ave}}} \cos \frac{\pi \ell}{\lambda} \sin \left(\phi - \frac{\pi \ell}{\lambda} \right)$$

And from (C.44), the average gravitational force is

$$mg\bar{\theta} = \frac{mg\Delta H}{\Lambda} - mg\pi \frac{A}{\lambda} \frac{B}{\dot{R}_x} \cos \frac{\pi \ell}{\lambda} \sin \left(\phi - \frac{\pi \ell}{\lambda} \right) \quad (C.63)$$

where the superscript 'A' on trailer mass is dropped henceforth.

The first term on the right hand side of the above equation has been employed in the onboard processing and therefore, the error term is

$$\varepsilon_g = -mg\pi \frac{A}{\lambda} \frac{B}{\dot{R}_{x_{ave}}} \cos \frac{\pi \ell}{\lambda} \sin \left(\phi - \frac{\pi \ell}{\lambda} \right) \quad (C.64)$$

where the fact that B is the maximum value of the speed variations $\Delta \dot{R}_x$ has been employed. Equation (C.64) shows that the error depends upon (i) ratio of track disturbance amplitude to wavelength (ii) ratio of maximum speed variation about the average speed to the average speed itself (iii) attenuation factor which is a function of the ratio of carbody bolster spacing to disturbance wavelength and (iv) phase angle between the track variations and the speed variations.

The maximum error in (C.64) occurs when both sine and cosine terms are unity, therefore,

$$|\varepsilon_g|_{\max} = mg\pi \frac{A}{\lambda} \frac{B}{\dot{R}_{x_{ave}}} \quad (C.65)$$

In order to evaluate the largest error from (C.65) the value of B is required. If $\Delta \dot{R}_x$ is derived from the track variations alone due to potential kinetic energy conversion (and vice versa),

$$\frac{1}{2} m \dot{R}_{x_{\max}}^2 - \frac{1}{2} m \dot{R}_{x_{\min}}^2 = mg(2A)$$

or

$$\frac{1}{2} \left(\dot{R}_{x_{\max}}^2 - \dot{R}_{x_{\min}}^2 \right) = 2gA \quad (C.66)$$

$$\frac{1}{2} \left(\dot{R}_{x_{\max}} + \dot{R}_{x_{\min}} \right) \left(\dot{R}_{x_{\max}} - \dot{R}_{x_{\min}} \right) = 2gA$$

Since,

$$\dot{R}_{x_{\text{ave}}} = \frac{1}{2} \left(\dot{R}_{x_{\max}} + \dot{R}_{x_{\min}} \right)$$

and,

$$B = \frac{1}{2} \left(\dot{R}_{x_{\max}} - \dot{R}_{x_{\min}} \right)$$

$$2\dot{R}_{x_{\text{ave}}} \left(\dot{R}_x \right)_{\max} = 2gA$$

or

$$\frac{B}{\dot{R}_{x_{\text{ave}}}} = \frac{gA}{\dot{R}_{x_{\text{ave}}}^2} \quad (C.67)$$

Given $A = 1/8$ -inch and $\dot{R}_{x_{ave}} = 50 \text{ mph} = 73.3 \text{ ft/sec}$

$$\begin{aligned} \frac{B}{\dot{R}_{x_{ave}}} &= (32.2) \frac{1}{(8)(12)} \frac{1}{(73.3)^2} \\ &= 6.24 \times 10^{-5} \text{ at } 50 \text{ mph} \end{aligned}$$

At 90 mph = 132 ft/sec

$$\begin{aligned} \frac{B}{\dot{R}_{x_{ave}}} &= 32.2 \frac{1}{(8)(12)} \frac{1}{(132)^2} \\ &= 1.93 \times 10^{-5} \text{ at } 90 \text{ mph} \end{aligned}$$

Finally, for a 9,850-lb. trailer,

$$\begin{aligned} \left| \epsilon_g \right|_{\max} &= (9,850) \pi \left(\frac{1}{8 \times 12} \right) \left(\frac{1}{78} \right) (6.24 \times 10^{-5}) \\ &= 2.58 \times 10^{-4} \text{ lb at } 50 \text{ mph} \end{aligned}$$

and

$$\begin{aligned} \left| \epsilon_g \right|_{\max} &= (9,850) \pi \left(\frac{1}{8 \times 12} \right) \left(\frac{1}{78} \right) (1.93 \times 10^{-5}) \\ &= 8.0 \times 10^{-5} \text{ lb at } 90 \text{ mph} \end{aligned}$$

Thus, the error is extremely small. It may be remarked that if the track variations are described in terms of a Fourier sine series

$$h(x) = \frac{\Delta H}{\Lambda} + \sum_{p=0}^{\infty} A_p \sin \frac{2\pi x}{\lambda_p} \quad (\text{C.68})$$

and if the speed variations are given by another Fourier series,

$$R_x = \sum_{q=0}^{\infty} B_q \sin 2\pi f_q t \quad (C.69)$$

then, the error becomes (ignoring the phase angle),

$$\epsilon_g = mg\pi \sum_{p=0}^{\infty} \sum_{q=0}^{\infty} \frac{A_p}{\lambda_p} \frac{B_q}{\dot{R}_{a\text{ave}}} \cos \frac{\pi \ell}{\lambda_p} \sin \left(\frac{\pi \ell}{\lambda_p} \right)$$

or

$$\epsilon_g = mg \frac{\pi}{2} \sum_{p=0}^{\infty} \sum_{q=0}^{\infty} \frac{A_p}{\lambda_p} \frac{B_q}{\dot{R}_{x\text{ave}}} \sin \frac{2\pi \ell}{\lambda_p} \quad (C.70)$$

Even in the presence of smaller wavelengths, λ_p , the total error is expected to be small because (i) convergence property of the Fourier axes ensures that successive coefficients A_p 's and B_q 's are small; (ii) within the framework of present analysis, the condition (C.51) need be satisfied by the largest wavelength in the truck and A_p/λ_p can locally be of the order of unity; and (iii) the attenuation factor may reduce contributions of some terms in the series.

APPENDIX C.5

ERROR IN AVERAGING A SINUSOIDAL SIGNAL

Consider a sinusoidal signal which is averaged over a finite time interval T (Figure C-5)

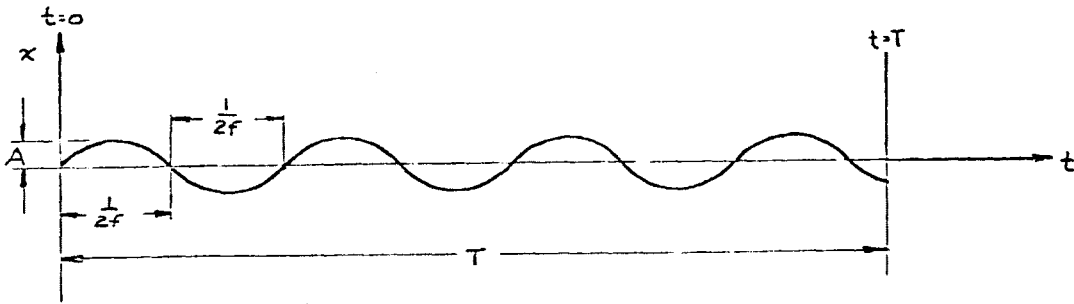


Figure C-5. Example of a Sinusoidal Time series

Let the signal be given by

$$x(t) = A \sin 2\pi ft \quad (C.71)$$

By definition the average value of $x(t)$ is

$$\bar{x} = \lim_{T \rightarrow \infty} \frac{A}{T} \int_0^T x(t) dt \quad (C.72)$$

The integral in Equation (C.72) represents area under the $x(t)$ vs t curve, and since a sinusoid is a bounded function, this area is finite. Therefore, the average (\bar{x}) approaches zero as T approaches infinity. For a finite averaging time T , \bar{x} will be zero only if T includes an even number of half cycles so that the positive areas under the curve $x(t)$ exactly cancel the negative ones. Hence, the maximum deviation from

$\bar{x} = 0$ will occur when a half cycle remains uncanceled; i.e. when T contains an odd number of half cycles. In this case, the average is

$$\begin{aligned}
 \bar{x}_T &= \frac{A}{T} \int_0^{1/2f} \sin 2\pi ft \, dt \\
 &= \frac{A}{2\pi fT} [\cos 2\pi ft]_0^{1/2f} \\
 &= \frac{A}{2fT} [\cos \pi - \cos 0] \\
 &= \frac{A}{2fT} [-1 - 1] \\
 &= \frac{A}{\pi fT}
 \end{aligned}$$

Thus the error in averaging, or deviation from a time average of zero, is

$$\epsilon_{ave} = \frac{A}{\pi fT} \tag{C.73}$$

It is noticed that this error goes to zero as the averaging time becomes infinitely large.

APPENDIX C.6

DETERMINATION OF ERROR IN MEASUREMENT OF INSTANTANEOUS TRAIN SPEED

Let V be the instantaneous train speed at time t and ' a ' be the acceleration at that instant. Let Δt be a 'sufficiently' small time interval over which a can be assumed constant. Then, the distance travelled by the train in time Δt is

$$s = V\Delta t + \frac{1}{2} a (\Delta t)^2 \quad (C.74)$$

If D_o is the nominal diameter of the wheelset, the number of wheel revolutions in time Δt is

$$\frac{s}{\pi D_o} = \frac{V\Delta t + \frac{1}{2} a (\Delta t)^2}{D_o} \quad (C.75)$$

If N pulses are put out by the encoder per wheel revolution, the total number of pulses is

$$q = \frac{N}{\pi D_o} V\Delta t + \frac{1}{2} a (\Delta t)^2 \quad (C.76)$$

Solving equation (C.76) for V , the train speed at instant t , one obtains

$$V = \frac{\pi D_o q}{N} - \frac{1}{2} a (\Delta t)^2 \frac{1}{\Delta t}$$

or

$$V = \frac{\pi D_o q}{N\Delta t} - \frac{1}{2} a \Delta t \quad (C.77)$$

Assume now that an error of Δq pulses is made in counting q_o pulses, or

$$q = q_o + \Delta q$$

Writing V as V_0 plus an error term ΔV_0 , Equation (C.77) becomes,

$$V_0 + \Delta V_0 = \frac{\pi D_0 q_0}{N \Delta t} + \frac{\pi D_0 \Delta q}{N \Delta t} - \frac{1}{2} a \Delta t \quad (\text{C.78})$$

If there were no errors in pulse counting and if there is no acceleration of the train over the period Δt , the last two terms are absent in the above equation. Thus,

$$V_0 = \frac{\pi D_0 q_0}{N \Delta t} \quad (\text{C.79a})$$

and

$$\Delta V_0 = \frac{\pi D_0 \Delta q}{N \Delta t} - \frac{1}{2} a \Delta t \quad (\text{C.79b})$$

Dividing the last equation by V_0 , the error is

$$\begin{aligned} \frac{\Delta V_0}{V_0} &= \frac{\pi D_0 \Delta q}{V_0 N \Delta t} - \frac{1}{2 V_0} a \Delta t \\ &= \epsilon_1 + \epsilon_2 \end{aligned} \quad (\text{C.80})$$

where,

$$\epsilon_1 = \frac{\pi D_0 \Delta q}{V_0 N \Delta t} \quad (\text{C.81a})$$

and

$$\epsilon_2 = - \frac{1}{2 V_0} a \Delta t \quad (\text{C.81b})$$

Since these errors are independent they can be combined in an RMS manner to yield the total error as follows,

$$\epsilon^2 = \epsilon_1^2 + \epsilon_2^2$$

$$\epsilon^2 = \left(\frac{\pi D_o \Delta q}{V_o N} \right)^2 \frac{1}{(\Delta t)^2} + \frac{a^2}{4V_o^2} (\Delta t)^2 \quad (C.82)$$

Equation (C.82) shows that the error (squared) consists of two parts, one which is directly proportional to $(\Delta t)^2$ and the other inversely proportional to $(\Delta t)^2$. Δt may now be identified as the time interval over which the pulses are counted. Thus, there is a value of this time interval (squared) for which ϵ^2 is a minimum. This is given by

$$\frac{d\epsilon^2}{d(\Delta t)^2} = 0$$

or

$$\left(\frac{\pi D_o \Delta q}{N V_o} \right)^2 \cdot \frac{-1}{(\Delta t^2)^2} + \frac{a^2}{4V_o^2}$$

Hence,

$$(\Delta t)^4 = \frac{4\pi^2 D_o^2 (\Delta q)^2}{N^2 a^2} \quad (C.83)$$

The minimum value of Δt from equation (C.83) is calculated below.

N = Pulses per revolutions = 1,000

a = Maximum acceleration (worst case) of the train = 2 ft/sec² typically.

q = Error in pulse counting = ± 1

D_o = Nominal wheel diameter = 3 ft

$$(\Delta t)^4 = \frac{4\pi^2(9)(1)}{10^6(4)} = 88.8 \times 10^{-6} \text{ sec}^4$$

$$(\Delta t)^2 = 9.4 \times 10^{-3} \text{ sec}^2$$

and

$$(\Delta t) = 9.673 \times 10^{-2} \text{ secs or } 96.73 \text{ msec.}$$

If a sampling rate of $\frac{1}{256} \text{ sec} = 3.9 \text{ msec}$ is used,

$$\Delta t = \frac{96.73}{3.9} = 24.8 \text{ sampling intervals.}$$

The minimum error is at $V_0 = 90 \text{ mph}$
 $= 132 \text{ ft/sec.}$

$$\epsilon^2 = \frac{\pi^2(9)(1)}{(132)^2 10^6} \frac{1}{(9.4 \times 10^{-3})}$$

$$+ \frac{4}{4(132)^2} (0.4 \times 10^{-3})$$

$$= 0.54 \times 10^{-6} + 5.4 \times 10^{-7}$$

$$= 1.08 \times 10^{-6}$$

$$\epsilon = 1.04 \times 10^{-3} \text{ or } \underline{0.10\%}$$

At $V_0 = 90$ mph,

$$\begin{aligned}\epsilon^2 &= \frac{\pi^2(9)(1)}{(132)^2(10^6)} \frac{1}{(\Delta t)^2} + \frac{4}{4(132)^2} (\Delta t)^2 \\ &= \frac{5.10 \times 10^{-9}}{(\Delta t)^2} + 5.74 \times 10^{-5} (\Delta t)^2\end{aligned}$$

Writing Δt in terms of the sampling rate (1/256 sec),

$$\Delta t = \frac{n}{256} \text{ sec, } n \geq 0.$$

$$\epsilon^2 = \frac{5.10 \times 10^{-9} (256)^2}{n^2} + \frac{5.74 \times 10^{-5}}{(256)^2} n^2$$

$$\epsilon^2 = \frac{3.34 \times 10^{-4}}{n^2} + 8.76 \times 10^{-10} n^2 \quad (\text{C.84})$$

Since $\epsilon^2 \propto \frac{1}{V_0^2}$ or $\epsilon \propto \frac{1}{V_0}$, the error at 50 mph is 1.8 times the error at 90 mph. A table of errors is given below.

<u>n</u>	<u>ε% at 90 mph</u>	<u>ε% at 50 mph</u>
0	∞	∞
1	1.83	3.3
2	0.91	1.64
4	0.46	0.83
6	0.30	0.54
10	0.18	0.32
15	0.13	0.23
20	0.11	0.20
25	0.10	0.18
30	0.11	0.20
35	0.12	0.22
50	0.15	0.27
100	0.30	0.54

These values are plotted in Figure C-6. For the AERO/TOFC-II tests Δt was chosen to be 10/256 sec and this leads to an error of 0.18% at 90 mph and 0.32% at 50 mph in the measurement of instantaneous train speed.

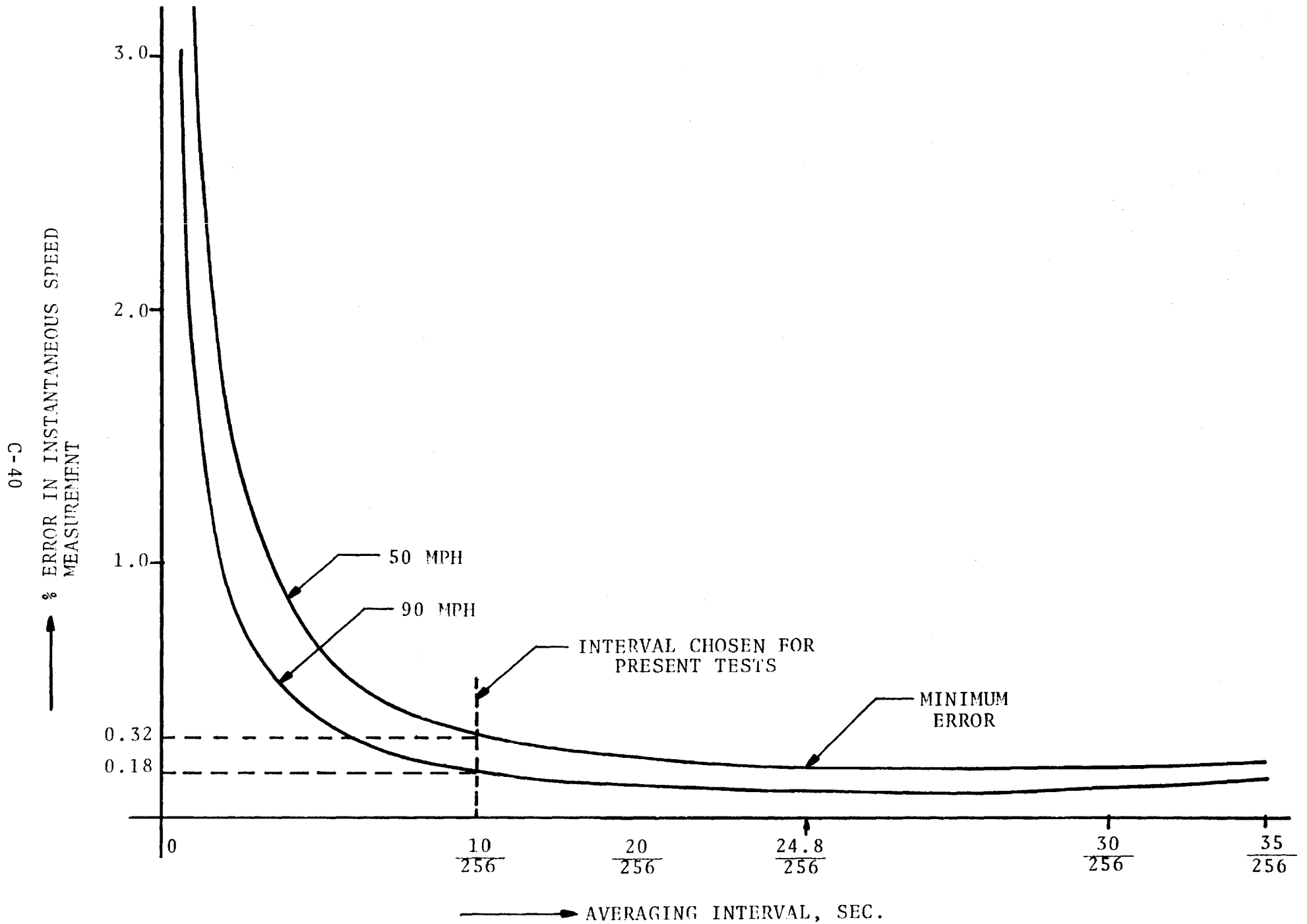


Figure C-5. Errors in Instantaneous Train Speed Measurement.

APPENDIX C.7

ERRORS IN SIDE FORCE DUE TO DECOUPLING BETWEEN
TRANSLATIONAL AND ROTATIONAL MOTIONS

Following the developments of Appendix C.2 it can be seen that the yaw rotation of the carbody is coupled to the translation of the trailer relative to the carbody in the \tilde{x} direction.

The term is of the form

$$s_{dc} = \frac{m}{T} \left[\omega_z(T) - \omega_z(0) \right] \tilde{x} \quad (C.85)$$

The frequency of yaw oscillations is typically around 2.5Hz as shown in Table III.1 and the amplitude may be 2 inches over the carbody wheelbase of 60 feet. Therefore,

$$\theta_z = \pm \frac{2}{60 \times 12} \sin 2\pi (2.5) t$$

or

$$\theta_z = \frac{1}{360} \sin 5\pi t$$

Hence,

$$\omega_z = \frac{d\theta_z}{dt} = \pm \frac{\pi}{72} \cos 5\pi t$$

and $[\omega_z(T) - \omega_z(0)]_{\max} = 2(\pi/72)$

Given the distance of trailer center of gravity from center of the carbody, \tilde{x} , to be 219 inches the decoupling error has the maximum value

$$s_{dc} = \frac{9850}{32.2} \frac{1}{30.3} 2 \frac{\pi}{72} \left(\frac{219}{12}\right) \text{ at 90 mph when } T = 30.3 \text{ seconds}$$

$$= 16.1 \text{ lbs at 90 mph}$$

At 50 mph, when T = 54.5 seconds

$$s_{dc} = \frac{9850}{32.2} \frac{1}{54.5}^2 \left(\frac{\pi}{72}\right) \left(\frac{219}{12}\right)$$
$$= 8.9 \text{ lbs at 50 mph}$$

In addition, following the deviation in Appendix C-2, the error due to translation of the trailer relative to carbody can be shown to be,

$$s_t = \frac{m}{T} [\dot{\tilde{y}}(T) - \dot{\tilde{y}}(0)] \quad (C.86)$$

Since the trailer motions relative to the carbody are expected to be very small, let $\dot{\tilde{y}} = \pm 0.01$ ft/sec, which yields

$$\alpha_t = \frac{9850}{32.2} \frac{1}{30.3} 2(0.01) = 0.20 \text{ lbs at 90 mph}$$
$$= \frac{9850}{32.2} \frac{1}{54.5} 2(0.01) = 0.11 \text{ lbs at 50 mph}$$

APPENDIX C.8

COMPUTATION OF ACCELERATION DUE TO GRAVITY

The value of local acceleration due to gravity 'g' depends upon the latitude and the elevation of the ground. 'g' is computed using Helmert's equation (Reference 11).

$$g = 980.616 - 2.5928 \cos 2\phi + 0.0069 \cos^2 2\phi - 3.086 \times 10^{-6}H \quad (\text{C.87})$$

where,

g = acceleration due to gravity in cm/sec²

ϕ = latitude

H = elevation in centimeters

The latitude for Pueblo, Colorado is 38°17'N (Reference 4): The elevations at track stations 140 and 180 are (Reference 5):

$$H_{140} = 4873.0 \text{ ft} = 1.485 \times 10^5 \text{ cm}$$

$$H_{180} = 4861.7 \text{ ft} = 1.482 \times 10^5 \text{ cm}$$

Since the test zone is between track stations 140 and 180 (Figure 1a), the average elevation is 1.4835×10^5 cm.

Now,

$$\cos(2\phi) = \cos[2(38.28)^\circ] = 0.2324$$

$$\cos^2(2\phi) = (0.2324)^2 = 0.0540$$

Hence,

$$\begin{aligned} g &= 980.616 - 2.5928(0.2324) + 0.0069(0.0540) - 3.086 \times 10^{-6} \\ &\quad (1.4835 \times 10^5) \\ &= 980.616 - 0.6026 + 0.00037 - 0.4578 \\ &= 979.556 \text{ cm/sec}^2 \end{aligned}$$

Or,

$$g = 32.138 \text{ ft/sec}^2$$

This value of 'g' was used as a constant in all computations.

APPENDIX C.9

DERIVATION OF ROLLING RESISTANCE INFORMATION

Consider the instrumental flat car with two trailers as shown in Figure C-6 below.

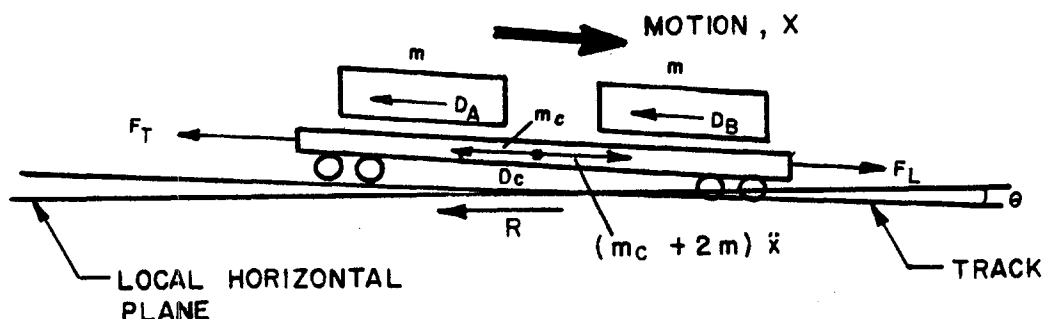


Figure C.6. Derivation of Rolling Resistance

F_{Lead} and F_{Trail} are leading and trailing coupler forces, respectively. D_A , D_B and D_C denote the drag force on trailer A, trailer B and the flat car C. R stands for the rolling resistance. The equation of motion for the total mass $(m_c + 2m)$ is

$$(m_c + 2m) \ddot{x} = (F_{Lead} - F_{Trail}) + (m_c + 2m)g \sin \theta - R - D_A - D_B - D_C \quad (C.88)$$

Where θ is the average downhill slope of the track. Integrating Equation (C.88) over the test duration T and dividing by T , one obtains

$$\begin{aligned} \frac{1}{T} (m_c + 2m) \int_0^T \ddot{x} dt &= \frac{1}{T} \int_0^T (F_{Lead} - F_{Trail}) dt \\ &+ \frac{1}{T} (m_c + 2m) g \sin \theta \int_0^T dt \\ &- \frac{1}{T} \int_0^T (D_A + D_B) dt - \frac{1}{T} \int_0^T (R + D_C) dt \end{aligned}$$

Introducing definition of an average.

$$\frac{1}{T} (m_c + 2m) [\dot{x}(r) - \dot{x}(o)] = (\bar{F}_{Lead} - \bar{F}_{Trail}) + (m_c + 2m)g \sin \theta - (\bar{D}_A + \bar{D}_B) - (\bar{R} + \bar{D}_C)$$

Therefore,

$$\begin{aligned} (\bar{R} + \bar{D}_C) &= (\bar{F}_{Lead} - \bar{F}_{Trail}) + (m_c + 2m)g \sin \theta - (\bar{D}_A + \bar{D}_B) \\ &- \frac{1}{T} (m_c + 2m) [\dot{x}(T) - \dot{x}(o)] \end{aligned}$$

(C.89)

This equation yields average rolling resistance combined with the aerodynamic drag of the flat car. Under the AERO/TOFC-II scheme of instrumentation it is not possible to evaluate the rolling resistance separately, except at low speeds (30-40 mph) when aerodynamic drag on the trailers and the flat car is small.

APPENDIX D

PROCEDURE FOR ONBOARD COMPUTATION
OF DRAG AND SIDE FORCES

D.1 LIST OF CHANNELS

FORCES

F1 A van vertical front force
F2 A van lateral front force
F3 A van longitudinal front force
F4 A van vertical rear left force
F5 A van vertical rear right force
F6 A van lateral rear force
F7 B van vertical front force
F8 B van lateral front force
F9 B van longitudinal front force
F10 B van vertical rear left force
F11 B van vertical rear right force
F12 B van lateral rear force
F13 Leading coupler longitudinal force
F14 Trailing coupler longitudinal force

ACCELERATIONS

A1 A van longitudinal accelration
A2 A van lateral acceleration
A3 B van longitudinal acceleration
A4 B van lateral acceleration
A5 Carbody longitudinal acceleration
A6 Carbody lateral acceleration

DISPLACEMENTS

D1 Carbody/Journal box relative displacement "A" end - right
D2 Carbody/Journal box relative displacement "A" end - left
D3 Carbody/Journal box relative displacement "B" end - right
D4 Carbody/Journal box relative displacement "B" end - left

VELOCITIES

\bar{T}	{ Tachometer counts (train displacement) Average train speed
U	Relative speed between T-5 and TTX
V	Wind speed relative to train (obtained from boom on locomotive)
α	Wind direction relative to train
W	Wind speed (wayside)
β	Wind direction (wayside)

PITCH AND ROLL ANGLES

θ	Pitch angle output of vertical gyro
ψ	Roll angle output of vertical gyro

D.2 COMPUTATION PROCEDURE

1. Read initial (i.e. zero) force values before the tests for each given test day. Denote these by

$$F_{i_0}, i = 1, 2, \dots, 12$$

Note that these values are obtained for the trailer in perfectly level position inside the Central Services Building.

2. Compute average values of the following channels over each 800-foot segment and over the entire test zone. The averages are computed in the form

$$\bar{x} = \frac{1}{n} \sum_{j=1}^n x_n \quad (\text{scale factor})$$

where the 'scale factor' converts the digitized output to appropriate physical units. The channels to be averaged are:

A. Force transducer readings

$$F_{1r} \quad \text{through} \quad F_{12r}$$

where the subscript 'r' denotes force reading. Let the corresponding averages be labeled:

$$\bar{F}_{1r} \quad \text{through} \quad \bar{F}_{12r}$$

B. Accelerations (optional)

A1 through A6 denoted by \bar{A}_1 through \bar{A}_6

C. Displacements

D1 through D4 denoted by \bar{D}_1 through \bar{D}_4

D. Velocities

- Train speed, \bar{T}
- Relative speed between T-5 and TTX, \bar{U}
- Component of wind speed relative to train along the direction of motion, \bar{V}_x = average value of $V \cos \alpha$, ft/sec.
- Component of wind speed relative to train across the direction of motion, \bar{V}_y = Average value of $V \sin \alpha$, ft/sec.
- Wind direction relative to train, $\bar{\alpha}$
- Component of wind speed (wayside) along the direction of motion, \bar{W}_x = Average value of $W \cos \beta$
- Component of wind speed (wayside) across the direction of motion, \bar{W}_y = Average value of $W \sin \beta$

3. Compute uncorrected average force values by subtracting the zero force values from the average transducer reading.

$$\bar{F}_{i_{\text{uncor}}} = \bar{F}_{i_r} - \bar{F}_{i_o}, \quad i = 1, 2, \dots, 12$$

where the subscript 'uncor' indicates that the force value has not been corrected for cross-axis response.

4. Compute force values corrected for cross-axis response for each trailer (A and B).

$$\bar{F}_i = a_{ij} \bar{F}_{j_{\text{uncor}}} \quad \text{or} \quad \{\bar{F}\} = [a] \{\bar{F}\}_{\text{uncor}}$$

with

$$\begin{aligned} i &= 1, 2, \dots, 6 \text{ and } j = 1, 2, \dots, 6 \text{ for trailer A} \\ i &= 7, 8, \dots, 12 \text{ and } j = 7, 8, \dots, 12 \text{ for trailer B} \end{aligned}$$

where

\bar{F}_i or $\{\bar{F}\}$ = column matrix of corrected average force

$\bar{F}_{j_{\text{uncor}}}$ or $\{\bar{F}\}_{\text{uncor}}$ = column matrix of uncorrected average force

a_{ij} of $[a]$ = calibration matrix (6x6)

Note that the calibration matrix $[a]$ is different for each trailer. For present test program, the flexure alignment procedures (Appendix A) performed by Brewer Engineering Laboratories assured that the calibration matrix a_{ij} is very nearly (within 2 percent) an identifying matrix.

5. Compute instantaneous train speed at the beginning and at the end of the test zone: T_{in} and T_{fin} in ft/sec.

6. Compute instantaneous speed of TTX relative to T-5 at the beginning and at the end of the test zone: U_{in} and U_{fin} in ft/sec. Note the sign convention for U :

$U > 0$ for coupler in buff

$U < 0$ for coupler in tension

7. Compute absolute speed of TTX at the beginning and at the end of the test zone.

$$\dot{x}_{in} = T_{in} + U_{in} \text{ ft/sec}$$

$$\dot{x}_{fin} = T_{fin} + U_{fin} \text{ ft/sec}$$

8. Compute the rate of change of momentum of TTX

$$\Delta M = \frac{m}{\Delta T} (\dot{x}_{fin} - \dot{x}_{in}) \text{ lbs}$$

where,

M = trailer mass in slugs - trailer weight/g

ΔT = duration of test run in seconds.

\dot{x}_{in} and \dot{x}_{fin} are in ft/sec and g is the acceleration due to gravity as computed in Appendix D.3

9. Compute absolute average speed of TTX over the test zone

$$\dot{x}_{ave} = \bar{T} + \bar{U} \text{ ft/sec}$$

10. Compute the average gravitational force contribution

$$\Delta \bar{G} = \frac{W \Delta H}{\dot{x}_{ave} \Delta T} \text{ ft/sec}$$

where,

W = trailer weight in lbs

ΔH = change in elevation between the beginning and end of the test zone

= final elevation - initial elevation

11. Compute average drag force on trailers A and B

$$\overline{DF}_A = F_3 - \Delta M - \Delta \overline{G} \quad \text{lbs}$$

$$\overline{DF}_B = F_9 - \Delta M - \Delta \overline{G} \quad \text{lbs}$$

12. Compute average side force on trailers A and B

$$\overline{SF}_A = F_2 + F_6 \quad \text{lbs}$$

$$\overline{SF}_B = F_8 + F_{12} \quad \text{lbs}$$

13. Computation of air density

$$\rho = 0.08071 (273.12/T) [(B-0.3783e)/760]$$

where

ρ = density of air in lb/ft³

T = dry bulb temperature in deg K

$$= 273 + 0.5556 (t-32)$$

B = barometer pressure in mm of Hg

$$= 25.4 P$$

e = vapor pressure of moisture in air in mm of Hg,
obtained from dew point tables in Reference 11,
page F-9.

14. Compute the square of average wind speed relative to the train

$$\overline{V}^2 = \overline{V}_x^2 + \overline{V}_y^2 \quad \text{ft}^2/\text{sec}^2$$

15. Compute average dynamic pressure

$$q = \frac{1}{2} \rho V^2 \left(\frac{1}{g}\right) \text{ lbs/ft}^2$$

where g has been computed in Appendix c.8.

16. Compute force areas for individual trailer

A. Drag Areas:

$$(C_D S)_A = \overline{DF}_A / \bar{q} \text{ ft}^2$$

$$(C_D S)_B = \overline{DF}_B / \bar{q} \text{ ft}^2$$

B. Side Force Areas:

$$(C_Y S)_A = \overline{SF}_A / \bar{q} \text{ ft}^2$$

$$(C_Y S)_B = \overline{SF}_B / \bar{q} \text{ ft}^2$$

17. Compute total force areas:

A. Drag Area:

$$C_D S = (C_D S)_A + (C_D S)_B \text{ ft}^2$$

B. Side Force Area:

$$C_Y S = (C_Y S)_A + (C_Y S)_B \text{ ft}^2$$

D.3 SAMPLE COMPUTER OUTPUT

Legend:

Ru	Run Number
TSP	Nominal Train Speed, MPH
WS	Nominal Wind Speed, MPH at OCC
D	Nominal Wind Direction, Degrees at OCC
T	Air Temperature, Degrees F
H	Present Humidity
P	Barometric Pressure
Gyro	
One	Pitch Angle (degrees)
Gyro	
Two	Roll Angle (degrees)
v	Onboard Wind Speed (ft/sec)
Alpha	Onboard Wind Direction
Beta	Wayside Wind Direction (4-1(a))
Pitch	Average Carbody Pitch Angle (Equation 3.28)
Roll	Average Carbody Roll Angle (Equation 3.33)
w	Onboard Wind Direction (Figure 4-1(b))

FTLE 02 TAPE 63 NC= 0090 SR= 0256 NS= 0041

12/16/77 AERO T0FC 2* (RU 98)(TSP 90)(WS 18)(D 270)(T 42)(H 17)(P 24.60)

AVERAGE CHANNEL	VALUES FOR MILEPOSTS 6301 TO 6309	DESCRIPTION	MEAN
71		VAN A VERTICAL FRONT FORCE	611.654
72		VAN A LATERAL FRONT FORCE	-814.720
73		VAN A LONGITUDINAL FRONT FORCE	-752.822
74		VAN A VERTICAL REAR LEFT FORCE	-652.334
75		VAN A VERTICAL REAR RIGHT FORCE	1174.149
76		VAN A LATERAL REAR FORCE	-774.297
77		VAN B VERTICAL FRONT FORCE	623.873
78		VAN B LATERAL FRONT FORCE	-650.903
40		VAN B LONGITUDINAL FRONT FORCE	-741.615
80		VAN B VERTICAL REAR LEFT FORCE	-495.155
81		VAN B VERTICAL REAR RIGHT FORCE	994.518
82		VAN B LATERAL REAR FORCE	-526.814
83		LEADING COUPLER LONGITUDINAL FORCE	1880.760
84		TRAILING COUPLER LONGITUDINAL FORCE	-81.808
85		A VAN LONGITUDINAL ACCELERATION	0.098
86		A VAN LATERAL ACCELERATION	0.085
87		B VAN LONGITUDINAL ACCELERATION	0.099
88		B VAN LATERAL ACCELERATION	0.039
69		RAILCAR LONGITUDINAL ACCELERATION	0.017
70		RAILCAR LATERAL ACCELERATION	-0.001
64		DISPLACEMENT A (END - RIGHT)	-0.552
65		DISPLACEMENT A (END - LEFT)	0.377
66		DISPLACEMENT B (END - RIGHT)	-0.481
67		DISPLACEMENT B (END - LEFT)	0.255
2		AVERAGE TRAIN SPEED (T)	127.550
3		RELATIVE SPEED BETWEEN TS AND TTX(U)	0.008
89		RELATIVE WIND SPEED (U)	151.287
46		RELATIVE WIND DIRECTION (ALPHA)	195.090
49		WAYSIDE WIND SPEED (W)	24.529
50		WAYSIDE WIND DIRECTION (BETA)	252.529
53		GYRO ONE	-1.011
54		GYRO TWO	0.567
		U*COS(ALPHA)	-145.945
		U*SIN(ALPHA)	-39.466
		W*COS(BETA)	-7.318
		W*SIN(BETA)	-23.031
		PITCH	-0.000
		ROLL	-0.007
		INITIAL TRAIN SPEED	131.453
		FINAL TRAIN SPEED	124.217
		INITIAL RELATIVE SPEED	-0.033
		FINAL RELATIVE SPEED	-0.003
		RATE OF CHANGE OF MOMENTUM	-71.166
		GRAVITATION CONTRIBUTION	-27.372
		TOTAL SAMPLES	8085

FORCES CORRECTED FOR CROSS-AXIS RESPONSE

71	VAN A VERTICAL FRONT FORCE	611.854
72	VAN A LATERAL FRONT FORCE	-814.720
73	VAN A LONGITUDINAL FRONT FORCE	-752.822
74	VAN A VERTICAL REAR LEFT FORCE	-652.334
75	VAN A VERTICAL REAR RIGHT FORCE	1174.149
76	VAN A LATERAL REAR FORCE	-774.297
77	VAN B VERTICAL FRONT FORCE	623.873
78	VAN B LATERAL FRONT FORCE	-650.903
40	VAN B LONGITUDINAL FRONT FORCE	-741.615
80	VAN B VERTICAL REAR LEFT FORCE	-495.155
81	VAN B VERTICAL REAR RIGHT FORCE	994.518
82	VAN B LATERAL REAR FORCE	-526.814

DYNAMIC PRESSURE = 22.901 LB/FT**2

FORCES AND FORCE AREAS

VAN A

DRAG FORCE	851.	LBS.
LATERAL FORCE	-1589.	LBS.
LIFT FORCE	1133.	LBS.
DRAG FORCE AREA	37.	FT**2
LATERAL FORCE AREA	-69.	FT**2
LIFT FORCE AREA	49.	FT**2

VAN B

DRAG FORCE	840.	LBS.
LATERAL FORCE	-1177.	LBS.
LIFT FORCE	1123.	LBS.
DRAG FORCE AREA	36.	FT**2
LATERAL FORCE AREA	-51.	FT**2
LIFT FORCE AREA	49.	FT**2

TOTAL FORCE AREAS

TOTAL DRAG FORCE AREA	73.	FT**2
TOTAL LATERAL FORCE AREA	-120.	FT**2
TOTAL LIFT FORCE AREA	98.	FT**2

AERODYNAMIC FORCES ON FREIGHT TRAINS
VOLUME II
TEST RESULTS REPORT
FULL-SCALE AERODYNAMIC VALIDATION TESTS
OF TRAILER-ON-A-FLAT CAR (SERIES II)
MARCH 1978

ERRATA SHEET

On page xii (Summary), second paragraph, the fifth sentence should read:

It was found that the configuration with the empty buffer car (Configuration 2) consistently experienced larger drag (10 percent for wind angles near zero and up to 20 percent at six degrees) than the configuration with the loaded buffer car (Configuration 1).

